

Reinforced Concrete Beams Subjected to Drop-Weight Impact

Experimental study of the influence of reinforcement properties on the structural response

Master's thesis in the Master's Programme Structural Engineering and Building Technology

MALIN ANDERSSON
EMMA PETTERSSON

MASTER'S THESIS ACEX30-19-27

Reinforced Concrete Beams Subjected to Drop-Weight Impact

Experimental study of the influence of reinforcement properties on the structural
response

*Master's Thesis in the Master's Programme Structural Engineering and Building
Technology*

MALIN ANDERSSON
EMMA PETTERSSON

Department of Architecture and Civil Engineering
Division of Structural Engineering
Concrete Structures

CHALMERS UNIVERSITY OF TECHNOLOGY

Göteborg, Sweden 2019

Reinforced Concrete Beams Subjected to Drop-Weight Impact

Experimental study of the influence of reinforcement properties on the structural response

Master's Thesis in the Master's Programme Structural Engineering and Building Technology

MALIN ANDERSSON

EMMA PETTERSSON

© MALIN ANDERSSON, EMMA PETTERSSON, 2019

Examensarbete ACEX30-19-27

Institutionen för arkitektur och samhällsbyggnadsteknik

Chalmers tekniska högskola, 2019

Department of Architecture and Civil Engineering

Division of Structural Engineering

Concrete Structures

Chalmers University of Technology

SE-412 96 Göteborg

Sweden

Telephone: + 46 (0)31-772 1000

Cover:

Illustration of drop-weight impact on reinforced concrete beam along with strain fields of beam I10-UD-B1-07 at different time steps after the impact and mechanical properties of undamaged, pre-stretched and bent reinforcement.

Chalmers Reproservice

Göteborg, Sweden, 2019

Reinforced Concrete Beams Subjected to Drop-Weight Impact

Experimental study of the influence of reinforcement properties on the structural response

Master's thesis in the Master's Programme Structural Engineering and Building Technology

MALIN ANDERSSON

EMMA PETTERSSON

Department of Architecture and Civil Engineering
Division of Structural Engineering
Concrete Structures
Chalmers University of Technology

ABSTRACT

Reinforced concrete is commonly used in protective structures, therefore it is of high interest how it is affected by impulse loads such as collisions or explosions. The general purpose of this thesis is to increase the understanding of the structural response of reinforced concrete structures subjected to impact loading. An important issue was to evaluate the influence of damaged reinforcement on the plastic deformation capacity.

A literature study was made on the mechanical properties of reinforcement that was damaged due to stretching, bending, welding and corrosion, together with its influence on the plastic deformation capacity. The mechanical properties of reinforcement damaged through stretching and bending were also tested experimentally. Furthermore, a literature study was made on impact loads, plastic rotation capacity and two-degree-of-freedom (2DOF) systems.

Experiments were conducted on reinforced concrete beams impacted by a drop-weight subsequently tested statically. Beams containing undamaged reinforcement and beams containing pre-stretched reinforcement were tested. The response was captured with cameras and was thereafter processed using digital image correlation (DIC). One objective was to use a 2DOF system to predict the response of the impacted beams. Additionally, simplified hand calculations were performed. The structural response of the dynamically impacted beams obtained from experiments was then compared to non-impacted beams and to the predicted results obtained from the 2DOF model and hand calculations.

The evaluation of the experiments showed that using pre-stretched reinforcement results in a smaller plastic deformation capacity and residual capacity after the impact, compared to using undamaged reinforcement. Furthermore, the 2DOF model generally underestimates the strength of the impacted beams which results in larger deflections than what was observed in the experiments. Thereby, the model predicts the dynamic response in a conservative way, though further developments of the model is desirable.

Key words: reinforced concrete, reinforcement, damaged, pre-stretching, bending, welding, corrosion, drop-weight impact, digital image correlation, DIC, 2DOF, plastic deformation capacity.

Armerade Betongbalkar Utsatta för Fallviktsförsök

Experimentell studie om påverkan av armeringens egenskaper på strukturens respons

Examensarbete inom masterprogrammet Konstruktionsteknik och Byggnadsteknologi

MALIN ANDERSSON

EMMA PETTERSSON

Institutionen för arkitektur och samhällsbyggnadsteknik

Avdelningen för Konstruktionsteknik

Betongbyggnad

Chalmers tekniska högskola

SAMMANFATTNING

Eftersom armerad betong ofta används till skyddande konstruktioner finns ett intresse för hur dessa påverkas av stötlaster såsom till exempel kollisioner eller explosioner. Det generella syftet med denna masteruppsats är att öka förståelsen för strukturens respons hos armerade betongstrukturer utsatta för stötlaster. En viktig del var att undersöka skadad armerings inverkan på den plastiska deformationskapaciteten.

En litteraturstudie i materialegenskaper hos armering som är skadad genom kalldragning, bockning, svetsning och rost utfördes, med fokus på dess inverkan på den plastiska deformationskapaciteten. Materialegenskaperna hos armering skadad genom kalldragning och bockning testades även experimentellt. Vidare gjordes även litteraturstudie angående stötlaster, plastisk rotationsförmåga och tvåfrihetsgradsystem (2DOF-system).

Experiment utfördes på armerade betongbalkar som stötblastades genom en fallvikt och därefter testades statiskt. Både balkar med oskadad och kalldragen armering testades. Responsen filmades med kameror och analyserades sedan genom digital image correlation (DIC). Ett delmål med studien var att förutspå de stötblastade balkarnas strukturens respons genom att använda ett 2DOF-system. Dessutom utfördes förenklade handberäkningar. Därefter jämfördes strukturens respons hos de dynamiskt belastade balkarna erhållen från experimenten med den hos obelastade balkar och de förutspådda resultaten från 2DOF-modellen och handberäkningarna.

Analysen av fallviktsförsöken visade att användning av kalldragen armering, i jämförelse med oskadad armering, resulterar i en lägre plastisk deformationskapacitet och återstående kapacitet efter stöten. Vidare tenderar 2DOF-modellen generellt att underskatta de stötblastade balkarnas styrka vilket resulterar i större plastisk deformation än vad som kunde observeras i fallviktsförsöken. Därmed förutspår modellen det dynamiska beteendet på ett konservativt sätt, men en vidare utveckling av den vore önskvärt för framtida studier.

Nyckelord: armerad betong, armering, skadad, kalldragning, bockning, svetsning, rost, fallviktsförsök, digital image correlation, DIC, 2DOF, plastisk deformationskapacitet.

Contents

1	INTRODUCTION	1
1.1	Background	1
1.2	Aim	1
1.3	Method	2
1.4	Limitations	2
2	STRUCTURAL RESPONSE AND MATERIALS	3
2.1	Linear elastic response	3
2.2	Plastic response	4
2.3	Elasto-plastic response	4
2.4	Tri-linear response	5
2.5	Concrete	6
2.5.1	Structural response in compression	6
2.5.2	Determination of concrete strength	8
2.5.2.1	Compressive strength	8
2.5.2.2	Tensile strength	8
2.5.2.3	Modulus of elasticity	9
2.6	Reinforcing steel	9
2.7	Reinforced concrete	11
2.7.1	Structural response in bending	11
2.7.2	Strain rate effects	12
3	IMPULSE LOADED STRUCTURES	15
3.1	Impulse, external work and kinetic energy	15
3.2	Equation of motion	16
3.3	Internal work and energy equilibrium	17
3.4	Collision of two bodies	18
4	PLASTIC ROTATION CAPACITY	21
4.1	Definition of plastic rotation	21
4.2	Influence of the mechanical properties of the reinforcement	25
4.3	Methods to predict the plastic rotation capacity	27
4.3.1	Bk25	27
4.3.2	Eurocode 2	30
4.3.3	Determination of plastic rotation capacity from experimental results	31

5	MECHANICAL PROPERTIES OF DAMAGED REINFORCEMENT	33
5.1	Investigated mechanical properties	33
5.2	Damage due to stretching	34
5.3	Damage due to bending	35
5.4	Damage due to welding	38
5.5	Damage due to corrosion	39
6	DISCRETE MODEL FOR DYNAMIC ANALYSIS	41
6.1	Definition of an SDOF system	41
6.2	Drop-weight load – dynamic interpretation	41
6.3	Transformation of structural members to equivalent SDOF systems	41
6.3.1	Transformation of a beam to equivalent SDOF system	41
6.3.2	Transformation of a drop-weight to equivalent SDOF system	44
6.4	Coupling of two SDOF systems into a 2DOF system	45
6.4.1	Equation of motion for a 2DOF system	46
6.4.2	2DOF system for a drop-weight and beam system	47
6.5	Central difference method	49
6.5.1	Numerical formulation	50
6.5.2	Stability of CDM	51
7	EXPERIMENT DESCRIPTION	52
7.1	Beam tests	52
7.1.1	Geometry of tested beams	53
7.1.2	Preparations	54
7.1.2.1	Moulds	54
7.1.2.2	Reinforcement	54
7.1.3	Casting	56
7.1.4	Demoulding and painting	57
7.1.5	Testing of the hardened concrete	57
7.1.6	Dynamic tests	58
7.1.7	Static tests	59
7.1.8	Digital image correlation	61
7.2	Reinforcement Testing Description	62
7.2.1	Modifications of the reinforcement	62
7.2.1.1	Pre-stretching	62
7.2.1.2	Bending	65
7.2.2	Testing procedure	67
8	PREDICTIONS	68
8.1	Static response	68
8.1.1	Ultimate limit state	68
8.1.2	Cracking	70
8.1.3	Yielding	70
8.1.4	Load-deflection curves	71

8.2	Rotation capacity	73
8.2.1	Bk25	73
8.2.2	Eurocode 2	73
8.2.3	Comparison	74
8.3	Dynamic response	74
8.3.1	2DOF	74
8.3.1.1	Input data	74
8.3.1.2	Results	75
8.3.2	Initial shear velocity	77
9	EXPERIMENTAL RESULTS	79
9.1	Hardened concrete properties	79
9.2	Reinforcement test results	80
9.2.1	Undamaged vs damaged reinforcement	80
9.2.2	Variation of testing speed	82
9.3	Dynamic testing of beams	83
9.3.1	Method	83
9.3.2	Applied force and impulse	83
9.3.2.1	Series I10-UD	83
9.3.2.2	Series I10-D	84
9.3.2.3	Series I20-UD	85
9.3.2.4	Series I20-D	86
9.3.2.5	Comparison	86
9.3.3	Velocity of drop-weight	87
9.3.4	Midpoint deflection over time	87
9.3.4.1	Series I10-UD	88
9.3.4.2	Series I10-D	89
9.3.4.3	Series I20-UD	90
9.3.4.4	Series I20-D	91
9.3.4.5	Comparison	91
9.3.5	Deformed shape	92
9.3.5.1	Series I10-UD	93
9.3.5.2	Series I10-D	94
9.3.5.3	Series I20-UD	95
9.3.5.4	Series I20-D	96
9.3.5.5	Comparison	97
9.3.6	Velocity of initial deflection	97
9.3.7	Strain fields	98
9.3.7.1	I10-UD	98
9.3.7.2	I10-D	100
9.3.7.3	I20-UD	101
9.3.7.4	I20-D	102
9.3.7.5	Comparison	102
9.4	Static testing of beams	103
9.4.1	Method	103
9.4.2	Results for Series S	103
9.4.2.1	Load-deflection relationship	103

9.4.2.2	Strain fields	111
9.4.3	Results for Series I10	112
9.4.3.1	Load-deflection relationship	112
9.4.3.2	Strain fields	115
9.4.3.3	Comparison with Series S	117
9.4.3.3.1	Load-deflection relationship	117
9.4.3.3.2	Approximation of internal work during impact	120
9.4.4	Results for Series I20	122
9.4.4.1	Load-deflection relationship	123
9.4.4.2	Strain fields	126
9.4.4.3	Comparison with Series S	127
10	COMPARISON BETWEEN EXPERIMENTAL RESULTS AND PREDICTIONS	128
10.1	Dynamic response	128
10.1.1	2DOF	128
10.1.2	Initial shear velocity	131
10.2	Static response	131
10.2.1	Series S	131
10.2.2	Series I10	133
10.2.3	Series I20	135
10.3	Rotation capacity	137
11	DISCUSSION	139
12	FINAL REMARKS	141
12.1	Conclusions	141
12.2	Future studies	142
13	REFERENCES	143
APPENDIX A	APPROXIMATION OF k_I IN 2DOF MODEL	A-1
APPENDIX B	2DOF CONVERGENCE STUDY	B-1
APPENDIX C	MATERIAL PROPERTIES OF CONCRETE	C-1
C.1	Compressive strength	C-1
C.2	Tensile strength	C-2
C.3	Fracture energy	C-2
APPENDIX D	MATERIAL PROPERTIES OF REINFORCEMENT	D-1
D.1	Undamaged reinforcement	D-1
D.2	Undamaged reinforcement tested with low speed	D-2

D.3	Pre-stretched reinforcement	D-3
D.4	Bent reinforcement	D-4
D.5	Reinforcement tested at RISE	D-7
D.6	Modulus of elasticity	D-8
APPENDIX E	DIC FACET ANALYSIS	E-1
APPENDIX F	IMPACT FORCE – ALTERNATIVE METHOD	F-1
APPENDIX G	VELOCITY OF DROP-WEIGHT	G-1
APPENDIX H	DETERMINATION OF PLASTIC DEFLECTION USING DIC	H-1
APPENDIX I	CALCULATION OF STIFFNESS	I-1
APPENDIX J	CALCULATION OF INTERNAL WORK	J-1
APPENDIX K	STRAIN FIELDS FROM STATIC TEST DISPLAYED ON BEAMS	K-1
K.1	Series S	K-1
K.2	Series I10	K-3
K.3	Series I20	K-4
APPENDIX L	APPROXIMATION OF INTERNAL WORK DURING IMPACT	L-1
APPENDIX M	MATLAB SCRIPT FOR 2DOF MODEL	M-1
APPENDIX N	MATHCAD CALCULATIONS	N-1

Preface

In this master thesis, drop-weight tests have been carried out in order to increase the understanding of the structural response of reinforced concrete beams subjected to impact loading. Focus has been on the influence of the mechanical properties of the reinforcement on the plastic deformation capacity.

The work was carried out between January and June 2019 at Chalmers and Norconsult in Gothenburg. This thesis is part of an ongoing research project at the Division of Structural Engineering at Chalmers University of Technology that is financed by the Swedish Civil Contingencies Agency. For the experiments, funding have also been provided by Fortifikationskårens forskningsfond and Brosamverkan. The project is carried out as a co-operation between Chalmers and Norconsult and is a continuation of four previous thesis projects carried out in 2016 to 2018.

First of all, we would like to express our deepest gratitude to Morgan Johansson for his invaluable guidance, knowledge and dedication throughout the whole project. We also want to evince great appreciation to Joosef Leppänen for his assistance during the experiments and very helpful feedback and advices during the project. Before, during and after the experiments, Sebastian Almfeldt contributed with much appreciated experience, knowledge and helpful supervision. Additionally, we want to thank Mathias Flansbjer for his help with the DIC equipment and useful tips regarding the postprocessing in GOM Correlate.

Gothenburg, June 2019

Malin Andersson and Emma Pettersson

Notations

Abbreviations

B	Batch
CDM	Central difference method
D	Damaged reinforcement
DIC	Digital image correlation
DIF	Dynamic increase factor
I10	Impact load case with 10 kg drop-weight
I20	Impact load case with 20 kg drop-weight
RC	Reinforced concrete
S	Static load case
SDOF	Single-degree-of-freedom
UD	Undamaged reinforcement
ULS	Ultimate limit state
WST	Wedge splitting test
2DOF	Two-degree-of-freedom

Roman upper case letters

A_{imp}	Impact area
A_s	Area of reinforcement
E_{cm}	Mean modulus of elasticity for concrete
E_k	Kinetic energy
F	Force
F_{cr}	Cracking load
$F_{dynamic}$	Dynamic force
F_{max}	Maximum load
F_{static}	Static force
G	Shear modulus
G_f	Fracture energy
I	Impulse, moment of inertia
I_k	Characteristic impulse
L_e	Length from support to plastic hinge
L_0	Length of span of the beam
M_{cr}	Cracking moment
M_u	Ultimate moment
M_y	Yield moment
R	Internal resisting force
R_{cr}	Internal resisting force when cracking occurs
R_{dyn}	Dynamic internal response
R_m	Maximum internal resistance
R_{sta}	Static internal response
T_n	Smallest period
W_e	External work
W_i	Internal work

Roman lower case letters

a	Acceleration, half of plastic hinge length, distance between support and load application
b	Width of beam
c	Damping coefficient, concrete cover
d	Effective height, bottom reinforcement
d'	Effective height, top reinforcement
f_c	Compressive cylinder strength of concrete
f_{ck}	Characteristic compressive cylinder strength of concrete
f_{cm}	Mean compressive cylinder strength of concrete
$f_{cm,cube}$	Mean compressive cube strength of concrete
f_{ct}	Tensile strength of concrete
$f_{ct,fl}$	Flexural tensile strength of concrete
f_{ctm}	Mean tensile strength of concrete
$f_{ct,sp}$	Splitting tensile strength of concrete
f_u	Ultimate tensile strength of steel
f_y	Yield strength of steel
$f_{0.2}$	Proof stress of steel
g_{beam}	Self-weight of beam
h	Height of beam cross-section
k	Linear elastic stiffness
k'	Stiffness after cracking has occurred
k_λ	Correction factor for slenderness
l_0	Distance from zero moment section to the point of maximum moment after redistribution
l_{pl}	Length of plastic hinge
m	Mass
p	Momentum
r	Radius, curvature radius
t	Time
t_l	Duration of load
t_0	Time for active portion of the beam to span the entire beam
u	Displacement
u_{cr}	Displacement when cracking occurs
u_{el}	Elastic deformation
u_{pl}	Plastic deformation
u_s	Displacement of system point
u_{SDOF}	Displacement of SDOF system
u_{tot}	Total displacement
\dot{u}	Velocity
\ddot{u}	Acceleration
v	Velocity
v_0	Velocity before impact
v_1	Velocity after impact
x	Height of compressive zone, transition point between active and inactive portion

Greek letters

α_R	Stress block factor
β_R	Stress block factor
Δt	Time step
δ	Deformation at impact zone
ε_c	Compressive strain
ε_{cc}	Compressive strain for concrete
ε_{ct}	Tensile strain for concrete
ε_{pl}	Plastic strain
ε_s	Tensile strain for steel
ε_{su}	Ultimate strain for steel
ε_{sy}	Tensile strain at yielding for steel
$\dot{\varepsilon}$	Strain rate
η_f	Ratio of ultimate and yield stress
η_M	Moment ratio
φ	Curvature
κ	Transformation factor
ν	Poisson's ratio
λ	Slenderness
ω	Eigenfrequency
ω_s	Mechanical reinforcement ratio
ϕ	Angle
ρ	Reinforcement ratio, density
σ_c	Compressive stress
θ_f	Plastic rotation in span
θ_{pl}	Plastic rotation
$\theta_{Rd,Bk25}$	Plastic rotation according to Bk25
$\theta_{Rd,Ec}$	Plastic rotation according to Eurocode 2
$\theta_{pl,x\%}$	Plastic rotation at given load level

Index

b	Beam
c	Concrete
$crit$	Critical
cy	Cracking to yielding
el	Elastic
F	Force
f	Span
I	State I
II	State II
III	State III
k	Characteristic, spring stiffness
m	Mean value, mass
max	Maximum
pl	Plastic
rel	Relative
s	Reinforcing steel, secant

<i>t</i>	Tangent
<i>tot</i>	Total
<i>u</i>	Ultimate
<i>y</i>	Yielding
0	Initial
1	Body 1, drop-weight
2	Body 2, beam
3 <i>P</i>	Three point bending
4 <i>P</i>	Four point bending
'	Top reinforcement

1 Introduction

1.1 Background

How impact loads such as collisions or explosions affect different types of concrete structures is an important issue since concrete is commonly used for protective structures. An impact load can be critical for the remaining capacity of a structure. The structural response of an impact loaded concrete beam may be different compared to when it is statically loaded. Hence, it is not sure that observations obtained for statically loaded structures also hold true for a case of impact loading.

The most effective way for a structure to resist an impact load is to withstand it through deformations. A large plastic deformation capacity in the structure is therefore essential to obtain a large energy absorption. Today, the plastic deformation capacity is determined using static load cases. However, it is of interest to investigate the influence of dynamic behaviour. Additionally, the influence of the properties of the reinforcement on the plastic deformation capacity is also of great interest.

This thesis is part of an ongoing research project at the Division of Structural Engineering at Chalmers University of Technology that is financed by the Swedish Civil Contingencies Agency. The project is carried out as a co-operation between Chalmers and Norconsult and is a continuation of four previous thesis projects carried out in 2016 to 2018; Lovén and Svavarsdóttir (2016), Lozano and Makdesi (2017), Jönsson and Stenseke (2018) and Munther and Runebrant (2018).

1.2 Aim

The aim of this project is to increase the understanding of the structural response of reinforced concrete members subjected to impact loading, with focus on damaged reinforcement, and serve as a support for the research in the field. The specific objectives are

- To study the influence of damaged reinforcement in reinforced concrete beams subjected to impact loading through experiments.
- To study the mechanical properties of the reinforcement on bars that are damaged due to stretching, bending, welding or corrosion to increase the knowledge of its impact.
- To investigate the capability to use a two-degree-of-freedom (2DOF) system to predict the results of the experiments in a simplified way. The calculations are compared to the experiments and analysed how and to what extent the dynamic response can be predicted.

1.3 Method

The project started with a literature study to increase the knowledge of impact loading, plastic deformation capacity and the effect of damaged reinforcement.

Thereafter, the main focus was the beam testing and analyses of the structural response. The manufacturing of the concrete beams was a part of the project. Half of the beams contained pre-stretched reinforcement while the rest were reinforced with undamaged bars.

During the testing, cameras filmed the beams and digital image correlation (DIC) was then used to analyse the structural behaviour. This was the basis for the evaluation and analysis of the results.

Predictions of the structural response of the beams were carried out by simplified hand calculations and a 2DOF system. The calculations of the 2DOF model were based on the methods found in the literature study.

The influence of damage on the reinforcement bars was investigated by tensile tests for stretched and bent bars. The influence of corrosion and welding was studied in the literature of previously carried out work.

1.4 Limitations

In the study of the response of the reinforced beams, the number of beams tested were limited to twelve for the dynamic tests and six for the static tests. The concrete mixer had a limited size which resulted in having to mix the concrete in two batches of equal quantity. The number of tests for the material properties of both the concrete and the reinforcement were also limited.

The study of the influence of the reinforcement's properties on the plastic deformation capacity was in the drop-weight impact and static tests limited to testing undamaged reinforcement and pre-stretched reinforcement. The investigation of the influence of bent reinforcement was limited to analysis and interpretation of results from the tests of the mechanical properties. The influence of corroded and welded reinforcement was analysed through a literature study.

The expected failure was bending failure and therefore shear failure was not taken into account in the study.

2 Structural Response and Materials

The structural response of a structure is in this thesis described with four different types of responses; linear elastic, plastic, elasto-plastic and tri-linear. In order to facilitate the understanding of results and discussions made in subsequent chapters, this chapter describes these responses using simplified idealized functions.

Furthermore, this chapter gives a brief description of all the materials used in the experiments, i.e. concrete, reinforcing steel and reinforced concrete.

2.1 Linear elastic response

A linear elastic response is characterized by a linear response where deformations go back to zero when the structure is unloaded (Lundh, 2000). The response can be described by

$$R(u) = k \cdot u_{el} \quad (2.1)$$

where R corresponds to the internal resisting force, k to the stiffness of the structure and u_{el} to the displacement. Accordingly, the relation between the internal resisting force and the displacement is linear and is illustrated in Figure 2.1.

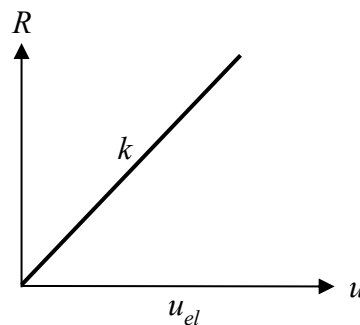


Figure 2.1 Relation between the internal resisting force R and displacement u for a linear elastic response. From Jönsson and Stenseke (2018).

2.2 Plastic response

A plastic response is characterised by lasting deformations when the structure is unloaded (Lundh, 2000). As seen in Figure 2.2 an ideally plastic response implies that there will be no lasting deformations if the applied load is less than the maximum internal resistance R_m .

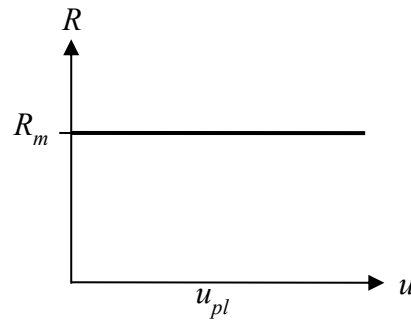


Figure 2.2 Relation between the internal resisting force R and displacement u for an ideally plastic response. From Jönsson and Stenseke (2018).

The ideally plastic response can be described by

$$R(u) = \begin{cases} F & \text{if } u = 0 \\ R_m & \text{if } u > 0 \end{cases} \quad (2.2)$$

where F is an external force that is smaller than the maximum internal resistance R_m and u is the displacement.

As can be seen in Figure 2.2 the relation between R and u for an ideally plastic response is horizontal. This is because ideal plasticity does not take hardening effects into account (Ljung, Saabye Ottosen and Ristinmaa, 2007).

2.3 Elasto-plastic response

An elasto-plastic response is a combination of an elastic response and a plastic response. This can be used to describe a structural response in a more accurate way. As can be seen in Figure 2.3 an elasto-plastic response will exhibit an elastic response until the maximum internal resistance is reached and thereafter exhibit a plastic response. The deformation arising from loading of the structure will contain one elastic and one plastic part. When the structure is unloaded the elastic deformation will go back to zero while the plastic deformation will remain. The same stiffness is assumed if the structure is reloaded. In design, it is common to approximate the load-deflection relation for concrete structures as elasto-plastic.

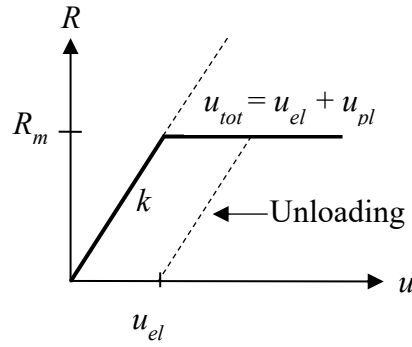


Figure 2.3 Relation between the internal resisting force R and displacement u for an elasto-plastic response. From Jönsson and Stenseke (2018).

The elasto-plastic response can be described by

$$R(u) = \begin{cases} k \cdot u & \text{if } u \leq u_{el} \\ R_m & \text{if } u > u_{el} \end{cases} \quad (2.3)$$

where R_m is the maximum internal resistance and u is the displacement. The total deformation u_{tot} can be described as

$$u_{tot} = u_{el} + u_{pl} \quad (2.4)$$

where u_{pl} is the plastic deformation and u_{el} is the elastic deformation.

2.4 Tri-linear response

A tri-linear response is an even more refined response which corresponds well with that of reinforced concrete which will have a change in stiffness when the first cracks appear (Jönsson and Stenseke, 2018). In a tri-linear response the part with an internal resistance below R_m is divided into two parts with different stiffnesses. The relation between the internal resisting force and displacement is depicted in Figure 2.4.

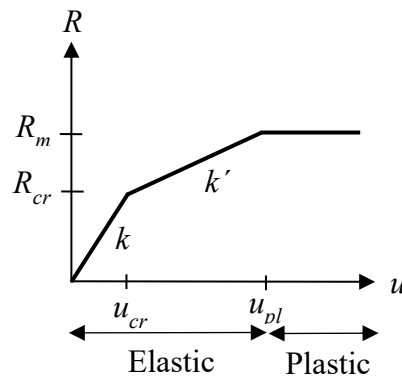


Figure 2.4 Relation between the internal resisting force R and displacement u for a tri-linear response. From Jönsson and Stenseke (2018).

The tri-linear response can also be described by

$$R(u) = \begin{cases} k \cdot u & \text{if } u \leq u_{cr} \\ R_{cr} + k'(u - u_{cr}) & \text{if } u_{cr} \leq u \leq u_{pl} \\ R_m & \text{if } u > u_{pl} \end{cases} \quad (2.5)$$

where u_{cr} corresponds to the displacement when cracking occurs, R_{cr} is the internal resisting force when cracking occurs, k is the stiffness before cracking occurs and k' is the stiffness after cracking has occurred.

2.5 Concrete

Concrete is a composite material containing a mixture of cement, aggregates and water (Al-Emrani, Engström, Johansson and Johansson, 2013). It is characterised by its difference in strength when subjected to tension and compression. This is illustrated in Figure 2.5 showing the stress-strain relation for concrete under uniaxial loading. The compressive strength, f_c , is markedly higher than the tensile strength, f_{ct} . This is why concrete structures subjected to tension often are provided with reinforcing steel. Reinforced concrete (RC) is further described in Section 2.7.

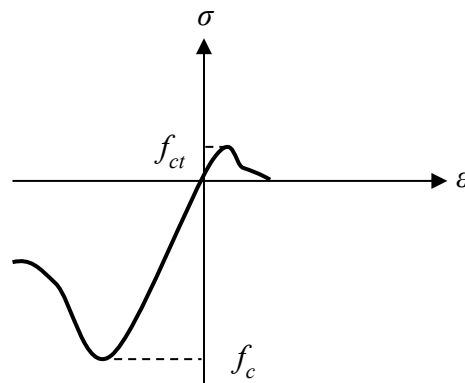


Figure 2.5 Stress-strain relation for concrete under uniaxial loading. f_c and f_{ct} correspond to the strength in compression and tension respectively. From Jönsson and Stenseke (2018).

2.5.1 Structural response in compression

The stress-strain relationship of concrete under compressive loading is of considerable interest since concrete often is used for its eligible properties in compression. According to Burström (2001) the compressive strength is the most tested property of concrete.

The failure mode for concrete with lower compressive strength is more ductile while the failure mode for concrete with higher compressive strength is more brittle (Al-Emrani et al, 2013). This is also indicated in Figure 2.6 where the compressive strain related to the maximum compressive stress is higher for concrete with higher compressive strength.

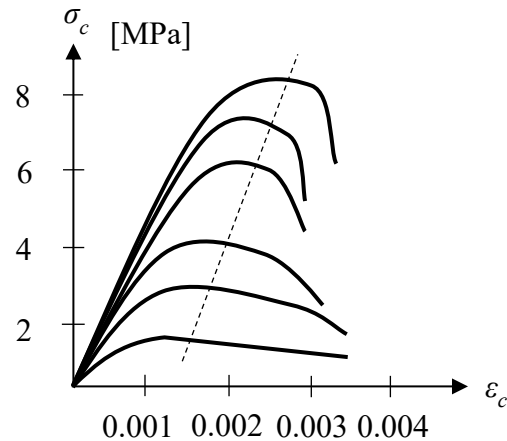


Figure 2.6 Typical compressive stress-strain relations for concrete with different strengths. σ_c and ε_c correspond to the compressive stress and compressive strain respectively. From Jönsson and Stenseke (2018).

Furthermore, the compressive strength of concrete is also depending on the loading rate. As can be seen in Figure 2.7 the compressive strength gets higher for a faster loading rate. This effect is further described in Section 2.7.2.

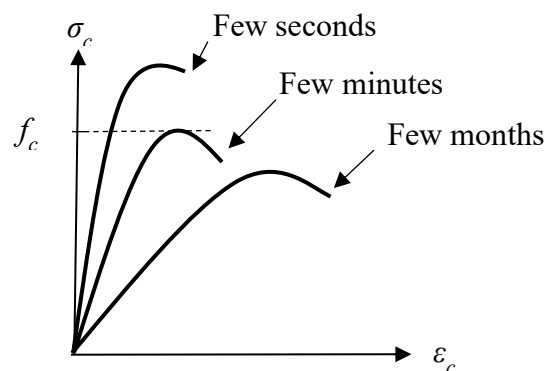


Figure 2.7 Illustration of compressive strengths dependency on loading rate. From Jönsson and Stenseke (2018).

In design there are several simplified stress-strain relations that can be used. Two examples of simplified stress-strain relations for concrete subjected to compression given in Al-Emrani et al (2013) are illustrated in Figure 2.8. The stress-strain relation can be assumed to be parabolic until maximum compressive strength is reached and thereafter constant until ultimate concrete strain, see Figure 2.8a. An even more simplified but also more conservative model is to assume a bi-linear model, see Figure 2.8b.

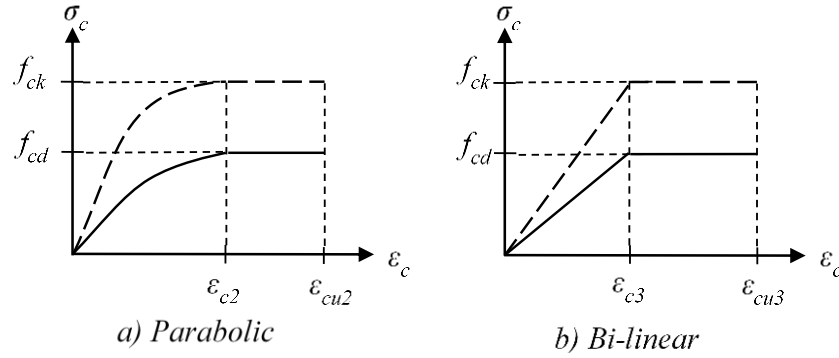


Figure 2.8 Simplified stress-strain relations for concrete subjected to compression. From Jönsson and Stenseke (2018).

2.5.2 Determination of concrete strength

This section describes ways of determining concrete strength from standard material tests. The tests treated here are regarding compressive strength, tensile strength and modulus of elasticity.

2.5.2.1 Compressive strength

The compressive strength of concrete is determined in a uniaxial loading test according to CEN (2009b). The test is normally performed using concrete cylinders. However, in Sweden cubes are often used instead of cylinders, which results in a higher strength. This is taken into account by

$$f_{cm} = 0.8 f_{cm,cube} \quad (2.6)$$

where f_{cm} is the mean compressive strength of a cylinder and $f_{cm,cube}$ is the mean compressive strength of a cube.

2.5.2.2 Tensile strength

The tensile strength of concrete can be determined in a splitting test according to CEN (2009c). An approximation of the axial tensile strength, f_{ct} , can be determined from the splitting tensile strength, $f_{ct,sp}$, as

$$f_{ct} = 0.9 f_{ct,sp} \quad (2.7)$$

Another way to determine the tensile strength is to do it based on the characteristic compressive strength as

$$f_{ct} = 0.3f_{ck}^{2/3} \quad \text{for concrete class} \leq \text{C50/60} \quad (2.8)$$

where

$$f_{ck} = f_{cm} - 8 \text{ MPa} \quad (2.9)$$

The flexural tensile strength, $f_{ct,fl}$, can be determined based on the axial tensile strength as

$$f_{ct,fl} = k \cdot f_{ctm} \quad \text{for concrete class} \leq \text{C50/60} \quad (2.10)$$

where

$$k = 0.6 + \frac{0.4}{h^{0.25}} \quad (2.11)$$

and h is the height of the cross-section.

2.5.2.3 Modulus of elasticity

The mean modulus of elasticity can be determined as the secant modulus between the origin and $\sigma_c = 0.4 f_{cm}$ in the stress-strain relation curve for concrete. However, the mean modulus of elasticity can also be approximately determined as

$$E_{cm} = 22 \left(\frac{f_{cm}}{10} \right)^{0.3} \quad [\text{GPa}] \quad (2.12)$$

where f_{cm} is the mean compressive strength in [MPa].

2.6 Reinforcing steel

Since, as mentioned in Section 2.5, reinforcement often is used to compensate for the low tensile strength of concrete, its behaviour under tension is the main interest.

Reinforcing steel is classified according to several properties such as its strength, fatigue strength, ductility class, size, weldability etc. (Engström, 2015). Considering the ability to take up impulse loads for reinforced concrete structures, a ductile response is preferred (Johansson and Laine, 2012). Plain concrete is in comparison to reinforcing steel a brittle material and therefore a reinforced concrete structure's ability to exhibit a ductile response is mainly depending on the ductility of the reinforcement. Hence, the ductility class of reinforcing steel is of special interest in this thesis. According to Eurocode 2 (CEN, 2005) reinforcement bars can be classified into three categories, summarized in Table 2.1.

Table 2.1 Classification of reinforcing steel with regard to ductility characteristics.

Property	Class		
	A	B	C
Characteristic yield strength, f_{yk} or $f_{0.2}$ [MPa]	400 to 600		
Ultimate strength / yield strength, $(f_u / f_y)_k$	≥ 1.05	≥ 1.08	≥ 1.15 < 1.35
Characteristic strain at maximum force, ε_{su}	≥ 0.025	≥ 0.05	≥ 0.075

The structural tensile response of reinforcing steel is depending on the manufacturing process (Engström, 2015). Distinction is made between reinforcing steel that is hot rolled and reinforcing steel that is cold worked. A comparison between the associated stress-strain relations for the two manufacturing processes is displayed in Figure 2.9, where f_u corresponds to maximum tensile strength, f_y to yield strength, $f_{0.2}$ to proof stress and ε_{su} to the ultimate strain at maximum strength, f_u .

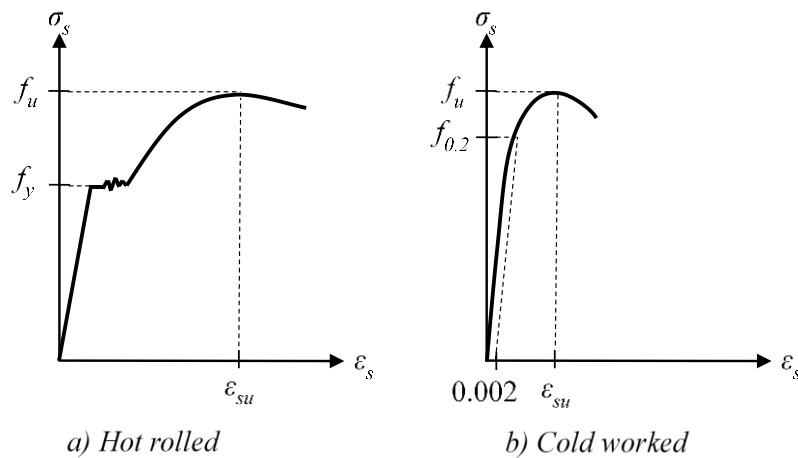


Figure 2.9 Stress-strain relation for reinforcing steel that is a) hot rolled and b) cold worked. From Jönsson and Stenseke (2018).

The stress-strain relation for hot rolled reinforcing steel distinguishes a clear plastic stage (yield plateau) and a large strain hardening stage. Cold worked reinforcing steel is lacking a clear yield plateau and has a smaller strain hardening stage. Hence, it is not possible to determine the yield stress for cold worked reinforcing steel. Instead the so called proof stress, $f_{0.2}$, is used for this type of reinforcement. The proof stress is further described in Section 5.2.

2.7 Reinforced concrete

Reinforced concrete can be seen as a composite material that utilizes the reinforcement's ductility and eligible properties in tension and the concrete's high strength in compression. This enables the use of reinforced concrete in many different structures.

2.7.1 Structural response in bending

In this thesis, experiments are executed on simply supported reinforced concrete beams. A typical load-deflection relation for that type of beam subjected to a concentrated force in the mid span is illustrated in Figure 2.10. The response can be brittle or ductile depending on the configuration and properties of the reinforcement.

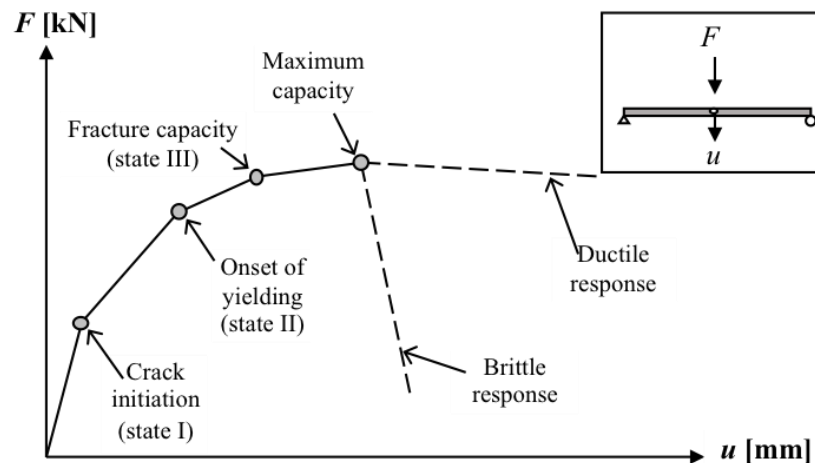


Figure 2.10 Schematic structural response of a simply supported reinforced concrete beam subjected to a concentrated load in the mid span. Modified from Johansson and Laine (2012).

The response can be divided into three stages; state I, state II and state III. In state I the concrete is assumed to be uncracked and the response is assumed to be linear elastic for both the reinforcing steel and the concrete. In design the influence of the reinforcement is often neglected and the stiffness of the uncracked section is determined based on the properties of the concrete only (Engström, 2015). However, the stiffness could be increased by over 20 % by including the reinforcement.

In state II, the concrete is assumed to be fully cracked and the response is, like in state I, assumed to be linear elastic for both the reinforcing steel and the concrete. The concrete in the tensile zone is considered not to contribute. The stiffness gets lower than in state I but will now also depend on the reinforcement configuration.

The uncracked concrete in between the cracks in a fully cracked region will still contribute to the stiffness of the region, this effect is referred to as tension stiffening. Hence, using a state II model to determine the stiffness of a cracked member will result in an underestimation of the real stiffness of the member. Though it should be noted

that the effect of tension stiffening will decrease when the load is increased above the cracking load.

In state III, the response of the reinforcing steel and/or the concrete are assumed to be non-linear.

The response of a simply supported reinforced concrete beam can according to Johansson and Laine (2012) be simplified to a bi-linear elasto-plastic response. This simplification is illustrated in blue colour in Figure 2.11. The beam is here assumed to be fully cracked already from the start of the application of load and the stiffness is determined based on a state II model. The response of the beam is up to its fracture capacity considered to be elastic and after that it is considered to be ideal plastic.

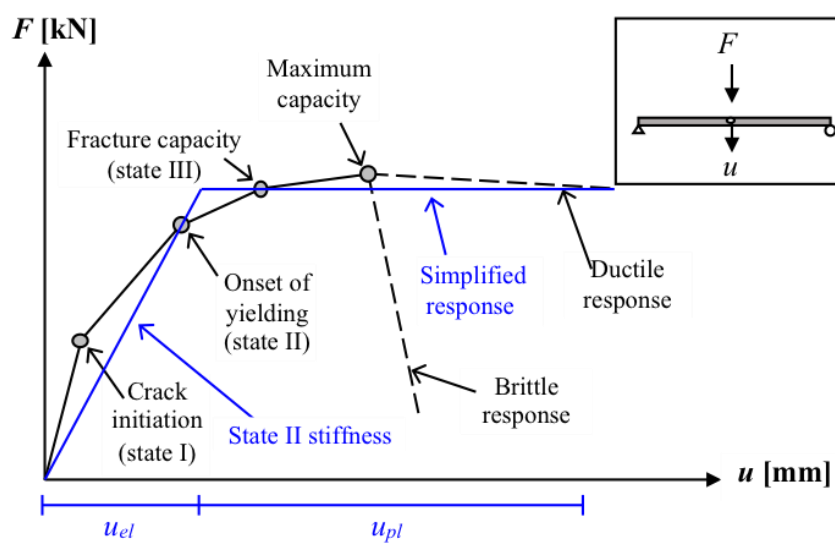


Figure 2.11 Schematic simplified structural response showing a bi-linear response of a simply supported reinforced concrete beam subjected to a concentrated load in the mid span. The simplified response is marked in blue. Modified from Johansson and Laine (2012).

2.7.2 Strain rate effects

The material properties of concrete and reinforcing steel are affected by the rate of loading (Johansson, 2000). When a load is applied fast the material tends to behave stronger and stiffer. This effect is referred to as strain rate effect, $\dot{\epsilon}$ [1/s]. Hence, the structural response of an impact loaded reinforced concrete beam may be different compared to a statically loaded beam. In other words, it is not sure that observations obtained for statically loaded structures hold true for a dynamic case of impact loading.

Furthermore, the degree of dynamic loading can vary widely between different load types. As an example, an earthquake load is considered to be 100 to 1 000 times faster than a static load. The difference in load rate is illustrated in relation to a static load in Figure 2.12.

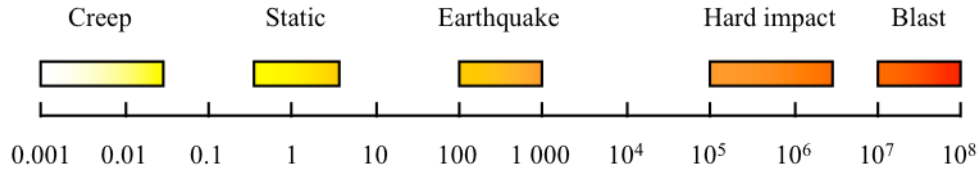


Figure 2.12 Principal difference in load rate for a building subjected to different load types. The values are normalized in relation to a static load. Modified from Johansson and Laine (2012).

A thorough investigation of strain rate effects is done in Johansson (2000). A common way to describe the increase in strength or stiffness due to dynamic loading in relation to its static counterpart is through a dynamic increase factor, DIF , which can be expressed as

$$DIF = \frac{F_{dynamic}}{F_{static}} \quad (2.13)$$

where $F_{dynamic}$ and F_{static} is the dynamic and static load respectively. The DIF for different strain rates according to some different studies are compared in Johansson (2000) and presented in Figure 2.13 for concrete in compression, Figure 2.14 for concrete in tension and Figure 2.15 for reinforcement in tension. It can be seen that the strain rate has largest effect on concrete strength. Regarding the reinforcement the yield and ultimate strength is somewhat affected by the strain rate but the modulus of elasticity is not. Though, it should be noticed that there are considerably large deviations between the different studies which implies that the effect of strain rates is uncertain.

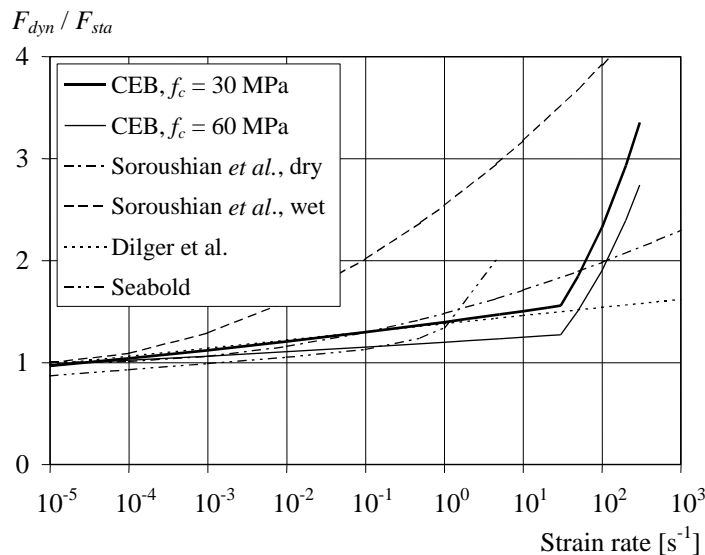


Figure 2.13 Relation between DIF and strain rate for concrete in compression according to different studies. From Johansson (2000).

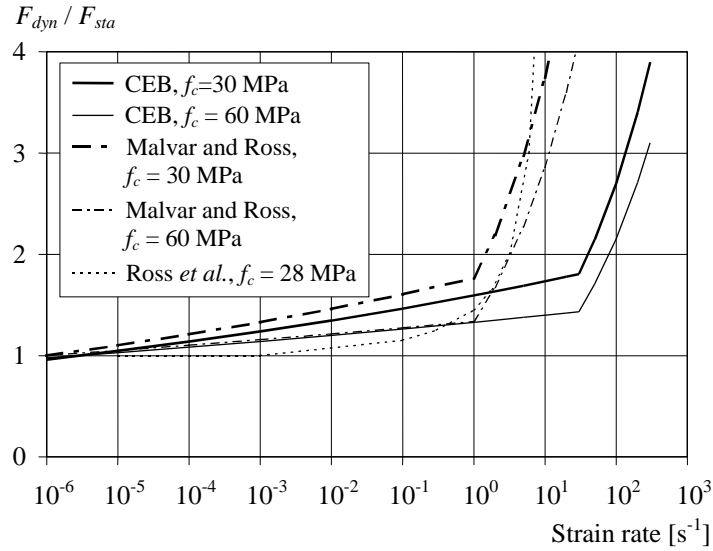


Figure 2.14 Relation between DIF and strain rate for concrete in tension according to different studies. From Johansson (2000).

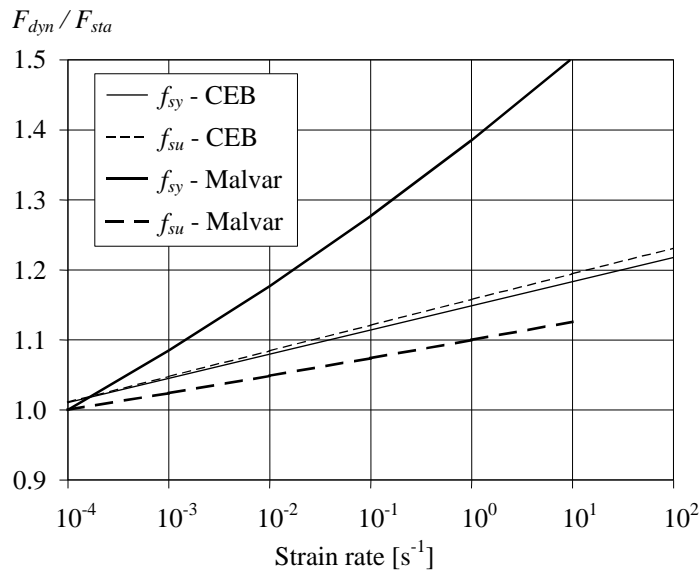


Figure 2.15 Relation between DIF and strain rate for reinforcement in tension according to different studies. From Johansson (2000).

3 Impulse Loaded Structures

An impulse load is a dynamic load with high intensity and short duration. It may be caused by e.g. an explosion or an impact between two objects. Explosions may be rare in urban areas but they may still be of interest to consider as a possible load case for a structure (Johansson and Laine, 2012). Furthermore, Johansson and Laine (2012) explains that different structures are exposed to different levels of explosion risks. Possible causes for the presence of an explosion load may be an accident involving a truck carrying gas or flammable liquid or even explosions from terrorists.

An explosion is a dynamic load acting on a structure. Figure 3.1 illustrates two extreme cases of dynamic loading, an ideal impulse load, here denoted as a characteristic impulse, and a pressure load. Figure 3.1a shows a characteristic impulse, I_k , with an infinitely large pressure that acts for an infinitesimal time. A pressure load, illustrated in Figure 3.1b, acts with a characteristic pressure at an infinite time. An impulse load can act as either of these extreme cases, though, the general interpretation is somewhere in between (Johansson and Laine, 2012). In this report the drop-weight hitting the beams is treated as an impulse load case. Therefore the case of impulse loading and how it can be interpreted will be further described in this chapter.

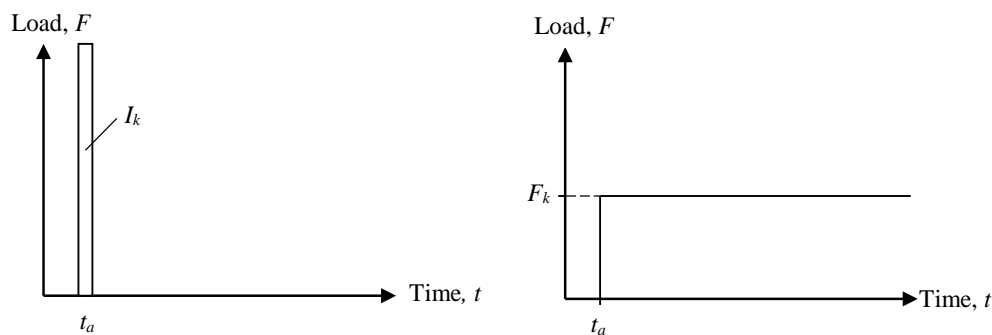


Figure 3.1 Illustration of extreme dynamic cases that start acting at the time t_a : a) characteristic impulse and b) characteristic pressure load. From Johansson and Laine (2012).

3.1 Impulse, external work and kinetic energy

According to Johansson and Laine (2012) the impulse on a body can be described by the change in the momentum, $p = mv$, of the body before and after impact as

$$I = m \cdot v_1 - m \cdot v_0 = \int_{t_0}^{t_1} F(t) dt \quad (3.1)$$

where I is the impulse, m the mass of the body, v_1 and v_0 the velocity of the mass after and before the impulse respectively, and F the force of the impulse.

In addition, the kinetic energy of the body, E_k , is defined as

$$E_k = \frac{m \cdot v^2}{2} \quad (3.2)$$

According to Jönsson and Stenseke (2018) the external work on the same body, W_e can be described by the change in kinetic energy as

$$W_e = \Delta E_k = \frac{m \cdot v_1^2}{2} - \frac{m \cdot v_0^2}{2} \quad (3.3)$$

Furthermore, for a body where $v_0 = 0$, the equation for external work can be combined with Equation (3.1) as

$$W_e = \frac{I_k^2}{2m} \quad (3.4)$$

where I_k is the characteristic impulse.

3.2 Equation of motion

The equation of motion is based on Newton's second law in accordance to Figure 3.2 as

$$F(t) - (R_{sta} + R_{dyn}) = ma \quad (3.5)$$

where R_{sta} , R_{dyn} and a are the static and dynamic internal response and the acceleration of the body, respectively.

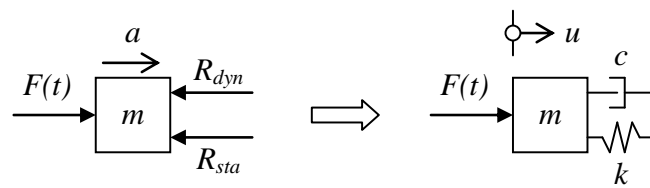


Figure 3.2 Free body diagram of a dynamically loaded accelerating body. From Johansson and Laine (2012).

For a linear elastic response the internal responses R_{sta} and R_{dyn} can be expressed as

$$R_{sta} = ku \quad (3.6)$$

$$R_{dyn} = c\dot{u} \quad (3.7)$$

where k is a linear spring stiffness, u is the deformation, c is the damping coefficient and \dot{u} is the velocity of the body. Inserting these expressions into Equation (3.5) with \ddot{u} as the acceleration results in the commonly used expression of the equation of motion

$$m\ddot{u} + c\dot{u} + ku = F(t) \quad (3.8)$$

3.3 Internal work and energy equilibrium

According to Johansson and Laine (2012), the response of an impulse loaded structure depends on energy equilibrium; i.e. the internal energy absorption is an important parameter. This is in contradiction to a statically loaded structure in which force equilibrium is essential. Energy equilibrium means that the external work on a body has to be balanced by an internal work, as illustrated in Figure 3.3, where the external and internal work are the integrals of the force and response curves, respectively.

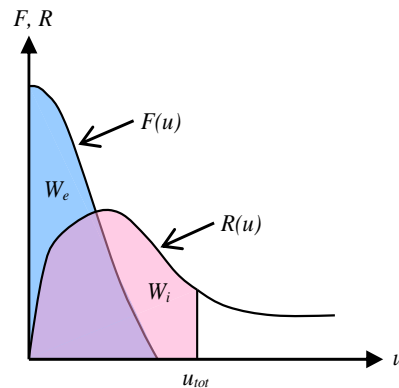


Figure 3.3 Schematic figure of the external work as the integral of an applied load $F(u)$ and the internal work as the integral of the structural response $R(u)$. From Johansson and Laine (2012).

The ability of a structure to absorb energy, as illustrated in Figure 3.3, is determined by a combination of the force and resulting deformation. The characteristics of this combination depends on the material and geometry of the structure. Furthermore, Johansson and Laine (2012) state that it is more desirable to have a large capacity to deform than a large stiffness for an impulse loaded structure. The response of a structure are often in a simplified manner described as elastic, plastic or elastoplastic, as described in Section 2.1 to 2.3. How the internal work, W_i , is determined from these three responses is illustrated in Figure 3.4. The plastic deformation capacity, u_{pl} , of a structure, is used as the definition of the structure's ductility by Johansson and Laine (2012). This is done in this report as well.

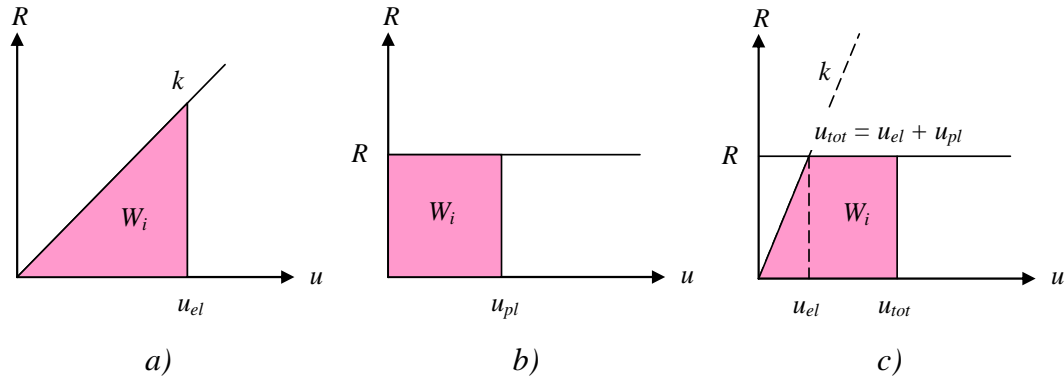


Figure 3.4 Structural response assuming a) linear elastic behaviour, b) plastic behaviour and c) elastic ideal plastic behaviour. From Johansson and Laine (2012).

3.4 Collision of two bodies

The mass has a large influence in the structural response of an impulse loaded structure, which can be interpreted from Equation (3.4). A collision of two particles can be described using two extreme cases; an elastic or plastic behaviour. Grahn and Jansson (2013), state that after an elastic collision the two bodies will have two different velocities while in a plastic case they will gain the same velocity after impact, see Figure 3.5 and Figure 3.6. After a perfectly elastic collision both the kinetic energy and momentum will remain, whereas after a perfectly plastic one the momentum remains while the kinetic energy is reduced. The amount of energy consumed is dependent of the masses of the particles, and the remaining energy has to be absorbed by the structure (Johansson and Laine (2012)).

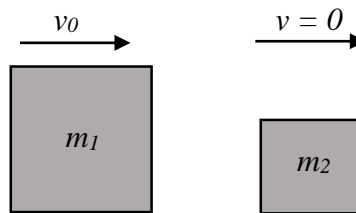


Figure 3.5 Before collision between two particles. From Jönsson and Stenseke (2018).

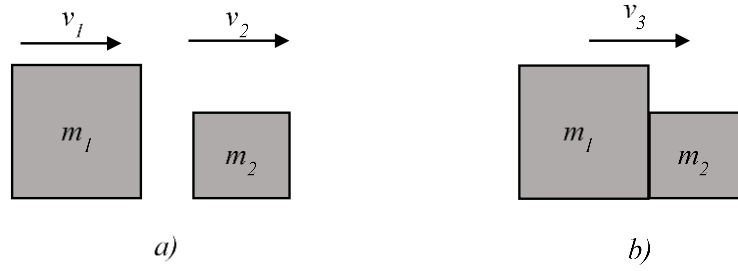


Figure 3.6 After collision between two particles, a) elastic collision and b) plastic collision. From Jönsson and Stenseke (2018).

The kinetic energy and momentum of the first body before impact can be described as

$$E_{k,0} = \frac{m_1 v_0^2}{2} \quad (3.9)$$

$$p_0 = m_1 v_0 \quad (3.10)$$

For an elastic collision, the velocities of the bodies after impact are calculated as

$$v_1 = \frac{m_1 - m_2}{m_1 + m_2} v_0 \quad (3.11)$$

$$v_2 = \frac{2m_1}{m_1 + m_2} v_0 \quad (3.12)$$

The kinetic energy for the particles after an elastic impact can be determined as

$$E_{k,1} = \frac{m_1 v_1^2}{2} = \frac{m_1}{2} \left(\frac{m_1 - m_2}{m_1 + m_2} \right)^2 v_0^2 = \left(\frac{m_1 - m_2}{m_1 + m_2} \right)^2 E_{k,0} \quad (3.13)$$

$$E_{k,2} = \frac{m_2 v_2^2}{2} = \frac{m_2}{2} \left(\frac{2m_1}{m_1 + m_2} \right)^2 v_0^2 = \frac{4m_1 m_2}{(m_1 + m_2)^2} E_{k,0} \quad (3.14)$$

The velocity of the bodies after a perfectly plastic impact can be determined as

$$v_3 = \frac{m_1}{m_1 + m_2} v_0 \quad (3.15)$$

Following, the kinetic energy after a plastic impact can be calculated as

$$\begin{aligned} E_{k,3} &= \frac{(m_1 + m_2)v_3^2}{2} = \frac{m_1 + m_2}{2} \left(\frac{m_1}{m_1 + m_2} \right)^2 v_0^2 \\ &= \frac{m_1}{m_1 + m_2} E_{k,0} \end{aligned} \quad (3.16)$$

4 Plastic Rotation Capacity

In Chapter 3 it is concluded that a ductile behaviour of an impulse loaded structure is desirable. When it comes to concrete structures, the properties of the reinforcement are essential to obtain such a response. A ductile response means formation of plastic hinges. A plastic hinge is a part of the structure where the reinforcement plasticise leading to the ability for the cross-section to keep its load capacity while the deformation is increased. According to Johansson and Laine (2012) this enables for redistributions in the structure and leads to an increased ability to absorb energy.

The plastic rotation of a structure is coupled to the deformation and therefore to the energy absorption. This is why a high value of plastic rotation capacity is desirable in an impulse loaded structure. It is often assumed in theory that plastic hinges are concentrated to a section in the structure while the real hinge is spread over a region, according to Jönsson and Stenseke (2018), see Figure 4.1.

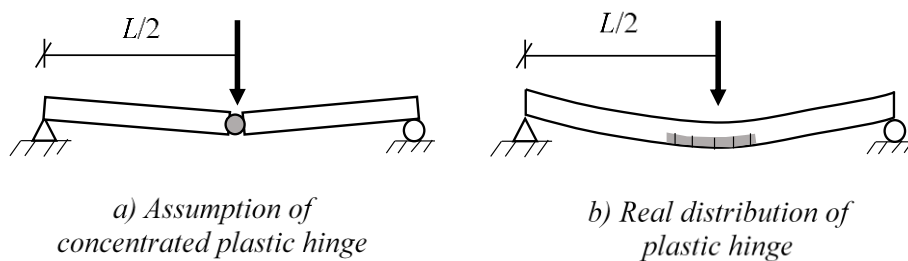


Figure 4.1 Plastic hinge in theory and reality. From Jönsson and Stenseke (2018).

In this chapter, a definition of the plastic rotation capacity is described, followed by an investigation of the influence of the mechanical properties of the reinforcement. Lastly, a few methods of determining the plastic rotation of a structure are described.

4.1 Definition of plastic rotation

When defining the plastic rotation of a concrete cross-section, the curvature is used. The curvature, φ , of a cross-section is according to Engström (2011) defined as the change of angle per unit length, as in Equation (4.1) with variables as in Figure 4.2.

$$\varphi = \frac{1}{r} = \frac{d\phi}{dx} \quad (4.1)$$

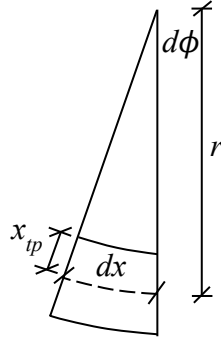


Figure 4.2 Relationship between curvature radius and flexural deformation of a beam element with constant curvature. From Jönsson and Stenseke (2018).

For a cross-section with known strain distribution, the curvature can be determined using known values of strains and the geometry of the section. For the cross-section in Figure 4.3, which is loaded in pure bending, the curvature can be determined as

$$\varphi = \frac{1}{r} = \frac{\varepsilon_{cc}}{x} = \frac{\varepsilon_s}{d - x} \quad (4.2)$$

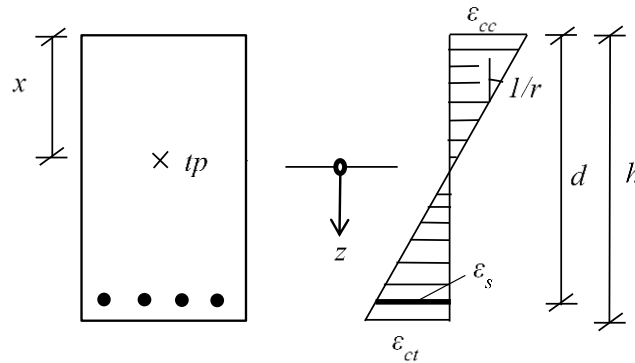


Figure 4.3 Definition of curvature from known strains. From Jönsson and Stenseke (2018).

For a region with length l_{pl} , where the steel strain exceeds the yield strain, the plastic rotation can be determined by integrating the plastic curvature from all sections along the length l_{pl} , as in Equation (4.3) (Engström, 2015). This is illustrated in Figure 4.4 in two simplified ways.

$$\theta_{pl} = \int_{l_{pl}} (\varphi(x) - \varphi_y) dx \quad (4.3)$$

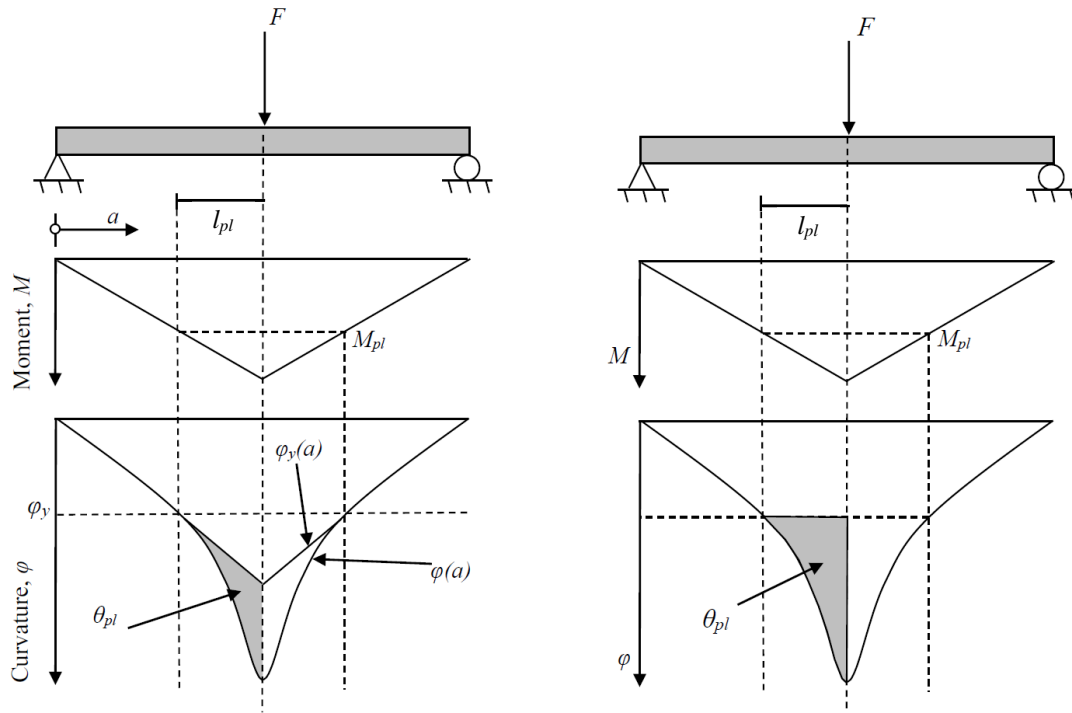


Figure 4.4 Schematic representation of different simplified models to determine plastic rotation capacity. Modified from Lozano and Makdesi (2017).

To determine the plastic rotation capacity of a cross-section, the upper limit for the curvature is needed. This is normally defined as the curvature at ultimate concrete strain. However, it can be determined as the curvature at ultimate steel strain (see Figure 4.5) in cases of high steel ratios or for steel with low ductility, according to Engström (2015). The definition of the plastic rotation capacity is therefore the difference between ultimate curvature and yield curvature. These definitions can be seen in Figure 4.5 for an under-reinforced concrete cross-section in accordance with Engström (2015).

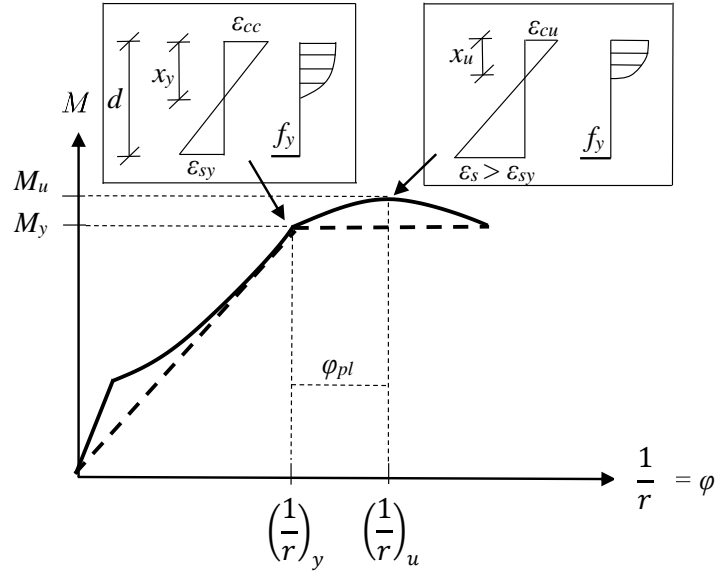


Figure 4.5 Typical moment-curvature diagram for an under-reinforced concrete cross-section. Modified from Engström (2015).

The definition for the curvature at yielding is

$$\varphi_y = \left(\frac{1}{r}\right)_y = \frac{\varepsilon_{cy}}{x_y} = \frac{\varepsilon_{sy}}{d - x_y} \quad (4.4)$$

where the parameters are defined as in Figure 4.5. Furthermore, the ultimate curvature is, for cases when ultimate concrete strain is reached first, defined as

$$\varphi_u = \left(\frac{1}{r}\right)_u = \frac{\varepsilon_{cu}}{x_u} = \frac{\varepsilon_s}{d - x_u} \quad (4.5)$$

and, for cases when the ultimate steel strain is reached first, as

$$\varphi_u = \left(\frac{1}{r}\right)_u = \frac{\varepsilon_{cc}}{x_u} = \frac{\varepsilon_{su}}{d - x_u} \quad (4.6)$$

The parameters are defined in Figure 4.5, and ε_{su} is defined as the ultimate steel strain.

Using these definitions of curvature at yielding and ultimate strain, the plastic curvature of a section can be defined using the steel strains as

$$\varphi_{pl} = \left(\frac{1}{r}\right)_{pl} = \left(\frac{1}{r}\right)_u - \left(\frac{1}{r}\right)_y = \frac{\varepsilon_s}{d - x_u} - \frac{\varepsilon_{sy}}{d - x_y} \approx \frac{\varepsilon_s - \varepsilon_{sy}}{d - x_u} \quad (4.7)$$

Moreover, the plastic curvature of a plastic region varies due to the variation of steel strains within the plastic region, l_{pl} . Combining Equation (4.3) and (4.7), the plastic rotation capacity of the region can be determined as the integral of the plastic curvature along this length, which results in

$$\theta_{pl} = \int_{l_{pl}} \left(\frac{\varepsilon_s(x) - \varepsilon_{sy}}{d - x_u} \right) dx \quad (4.8)$$

Engström (2015) states that this way of calculating the plastic rotation of a plastic hinge is theoretically correct though it is quite difficult to use since the parameters are quite complex. Therefore, other ways of determining the plastic rotation capacity of a plastic hinge are described in Section 4.3 with this definition as a theoretical background. The physical definition of the plastic rotation in Engström (2015) is presented in Figure 4.6.

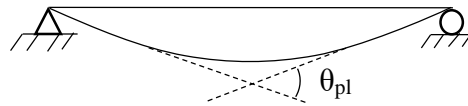


Figure 4.6 Definition of plastic rotation of a plastic hinge as in Engström (2015). From Jönsson and Stenseke (2018).

Further, Engström (2015) mentions ways of improving the rotation capacity of a concrete member, where one method is to use reinforcing steel with high ductility. This influence of reinforcement mechanical properties on the plastic rotation capacity is further described in Section 4.2.

4.2 Influence of the mechanical properties of the reinforcement

As described in Section 4.1, the plastic rotation capacity is defined by the integral of the difference in ultimate and yield curvature of a concrete region. These curvatures represent moments at different states of the concrete, as illustrated in Figure 4.7. The yield curvature gives a yield moment, M_y , and the ultimate curvature gives an ultimate moment, M_u . A high ratio of these moments, η_M (defined in Equation (4.9)), is, according to M. Johansson (technical specialist, Norconsult) needed for a high plastic rotation capacity (personal communication, 2 April, 2019).

$$\eta_M = \frac{M_u}{M_y} \quad (4.9)$$

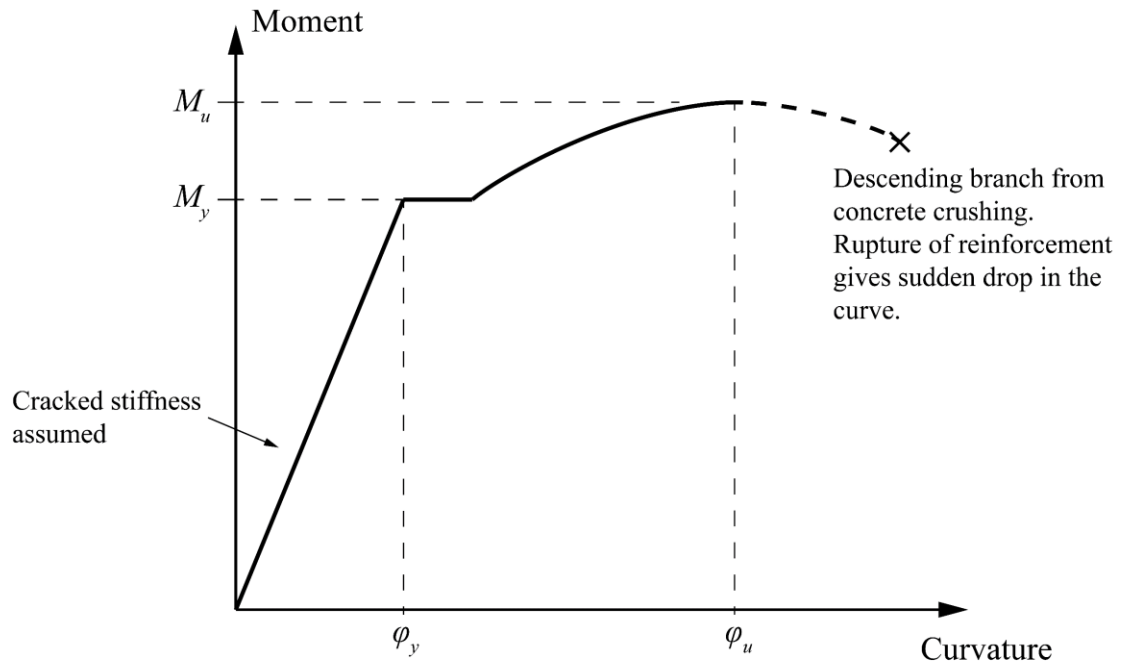


Figure 4.7 Moment-curvature diagram for reinforced concrete. Inspired by M. Johansson (personal communication, 2 April, 2019).

The load-case studied in this project is a simply supported beam subjected to a point load in the middle of the span. This gives a moment distribution as shown in Figure 4.8. Accordingly, it can be noted that for an increased value of η_M the plastic hinge length, l_{pl} , also increases. To obtain a high plastic rotation capacity a large l_{pl} is desired as previously understood by the definition which is based on integrating the curvature over the plastic hinge length.

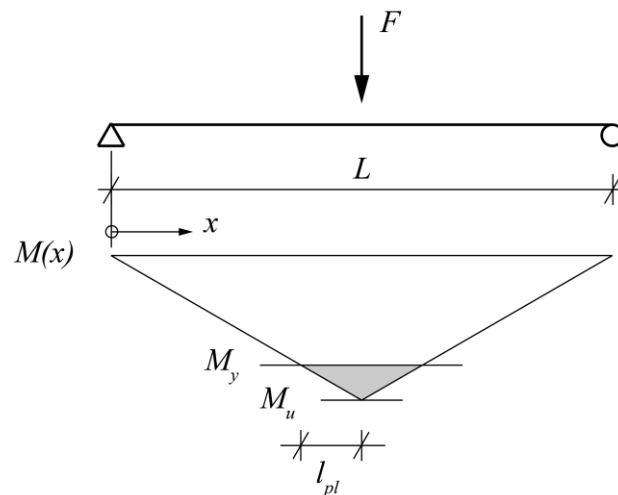


Figure 4.8 Moment distribution of simply supported beam subjected to point load in the middle of the span. Inspired by M. Johansson (personal communication, 2 April, 2019).

Furthermore, when a concrete section has cracked, the stiffness and bending capacity are mostly dependent on the properties of the reinforcement, and behaves thereafter. Therefore, the moment ratio, η_M , can approximately be treated as almost equal to the reinforcement ratio, η_f , as

$$\eta_f = \frac{f_u}{f_y} \approx \frac{M_u}{M_y} = \eta_M \quad (4.10)$$

Based on this, it can be concluded that the strain hardening effects of the reinforcement are important for a high plastic rotation capacity. However, this is mainly the case for concrete structures with high reinforcement ratios, where concrete crushing is the determining failure mode (M. Johansson, personal communication, 28 May, 2019). On the other hand, when rupture of the reinforcement is the determining failure mode (for low reinforcement ratios), the plastic strain capacity, ε_{pl} , of the reinforcement may also have large influence on the plastic rotation capacity.

4.3 Methods to predict the plastic rotation capacity

In this section three different methods of determining the plastic rotation capacity of a structure are presented. Bk25 is intended to be used in case of impulse loading while Eurocode 2 is intended to be used in case of static loading. Another determining difference between the methods is the loadcase they are based on, Bk25 is based on an evenly distributed load over the entire span while Eurocode 2 is based on a point load in midspan. These methods are described based on the work of Johansson and Laine (2012). Additionally, the method of how to determine the plastic rotation capacity from experimental results is described.

4.3.1 Bk25

This method of determining the plastic rotation capacity of a concrete beam comes from Fortifikationsförvaltningen, published 1973, and is meant for determining the capacity of an impulse loaded beam.

An illustration of the rotation capacity of a plastic hinge in a simply supported beam according to Bk25 can be seen in Figure 4.9. The plastic hinge is here represented by the length $2a$ where it has a curvature with a radius r .

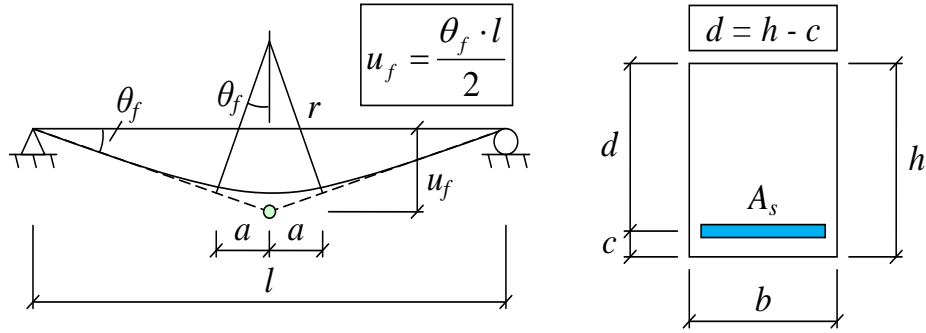


Figure 4.9 Model for rotation capacity of a plastic hinge in a simply supported beam. From Johansson and Laine (2012).

The length a is calculated as

$$a = 0.5 \cdot d + 0.15 \cdot l \quad (4.11)$$

The rotation capacity θ_f is linearly dependent on the plastic hinge length a as

$$\theta_f = \frac{a}{r} \quad (4.12)$$

The maximum allowed strain in the reinforcement or in the concrete determines the maximum curvature radius, r . The curvature can be calculated as below

$$\frac{1}{r} = \frac{\varepsilon_{cu}}{x} = \frac{\varepsilon_s}{d - x} \quad (4.13)$$

where ε_{cu} is the ultimate strain in the concrete, ε_s is the mean strain in the steel over the length a , x is the height of the compressive zone and d the effective height of the cross-section as shown in Figure 4.10 below.

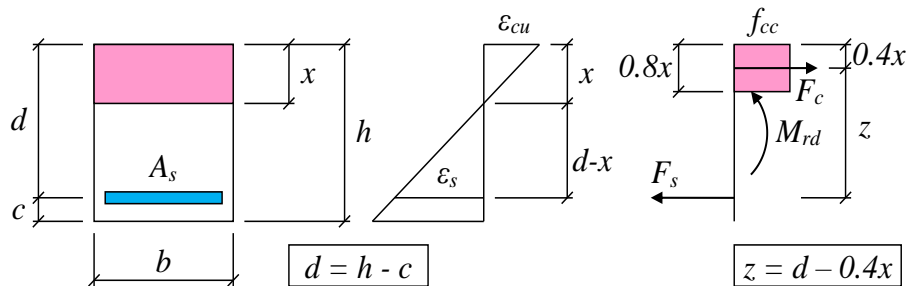


Figure 4.10 Cross-sectional analysis of a concrete cross-section under impact from a bending moment. From Johansson and Laine (2012).

A horizontal force balance, $F_c = F_s$, for the cross-section in Figure 4.10 gives

$$f_{cc} \cdot b \cdot 0.8x = f_y \cdot A_s \quad (4.14)$$

This combined with the definition of reinforcement ratio

$$\rho = \frac{A_s}{bd} \quad (4.15)$$

and the mechanical reinforcement ratio as

$$\omega_s = \frac{A_s}{bd} \cdot \frac{f_y}{f_{cc}} \quad (4.16)$$

gives the height of the compressive zone, x , as

$$x = \frac{1}{0.8} \cdot \rho d \cdot \frac{f_y}{f_{cc}} = \frac{\omega_s d}{0.8} \quad (4.17)$$

or

$$\frac{x}{d} = \frac{\omega_s}{0.8} \quad (4.18)$$

From this, the limit for change in failure mode based on Equation (4.13) can be written as

$$\omega_{s,crit} = \frac{0.8 \cdot \varepsilon_{cu}}{\varepsilon_{cu} + \varepsilon_s} \quad (4.19)$$

Values of the mechanical reinforcement ratio lower than $\omega_{s,crit}$ indicate that the failure mode is rupture of the reinforcement and for values higher than the limit, the failure is due to crushing of the concrete.

When concrete crushing is the assumed failure mode, $\omega_s > \omega_{s,crit}$, the rotation capacity can be determined with Equation (4.12) and (4.17) as

$$\theta_{Rd,Bk25} = \frac{0.8\varepsilon_{cu}}{\omega_s d} \cdot (0.5d + 0.15l) = \frac{0.4\varepsilon_{cu}}{\omega_s} \cdot \left(1 + 0.3 \frac{l}{d}\right) \quad (4.20)$$

If the failure mode is rupture of the reinforcement instead, i.e. $\omega_s < \omega_{s,crit}$, the rotation capacity can be determined in the same way as

$$\begin{aligned}\theta_{Rd,Bk25} &= \frac{0.8\varepsilon_s}{d(0.8 - \omega_s)} \cdot (0.5d + 0.15l) \\ &= \frac{0.4\varepsilon_s}{0.8 - \omega_s} \cdot \left(1 + 0.3\frac{l}{d}\right)\end{aligned}\quad (4.21)$$

4.3.2 Eurocode 2

The plastic rotation capacity is in Eurocode 2 (CEN, 2005) determined by the ratio x_u / d along with the concrete and steel class of the structural member. This is done using the diagram in Figure 4.11.

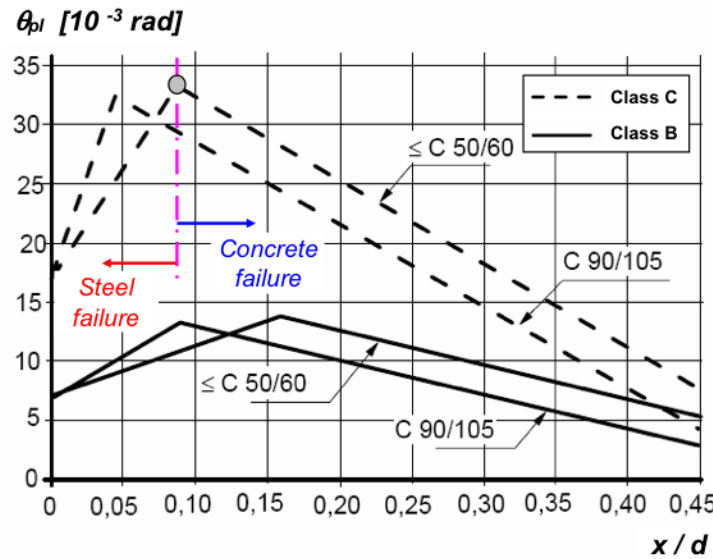


Figure 4.11 Diagram for determination of the allowed plastic rotation capacity θ_{pl} for different concrete and reinforcement classes. Values for structural members with shear slenderness $\lambda = 3.0$. Based on CEN (2005).

The rotation of a plastic hinge, θ_s , shall be lower than θ_{pl} obtained from Figure 4.11. Within zones with plastic hinges, the x/d ratio is limited to

$$\begin{aligned}x/d &\leq 0.45 && \text{for concrete classes } \leq C50/60 \\ x/d &\leq 0.35 && \text{for concrete classes } \geq C55/67\end{aligned}$$

Furthermore, the base value for the plastic rotation, θ_{pl} , should be multiplied with a correction factor, k_λ , as in Equation (4.22) if the structural member does not have a shear slenderness of $\lambda = 3.0$.

$$\theta_{Rd,Ec} = k_\lambda \theta_{pl} \quad (4.22)$$

where k_λ is determined as

$$k_\lambda = \sqrt{\frac{\lambda}{3}} \quad (4.23)$$

with

$$\lambda = \frac{l_0}{d} \quad (4.24)$$

where l_0 is the distance from the zero moment section to the point of maximum moment after redistribution.

4.3.3 Determination of plastic rotation capacity from experimental results

According to Jönsson and Stenseke (2018), the plastic rotation capacity can be determined from the load-displacement curve obtained from experimental static loading test results. An example of response of a deformation-controlled test is illustrated in Figure 4.12.

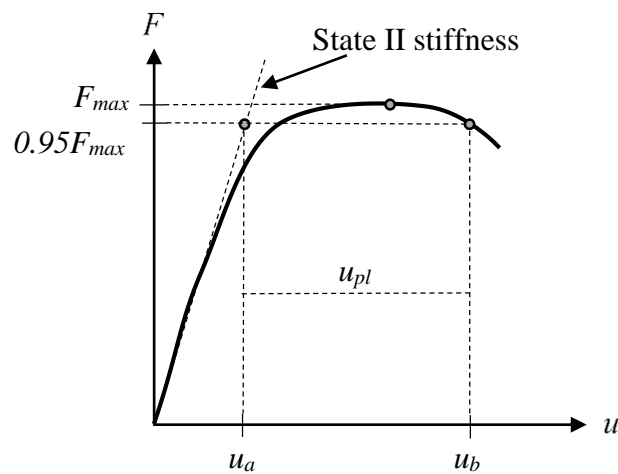


Figure 4.12 Response of a deformation-controlled test where the rotation capacity is determined at 95% of the ultimate load. From Jönsson and Stenseke (2018).

Depending on the deformations, the plastic rotation capacity $\theta_{pl,x\%}$ is determined at the descending branch of the load-displacement curve at a certain percentage of the ultimate load $(x\%/100) \cdot F_{max}$. The elastic and plastic deformation at that certain load is represented by u_a and $u_{pl} = u_b - u_a$, respectively.

In a simply supported reinforced concrete beam, subjected to a concentrated force in the midspan, a plastic hinge will form at the location of maximum moment when the reinforcement starts to yield. That will in this case occur in the midspan of the beam, see Figure 4.13.

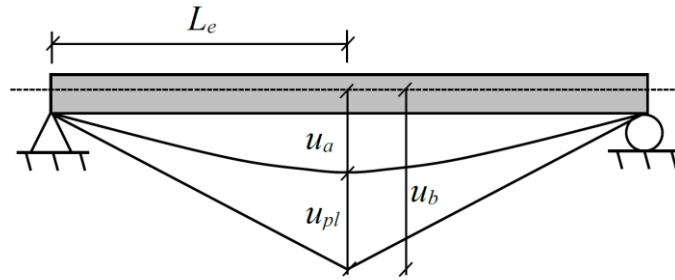


Figure 4.13 Illustration of elastic plastic deformation measured from experiments. From Lozano and Makdesi (2017).

If L_e is defined as the length from the support of the beam to the plastic hinge, the plastic rotation capacity can be determined as

$$\theta_{pl,x\%} = \frac{u_{b,x\%} - u_{a,x\%}}{L_e} = \frac{u_{pl,x\%}}{L_e} \quad (4.25)$$

5 Mechanical Properties of Damaged Reinforcement

One aim of this study is to investigate the influence of damage on the reinforcement in a reinforced concrete structure. This is done by studying how the deformation capacity of a structure is affected by the mechanical properties of the reinforcement. As mentioned in Chapter 3, a high deformation capacity is sought for in an impulse loaded structure. Four different kinds of damages are studied through a literature survey to get a proper understanding of the influence. The damage comes from stretching, bending, welding and corrosion of the reinforcement.

5.1 Investigated mechanical properties

Following Section 4.2 the deformation capacity of a plastic hinge is defined by a high M_u / M_y ratio. This can approximately be related to the reinforcement by a high ratio of f_u / f_y (η_f). The general behaviour of undamaged steel can be seen in Figure 5.1. This chapter is further related to this general behaviour when the changes in mechanical properties are described.

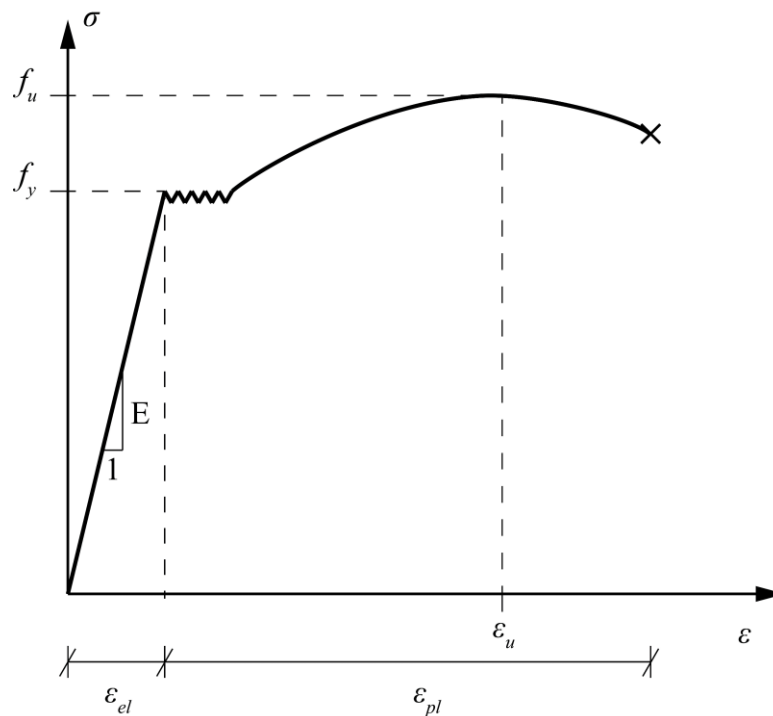


Figure 5.1 General stress-strain curve for steel.

In Figure 5.1, f_u is the ultimate stress, f_y is the yield stress, E is the modulus of elasticity, ϵ_{el} is the elastic strain, ϵ_{pl} is the plastic strain and ϵ_u is the strain at ultimate load.

5.2 Damage due to stretching

Stretching the reinforcement is a way of cold working it. Burström (2001) describes the change in mechanical properties due to stretching according to Figure 5.2 due to stretching. First, the steel responds elastically up to yielding when it starts to plasticize. As loading continues, strain hardening occurs in the steel which results in a higher strength as it is loaded. As a plastic deformation cannot be undone, unloading results in a reversed elastic response as during loading. If the steel is loaded once again the stress-strain curve follows the path of unloading, which results in a higher immediate strength but a reduction in deformation capacity.

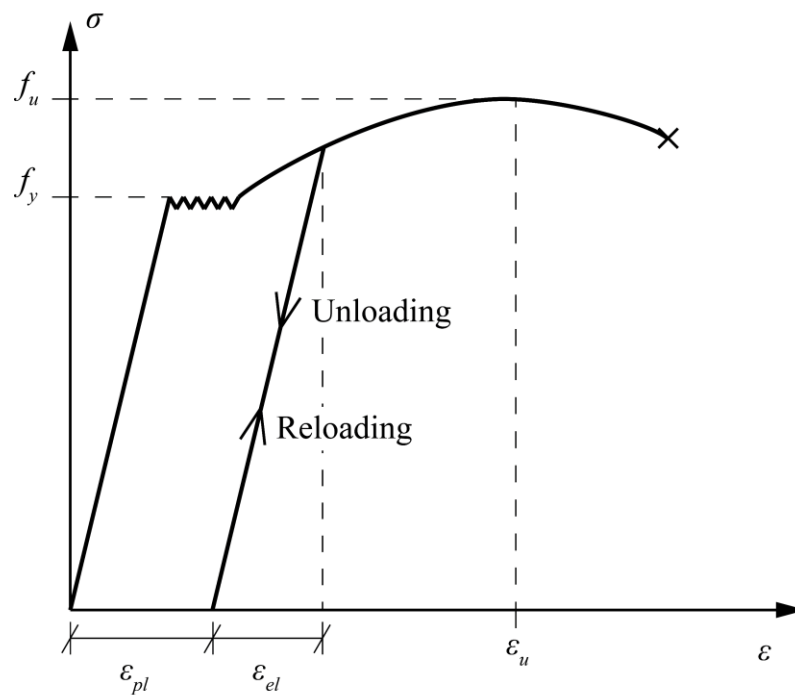


Figure 5.2 Stress-strain curve for steel during loading and reloading.

Following this behaviour, pre-stretched reinforcement is expected to get a higher “yield stress”, “ f_y ”, or proof stress, $f_{0.2}$, as it is called when there is no clear yield plateau, see Figure 5.3. The $f_{0.2}$ value represents the stress where an unloading results in a plastic strain of 0.2 %. A higher $f_{0.2}$ along with remaining f_u results in a lower η_f ratio. Further, as part of ϵ_{pl} is consumed during the first loading, the ductility is reduced.

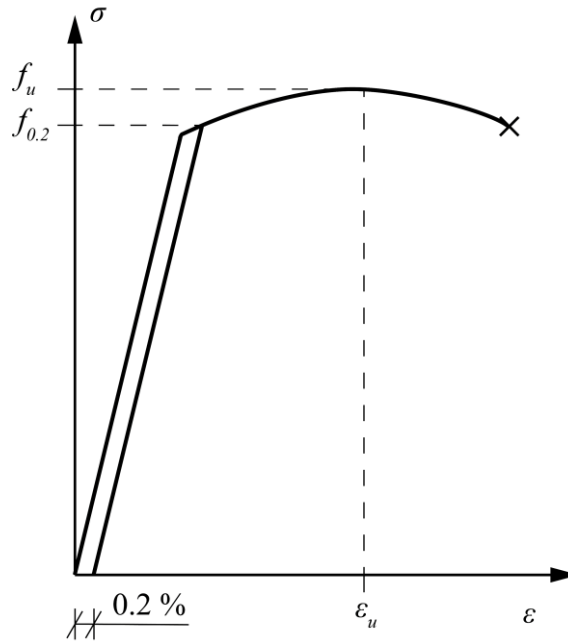


Figure 5.3 Stress-strain curve for cold-worked steel.

5.3 Damage due to bending

Bending is another way in which a reinforcing bar can be cold-worked. It can be regarded as locally stretching the bar, affecting only the bent part. A study has been performed in the matter by Chun and Ha (2014). The study was performed on bars with diameter 10, 13, 16 and 22 mm, with grade Gr 280 and Gr 420 (corresponding to a yield strength of 280 and 420 MPa, respectively). The bars were cold-bent at three different bend radii, $2d$, $3d$ and $4d$, where d was the diameter of the bar. According to Chun and Ha (2014), $3d$ is the minimum bend radius allowed for these grades of steel, established in the American standard ACI 318-11. The bars were bent to 90 degrees angle and then aged indoors for either one week, one month or three months. After the aging, the bars were straightened and then evaluated in a tensile test. The straightening was done using a pressing and bending machine. Two bars of each type were tested.

When bending a reinforcing bar, the plastic strain in the cross-section vary, since the inner side of the bend is subjected to compression and the outer side is subjected to tension. Chun and Ha (2014) display a determination of the tensile strain on the outside of the bend as

$$\varepsilon_t = \frac{\pi(r_0 + d) - \pi\left(r_0 + \frac{d}{2}\right)}{\pi\left(r_0 + \frac{d}{2}\right)} = \frac{\frac{d}{2}}{r_0 + \frac{d}{2}} \quad (5.1)$$

where r_0 is the bending radius and d_b the bar diameter. This yields a tensile strain of 14.3 % for the minimum allowed bend radius previously mentioned, which is beyond the limit of elongation for Gr 280 rebars from 10 to 19 mm diameter, established by the American standard ASTM A615-12 (Chun and Ha, 2014).

Furthermore, Chun and Ha (2014) state that after straightening the rebar, loading it in tension gives a reduced yield strength, plastic hardening without a yield plateau and a reduced elongation. Moreover, if the bar is not perfectly straightened, the modulus of elasticity is reduced.

The results of the experiments performed in the study show that the straightened bars exhibited non-linearity earlier than the non-bent ones, without a clear proportional limit. For all the Gr 280 bars, the yield strength showed almost no effect when they had aged for one week and for one month. However, all the specimen showed an increase in yield strength after three months aging, the increase was of 18 % in average in comparison to an unbent bar. The bars with higher strength, Gr 420, exhibited a reduction in yield strength for all aging periods, however, the reduction was of 25 % for one week and month and 10 % for three months aging. When it came to yield strength, diameter or bend radius showed no influence.

Furthermore, the experiments showed a clear trend that the cold-bending and straightening had no influence on the ultimate strength. This was assumed to be due to the well-performed straightening, which was done using a pressing and bending machine. However, on construction sites the straightening conditions are not as in these tests, which is why a reduction in the tensile strength is expected for bars straightened on site.

Lastly, the bars generally showed reductions of the elongation and the modulus of elasticity, though no clear patterns based on the variables were observed for either of the parameters.

The results obtained in the study by Chun and Ha (2014), are illustrated principally in Figure 5.4 and Figure 5.5. Note that the differences in the curves are not quantitative, but purely qualitative, the values of change are stated above.

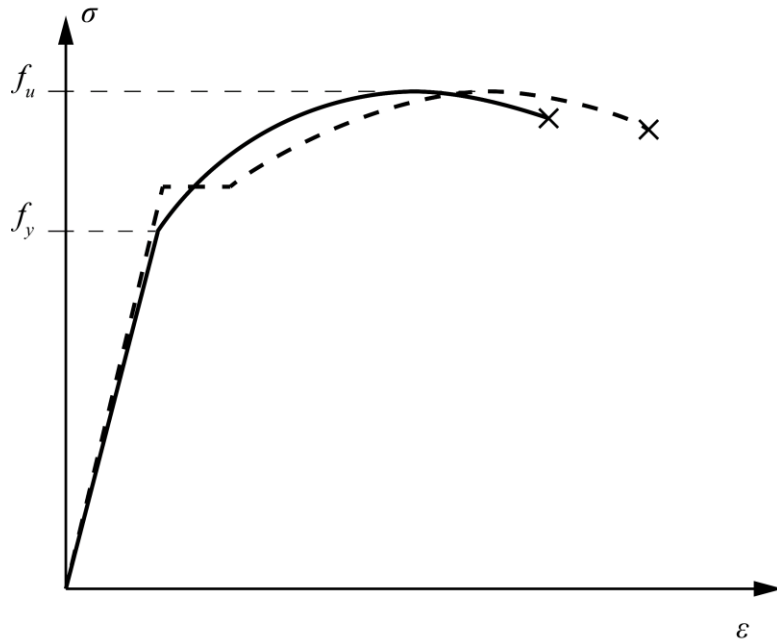


Figure 5.4 Principle illustration of the influence of cold-bending and straightening a reinforcing bar of Gr 420 for all three aging periods, based on the results from Chun and Ha (2014).

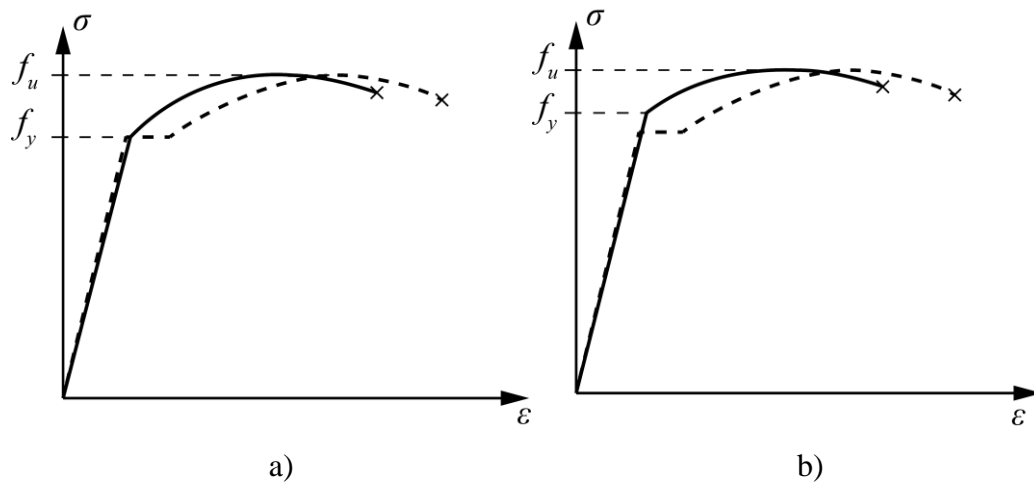


Figure 5.5 Principle illustration of the influence of cold-bending and straightening a reinforcing bar of Gr 280 a) for 1 week and 1 month aging and b) for 3 months aging, based on the results from Chun and Ha (2014).

Relating the results from Chun and Ha (2014) to the f_u / f_y ratio gives an increased η_f for bent reinforcement and a decreased ratio for the case of low steel strength and short aging.

5.4 Damage due to welding

The change in mechanical properties of reinforcing bars from welding has been studied by Mo and Kuo (1995). The study was performed to understand how welds in reinforcing cages affect the properties. Three bars were welded on each specimen with a spacing of 100 mm, using fillet welds, see Figure 5.6. The specimens tested were of four different sizes; #3, #4, #7 and #8 in American notations, which corresponds to about 10, 13, 22 and 25 mm. Three specimens of each type were tested. The rebars were of Grade 60 which corresponds to a minimum yield strength of 420 MPa. The weld material was E70 electrodes corresponding to an ultimate tensile strength of 490 MPa.

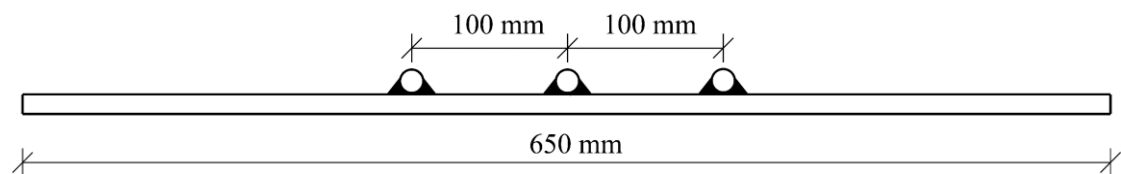


Figure 5.6 Illustration of the welded bars used in Mo and Kuo (1995).

The results from the study show that the bars ruptured by the welds, which was assumed to come from notches from the welding. The effect on the yield properties were negligible and the ultimate tensile strength only obtained a slight decrease up to 4 %. However, the ultimate strain decreased significantly, with values up to 46 %. Moreover, the bars with the most reduced ultimate strain still had a ductility sufficient for American standards, according to Mo and Kuo (1995). The ductility was defined as the difference in strain between rupture of the bar and yielding. The principle changes in the stress-strain curve of welded rebars are illustrated in Figure 5.7 qualitatively. Based on this study, the η_f ratio can be expected to only decrease slightly for welded rebars, but the strain at ultimate stress would decrease significantly.

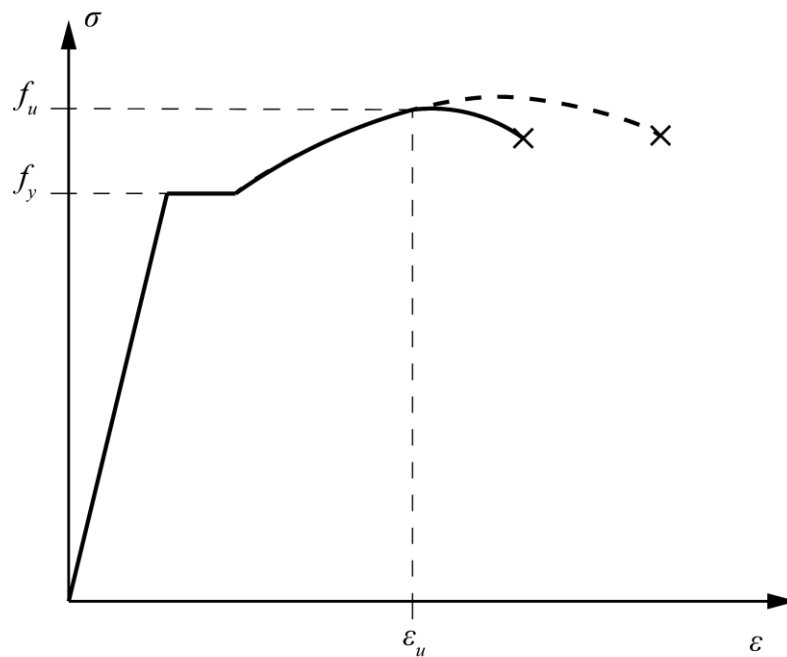


Figure 5.7 Principle illustration of the influence of welding on the stress-strain curve based on the results from Mo and Kuo (1995).

Mo and Kuo (1995) also studied the effect of annealing in addition to the welding, and showed that it had positive effects on the mechanical properties of the rebars. When this treatment was used, not all bars broke at the welds, and the ductility was recovered by 86 % due to the favourable microstructural change in the weld metal. However, the yield and ultimate stresses were slightly decreased, by 6 and 7 %, respectively.

5.5 Damage due to corrosion

One widely recognised issue with reinforced concrete is the event of corrosion in the reinforcement. Corrosion occurs if the passive layer of the concrete is broken or if the concrete cracks and the reinforcement is exposed to the environment. How corrosion affects the mechanical properties of the reinforcing steel has been studied by researchers to further understand how the service life of the structure is influenced.

Previous studies have been performed on both artificially and naturally corroded reinforcing steel bars. According to Apostolopoulos and Papadakis (2007) both events show similar impact on the yield and ultimate stress and the elongation to failure. However, they mention that there is no direct correlation between artificially and naturally corroded reinforcement, the observed similarities are solely qualitative. Furthermore, Apostolopoulos and Papadakis (2007) state that the artificial corrosion, intended to represent a coastal area, show a more aggressive attack on the reinforcing bars than what resulted from naturally corroded bars.

The most important issue from the corrosion on the reinforcement is the loss of mass, in correlation to the variation of cross-sectional area according to Apostolopoulos and Papadakis (2007). This is also proved by Du, Clark and Chan (2005) and by Fernandez and Berrocal (2019). The loss of cross-sectional area leads to a loss of yield and

ultimate load in all the investigations, see Figure 5.8 as an example from Fernandez and Berrocal (2019). The reduction of load capacity shows a linear correlation to the level of corrosion. Furthermore, Fernandez and Berrocal (2019) show that the yield and ultimate stresses are not affected by corrosion, since the material itself is not affected. Note that Figure 5.8 shows the load level, which is directly correlated to the cross-sectional area, which in turn is decreased by corrosion as proven by all the studies referred to here. From this, the expected f_u / f_y ratio would be indifferent to the undamaged case, however, the values of F_u and F_y are lowered significantly (proportionally to the level of corrosion), which indicates that the load capacity of the structure is reduced.

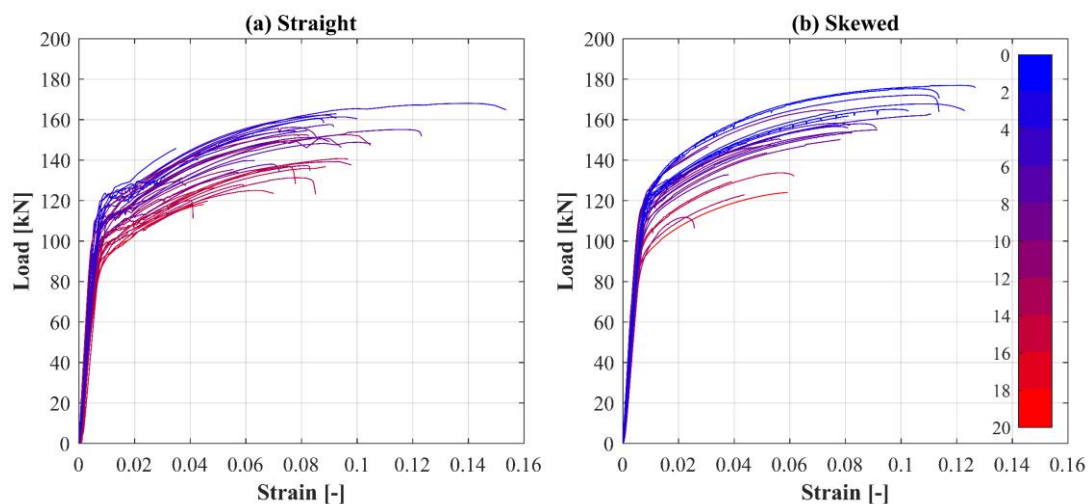


Figure 5.8 Load-strain curves for naturally corroded reinforcing bars with a) straight ribs and b) skewed ribs (Fernandez and Berrocal, 2019). The colour scale shows level of corrosion, which is represented by percentage of cross-sectional area loss.

Moreover, the effect of corrosion on the ductility is more difficult to find a correlation for. All the previously mentioned studies show that the ductility is significantly reduced by corrosion, though a clear trend is hard to define. Apostolopoulos and Papadakis (2007) show that the elongation to failure was reduced exponentially to the corrosion level, based on their tests on artificially corroded reinforcement. They also mention pitting as a large impact on the ductility. This is confirmed by Fernandez and Berrocal (2019) who present a clear trend with the pit depth of the reinforcement, based on tests on naturally corroded reinforcement. They further state that pits are common in naturally corroded structures. Moreover, it is proven by Fernandez and Berrocal (2019) that the appearance of pitting in reinforcement removes the necking and therefore the descending branch of the stress strain curve. The difference between the total strain and the strain at maximum load is therefore reduced significantly. The strain at maximum load is decreased for increased corrosion level, though the reduction is low for low levels of corrosion. In contrast the strain at yielding shows an increasing trend with increasing corrosion which they relate to the loss of stiffness due to the reduction of cross-section area.

6 Discrete Model for Dynamic Analysis

The response of a dynamically loaded beam can be described by a discrete model that originates from a single-degree-of-freedom model (SDOF) for the beam and an SDOF model for the drop-weight. The two SDOF models are then joined and transformed into one two-degree-of-freedom model (2DOF). This chapter is based on (Johansson and Laine, 2012).

6.1 Definition of an SDOF system

The definition of a dynamic SDOF system is illustrated in . It consists of a mass m that is exposed to an external time dependent load $F(t)$. An internal static resistance $R(u)$ and a viscous damper $c(\dot{u})$ work as counterparts to this load and generate a static force $R_{sta}(u)$ and a viscous force $R_{dyn}(\dot{u})$. However, Johansson and Laine (2012) consider it reasonable to neglect the effect of damping since the load duration is very short and it is solely the maximum displacement that is of interest. Hence, only the static force remains as a counteracting force here.

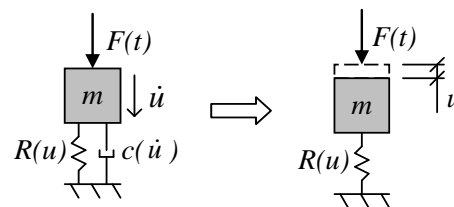


Figure 6.1 Definition of a dynamic SDOF system where the viscous damping c is neglected. From Johansson and Laine (2012).

6.2 Drop-weight load – dynamic interpretation

As stated in Chapter 3, there are two dynamic extreme cases; ideal impulse load I_k and pressure load F_k . An arbitrary case will be somewhere in between the two extreme cases depending not only on how long the load duration is but also on the structural response of the loaded structure. Simplified, it is reasonable to interpret a load with long duration as a pressure load and a load with short duration as an impulse load. The drop-weight used in the experiments in this thesis is considered to have a relatively short duration and may therefore be treated approximately as a characteristic impulse load.

6.3 Transformation of structural members to equivalent SDOF systems

To be able to analyse the structural response of a dynamically loaded structure all structural members need to be simplified and transformed to equivalent SDOF systems. In this case that is the reinforced concrete beam and the drop-weight.

6.3.1 Transformation of a beam to equivalent SDOF system

A statically loaded beam with a linear elastic response gets a deformation shape that is a function of the load acting on it and the boundary conditions. Hence the deformation

shape is the same regardless of the magnitude of the load which makes it possible to describe the deflection along the beam using one system point. The deformed shape scales linearly with a factor α , see Figure 6.2. The system point is attributed to properties so that its displacement u_s is equal to the displacement in an SDOF system u_{SDOF} , see Equation (6.1).

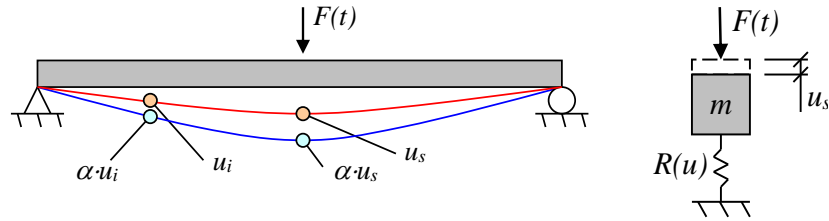


Figure 6.2 Beam subjected to a concentrated load $F(t)$ (to left) and an equivalent SDOF system (to right). The beam is assumed to behave linear elastic and the deformed shape scales linearly with α . Modified from Johansson and Laine (2012).

$$u_s = u_{SDOF} \quad (6.1)$$

In order to transform a real beam to an equivalent SDOF system its real parameters of mass m_b , stiffness k_b , and external load F_b are multiplied with transformation factors κ_m , κ_k and κ_F respectively, see Figure 6.3.

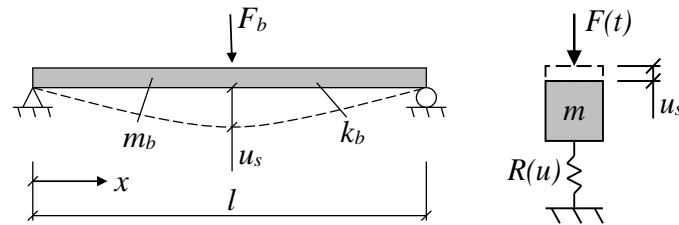


Figure 6.3 Transformation of a beam to an equivalent SDOF system. Modified from Johansson and Laine (2012).

The mass m , stiffness k and external load F for the SDOF system can then be expressed as

$$m = \kappa_m m_b \quad (6.2)$$

$$k = \kappa_k k_b \quad (6.3)$$

$$F = \kappa_F F_b \quad (6.4)$$

Equation (6.2) to (6.4) inserted in Equation (3.8) with the damping neglected gives

$$\kappa_m m_b \ddot{u} + \kappa_k k_b u = \kappa_F F_b \quad (6.5)$$

Equation (6.5) can also be written as

$$\frac{\kappa_m}{\kappa_F} m_b \ddot{u} + \frac{\kappa_k}{\kappa_F} k_b u = F_b \quad (6.6)$$

According to Biggs (1964)

$$\kappa_k = \kappa_F \quad (6.7)$$

and Equation (6.6) can then be rewritten as

$$\kappa_{mF} m_b \ddot{u} + k_b u = F_b \quad (6.8)$$

where

$$\kappa_{mF} = \frac{\kappa_m}{\kappa_F} \quad (6.9)$$

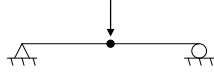
Equation (6.5) can then for an arbitrary system be expressed as

$$\kappa_{mF} m_b \ddot{u} + R_b(u) = F_b \quad (6.10)$$

where $R_b(u)$ describes the response of the beam at static loading.

The transformation factors κ are derived from the principle of energy conservation in the real beam system. κ_m is determined from conservation of the kinetic energy in the system while κ_k and κ_F are determined from conservation of the internal and external energy, respectively. Hence, the transformation factors depend on the boundary conditions and loading conditions; i.e. the elastic or plastic strain range. The beams in the experiments carried out in this master thesis are simply supported and subjected to three-point loading. Therefore only those transformation factors are treated in this report, presented in Table 6.1. E.g. Johansson and Laine (2012) and Biggs (1964) treat transformation factors for several boundary conditions, loading conditions and strain ranges.

Table 6.1 Transformation factors for a simply supported beam subjected to three-point-loading (Johansson and Laine, 2012).

	Strain range	κ_m	κ_F	κ_k	κ_{mF}
	Elastic	0.486	1.000	1.000	0.486
	Plastic	0.333	1.000	1.000	0.333

6.3.2 Transformation of a drop-weight to equivalent SDOF system

The drop-weight can be simplified and transformed to an equivalent SDOF system by using transformation factors in a similar way as described in Section 6.3.1. The major difference in this case is that the drop-weight will exhibit an axial deformation instead of a transverse deformation as for the beam, i.e. it can be treated as a bar (Lovén and Svavarsdóttir, 2016). The transformation of the drop-weight is illustrated in Figure 6.4. The system point u_s is placed where the maximum deformation occurs. That is at the surface where the impact occurs, i.e. at the bottom of the drop-weight.

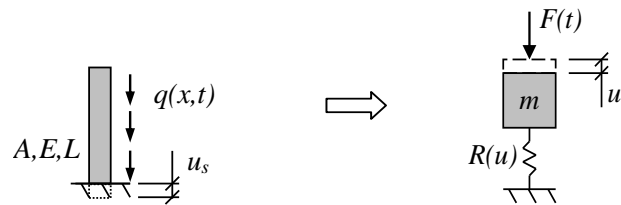
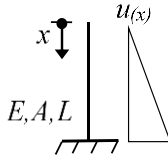
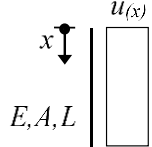


Figure 6.4 Transformation of the drop-weight to an equivalent SDOF system. From Johansson and Laine (2012).

The transformation factors used for transformation of the drop-weight to an equivalent SDOF system depend on whether the bar is seen as a rigid body, i.e. very stiff in comparison to the impacted surface (in this case the beam), or if the impacted surface is seen as a rigid body, i.e. the beam is very stiff in comparison to the falling drop-weight. The corresponding transformation factors are presented in Table 6.2.

Table 6.2 Transformation factors for drop-weight considered as a bar (Jönsson and Stenseke, 2018).

Case	κ_m	κ_F	κ_k	κ_{mF}
Rigid surface: 	0.333	0.500	0.500	0.667
Rigid bar: 	1.000	1.000	1.000	1.000

In an arbitrary case the drop-weight is somewhere in between these two extreme cases. Lovén and Svavarsdóttir (2016) give a more thorough description of the determination of the transformation factors. However, in this thesis the drop-weight is considered to have a very stiff base in comparison to the surface of the beam. Furthermore, the drop-weight is made of solid steel with a considerably high axial stiffness compared to the bending stiffness of the reinforced concrete beam that it impacts. Therefore the transformation factors for the drop-weight is taken for a rigid bar as

$$\kappa_m = \kappa_F = \kappa_k = \kappa_{mF} = 1.000 \quad (6.11)$$

6.4 Coupling of two SDOF systems into a 2DOF system

The two equivalent SDOF systems, the beam and the drop-weight, now need to be coupled together into a 2DOF system. The coupling is illustrated in Figure 6.5. Note that henceforth the subscript 1 refers to the drop-weight and subscript 2 refers to the impacted beam.

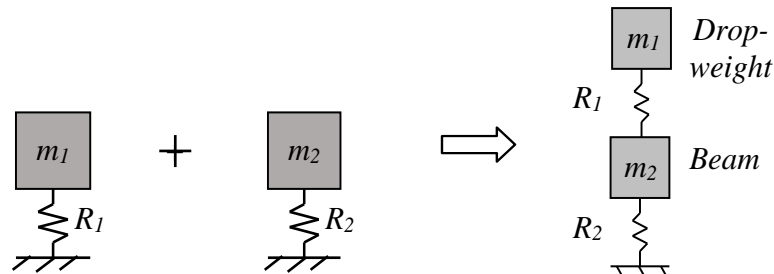


Figure 6.5 Illustration of how two equivalent SDOF systems are coupled into one 2DOF system. Modified from Lozano and Makdesi (2017).

6.4.1 Equation of motion for a 2DOF system

In order to establish the equation of motion for a 2DOF system a free-body diagram can be used, see Figure 6.6.

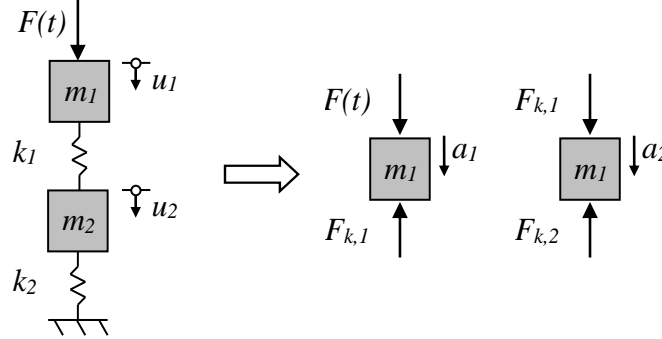


Figure 6.6 Free-body diagram of the 2DOF system used to describe the collision between the beam and the drop-weight. Note that the drop-weight is represented by m_1 and the beam by m_2 . Modified from Jönsson and Stenseke (2018).

Newton's second law gives the force equilibrium for the two bodies as:

$$F_1(t) - F_{k,1} = m_1 \ddot{u}_1 \quad (6.12)$$

$$F_2(t) - F_{k,2} = m_2 \ddot{u}_2 \quad (6.13)$$

By using constitutive relations this can be expressed as:

$$m_1 \ddot{u}_1 + k_1(u_1 - u_2) = F_1(t) \quad (6.14)$$

$$m_2 \ddot{u}_2 - k_1 u_1 + u_2(k_1 + k_2) = F_2(t) \quad (6.15)$$

where k_i corresponds to the spring stiffness, \ddot{u}_i to the acceleration and u_i to the displacement. This can also be expressed in matrix form as:

$$\begin{bmatrix} m_1 & 0 \\ 0 & m_2 \end{bmatrix} \begin{bmatrix} \ddot{u}_1 \\ \ddot{u}_2 \end{bmatrix} + \begin{bmatrix} k_1 & -k_1 \\ -k_1 & k_1 + k_2 \end{bmatrix} \begin{bmatrix} u_1 \\ u_2 \end{bmatrix} = \begin{bmatrix} F_1(t) \\ F_2(t) \end{bmatrix} \quad (6.16)$$

By inserting the transformation factors the expression becomes

$$\begin{bmatrix} \kappa_{m,1} m_1 & 0 \\ 0 & \kappa_{m,2} m_2 \end{bmatrix} \begin{bmatrix} \ddot{u}_1 \\ \ddot{u}_2 \end{bmatrix} + \begin{bmatrix} \kappa_{F,1} k_1 & -\kappa_{F,1} k_1 \\ -\kappa_{F,1} k_1 & \kappa_{F,1} k_1 + \kappa_{F,2} k_2 \end{bmatrix} \begin{bmatrix} u_1 \\ u_2 \end{bmatrix} = \begin{bmatrix} \kappa_{F,1} F_1(t) \\ \kappa_{F,2} F_2(t) \end{bmatrix} \quad (6.17)$$

By using the following relations

$$\alpha_m = \frac{\kappa_{m,1}}{\kappa_{m,2}} \quad (6.18)$$

$$\alpha_F = \frac{\kappa_{F,1}}{\kappa_{F,2}} \quad (6.19)$$

$$\kappa_{mF,2} = \frac{\kappa_{m,2}}{\kappa_{F,2}} \quad (6.20)$$

it can be rewritten as

$$\begin{aligned} \kappa_{mF,2} \begin{bmatrix} \alpha_m m_1 & 0 \\ 0 & m_2 \end{bmatrix} \begin{bmatrix} \ddot{u}_1 \\ \ddot{u}_2 \end{bmatrix} + \begin{bmatrix} \alpha_F k_1 & -\alpha_F k_1 \\ -\alpha_F k_1 & \alpha_F k_1 + k_2 \end{bmatrix} \begin{bmatrix} u_1 \\ u_2 \end{bmatrix} \\ = \begin{bmatrix} \alpha_F F_1(t) \\ F_2(t) \end{bmatrix} \end{aligned} \quad (6.21)$$

which also can be written as

$$\mathbf{M}\ddot{\mathbf{u}} + \mathbf{K}\mathbf{u} = \mathbf{F}(t) \quad (6.22)$$

Equation (6.22) can be solved numerically or analytically. An example of an appropriate numerical method to solve the equation, the central difference method, is described in Section 6.5.

6.4.2 2DOF system for a drop-weight and beam system

To establish an equivalent 2DOF model of the impact loaded reinforced concrete beam in this thesis, the transformation factors treated in Section 6.3.1 and 6.3.2 are inserted in Equations (6.18), (6.19) and (6.20). No external forces $F_i(t)$ are considered to act on the two bodies. Instead, the impact is represented by an initial velocity of the drop-weight.

For an elastic response of the specific case Equation (6.21) then becomes

$$\kappa_{mF,2} \begin{bmatrix} \alpha_m m_1 & 0 \\ 0 & m_2 \end{bmatrix} \begin{bmatrix} \ddot{u}_1 \\ \ddot{u}_2 \end{bmatrix} + \begin{bmatrix} k_1 & -k_1 \\ -k_1 & k_1 + k_2 \end{bmatrix} \begin{bmatrix} u_1 \\ u_2 \end{bmatrix} = \begin{bmatrix} 0 \\ 0 \end{bmatrix} \quad (6.23)$$

For an elasto-plastic response of the specific case Equation (6.21) then becomes

$$\kappa_{mF,2} \begin{bmatrix} \alpha_m m_1 & 0 \\ 0 & m_2 \end{bmatrix} \begin{bmatrix} \ddot{u}_1 \\ \ddot{u}_2 \end{bmatrix} + \begin{bmatrix} R_1 & -R_1 \\ -R_1 & R_1 + R_2 \end{bmatrix} \begin{bmatrix} u_1 \\ u_2 \end{bmatrix} = \begin{bmatrix} 0 \\ 0 \end{bmatrix} \quad (6.24)$$

with the relation between R and u according to Equation (2.3). However, an additional condition needs to be considered in this case. That is when the drop-weight moves

upwards after the collision, away from the beam. The modelled spring between the bodies is in this case subjected to tension. However, in reality there is no connection between the bodies preventing such a movement, i.e. the stiffness of the spring in tension must be equal to zero. Equation (2.3) is then extended to

$$R_1 = \begin{cases} k_1 \cdot u & \text{if } u_1 \leq u_{el,1} \\ R_{m,1} & \text{if } u_1 > u_{el,1} \\ 0 & \text{if } u_1 \leq 0 \end{cases} \quad (6.25)$$

The internal resistance of the drop-weight $R_{m,1}$ is determined from

$$R_{m,1} = f \cdot A_{imp} \quad (6.26)$$

where f is the strength of the material and A_{imp} is the impact area. The value of f depends on both the strength of the drop-weight and the local behaviour of the concrete where the impact occurs. This gives an interval for $R_{m,1}$

$$f_{cm}A_{imp} \leq R_{m,1} \leq f_{ym}A_{imp} \quad (6.27)$$

where f_{cm} is the compressive strength of concrete and f_{ym} is the yielding of steel.

The stiffness of the drop-weight k_1 can be determined based on Hertz contact theory, described in Fujikake, Senga, Ueda, Ohno and Katagiri (2006), as

$$k_1 = \frac{4\sqrt{r_1}}{3} \left[\frac{1 - \nu_1^2}{E_1} + \frac{1 - \nu_2^2}{E_2} \right]^{-1} \quad (6.28)$$

where r_1 is the radius of the hitting surface of the drop-weight, E_{sm} and E_{cm} are the mean modulus of elasticity of the drop-weight (steel) and the beam (concrete), respectively. ν_1 and ν_2 are the Poisson's ratio for the drop-weight (steel) and the beam (concrete), respectively. The relation between the impact force, F_1 , and the local deformation at the impact zone, δ , is through the contact law described as

$$F_1 = k_1 \cdot \delta^{3/2} \quad (6.29)$$

The relation in Equation (6.29) is non-linear. However, in this thesis a linear relationship was assumed at a certain internal resistance and a “new” stiffness, an approximation of k_1 , was determined. This is further treated in Appendix A.

The internal resistance of the beam, $R_{m,2}$, is determined from

$$R_{m,2} = \frac{4M_u}{L_2} \quad (6.30)$$

where M_u is the maximum moment at ultimate limit state for a point load at the midspan and L_2 is the length of the beam. Additionally, the beam is subjected to a static load, its self-weight g_{beam} . To account for the self-weight, Equation (6.30) is modified into Equation (6.31). This is illustrated in Figure 6.7.

$$R_{m,2,mod} = \frac{4M_u}{L_2} - \frac{g_{beam}L_2}{2} \quad (6.31)$$

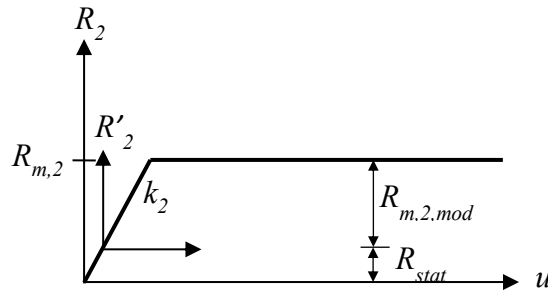


Figure 6.7 Illustration of the internal resistance of the beam. From Jönsson and Stenseke (2018).

The stiffness of the beam, k_2 , can be determined according to

$$k_2 = \frac{48E_{cm}I_{II}}{L_2^3} \quad (6.32)$$

where E_{cm} is the mean modulus of elasticity of concrete and I_{II} is the moment of inertia in state II.

6.5 Central difference method

The central difference method (CDM) is an explicit method to determine an approximate solution to a second-order differential equation such as for example the equation of motion, see Equation (3.8). The method is described in e.g. Jönsson and Stenseke (2018) and Johansson (2012). Though, as discussed in Section 6.1, the damping c is neglected in this thesis, so it is neglected in this description of CDM as well.

6.5.1 Numerical formulation

A scheme of the concept used in CDM can be seen in Figure 6.8.

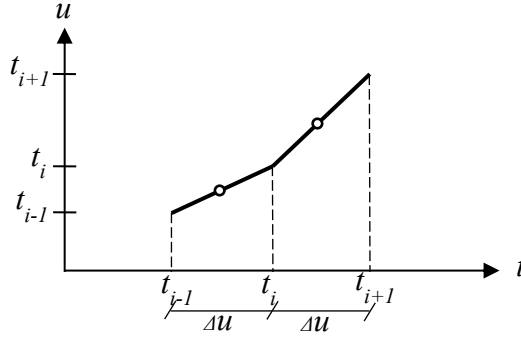


Figure 6.8 Scheme over the central difference method. From Jönsson and Stenseke (2018).

The velocity, \dot{u} , and acceleration, \ddot{u} , at time, i , can be expressed as

$$\dot{u}_i = \frac{u_{i+1} - u_{i-1}}{2\Delta t} \quad (6.33)$$

$$\ddot{u}_i = \frac{\frac{u_{i+1} - u_i}{\Delta t} - \frac{u_i - u_{i-1}}{\Delta t}}{\Delta t} = \frac{u_{i+1} - 2u_i + u_{i-1}}{(\Delta t)^2} \quad (6.34)$$

Inserting Equation (6.33) and Equation (6.34) into Equation (6.22) gives an approximation of the equation of motion

$$\mathbf{M} \frac{\mathbf{u}_{i+1} - 2\mathbf{u}_i + \mathbf{u}_{i-1}}{(\Delta t)^2} + \mathbf{K}\mathbf{u}_i = \mathbf{F}_i(t) \quad (6.35)$$

where \mathbf{u}_i and \mathbf{u}_{i-1} are assumed to be known. This expression can be solved for \mathbf{u}_{i+1} by introducing the initial conditions

$$\mathbf{u}(0) = \mathbf{u}_0 \quad (6.36)$$

$$\ddot{\mathbf{u}}(0) = \ddot{\mathbf{u}}_0 \quad (6.37)$$

$$\ddot{\mathbf{F}}(0) = \ddot{\mathbf{F}}_0 \quad (6.38)$$

for an initial value of $i = 0$. The solution can then be expressed as

$$\begin{aligned} \mathbf{u}_{i+1} &= (\Delta t)^2 \mathbf{M}^{-1} (\mathbf{F}_i(t) - \left(\mathbf{K} - \frac{2}{(\Delta t)^2} \mathbf{M} \right) \mathbf{u}_i - \frac{1}{(\Delta t)^2} \mathbf{M} \mathbf{u}_{i-1}) \\ &= \mathbf{F}_i(t) \end{aligned} \quad (6.39)$$

The starting step, where $i = 0$, for solving the central difference method is given as

$$\mathbf{u}_{-1} = \mathbf{u}_0 - \Delta t \dot{\mathbf{u}}_0 + \frac{(\Delta t)^2}{2} \ddot{\mathbf{u}}_0 \quad (6.40)$$

When deriving Equation (6.39) a linear elastic material response is assumed in the stiffness matrix, \mathbf{K} . Hence, this equation needs to be adjusted if the material response instead is assumed to be non-linear. A suggestion of how this can be done is described in Johansson and Laine (2012).

6.5.2 Stability of CDM

If the time step Δt is chosen too large, the errors in the initial conditions can easily grow during the iterations and the solution is then considered as unstable. To get a stable solution the time step should be chosen smaller than

$$\Delta t_{crit} = \frac{2}{\omega_{max}} = \frac{T_n}{\pi} \quad (6.41)$$

where ω_{max} corresponds to the highest eigenfrequency determined from Equation (6.42) and T_n is the smallest period.

$$\det(\mathbf{K} - \omega^2 \mathbf{M}) = 0 \quad (6.42)$$

According to Johansson and Laine (2012) a significantly smaller time step might be required when a high level of accuracy is needed. A suitable timestep is dependent on both loading conditions and response time of the system. Though, a time step that is smaller than one percent of the load duration is usually sufficient. That gives an appropriate time step as

$$\Delta t \leq \begin{cases} \Delta t_{crit} \\ \frac{t_l}{100} \end{cases} \quad (6.43)$$

where t_l is the duration of the load.

7 Experiment Description

This chapter gives a detailed description of the experiments performed. The first part describes the beam tests and the second part describes the reinforcement tests.

7.1 Beam tests

In total 18 beams were cast and tested under different loading conditions. Half of the beams were provided with normal reinforcement and the other half were provided with pre-stretched reinforcement. The beams were then divided into three series of which each were subjected to different load conditions. The beams in Series S were only tested statically and used as a reference. The beams in Series I10 and Series I20 were tested dynamically by a drop-weight impact of 10 kg and 20 kg respectively, released from a height of five meters. The residual capacities of the impacted beams were thereafter determined by a static test.

Due to limited size of the concrete mixer the concrete was mixed in two batches. The two batches of concrete were distributed evenly between the different beams. To be able to compare the results obtained from the dynamical testing of beams with undamaged reinforcement and beams with pre-stretched reinforcement, concrete from one batch was used within all beams in Series I10 and the other batch was used for beams in Series I20.

The beams were named with reference to its load case, reinforcement type, concrete batch and beam number, respectively. Static load case was indicated by *S* while dynamic load case with 10 kg and 20 kg drop-weight impact was indicated by *I10* and *I20*, respectively. Damaged reinforcement was abbreviated to *D*, undamaged reinforcement to *UD* and batch to *B*. Here damaged reinforcement refers to the pre-stretched reinforcement. A scheme over the beams and associated loading condition, reinforcement type and batch used can be found in Table 7.1.

Table 7.1 Scheme over beam number and associated loading condition, reinforcement type and batch used. Here damaged reinforcement refers to pre-stretched reinforcement.

Beam number	Load case	Reinforcement type	Batch number	Beam name	Series	Sub-series
1	Static	Undamaged	1	S-UD-B1-01	S	UD
2	Static	Undamaged	1	S-UD-B1-02		
3	Static	Undamaged	2	S-UD-B2-03		
4	Static	Damaged	1	S-D-B1-04		D
5	Static	Damaged	2	S-D-B2-05		
6	Static	Damaged	2	S-D-B2-06		
7	10 kg	Undamaged	1	I10-UD-B1-07	I10	UD
8	10 kg	Undamaged	1	I10-UD-B1-08		
9	10 kg	Undamaged	1	I10-UD-B1-09		
10	10 kg	Damaged	1	I10-D-B1-10		D
11	10 kg	Damaged	1	I10-D-B1-11		
12	10 kg	Damaged	1	I10-D-B1-12		
13	20 kg	Undamaged	2	I20-UD-B2-13	I20	UD
14	20 kg	Undamaged	2	I20-UD-B2-14		
15	20 kg	Undamaged	2	I20-UD-B2-15		
16	20 kg	Damaged	2	I20-D-B2-16		D
17	20 kg	Damaged	2	I20-D-B2-17		
18	20 kg	Damaged	2	I20-D-B2-18		

The material properties of the concrete and the reinforcement were determined according to standard material tests. A number of 16 concrete cubes were cast to determine the compressive and tensile strength of the concrete. Additionally, six cubes with a notch were cast to determine the fracture energy of the concrete.

7.1.1 Geometry of tested beams

The geometry of the beams can be seen in Figure 7.1. The beams had a total length of 1 400 mm and a cross-sectional area of 100 x 100 mm². Four longitudinal reinforcement bars with a nominal diameter of 6 mm were placed symmetrically in the beams. The distance from the free concrete edge to the centre of the bar was 20 mm.

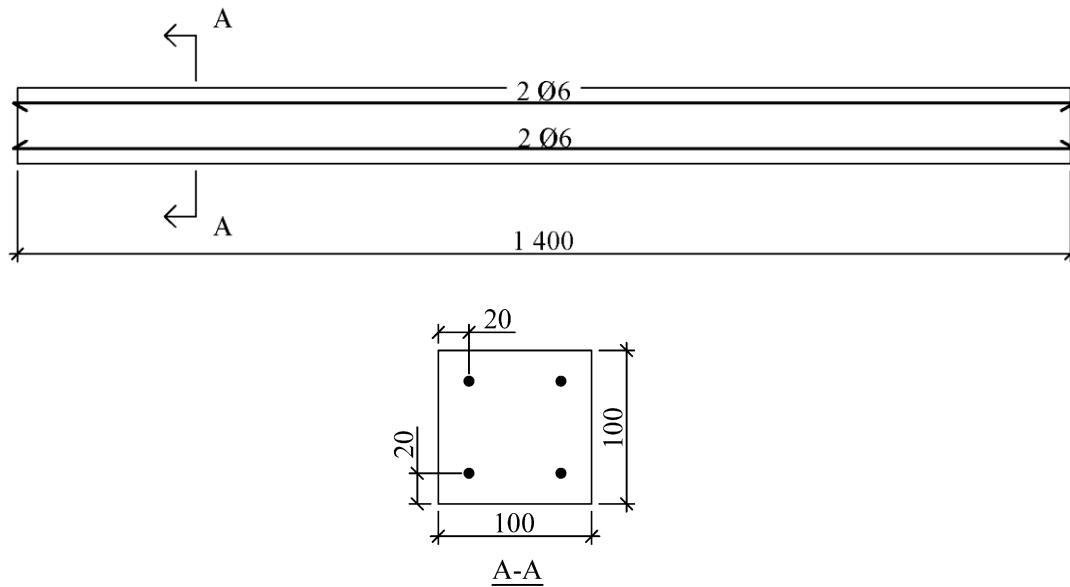


Figure 7.1 Geometry and reinforcement arrangement of the tested beams [mm].

7.1.2 Preparations

7.1.2.1 Moulds

The moulds for the beams were made before this project started. They were made of timber boards and screwed together with inner dimensions according to the beam geometry described in Figure 7.1. The moulds had four bored holes on each short end as support for the reinforcement, see Figure 7.2. The preparations started with cleaning and oiling the moulds for both the beams and the cubes and wedge splitting test (WST) cubes. The nominal size of the cubes was aimed for 150 mm according to CEN (2012).

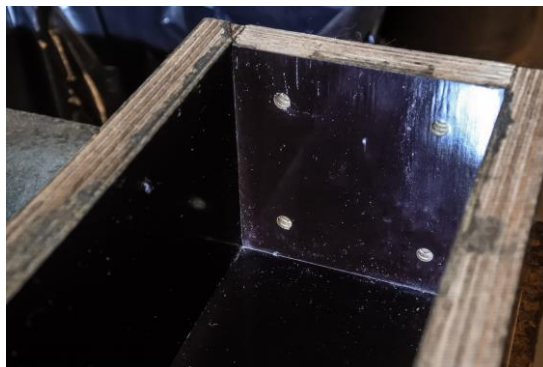


Figure 7.2 Example of short end of the beam moulds with bored holes as support for the reinforcement.

7.1.2.2 Reinforcement

The reinforcement used in the beams was K500C-T with a nominal diameter of 6 mm. The bars were cut from a 6 m long bar at a length of 1 410 mm so that the bars would be supported by the holes on the short sides of the mould. Half of the bars were first

pre-stretched to a plastic deformation of 3 %, this procedure is described in Section 7.2.1.1.

The reinforcement was put in the beam moulds and further kept in place by steel wires hung from a transverse reinforcement bar laying on top of the mould. The steel wires acted at approximately one third of the beam's length from the end, see Figure 7.3. The length of the steel wire (resulting in the height of the reinforcing bar) was assured by placing a timber block beneath the bar right by the steel wire, this block had a height of 17 mm which put the centre line of the bottom reinforcement at a height of 20 mm. The top reinforcement was put in place by a similar manner. The block below the bottom reinforcement was kept where it lay and then blocks were put between the bottom and top reinforcement to assure the concrete cover of 17 mm there as well. Thereafter, the steel wires for the top reinforcement were placed at the same distance along the length as for the bottom reinforcement. This procedure is shown in Figure 7.4. After the tests, the position of the reinforcement was measured for a few beam specimen and it was confirmed that the bars' centre lines were at 20 mm from the edge.



Figure 7.3 Location of the hanging arrangement for the reinforcement.

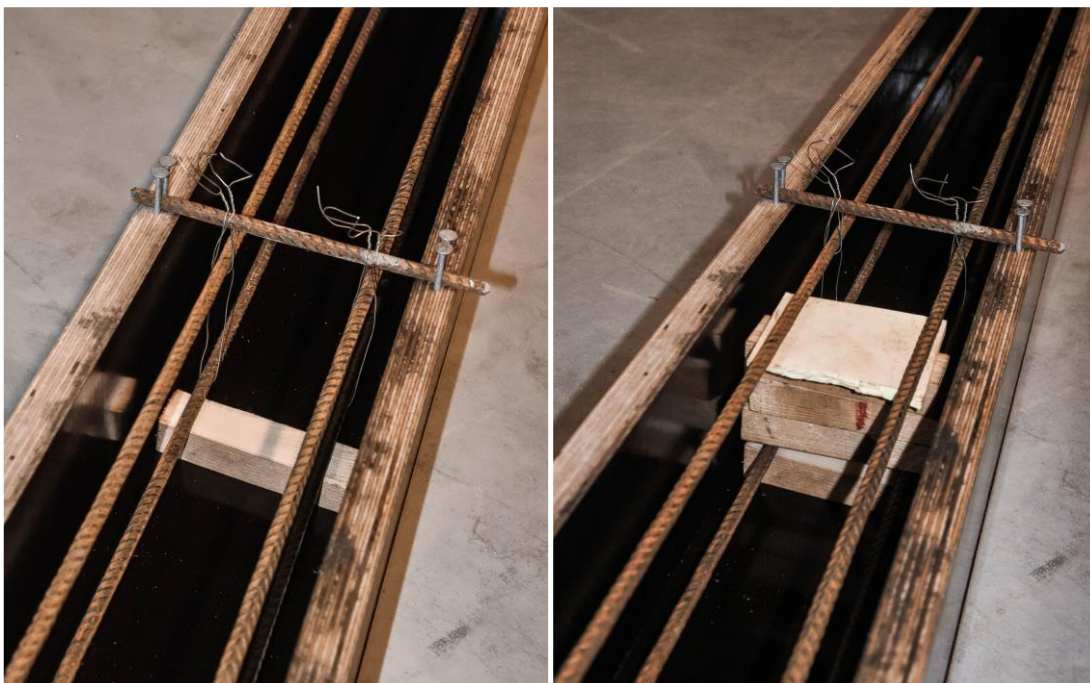


Figure 7.4 Procedure for hanging the reinforcement bars in steel wires, a) for bottom reinforcement, b) for top reinforcement.

7.1.3 Casting

The concrete was mixed according to the recipe in Table 7.2. As previously mentioned, the concrete was mixed in two batches due to the limiting size of the mixer. The recipe was developed by Ingemar Löfgren, Thomas Concrete Group AB. The materials used in the mixture were dry.

Table 7.2 Concrete recipe for one batch.

Material	Supplier	Quantity per batch [kg]
Sand 0/8 Sköllunga	Ucklums grus	157.4
Stone 5/8 Vikan	Skanska	16.7
Stone 8/16 Vikan	Skanska	140.5
Byggcement CEM II/A-LL 42,5R	Cementa	57.8
Glenium 51/18	BASF	0.635
Water	-	35.3

Slump tests were performed on the two batches to establish the consistence of the concrete before casting. After the slump tests were performed and the consistence of the concrete validated, the beams, cubes and WSTs were cast. The concrete was compacted using a vibrating rod, see Figure 7.5. Lastly, the top surface of the beams was evened out for a smooth surface and covered with a plastic film.



Figure 7.5 Compacting of the concrete using a vibrating rod.

The day after casting (25 h later for batch 1 and 22 h later for batch 2), water was poured over the beams and then the plastic film was reapplied. At the same time, the cubes and WSTs were demoulded and put in water for curing. The specimens cured for 27 and 28 days before testing.

The consistence of the fresh concrete was tested with slump test according to CEN (2009a). The target slump height for the concrete was 200 ± 20 mm. The measured slump heights for the two batches are listed in Table 7.3. The slump heights resulted within the target interval.

Table 7.3 Slump test results.

Batch	Slump height [mm]
1	215
2	200

7.1.4 Demoulding and painting

The beams were demoulded 23 days after casting. Then the beams were painted in a black and white random pattern in order to give good result from both the high speed camera and the one used in the static tests. An example of this pattern is presented using beam S-D-B2-05 in Figure 7.6.



Figure 7.6 Painted pattern of beam S-D-B2-05.

After the painting, two snapshots were taken of all the beams using the same cameras as for the static tests (note that this was before any impact). These were later used as reference frames in the analysis of the static tests.

7.1.5 Testing of the hardened concrete

The concrete material properties of importance were the compressive strength, the modulus of elasticity, the tensile strength and the fracture energy. Therefore, compressive tests were performed in accordance with CEN (2009b) and tensile splitting tests were performed in accordance with CEN (2009c). To estimate the fracture energy wedge splitting tests were performed according to Tschegg (1991). The number of cubes tested of each type are presented in Table 7.4. Additionally, the density was determined.

Table 7.4 Total number of tests performed to determine the material properties of the hardened concrete. Number from each batch within parentheses.

Test	27 days after casting	28 days after casting
Compressive test	4 (2)	6 (3)
Tensile splitting tests	6 (3)	-
WST	6 (3)	-

7.1.6 Dynamic tests

The drop-weight tests took place 27 days after casting of the beams. A schematic illustration of the set-up for the drop-weight tests can be found in Figure 7.7, and in Figure 7.8, a photo of the actual set-up is shown. The beams were placed freely on two rigid supports that had a distance of 1.3 m. Thus, the beam was acting simply supported with a 1.3 m span. The fact that the supports were rigid assured the assumptions of only the beam deforming under the load.

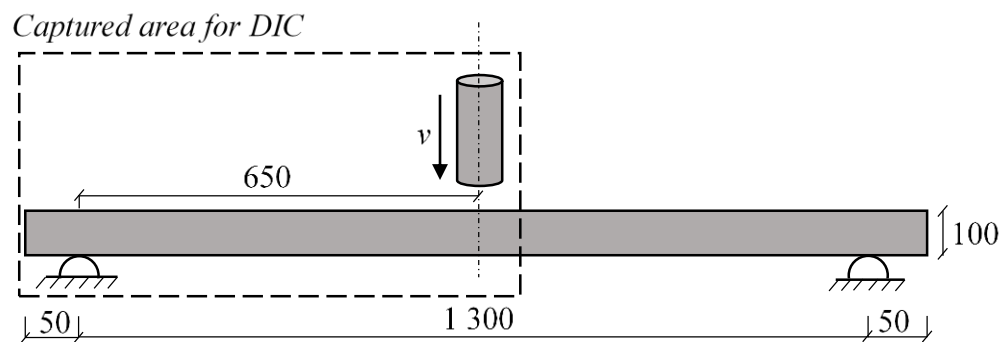


Figure 7.7 Dynamic test set-up. Modified from Jönsson and Stenseke (2018).



Figure 7.8 Set-up of the dynamic testing. Photo taken after the impacting of beam I10-UD-B1-09.

As seen in Figure 7.8, the drop-weight was a cylindrical steel rod with a rounded tip. The dimensions are presented in Figure 7.9. The drop-weight was lifted to a height of 5 m above the beam and there released. There were vertical guiding rails to assure that the weight would hit the centre point of the beam. As seen in Figure 7.8, the drop-weight also had the black and white pattern so it could be digitally analysed in the same manner as the beams.

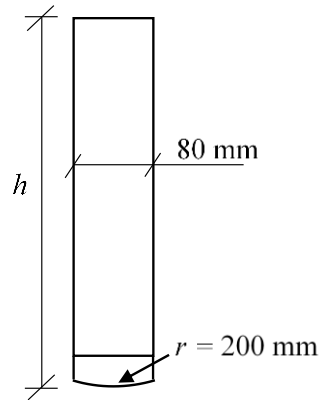


Figure 7.9 Dimensions of drop-weight with different heights for 10 and 20 kg.

The high speed camera used, captured half the beam span, as shown in Figure 7.7, in order to get as high resolution as possible. The camera specifications and conditions for the set-up are listed in Table 7.5.

Table 7.5 Camera specifications and setup.

High speed camera	Photron SA4
Distance from front of the beam to camera house	1 979 mm
Zoom	Tamron Zoom lens 28-75. Set to 50
Resolution	1 024×400 pixels
Spatial scale	Calibrated with a 200 mm measuring scale. 200 mm = 267 pixels \Rightarrow 1 pixel = 0.7491 mm
Approximate measured area	767×300 mm
Frame rate	5 000 fps (every 0.2 ms)
Triggering	Manual triggering with “centre trigger” which approximately captures 1 s before and 1 s after impact
Saved data	Approximately 140 ms (700 frames) were saved for each test

7.1.7 Static tests

The static testing was performed 27 and 28 days after casting. The aim of the static testing was to analyse the residual capacity of the beams tested dynamically and to compare structural response with beams that had not been tested before, i.e. the reference beams. Series S and I10 were tested in three point bending while Series I20 was tested in four point bending. The reason for the different loading conditions was that the beams subjected to the 20 kg drop-weight had a high level of concrete spalling after the impact, resulting in three point bending being unsuitable for these beams.

The beams were placed on two roller supports, with a distance of 1.3 m. The set-up for the three point and four point bending are illustrated in Figure 7.10 and Figure 7.11, respectively. Photos of the same set-ups are shown in Figure 7.12 and Figure 7.13. The

distance between the two point loads in the four point bending was 300 mm. In the static tests, two cameras were used which created a 3D view of the beam. The cameras captured the middle 1.0 m of the beam. The deformation speed in the static tests was 2 mm/min until a deformation of 10 mm was reached and thereafter it was increased to 10 mm/min.

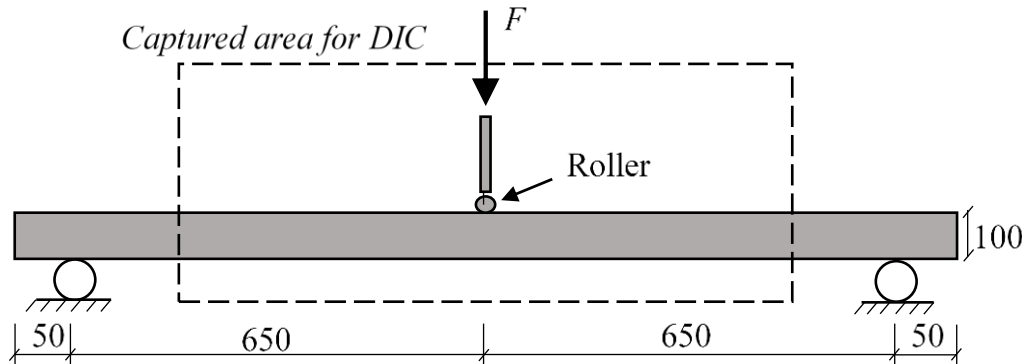


Figure 7.10 Static test set-up, three point bending. Modified from Jönsson and Stenseke (2018).

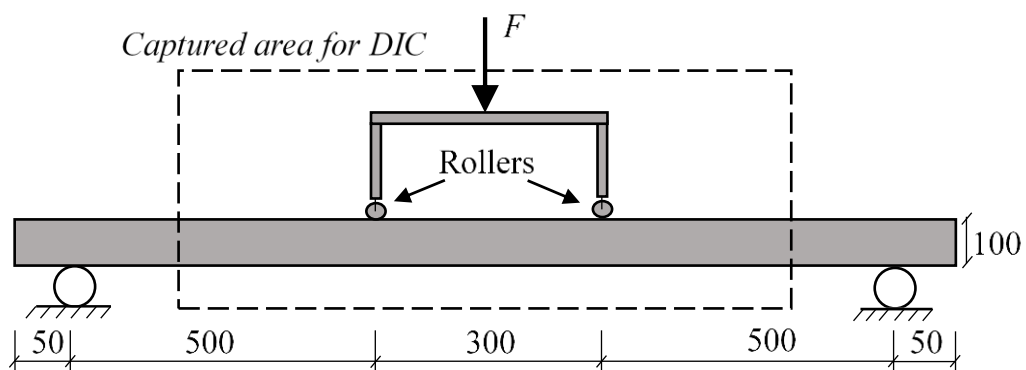


Figure 7.11 Static test set-up, four point bending. Modified from Jönsson and Stenseke (2018).



Figure 7.12 Photo of static test set-up with three point bending.



Figure 7.13 Photo of static test set-up with four point bending (picture taken from the back).

7.1.8 Digital image correlation

To analyse the structural behaviour of the dynamically and statically tested beams the frames collected by the cameras during the tests were processed by digital image correlation (DIC). This is an optical non-contact method that utilizes the stochastic pattern painted on the beams to describe discrete image areas. Structural behaviour such as for example deformation or strain can be determined from these images. The DIC

analysis was made using the programme GOM Correlate Professional 2018 (GOM, 2018).

7.2 Reinforcement Testing Description

An investigation was made on the properties of the reinforcement in order to further understand how it influences the behaviour of the beams. This was made through tensile tests on undamaged reinforcement and on reinforcement that was damaged in different ways. Moreover, an investigation of the strain rate at testing was performed to further understand the meaning of the measured values.

7.2.1 Modifications of the reinforcement

To understand the structural behaviour of damaged reinforcement better, tensile tests were performed on normal (undamaged), pre-stretched and bent bars. The mechanical properties for the bars were tested on six undamaged bars, six pre-stretched bars and 18 bent bars. The pre-stretched specimens were extracted from the bars that were pre-stretched for the beams. The group of bent bars was divided into three subgroups of equal quantity (six per group), where the bars in the first group were bent and re-bent once. The second group was bent and re-bent twice, and the last group was bent and re-bent four times.

7.2.1.1 Pre-stretching

A number of 14 uncut, 6 m long bars were pre-stretched using a hydraulic pump from Enepac (model SPR 36 0 E8) and a hydraulic cylinder that performed the stretching. The setup is depicted in Figure 7.14. The bar was anchored as depicted in Figure 7.15.



Figure 7.14 Setup for the pre-stretching of the reinforcement.



Figure 7.15 Anchorage of the reinforcement bar at a) end 1 and b) end 2.

The target plastic strain of the pre-stretched bars was 3 %. The resulting plastic strains were within an interval of 2.95 % and 3.04 %, as seen in Table 7.6. The bars marked with an asterisk had a too large plastic strain which is why they were excluded and two new bars were stretched to a value closer to 3 %. The resulting plastic strain was measured based on the total length of the bar.

Table 7.6 Plastic strain, $\epsilon_{s,pl}$, of the pre-stretched bars. The bars marked with an asterisk had a too large plastic strain and were excluded from the experiments.

Bar	$\epsilon_{s,pl}$ [%]	Bar	$\epsilon_{s,pl}$ [%]
1	2.97	8	3.00
2*	3.09	9*	3.06
3	3.00	10	3.04
4	3.03	11	2.95
5	2.97	12	2.97
6	3.03	13	2.98
7	2.96	14	2.97

After the stretching was performed, three 1 410 mm bars were cut from each stretched bar for the beams. As there were bent parts at the ends that were not desired to be used they were cut off as shown in Figure 7.16 and Figure 7.17. The bending of the end parts came from the tilting of the ground anchors as the bar was stretched; this is shown in Figure 7.18. There was enough material on each stretched bar to retrieve one specimen for the material tests later performed.



Figure 7.16 At the cylinder end 900 mm were cut off the bar.



Figure 7.17 At the other end 200 mm were cut off the bar.



Figure 7.18 Photograph of how one of the ground anchors tilted due to the stretching of the steel bar.

7.2.1.2 Bending

The bending was made in accordance with CEN (2016), bending around a mandrel using a clamp. The mandrel had a diameter of 71 mm, which equals 11.8ϕ . The aim of the angle of the bend was 90° and the resulting angle of a representative specimen can be seen in Figure 7.19, along with the general setup of the bending.



Figure 7.19 Resulting shape of a representative bar specimen after bending.

The bending was performed using a tube with an inner diameter of 11 mm to control the bending as seen in Figure 7.20.

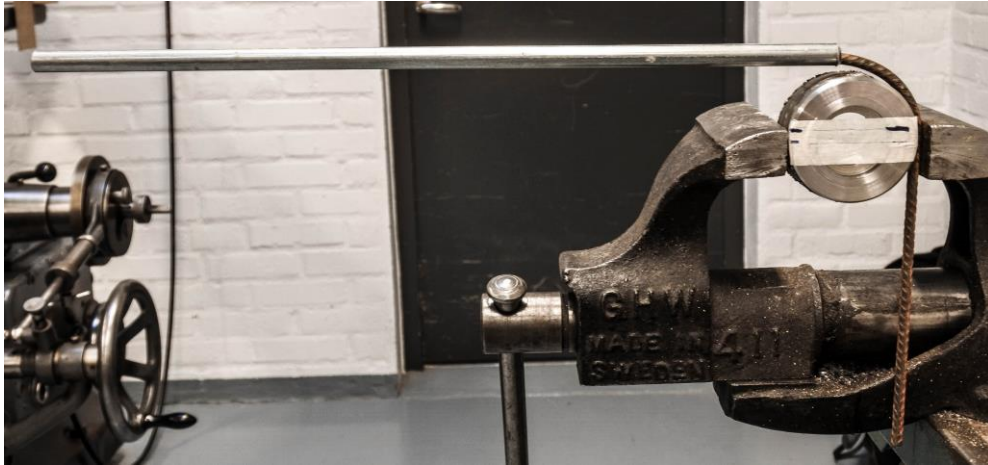


Figure 7.20 Photograph of the tube used for the bending.

After the bar was bent it was turned 180° horizontally to perform the re-bending using the same mandrel, the position was assured by marking the bar before moving it. The position can be seen in Figure 7.21.

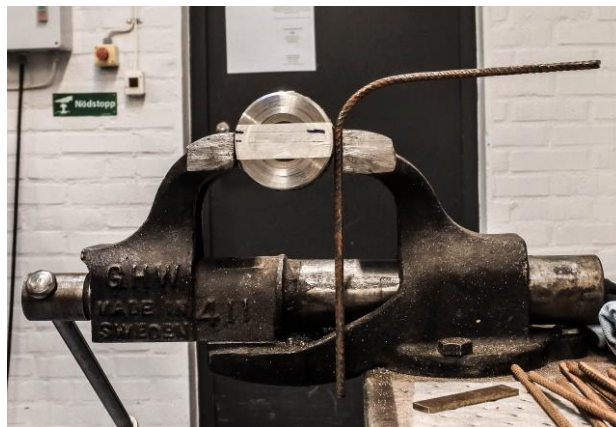


Figure 7.21 Position of bar specimen for re-bending.

The re-bending of the specimens was aimed for making the bars as straight as possible to fit in the grips of the testing machine and to reduce the impact of the straightening of the bar in the stress-strain curves. The resulting straightness of a representative specimen can be seen in Figure 7.22. The bending and re-bending was made one time for six bars, two times for another six bars and lastly four times for the last group of six bars.



Figure 7.22 Straightness of a representative bar specimen that has been re-bent.

7.2.2 Testing procedure

The tensile testing was performed for bar specimens that were 400 mm long. The parallel length of the bar was 300 mm (the length between the grips in the machine). The tests were performed using an MTS 380 machine. The tests were deformation controlled, with two different strain rates for different stages of the stress-strain curve according to proposed strain rates in CEN (2016). It was also of interest to investigate what influence the testing speed would have on the results. Therefore, another deformation rate was also used, which was slower than that proposed by CEN (2016). The different speed levels used in the testing are presented in detail in Table 7.7. The properties of interest were the modulus of elasticity, yield strength, tensile strength and ultimate strain.

Table 7.7 Speed used in the testing of the reinforcement properties.

Type	Stage	Deformation speed [mm/min]	Strain rate [s^{-1}]
Normal	1	5	$2.8 \cdot 10^{-4}$
	2	120	$67 \cdot 10^{-4}$
Slow	1	0.5	$0.28 \cdot 10^{-4}$
	2	4	$2.2 \cdot 10^{-4}$

To get more accurate results of the elastic and initial yielding part of the stress-strain curve an extensometer was used of model MTS 634.25F-24 with serial number 10504454C. It was removed at 10 mm, 15 mm and 20 mm deformation for different groups of bars.

8 Predictions

This chapter presents the expected behaviour of the beams tested both under dynamic and static loading. The material properties used in these calculations are the measured mean values that are presented in Section 9.1 and 9.2, to get a behaviour that would reflect the beams used in the tests more accurately.

8.1 Static response

The static tests in the experimental part of this project were performed in two different ways; using three-point or four-point bending. Therefore, predictions were made for both cases. The responses of interest for later comparison with experimental results are load and moment in ultimate limit state (ULS), cracking and yielding and lastly the general behaviour is presented by load-deflection curves. The calculations for the static response are made using the software Mathcad 15.0 and are presented in Appendix N.

8.1.1 Ultimate limit state

In ULS, it is assumed that the ultimate concrete strain, $\varepsilon_{cu} = 3.5 \text{ ‰}$, is reached. Furthermore, a linear strain distribution is assumed over the cross-section. It is also assumed that the stress distribution in the compressive zone follows an idealised parabolic-rectangular stress-strain relationship. The strain and stress distributions at failure are illustrated in Figure 8.1.

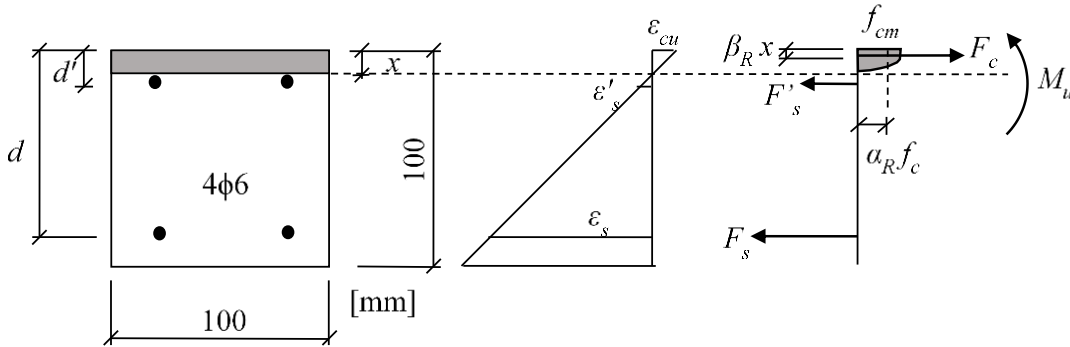


Figure 8.1 Assumed response in ULS. Modified from Lozano and Makdesi (2017).

Both Lozano and Makdesi (2017) and Jönsson and Stenseke (2018), who used the same cross-section as in this project, observed that the height of the compressive zone was lower than the concrete cover in ULS, meaning that the top reinforcement was subjected to tensile stresses. Therefore, these calculations are based on that assumption, which was later confirmed. Furthermore, the equilibrium conditions for the cross-section are

$$\alpha_R \cdot f_{cm} \cdot b \cdot x = \sigma_s \cdot A_s + \sigma'_s \cdot A'_s \quad (8.1)$$

$$M_u = \alpha_R \cdot f_{cm} \cdot b \cdot x \cdot (d - \beta_R \cdot x) - \sigma'_s \cdot A'_s \cdot (d - d') \quad (8.2)$$

The stress block factors used in ULS are

$$\alpha_R = 0.81 \quad (8.3)$$

$$\beta_R = 0.42 \quad (8.4)$$

The steel strains were determined from the geometry of the cross-section and the concrete strain as

$$\varepsilon_s = \frac{d - x}{x} \cdot \varepsilon_{cu} \quad (8.5)$$

$$\varepsilon'_s = \frac{d' - x}{x} \cdot \varepsilon_{cu} \quad (8.6)$$

The reinforcement stresses were determined from these strains using a bilinear relationship based on the measured values of the reinforcement used in the experiments (i.e. considering strain hardening effects), as

$$\sigma_s = \begin{cases} E_{sm} \cdot \varepsilon_s & \text{if } \varepsilon_s \leq \varepsilon_{sy} \\ f_{ym} + \frac{\varepsilon_s - \varepsilon_{sy}}{\varepsilon_{su} - \varepsilon_{sy}} (f_{tm} - f_{ym}) & \text{if } \varepsilon_s > \varepsilon_{sy} \end{cases} \quad (8.7)$$

Lastly, the ultimate load was determined from the moment in Equation (8.2). The value for three point bending was determined as

$$F_{u,3P} = \frac{4 \cdot M_u}{L} \quad (8.8)$$

and the value for four point bending as

$$F_{u,4P} = 2 \cdot \frac{M_u}{a} \quad (8.9)$$

where a is the distance between support and load application which is 0.5 m in this case. The factor 2 in Equation (8.9) results in F_u being the applied load from both point loads, which is the value retrieved from the experiments. In Equation (8.8) and (8.9) the self-weight of the beam has been disregarded due to its low impact.

The resulting ultimate moment and load are presented in Table 8.1 for three point bending and Table 8.2 for four point bending. The calculations were also made disregarding the top reinforcement, which were used in the later calculations of the rotation capacity since those are based on a cross-section with top reinforcement subjected to compressive stresses or without top reinforcement. Furthermore, the calculations were made using material properties of the undamaged and pre-stretched reinforcement measured, see Section 9.2.

Table 8.1 Moment and load capacity in ultimate limit state for different reinforcement cases for three point bending.

Reinforcement	Layers of reinforcement	M_u [kNm]	F_u [kN]
Undamaged	Top and bottom	2.49	7.68
	Only bottom	2.43	7.48
Damaged	Top and bottom	2.78	8.56
	Only bottom	2.73	8.40

Table 8.2 Moment and load capacity in ultimate limit state for different reinforcement cases for four point bending.

Reinforcement	Layers of reinforcement	M_u [kNm]	F_u [kN]
Undamaged	Top and bottom	2.49	9.98
	Only bottom	2.43	9.73
Damaged	Top and bottom	2.78	11.13
	Only bottom	2.73	10.92

8.1.2 Cracking

For the state of cracking the applied moment was determined as

$$M_{cr} = \frac{f_{ct,fl} \cdot I_I}{h/2} \quad (8.10)$$

using the flexural tensile concrete strength, $f_{ct,fl}$. Then, the cracking force was determined in the same manner as in ULS, using Equation (8.8) or (8.9), though M_{cr} was inserted. The resulting cracking moment and load are presented in Table 8.3.

Table 8.3 Moment and load at cracking for different loading and reinforcement cases.

Loading case	Reinforcement	M_{cr} [kNm]	F_{cr} [kN]
Three point bending	Undamaged	1.03	3.18
	Damaged	1.03	3.17
Four point bending	Undamaged	1.03	4.13
	Damaged	1.03	4.12

8.1.3 Yielding

The moment at onset of yielding was calculated in a similar manner as in ULS, though the top reinforcement was contributing to the compressive part of the cross-section. Here, the concrete strain was unknown, $\varepsilon_{cc} < \varepsilon_{cu}$, while the steel strain in the bottom reinforcement layer was known. At yielding, the stress block factors, α_R and β_R , were unknown, which is why an iterative process of determining the height of the

compressive zone was used. Initially, the position of the neutral axis was assumed, then, the concrete and top reinforcement strains were calculated as

$$\varepsilon_{cc,y} = \frac{x_y}{d - x_y} \cdot \varepsilon_{sy} \quad (8.11)$$

$$\varepsilon'_{sy} = \frac{x_y - d'}{x_y} \cdot \varepsilon_{cc,y} \quad (8.12)$$

Then, the stress block factors were determined and the condition for horizontal equilibrium was checked. The position of the neutral axis was adjusted until the horizontal equilibrium was fulfilled. Then, the yielding moment and load were determined for both three and four point bending, the results are presented in Table 8.4 and Table 8.5, respectively.

Table 8.4 *Moment and load at yielding for different reinforcement cases for three point bending.*

Reinforcement	Layers of reinforcement	M_y [kNm]	F_y [kN]
Undamaged	Top and bottom	2.26	6.95
	Only bottom	2.27	6.98
Damaged	Top and bottom	2.62	8.07
	Only bottom	2.63	8.09

Table 8.5 *Moment and load at yielding for different reinforcement cases for four point bending.*

Reinforcement	Layers of reinforcement	M_y [kNm]	F_y [kN]
Undamaged	Top and bottom	2.26	9.04
	Only bottom	2.27	9.07
Damaged	Top and bottom	2.62	10.49
	Only bottom	2.63	10.52

8.1.4 Load-deflection curves

In order to determine the expected load-deflection curves, the stiffnesses in state I and II are needed. The stiffness for three point bending is determined according to Equation (8.13) and that for four point bending according to Equation (8.14). In these equations, the second moment of inertia, I , can be inserted using either the value for state I or II which results in the stiffness for state I or II, respectively.

$$k_{3P} = \frac{48 \cdot E_{cm} \cdot I}{L^3} \quad (8.13)$$

$$k_{4P} = \frac{48 \cdot E_{cm} \cdot I}{a \cdot L^2 \left(3 - \frac{4a^2}{L^2} \right)} \quad (8.14)$$

The response is then presented using a bilinear and a trilinear load-deflection curve, where the trilinear curve takes cracking into account. The beam was assumed to be plastic after the ultimate load was reached. The load deflection curves for the four cases studied in this project are presented in Figure 8.2 and Figure 8.3. Lastly, the calculated stiffnesses are presented in Table 8.6. The ultimate load levels presented here are used in the 2DOF calculations in Section 8.3.1, and there called R_2 Predicted.

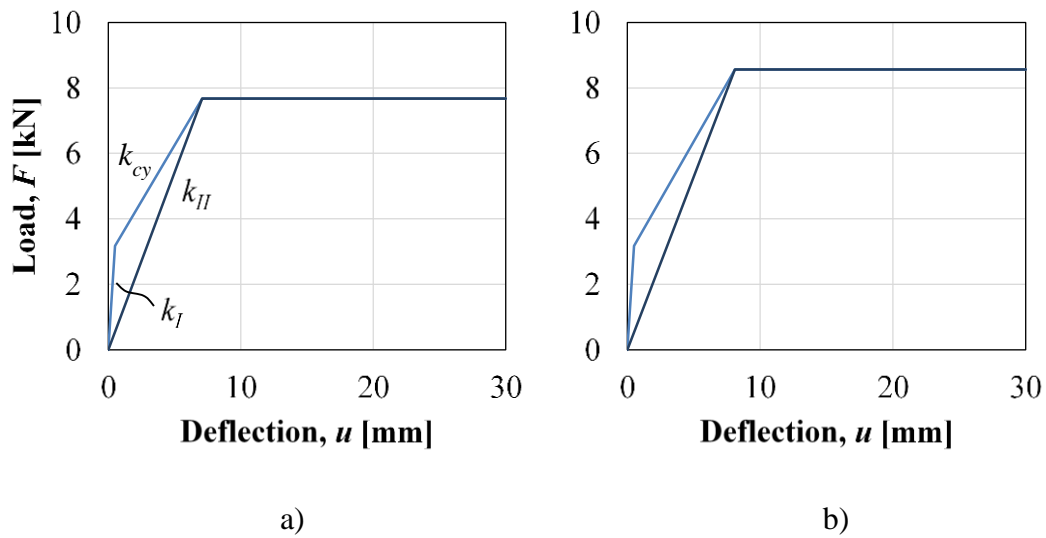


Figure 8.2 Load-deflection curve for three point bending for a) undamaged reinforcement and b) damaged reinforcement.

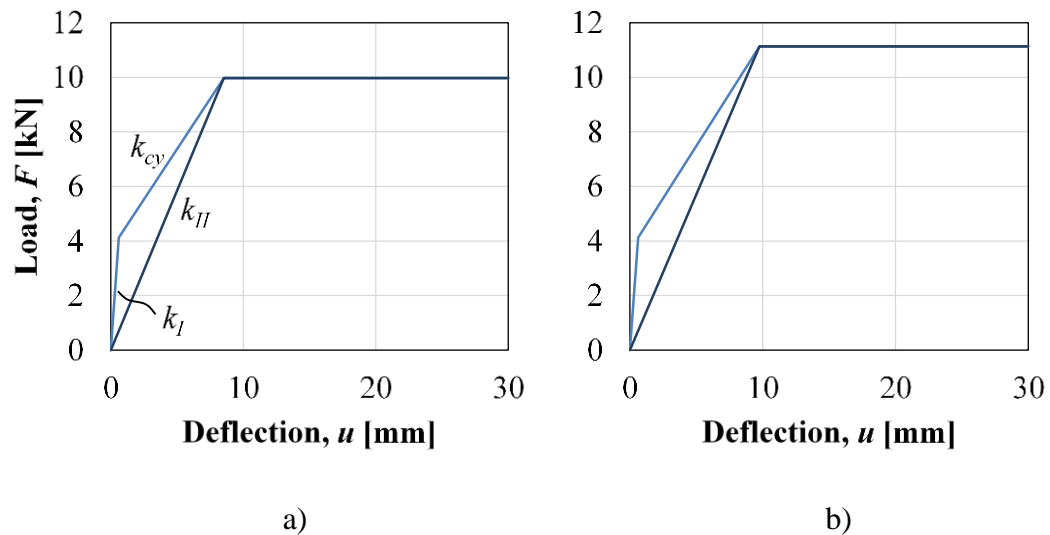


Figure 8.3 Load-deflection curve for four point bending for a) undamaged reinforcement and b) damaged reinforcement.

Table 8.6 Expected stiffnesses based on loading case and reinforcement properties.

Loading case	Reinforcement	k_I [MN/m]	k_{cy} [MN/m]	k_{II} [MN/m]
Three point bending	Undamaged	6.11	0.684	1.08
	Damaged	6.10	0.710	1.06
Four point bending	Undamaged	6.60	0.738	1.17
	Damaged	6.59	0.766	1.14

Futhermore, the moment ratios, η_M , for different reinforcement cases are presented in Table 8.7.

Table 8.7 Moment ratio for different reinforcement cases.

Reinforcement	Layers of reinforcement	M_y / M_y [kNm]
Undamaged	Top and bottom	1.10
	Only bottom	1.07
Damaged	Top and bottom	1.06
	Only bottom	1.04

8.2 Rotation capacity

As previously mentioned, the methods of predicting the rotation capacity are based on a cross-section with top reinforcement subjected to compressive stresses, however, that was not the case here. Therefore, the values used in these calculations were those disregarding the top reinforcement. The calculation were made in Mathcad 15.0 and are presented in Appendix N.

8.2.1 Bk25

The calculations using the Bk25 method were performed in accordance with Section 4.3.1. The calculated values are presented in Table 8.8.

Table 8.8 Expected plastic rotation capacity and plastic deformation according to Bk25.

Loading case	Reinforcement	θ_{pl} [mrad]	u_{pl} [mm]
Three point bending	Undamaged	69.2	45.0
	Damaged	59.5	38.7
Four point bending	Undamaged	69.2	34.6
	Damaged	59.5	29.8

8.2.2 Eurocode 2

The calculations using the Eurocode 2-method were performed in accordance with Section 4.3.2. The values of plastic rotation for Eurocode 2 were divided by two to compare with the results obtained from Bk25 and the experiments. The calculated values are presented in Table 8.9. The calculations for damaged rebars are based on

both class C and B reinforcement. The pre-stretched reinforcement does not fulfil the ductility requirements for any of the reinforcement classes, see Table 2.1 and Table 9.3. However, only class B and C are to be used in a plastic analysis according to Eurocode 2, which is why the calculations were made for these two classes.

Table 8.9 Expected plastic rotation capacity and plastic deformation according to Eurocode 2.

Loading case	Reinforcement	θ_{pl} [mrad]	u_{pl} [mm]
Three point bending	Undamaged	23.0	15.0
	Damaged – class B	11.1	7.22
	Damaged – class C	22.2	14.4
Four point bending	Undamaged	20.2	10.1
	Damaged – class B	9.74	4.87
	Damaged – class C	19.5	9.74

8.2.3 Comparison

The values obtained for the plastic rotation capacity are quite different in magnitude. This is assumed to partly be due to the difference in loading conditions. Bk25 is based on a uniformly distributed load. This results in a more favourable moment distribution and thereby a longer plastic hinge length, than for a case of point load in the middle of the span, which is the case for Eurocode 2.

8.3 Dynamic response

The predictions of the dynamic response are mostly made using the 2DOF model, additionally, calculations of the initial shear velocities are presented.

8.3.1 2DOF

The predictions using the 2DOF model were made in accordance with Chapter 6. The calculations were performed in the software Matlab R2016b and the script, based on the one written by Lozano and Makdesi (2017), is presented in Appendix M.

8.3.1.1 Input data

The input data for the 2DOF model is presented in Table 8.10. The velocity is determined by a mean value of the velocity during the 3 ms before impact for all the beams from the DIC analysis. This is presented in Section 9.3.3. The internal resistance of the drop-weight, R_I , and the stiffness of the spring between drop-weight and beam, k_I , are determined according to Hertz contact theory, explained in Section 6.4.2 and Appendix A, and determined from a convergence study, see Appendix B. The value of the stiffness of the beam is the one calculated for state II in Section 8.1.4. The density used is the one measured during testing of the material properties of the concrete, see Section 9.1. The mass of the reinforcement is disregarded in the density, however, it has a small impact in these tests. Lastly, there were two input data parameters that were varied depending on the loading and reinforcement case etc. The internal resistance of the beam, R_2 , was determined according to the ultimate load for three point bending in

Section 8.1.1 for both undamaged and damaged reinforcement. This was compared to the behaviour when the measured value of the ultimate load during the experimental static tests was used, from Section 9.4.2, this value was also taken for both undamaged and damaged reinforcement. The second parameter that was varied was the mass of the drop-weight, varying from 10 kg to 20 kg, as in the experiments.

Table 8.10 Input data for the 2DOF-model.

Parameter	Description	Value
v_0 [m/s]	Initial velocity of drop-weight	9.84
$R_{1,10}$ [kN]	Internal resistance of 10 kg-drop-weight	50
$k_{1,10}$ [N/m]	Stiffness of the spring between drop-weight and beam for 10 kg-drop-weight	$2.38 \cdot 10^8$
$R_{1,20}$ [kN]	Internal resistance of 20 kg-drop-weight	70
$k_{1,20}$ [N/m]	Stiffness of the spring between drop-weight and beam for 20 kg-drop-weight	$2.69 \cdot 10^8$
k_2 [N/m]	Stiffness of the beam spring	$1.08 \cdot 10^6$
ρ [kg/m ³]	Density of the beam	2 420

The results of the 2DOF model were solved using the central difference method described in Section 6.5. To get the starting step for solving the central difference method, $\dot{\mathbf{u}}_0$ was put into Equation (6.40) as load together with

$$\mathbf{u}_0 = 0 \quad (8.15)$$

$$\ddot{\mathbf{u}}_0 = 0 \quad (8.16)$$

8.3.1.2 Results

The maximum and plastic deflections of body 2, the beam, are tabulated in Table 8.11. The deflection of the beam and the velocity of the drop-weight at impact are presented in Figure 8.4 to Figure 8.7 for all the series.

Table 8.11 Predicted deflections with the 2DOF-model.

Drop-weight [kg]	Reinforcement	R_2 [kN]		u_{max} [mm]	u_{pl} [mm]
10	Undamaged	Predicted	7.68	35.0	28.1
		Measured	9.00	30.8	22.6
	Damaged	Predicted	8.56	32.0	24.2
		Measured	9.50	29.5	20.9
20	Undamaged	Predicted	7.68	88.8	81.9
		Measured	9.00	76.6	68.4
	Damaged	Predicted	8.56	80.2	72.4
		Measured	9.50	72.9	64.2

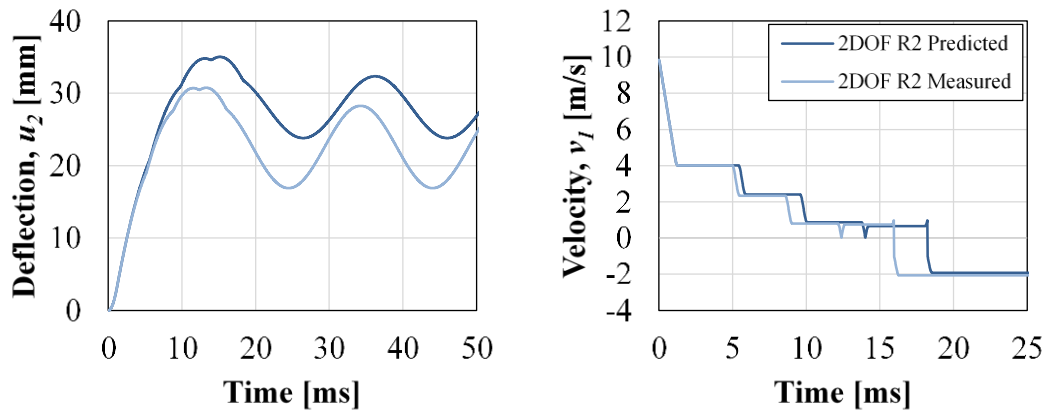


Figure 8.4 Deflection of beam, u_2 , and velocity of drop-weight, v_1 , after impact for I10-UD in 2DOF-model.

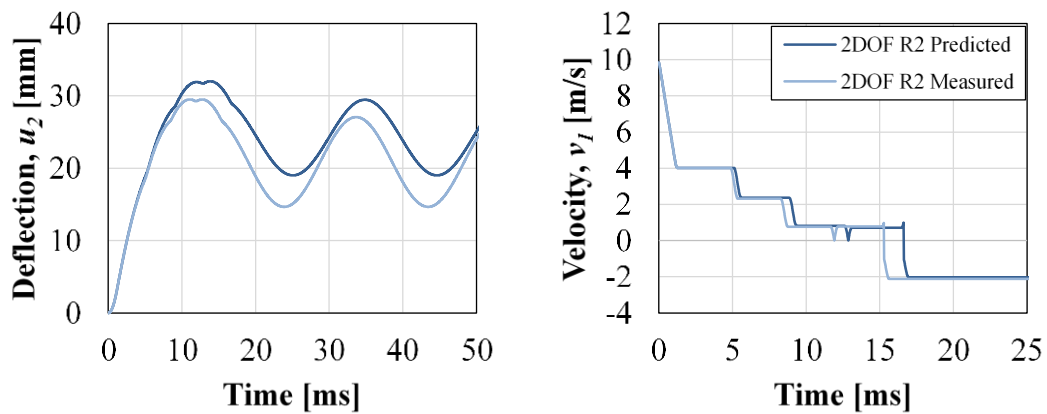


Figure 8.5 Deflection of beam, u_2 , and velocity of drop-weight, v_1 , after impact for I10-D in 2DOF-model.

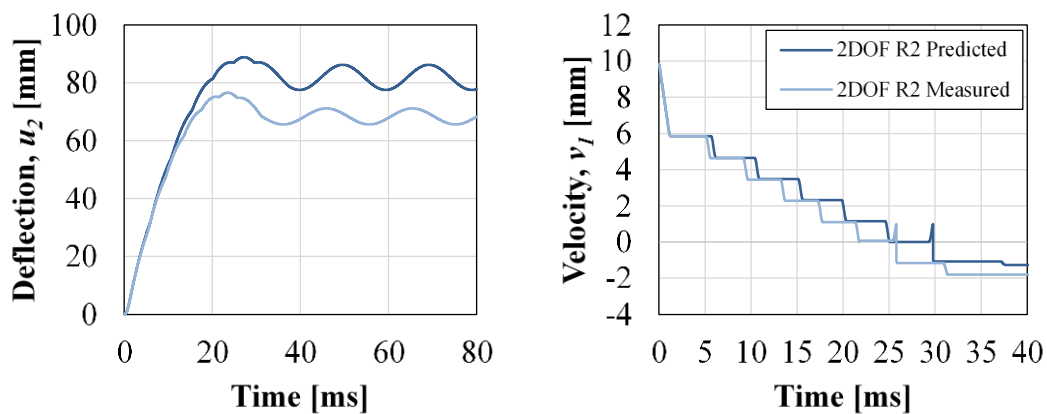


Figure 8.6 Deflection of beam, u_2 , and velocity of drop-weight, v_1 , after impact for I20-UD in 2DOF-model.

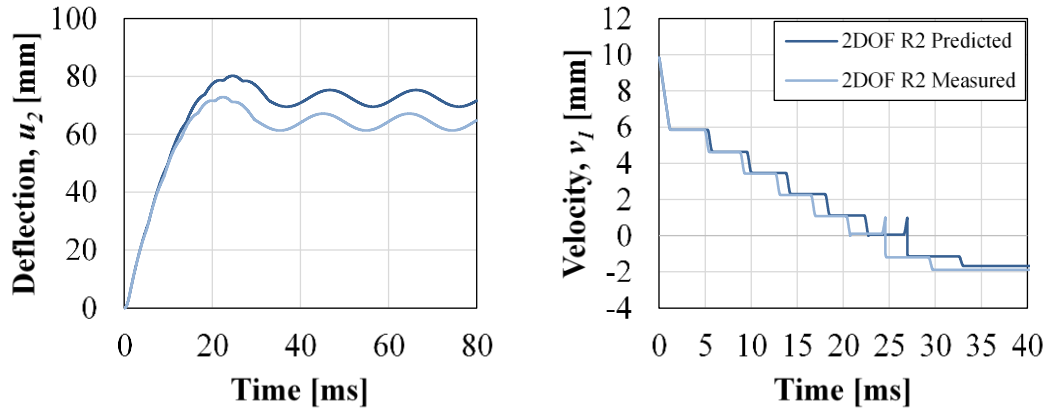


Figure 8.7 Deflection of beam, u_2 , and velocity of drop-weight, v_1 , after impact for I20-D in 2DOF-model.

When using the predicted R_2 the deflections become greater since the predicted beam resistance is less than the measured one. This is evident in all the deflection-time curves.

The beams with damaged reinforcement present slightly smaller deflections than the ones with undamaged reinforcement. This holds for both the I10 and I20-series.

8.3.2 Initial shear velocity

The shear wave propagation is studied by Yi, Zhao and Kunnath (2016) where a time, t_0 , is proposed as the time it takes for the active portion of the beam to span the entire beam. The definition of active part is illustrated in Figure 8.8.



Figure 8.8 Illustration of active and inactive part of the beam span.

The time, t_0 is given as

$$t_0 = \frac{L_0}{2v_s} \quad (8.17)$$

where L_0 is the span of the beam and v_s is determined as

$$v_s = \sqrt{\frac{G}{\rho}} \quad (8.18)$$

where ρ is the density and G is the shear modulus, determined from the modulus of elasticity, E , and Poisson's ratio, ν , as

$$G = \frac{E}{2(1 + \nu)} \quad (8.19)$$

The parameters used and the resulting t_0 are presented in Table 8.12. The detailed calculations are presented in Appendix N.

Table 8.12 Parameters for calculating shear velocity and resulting t_0 .

Parameter	Value
ρ	2420 kg
G	13.1 GPa
L_0	1.3 m
t_0	0.28 ms

9 Experimental results

Presented in this chapter are the results from the experiments performed on concrete and reinforcement material properties and the structural response of the beams under both dynamic and static loading. Note that in this section damaged reinforcement refers to pre-stretched reinforcement.

9.1 Hardened concrete properties

The testing of the hardened concrete was made in accordance with Section 7.1.5 and the results are presented in Table 9.1. For more detailed results see Appendix C. There are no apparent differences between the two batches, therefore, they are not expected to behave differently in the beams either. The observant reader sees that the compressive strength in batch 2 is somewhat lowered from 27 to 28 days after casting. This is assumed to be a coincidence and there were probably cubes in the higher range of the normal distribution curve tested on day 27, rather than that the strength would have lowered. The average cube compressive strengths between the batches are the same for day 27 and 28 which is a reasonable behaviour of concrete.

Table 9.1 Experimentally determined average values of concrete properties.

Property	Description	Batch 1	Batch 2	Average
$f_{cm,cube,27}$	Mean compressive cube strength after 27 days [MPa]	40.2	42.2	41.2
$f_{cm,cube,28}$	Mean compressive cube strength after 28 days [MPa]	41.0	41.3	41.2
$f_{ctm,sp,27}$	Mean splitting tensile strength after 27 days [MPa]	4.94	4.90	4.92
ρ	Density [kg/m ³]	2 420	2 410	2 420
$G_{f,28}$	Fracture energy after 28 days [Nm/m ²]	112	114	113

Then, the measured cube properties were transformed into cylinder properties according to Section 2.5.2. These values are presented in Table 9.2 and are the ones used in the calculations made.

Table 9.2 Calculated cylinder properties of concrete.

Property	Description	Average
$f_{cm,27}$	Mean compressive strength after 27 days [MPa]	33.0
$f_{cm,28}$	Mean compressive strength after 28 days [MPa]	32.9
$f_{ctm,27}$	Mean tensile strength after 27 days [MPa]	4.43
$E_{cm,27}$	Modulus of elasticity after 27 days [GPa]	31.5
$E_{cm,28}$	Modulus of elasticity after 28 days [GPa]	31.5

9.2 Reinforcement test results

The testing of the reinforcement was made in accordance with Section 7.2. The detailed results including properties of all bars can be seen in Appendix D. In the charts in this section, representative bars have been used, and the relation used is stated in the appendix. The values of the properties in the tables are presented using mean values.

9.2.1 Undamaged vs damaged reinforcement

In the testing, values of proof stress, $f_{0.2}$ [MPa], ultimate stress, f_u [MPa], ultimate strain, ϵ_u [%], and modulus of elasticity, E [GPa], were measured and are presented in Table 9.3 for the undamaged and damaged reinforcement. In the table, the $f_u / f_{0.2}$ ratio is also presented. The stress-strain curves of the undamaged and pre-stretched reinforcement are presented in Figure 9.1. The increase of yield stress and loss of ductility is clear from this chart. One observation for the pre-stretched reinforcement in Table 9.3 is that the η_f ratio is lower than what is accepted for all three ductility categories for reinforcement, presented in Table 2.1.

Table 9.3 Material properties for the different types of reinforcement.

Reinforcement	$f_{0.2}$ [MPa]	f_u [MPa]	ϵ_u [%]	E [GPa]	$f_u / f_{0.2}$ [-]
Undamaged	555	656	9.38	202	1.18
Pre-stretched	645	664	5.80	196	1.03
Bent one time	553	651	8.29	166	1.18
Bent two times	556	649	7.58	133	1.17
Bent four times	554	645	6.97	146	1.16

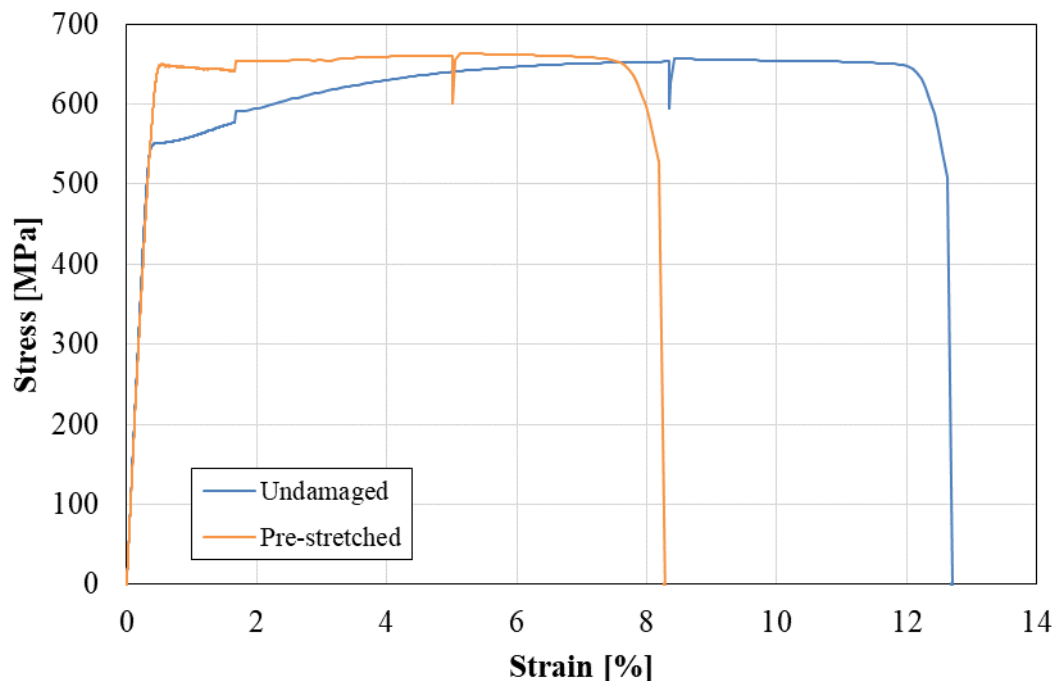


Figure 9.1 Stress-strain curves for undamaged and pre-stretched reinforcement.

The stress-strain curves for undamaged and bent reinforcement are presented in Figure 9.2. The bent reinforcement showed a slightly softer behaviour by the end of the elastic range, which is assumed to come from the straightening of the slight bend that remained. This made it unreasonable to use the proof stress since it resulted in very low values when it is clear in the chart that yielding is at the same level as for the undamaged bars. Therefore, the yield stress for the bent bars were taken as the stress at the plateau seen in the chart. Moreover, it does not seem to be any apparent differences of the yield stress between the undamaged and bent bars, though the ultimate stress and strain are both lowered proportionally to the amount of bendings. Furthermore, the moduli of elasticity appear to differ for the different groups of bars, which is not visible in the graphs. This is assumed to be due to the fact that the extensometer is more sensitive to the straightening of the bar than the values from the machine, which are the values that the graphs are based on. This is further commented on in Appendix D.

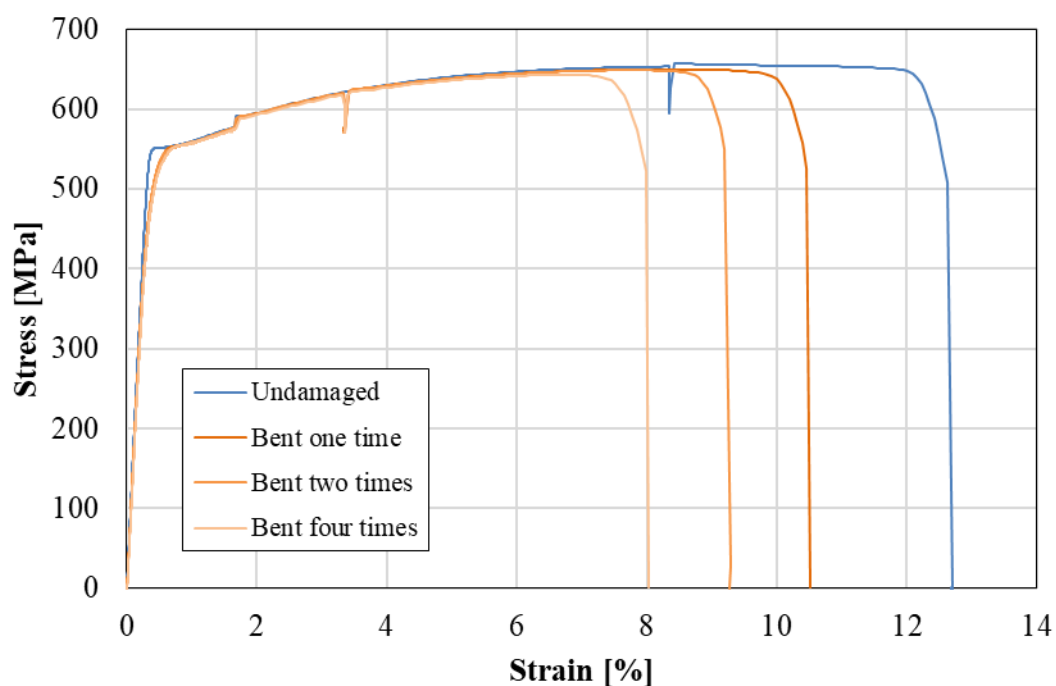


Figure 9.2 Stress-strain curves for undamaged and bent reinforcement.

9.2.2 Variation of testing speed

The difference in properties and stress-strain relationship for the two speeds introduced in Section 7.2.2 can be seen in Table 9.4 and Figure 9.3, respectively. Note that the group called fast here is the same as the one called undamaged in the previous section. This is the speed recommended by CEN (2016). It is apparent here that there is a slight decrease in all the properties (except for the modulus of elasticity), this decrease is of about 1.5 – 2.0 % depending on which property is studied.

Table 9.4 Material properties based on testing speed.

Reinforcement	$f_{0.2}$ [MPa]	f_u [MPa]	ϵ_u [%]	E [GPa]	$f_u / f_{0.2}$ [-]
Fast	555	656	9.38	202	1.18
Slow	546	643	9.24	203	1.18

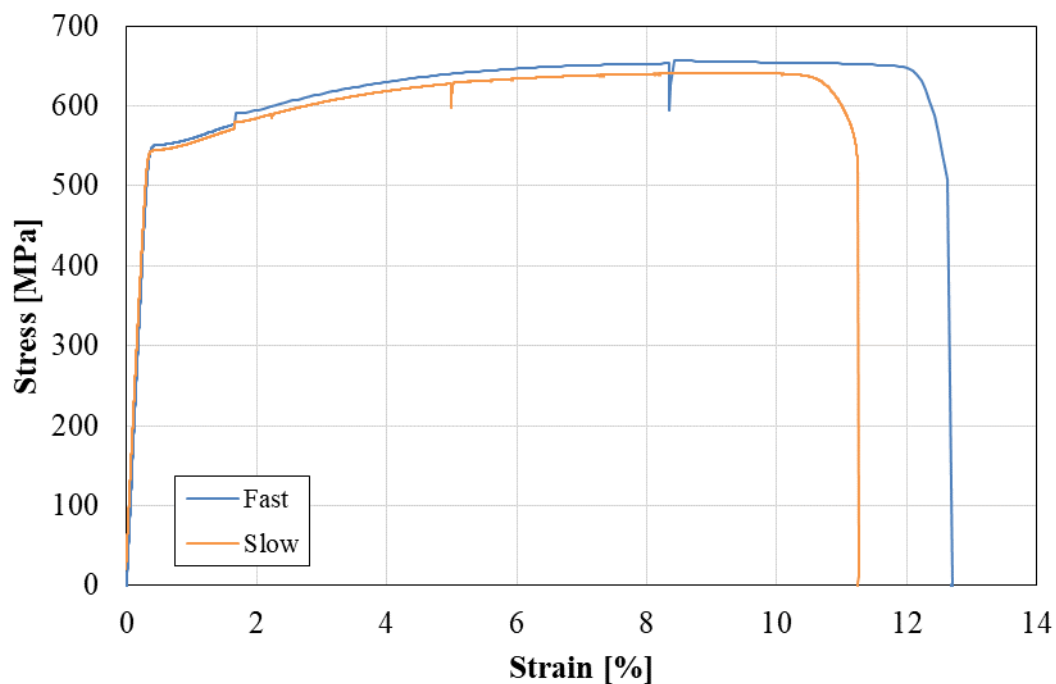


Figure 9.3 Stress-strain curves for reinforcement specimens tested with different speed.

9.3 Dynamic testing of beams

This section treats the drop-weight testing of the beams. The results are based on the high speed camera used. The films from the high speed camera were processed and retrieved from GOM Correlate Professional 2018. The section treats the force at impact, the midpoint deflection over time, the initial deformed shape of the beams, the velocities of the initial deflections and lastly the crack patterns on the concrete face.

9.3.1 Method

Initially, a study was made in the mesh of the surface component in GOM Correlate, to get clear results. This investigation is presented in Appendix E. It resulted in a facet size of 15 pixels and a point distance of 5 pixels for this project, which gave readable strain fields. The strain fields were displayed against the reference stage, namely the first picture in the film.

Then, surface points were applied straight under the drop-weight and over the support in mid-height of the beam to extract the beam deflections. The deflection in the middle of the span, u_{mid} , were then analysed relative the support point, u_{sup} ; i.e. all deflections given here have been adjusted as

$$u(t) = u_{mid}(t) - u_{sup}(t) \quad (9.1)$$

To analyse the deformed shape of the beam a section was created through the beam at mid-height along the horizontal axis. The deformations were extracted at different time steps.

Lastly, three facet points were set on the drop-weight, close to the head, where the acceleration and velocity were extracted.

These steps were made for all the beams, except for the facet analysis, which was only made once.

9.3.2 Applied force and impulse

The force from the drop-weight and its corresponding impulse are presented within this section. The force was established from the acceleration in several points on the drop-weight in GOM Correlate. An average value was taken from these points in order to get rid of the noise in this process, also observed by Jönsson and Stenseke (2018).

9.3.2.1 Series I10-UD

The peak force and impulse on series I10-UD are presented in Table 9.5. The impact is taken as the integral of the peak in the force-time curve, which is presented in Figure 9.4. The highspeed camera may not have captured the actual peak acceleration in these tests, it may have occurred between two frames which is why trend lines are presented of the peaks to get a better understanding of how the curve could be assumed to look if more frames had been captured per second. Note therefore that the peak loads

presented in the table may not be the actual peak load, but the highest one captured with the camera. An alternative method to determine this can be found in Appendix F.

Table 9.5 *Impact force and impulse for series I10-UD.*

Beam	F [kN]	I [Ns]
I10-UD-B1-07	97.6	53.7
I10-UD-B1-08	95.2	55.9
I10-UD-B1-09	96.9	53.7
Average	96.6	54.5

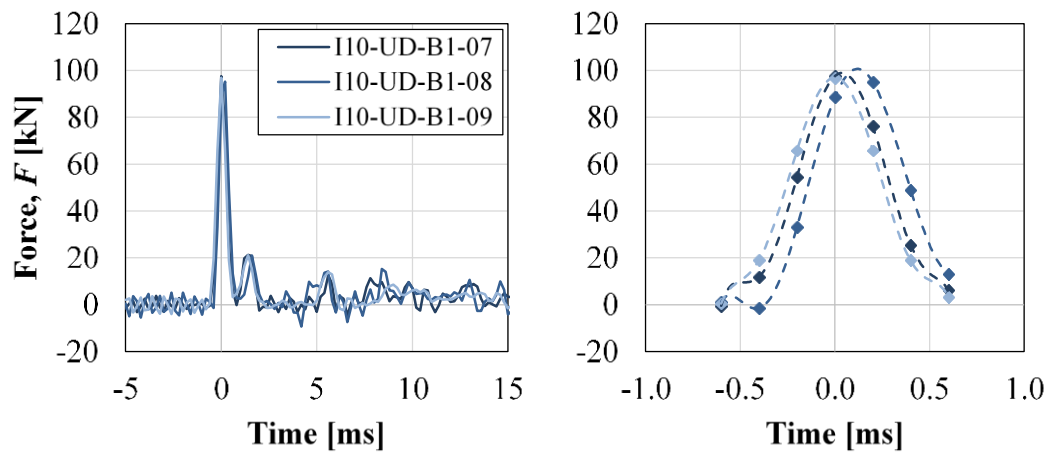


Figure 9.4 *Applied force of series I10-UD. The diagram to the right is zoomed in on the peak of the left one. Dashed lines are trendlines for each beam with corresponding shade.*

9.3.2.2 Series I10-D

The peak force and impulse on series I10-D are presented in Table 9.6. The force-time curve is presented in Figure 9.5.

Table 9.6 *Impact force and impulse for series I10-D.*

Beam	F [kN]	I [Ns]
I10-D-B1-10	99.6	53.5
I10-D-B1-11	92.2	52.9
I10-D-B1-12	96.7	53.4
Average	96.2	53.2

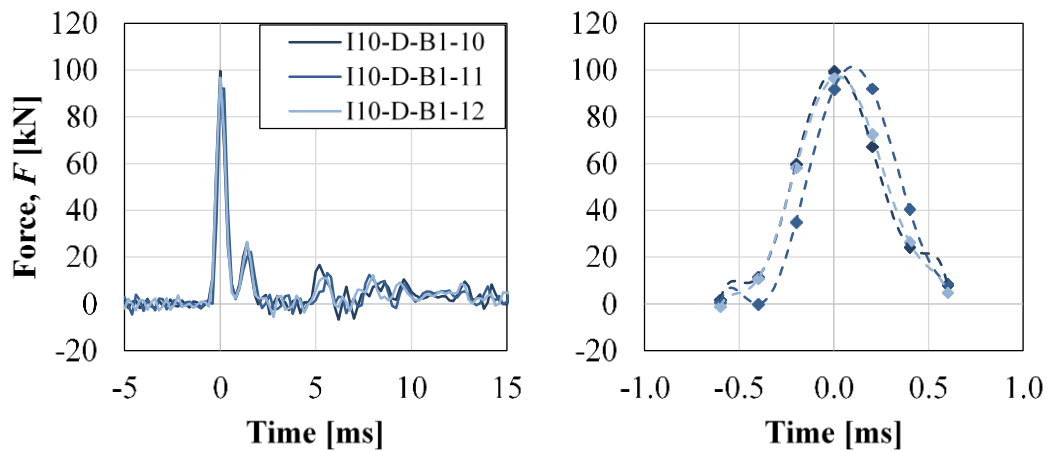


Figure 9.5 Applied force of series I10-D. Right diagram is zoomed in on the peak of the left one. Dashed lines are trendlines for each beam with corresponding shade.

9.3.2.3 Series I20-UD

The peak force and impulse on series I20-UD are presented in Table 9.7. The force-time curve is presented in Figure 9.6.

Table 9.7 Impact force and impulse for series I20-UD.

Beam	F [kN]	I [Ns]
I20-UD-B2-13	102	69.4
I20-UD-B2-14	105	72.0
I20-UD-B2-15	96.4	68.2
Average	101	69.9

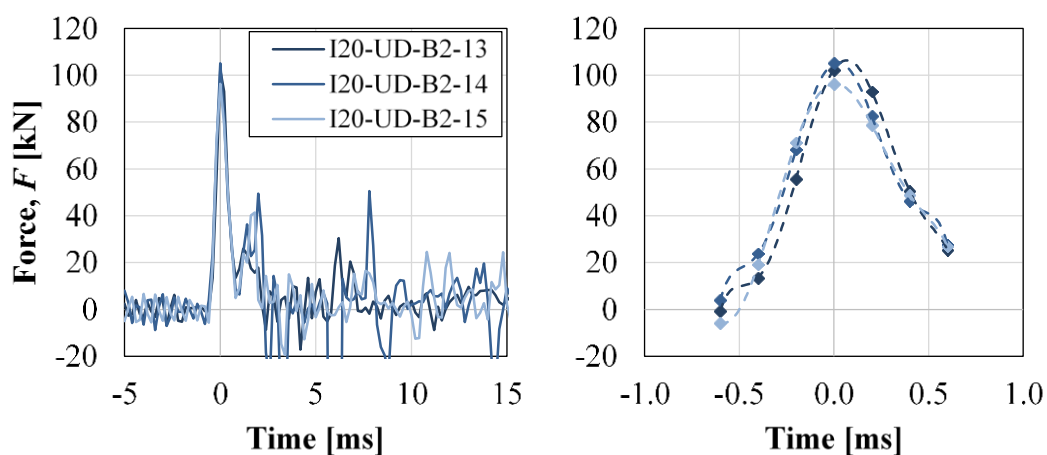


Figure 9.6 Applied force of series I20-UD. Right diagram is zoomed in on the peak of the left one. Dashed lines are trendlines for each beam with corresponding shade.

9.3.2.4 Series I20-D

The peak force and impulse on series I20-D are presented in Table 9.8. The force-time curve is presented in Figure 9.7.

Table 9.8 Impact force and impulse for series I20-D.

Beam	F [kN]	I [Ns]
I20-D-B2-16	101	73.6
I20-D-B2-17	106	67.0
I20-D-B2-18	112	69.4
Average	106	70.0

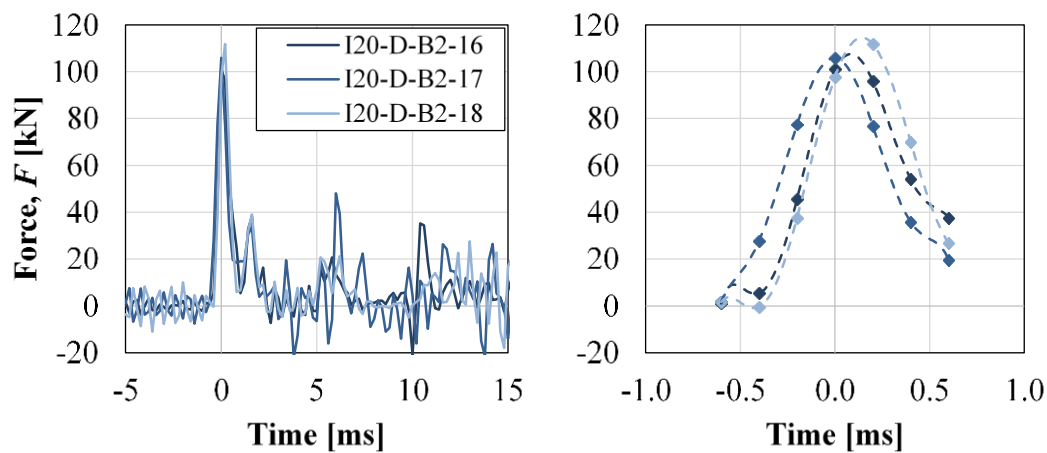


Figure 9.7 Applied force of series I20-D. Right diagram is zoomed in on the peak of the left one. Dashed lines are trendlines for each beam with corresponding shade.

9.3.2.5 Comparison

The I10 series show a rather well gathered response on all fronts, which is not the case for the I20 beams. Both beam I20-UD-B2-14 and I20-D-B2-17 show a large noise in the tests results. However, they do show a behaviour similar to the other beams during the peak loading, i.e. at the impact.

All beams show a smaller second peak at around 1.6 ms which is interesting. This can be interpreted as a second impact between the drop-weight and the beam, and occurs at the same time as the beam has straightened out, shown in the deformed shape of the beams, which is presented in Section 9.3.5.

Furthermore, the impact forces and impulses from the 20 kg drop-weight are slightly higher than those of the 10 kg impact. This is in line with observations made by Jönsson and Stenseke (2018), who additionally showed that the drop height had most influence on the force, rather than the mass of the drop-weight.

9.3.3 Velocity of drop-weight

The velocity of the drop-weight is presented in Figure 9.8 using average values for each series. The velocities for all the beam can be viewed in Appendix G. Here, the same process was made as for the acceleration, where the velocity was established from several points on the drop-weight in GOM Correlate.

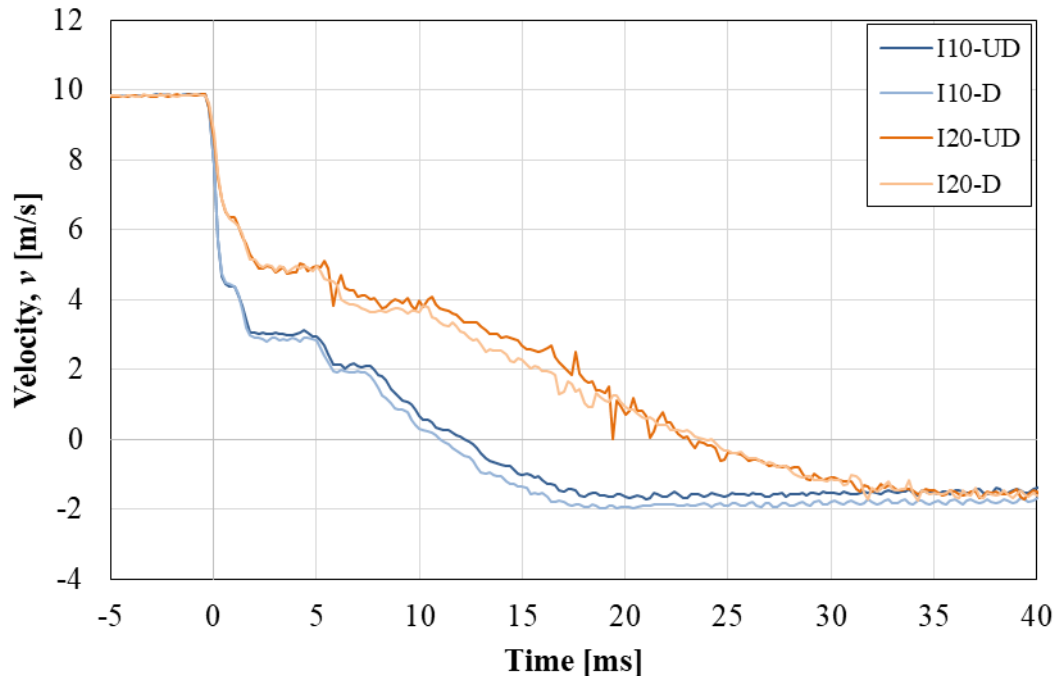


Figure 9.8 Velocity of drop-weight for all series.

The 20 kg drop-weight takes longer time to slow down due to its higher kinetic energy. There is also a systemic difference between undamaged and damaged reinforcement where it takes slightly longer time for the beams with undamaged reinforcement to slow down the drop-weight. It is seen in the figure that series I20-UD has a curve that is more noisy than the other ones, this is due to noise in the curve from beam I20-UD-B2-14, which is in correspondence with Section 9.3.2.3.

9.3.4 Midpoint deflection over time

In this section, the midpoint deflection over time is presented. The value was taken relative the support deflection, as in Equation (9.1), in GOM Correlate by setting points in mid-height of the beam straight over the support and under the drop-weight. The reason for the initial, small bulge in the curves, after about 5 ms, is the fact that the beam rose from the support initially and when it was lowered to the support level again, this behaviour is apparent. The plastic deflection of the beams was determined according to Appendix H.

9.3.4.1 Series I10-UD

The midpoint deflection during the first 50 ms after impact of the beams in Series I10-UD is presented in Figure 9.9. The initial velocities of the drop-weight along with the maximum deflection and the plastic deflection of the beam's midpoint are presented in Table 9.9.

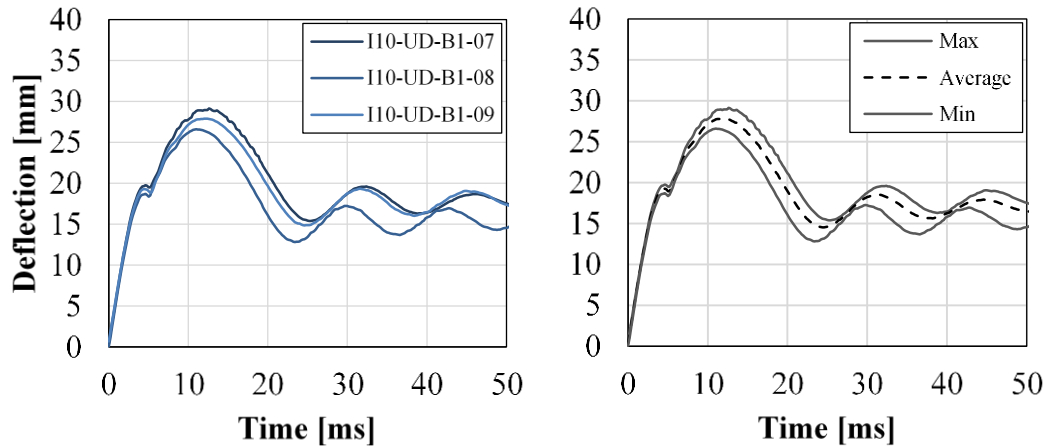


Figure 9.9 Midpoint deflection of beams with undamaged reinforcement during the first 50 ms after impact from the 10 kg drop-weight.

Table 9.9 Initial velocity of drop-weight, maximum deflection and plastic deflection of beams subjected to 10 kg dropweight with undamaged reinforcement.

Beam	v_0 [m/s]	u_{max} [mm]	u_{pl} [mm]
I10-UD-B1-07	9.83	29.1	18.0
I10-UD-B1-08	9.86	26.6	15.3
I10-UD-B1-09	9.83	27.9	17.5
Average	9.84	27.9	17.0

9.3.4.2 Series I10-D

The midpoint deflection during the first 50 ms after impact of the beams in Series I10-D is presented in Figure 9.10. The initial velocities of the dropweight along with the maximum deflection and the plastic deflection of the beam midpoint are presented in Table 9.10.

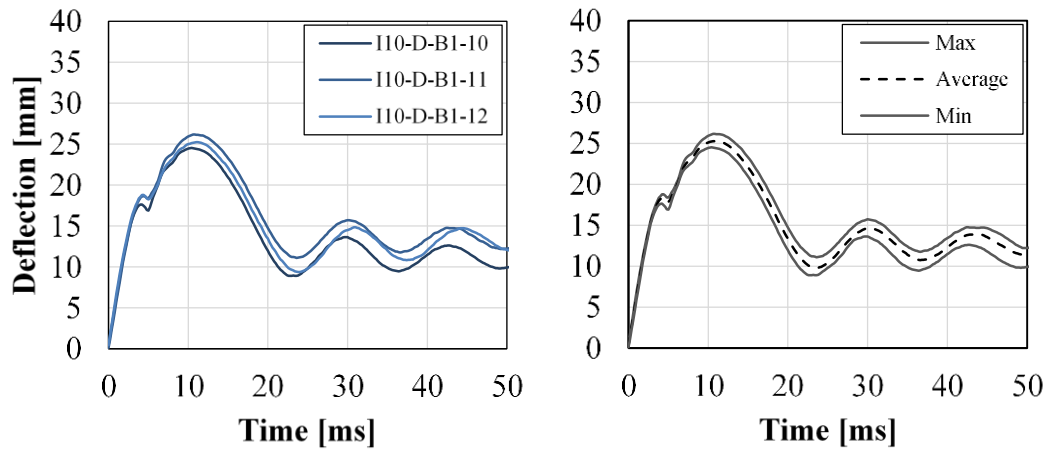


Figure 9.10 Midpoint deflection of beams with damaged reinforcement during the first 50 ms after impact from the 10 kg drop-weight.

Table 9.10 Initial velocity of drop-weight, maximum deflection and plastic deflection of beams subjected to 10 kg dropweight with damaged reinforcement.

Beam	v_0 [m/s]	u_{max} [mm]	u_{pl} [mm]
I10-D-B1-10	9.84	24.5	12.0
I10-D-B1-11	9.85	26.2	14.0
I10-D-B1-12	9.82	25.2	12.1
Average	9.84	25.3	12.7

9.3.4.3 Series I20-UD

The midpoint deflection during the first 80 ms after impact of the beams in Series I20-UD is presented in Figure 9.11. The initial velocities of the dropweight along with the maximum deflection and the plastic deflection of the beam midpoint are presented in Table 9.11. Note that beam I20-UD-B2-15 was first accidentally subjected to a load of the 20 kg weight dropped from a height of approximately 2 m. This is assumed to be the reason for the different behaviour of that one. Therefore, it is not included in the average and envelope curves in Figure 9.11. It is also observed to have lower deflections in Table 9.11, which can be assumed to be due to the strain hardening of the reinforcement due to the accidental impact. Furthermore, be aware that the measured data from beam I20-UD-B2-15 is from the second impact only; the deflection from the accidental impact is not included. In the figure, the curve for beam I20-UD-B2-14 lack information around the maximum deflection, where the curve is dashed. The maximum is therefore taken as the highest measured value of the deflection.

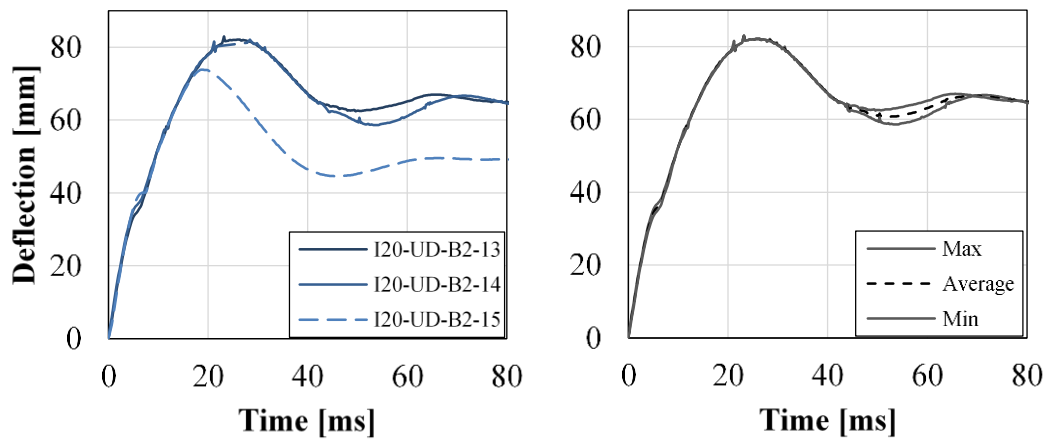


Figure 9.11 Midpoint deflection of beams with undamaged reinforcement during the first 80 ms after impact from the 20 kg drop-weight. Note that beam I20-UD-B2-15 is not included in the average and envelope curves.

Table 9.11 Initial velocity of drop-weight, maximum deflection and plastic deflection of beams subjected to 20 kg dropweight with undamaged reinforcement.

Beam	v_0 [m/s]	u_{max} [mm]	u_{pl} [mm]
I20-UD-B2-13	9.80	82.1 ⁽¹⁾	69.1
I20-UD-B2-14	9.83	82.1	67.1
I20-UD-B2-15	9.85	73.6 ⁽²⁾	54.2 ⁽²⁾
Average	9.83	82.1	68.1

⁽¹⁾ Note that in the maximum deflection for beam 13 the small top before the smooth rounded curve top is disregarded as it is assumed to come from noise in the measuring data in GOM Correlate.

⁽²⁾ Deflection values for beam I20-UD-B2-15 are not included in the average values.

9.3.4.4 Series I20-D

The midpoint deflection during the first 80 ms after impact of the beams in Series I20-D is presented in Figure 9.12. The initial velocities of the dropweight along with the maximum deflection and the plastic deflection of the beam midpoint are presented in Table 9.12.

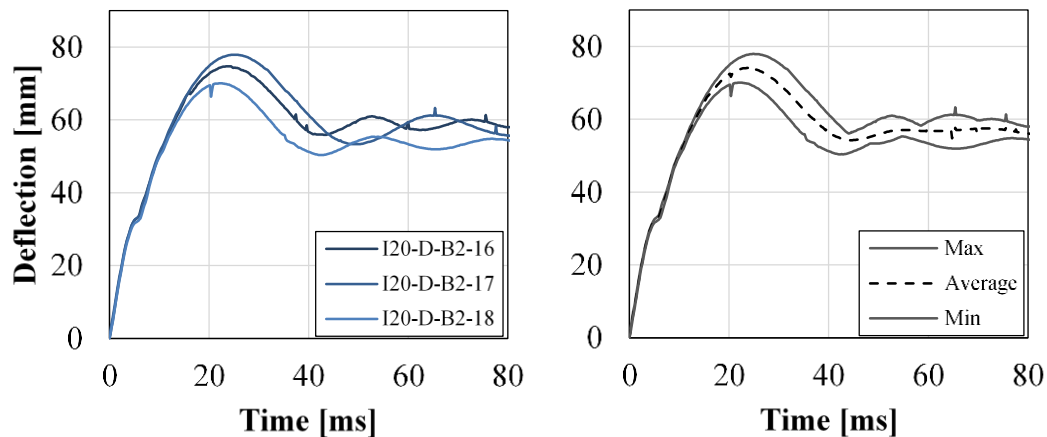


Figure 9.12 Midpoint deflection of beams with damaged reinforcement during the first 80 ms after impact from the 20 kg drop-weight.

It is apparent that beam I20-D-B2-17 has a shift in its time period compared to the other two in Figure 9.12. This is assumed to be due to the high level of concrete spalling during the impact which resulted in a greater loss of mass and stiffness compared to the other two beams.

Table 9.12 Initial velocity of drop-weight, maximum deflection and plastic deflection of beams subjected to 20 kg dropweight with damaged reinforcement.

Beam	v_0 [m/s]	u_{max} [mm]	u_{pl} [mm]
I20-D-B2-16	9.90	74.7	58.6
I20-D-B2-17	9.80	77.9	61.8
I20-D-B2-18	9.82	70.0	55.5
Average	9.84	74.2	58.6

9.3.4.5 Comparison

The average midpoint deflection curves for all beam series are presented in Figure 9.13. It is evident that the 20 kg-drop-weight gives a more severe impact on the beams. Moreover, it can be seen that the beams containing damaged reinforcement gives a smaller overall deflection compared to those with undamaged reinforcement. This comes from the reduction of plastic deformation capacity in the reinforcement bars due to pre-stretching, as shown in Figure 9.1. Exactly how much the maximum deflection has been lowered due to the reinforcement properties is presented in Table 9.13.

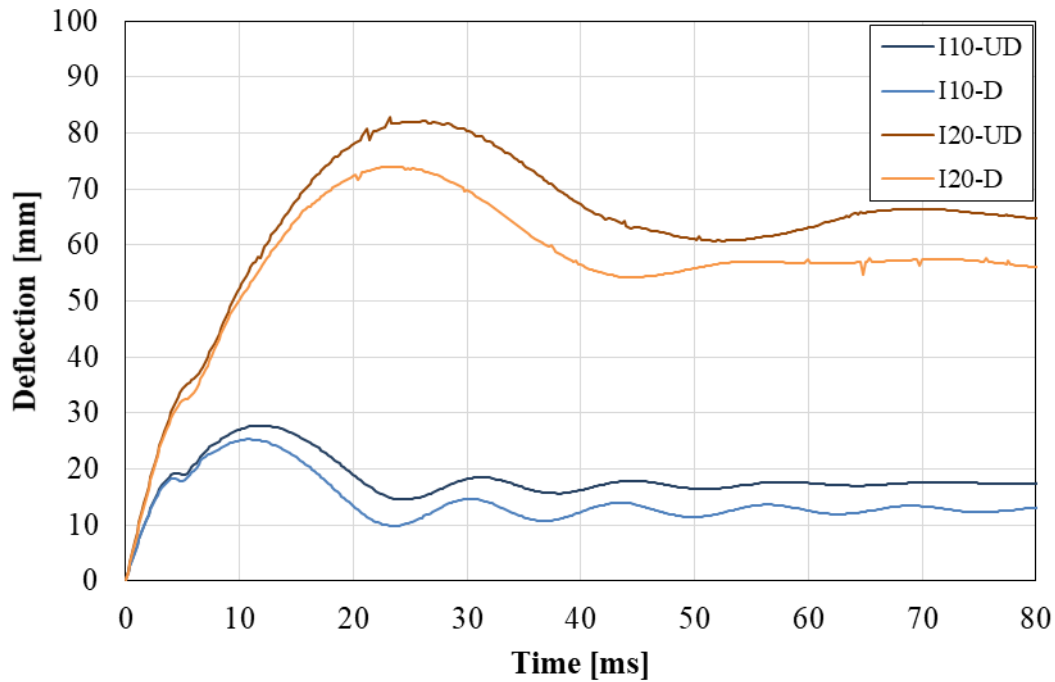


Figure 9.13 Midpoint deflection of all beam groups (presented using average curves) during the first 80 ms after impact.

Table 9.13 Comparison of deflection between beams with undamaged vs damaged reinforcement.

Comparison	$\frac{u_{max,D} - u_{max,UD}}{u_{max,UD}}$ [%]	$\frac{u_{pl,D} - u_{pl,UD}}{u_{pl,UD}}$ [%]
I10-UD vs I10-D	-9	-25
I20-UD vs I20-D	-10	-14

9.3.5 Deformed shape

The variation of the deformed shape of the beams is of interest to get an explanation on how the load is transferred through it. This was done by taking a section through the middle part of the beam, in the vertical direction, that was parallel to the horizontal axis in GOM Correlate. The deflections in the sections were retrieved for the first two milliseconds after impact. This was done for only four beams, one representative beam from each series. The choice was based on the midpoint deflection over time curves where the one chosen was the one closest to average in the beginning of the curve.

9.3.5.1 Series I10-UD

For this series, beam I10-UD-B1-07 was used to represent the group. The variation of the deformed shape is presented in Figure 9.14. The relative deformed shape is presented in Figure 9.15. In this figure, the deflection was normalized to the maximum value at each time step.

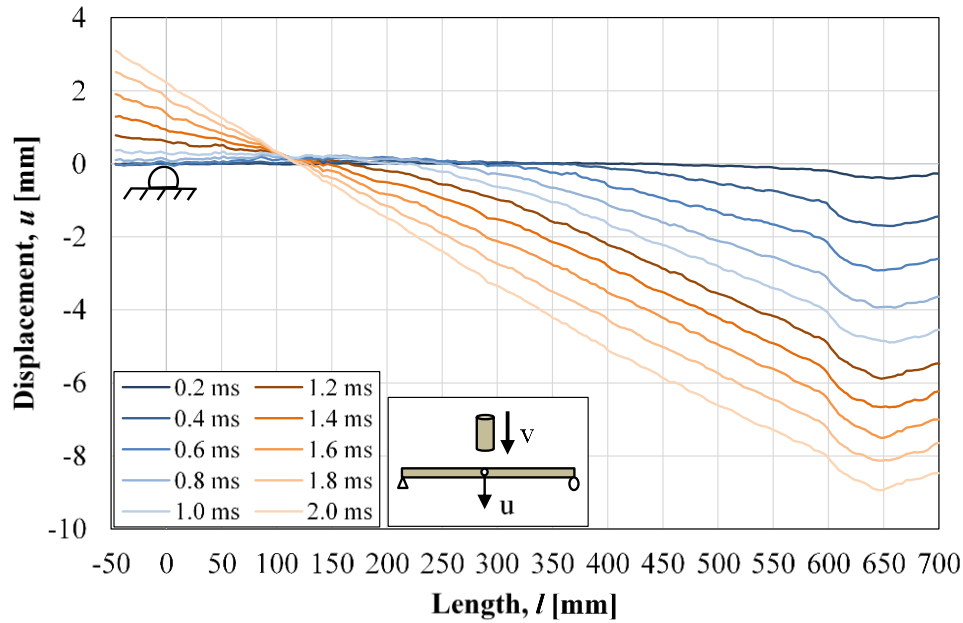


Figure 9.14 Variation of deformed shape of half of beam I10-UD-B1-07 during the first 2 ms after impact.

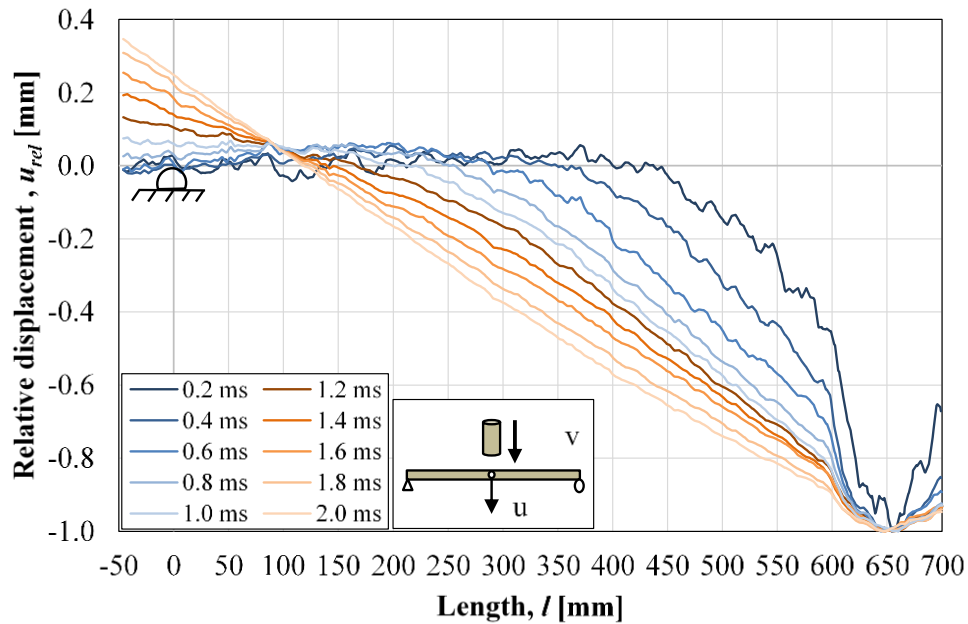


Figure 9.15 Variation of relative deformed shape of half of beam I10-UD-B1-07 during the first 2 ms after impact.

9.3.5.2 Series I10-D

For this series, beam I10-D-B1-10 was used to represent the group. The variation of the deformed shape is presented in Figure 9.16. The relative deformed shape is presented in Figure 9.17.

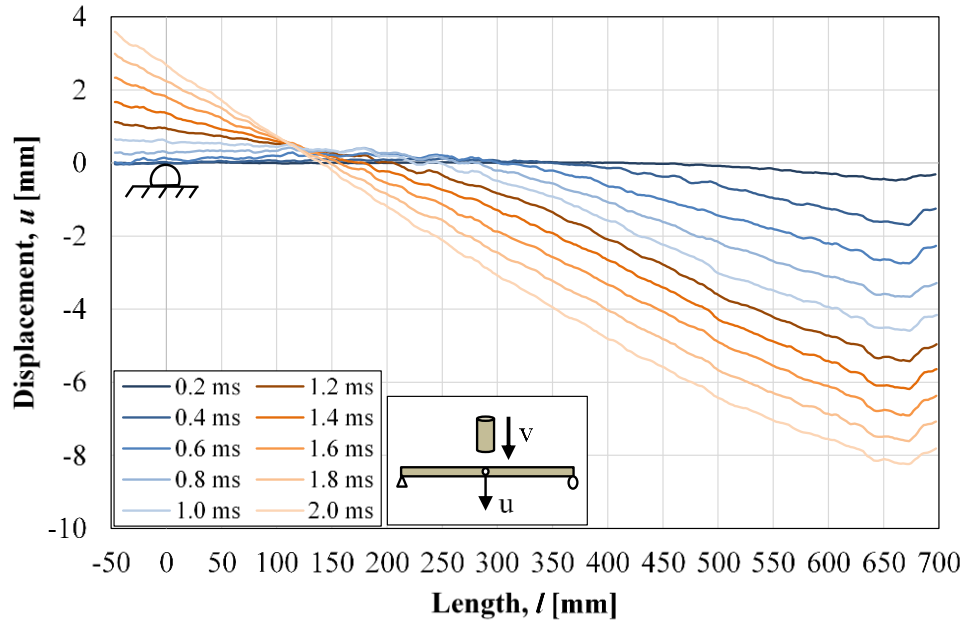


Figure 9.16 Variation of deformed shape of half of beam 10 during the first 2 ms after impact.

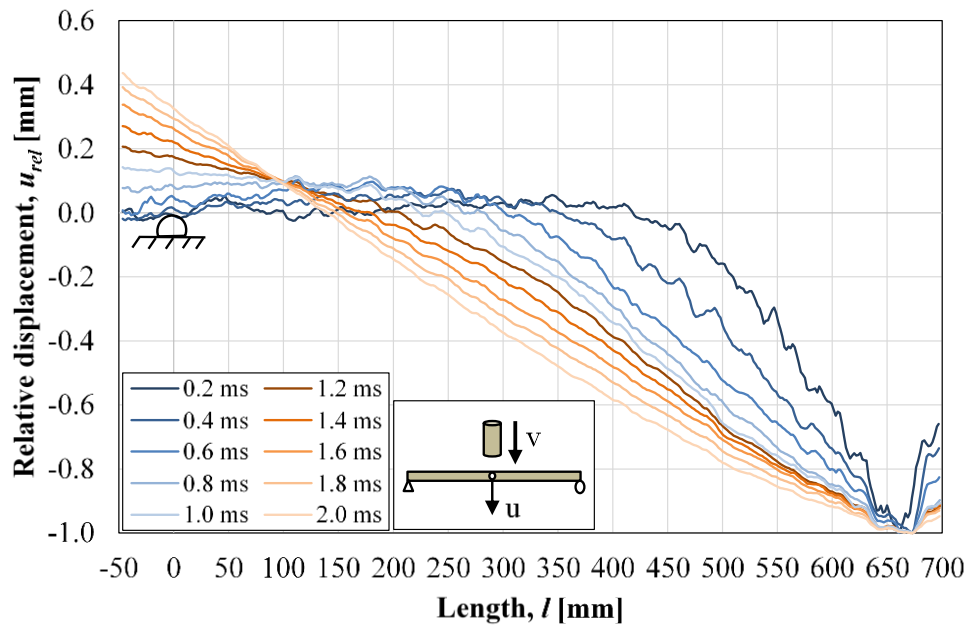


Figure 9.17 Variation of relative deformed shape of half of beam 10 during the first 2 ms after impact.

9.3.5.3 Series I20-UD

For this series, beam I20-UD-B2-13 was used to represent the group. The variation of the deformed shape is presented in Figure 9.18. The relative deformed shape is presented in Figure 9.19.

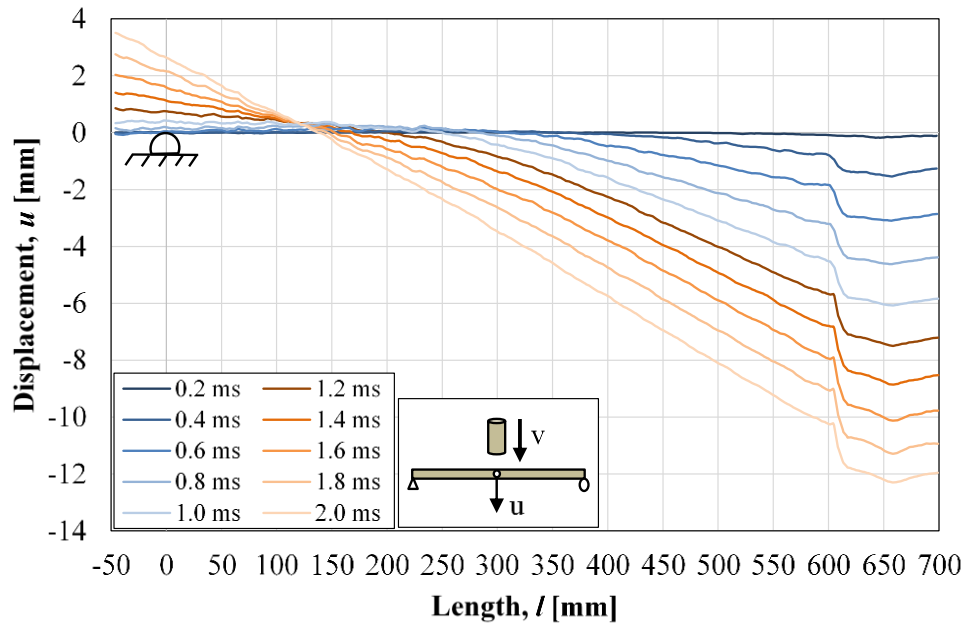


Figure 9.18 Variation of deformed shape of half of beam 13 during the first 2 ms after impact.

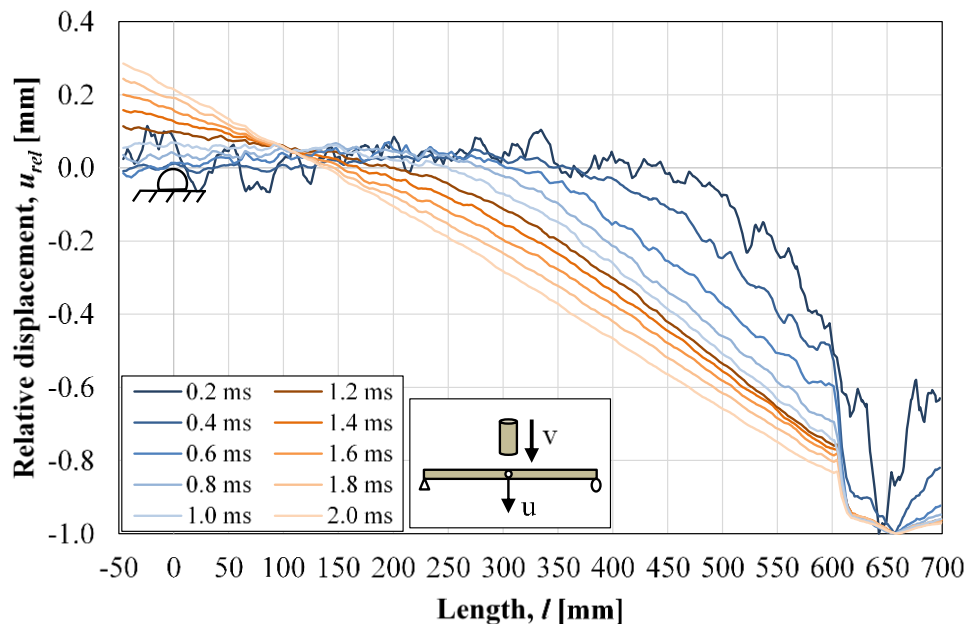


Figure 9.19 Variation of relative deformed shape of half of beam 13 during the first 2 ms after impact.

9.3.5.4 Series I20-D

For this series, beam I20-D-B2-16 was used to represent the group. The variation of the deformed shape is presented in Figure 9.20. The relative deformed shape is presented in Figure 9.21.

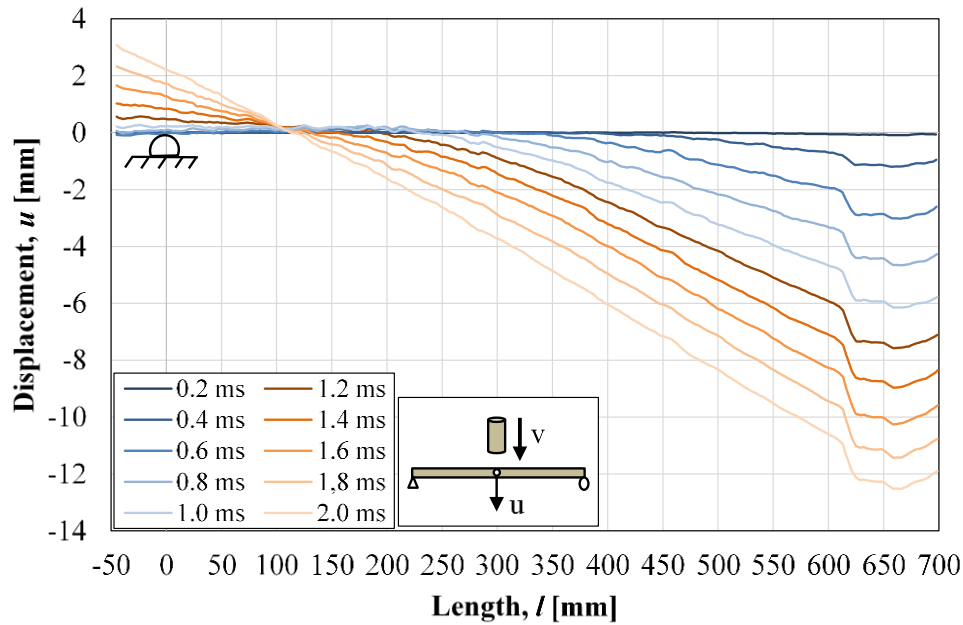


Figure 9.20 Variation of deformed shape of half of beam 16 during the first 2 ms after impact.

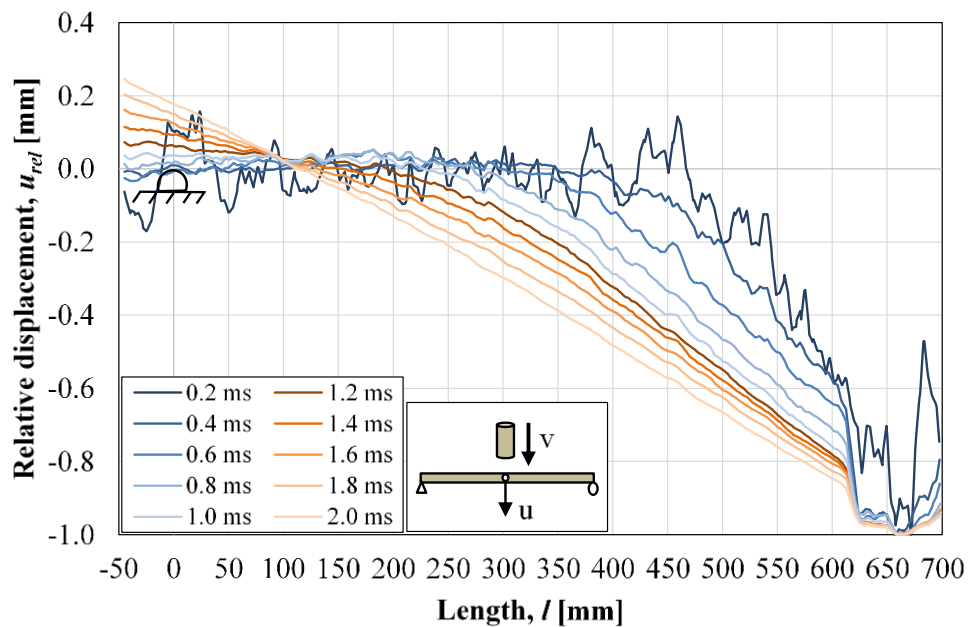


Figure 9.21 Variation of relative deformed shape of half of beam 16 during the first 2 ms after impact.

9.3.5.5 Comparison

From the figures of the absolute deformed shape it is clear that the 20 kg drop-weight gave a higher deflection in general. It is also visible that there immediately appeared severe cracks close to the middle in the I20-beams, due to the excess deflection directly below the point of impact. This behaviour is not as severe in the I10-beams.

The influence of the reinforcement is not distinct in either the absolute or relative deformed shapes. Therefore, the information seems to travel at almost the same pace in all the beams. However, it is difficult to study in these rough curves, which is why this is evaluated further.

9.3.6 Velocity of initial deflection

How the deflection propagates through the beam is here studied in a more detailed manner. This was done by calculating how the active portion of the beam increased in length between two time steps. This velocity was calculated as

$$v = \frac{x(t_2) - x(t_1)}{t_2 - t_1} \quad (9.2)$$

where x is the transition point between active and inactive portion in each time step. The method is schematically shown in Figure 9.22.

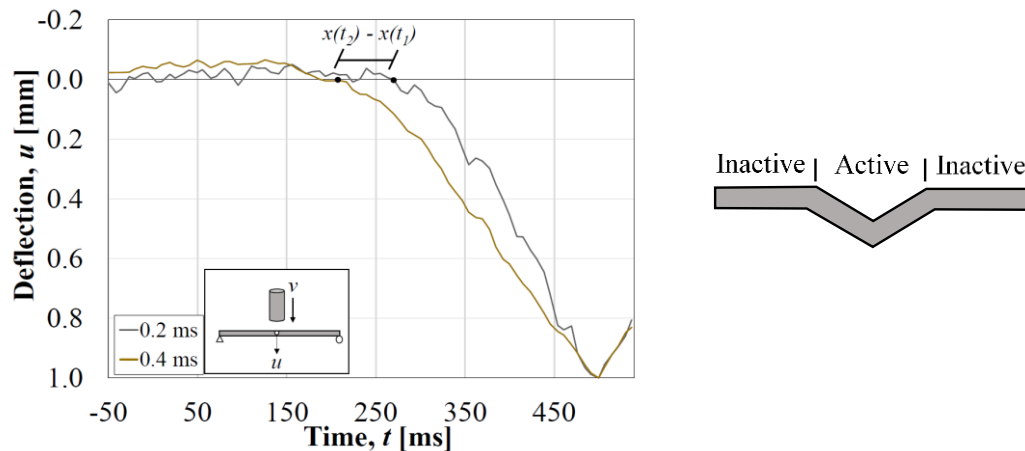


Figure 9.22 Transition point between active and inactive part. From Jönsson and Stenseke (2018).

The velocities were calculated for the beams studied in the previous section, and they are presented in Table 9.14.

Table 9.14 Shear velocities of representative beams during the first two milliseconds after impact. [m/s]

Beam	0.4 ms	0.6 ms	0.8 ms	1.0 ms	1.2 ms	1.4 ms	1.6 ms	1.8 ms	2.0 ms
I10-UD-B1-07	446	318	149	282	169	131	37.5	37.2	37.5
I10-D-B1-10	337	252	84	178	207	140	112	37.7	46.8
I20-UD-B2-13	431	281	112	149	245	168	75.6	37.2	59.9
I20-D-B2-16	262	262	112	224	170	206	113	37.6	55.5

It is evident that the velocities decrease with time and that they quickly stabilize. Though it seems that for all the beams, the velocity is increased between 0.8 and 1.0 ms. This could come from the fact that this is the point at which the beams seem to lift from the support and therefore behave quite differently. Additionally, it seems that the velocity in the beams with damaged reinforcement start at a lower value than those with undamaged bars. This indicates that the reinforcement reaches its yield limit in either the top bars or the bottom bars in mid-span. In this part of the stress-strain curve the different types of reinforcement respond differently due to strain hardening effects in the pre-stretched bars. The beams with damaged reinforcement also seem to stabilize one time step later, at 1.8 ms rather than 1.6 ms which seems to be the case for the undamaged ones. Furthermore, there does not seem to be any apparent difference in impacting with 10 kg or 20 kg.

9.3.7 Strain fields

Strain fields were retrieved from GOM Correlate for the dynamic testing to get an overview of the crackpattern of the beams during the dynamic tests. The strain fields were taken for the first two milliseconds after impact and at the time of maximum deflection.









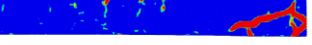

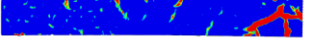
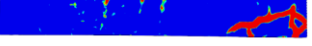


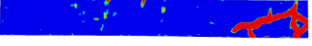
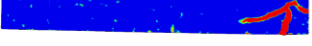


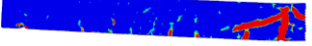
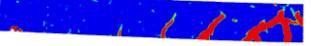
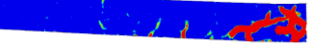

9.3.7.1 I10-UD

The strain fields for Series I10-UD are presented in Table 9.15. Between the time steps 0.6 and 1.0 ms one can see that cracks form in the top of the beam at approximately one fourth of the beam span from the support. They seem to have closed by 2.0 ms. This is assumed to come from the behaviour studied in the previous sections where the deflection propagates.

The strain fields are similar for the three beams, where three major cracks appear in the middle of the span, of which one is vertical and two inclined.

Note that the white spots in the strain fields solemnly mean that there is no information available there. This either indicates that there is excessive concrete spalling or that the concrete is there, yet that the surface component has lost vital information.




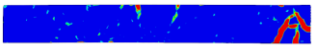
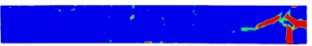
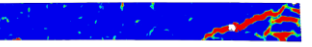
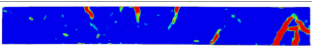
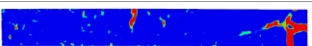
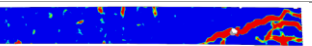
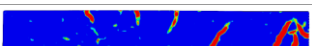
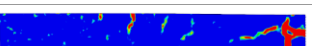
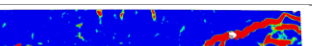
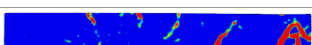
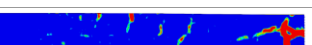
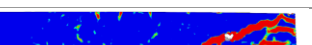


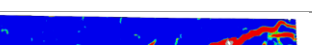
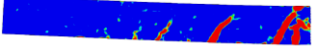
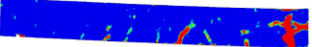
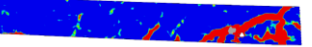

Table 9.15 Strain fields during the first two milliseconds and at the maximum deflection for beams with undamaged reinforcement dynamically loaded with 10 kg drop-weight.

[ms]	I10-UD-B1-07	I10-UD-B1-08	I10-UD-B1-09
0.2			
0.4			
0.6			
0.8			
1.0			
2.0			
u_{max}	 $t = 12.6 \text{ ms}$ $u_{max} = 29.1 \text{ mm}$	 $t = 11.0 \text{ ms}$ $u_{max} = 26.6 \text{ mm}$	 $t = 12.4 \text{ ms}$ $u_{max} = 27.9 \text{ mm}$
[%]			

9.3.7.2 I10-D

The strain fields for Series I10-D are presented in Table 9.16. These show the same behaviour as I10-UD with the initial cracks in the top that later closes. The I10-D beams show a larger variation than the former ones. However, the cracks seem to follow the same general pattern as in the undamaged beams.





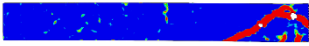

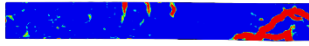
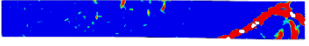
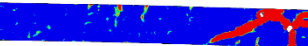
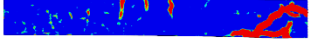
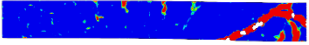
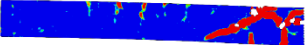
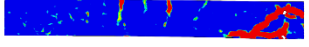
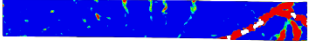
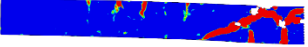



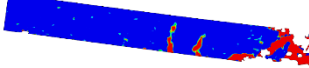
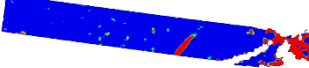
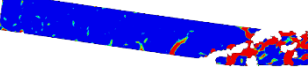
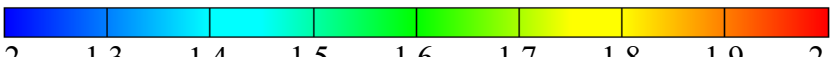
Table 9.16 Strain fields during the first two milliseconds and at the maximum deflection for beams with damaged reinforcement dynamically loaded with 10 kg drop-weight.

[ms]	I10-D-B1-10	I10-D-B1-11	I10-D-B1-12
0.2			
0.4			
0.6			
0.8			
1.0			
2.0			
u_{max}	 $t = 10.4 \text{ ms}$ $u_{max} = 24.5 \text{ mm}$	 $t = 11.0 \text{ ms}$ $u_{max} = 26.2 \text{ mm}$	 $t = 11.2 \text{ ms}$ $u_{max} = 25.2 \text{ mm}$
[%]			

9.3.7.3 I20-UD

The strain fields for Series I20-UD are presented in Table 9.17. The beams I20-UD-B2-13 and -14 show similar crack patterns. Beam I20-UD-B2-15, however, shows a larger deflection along with more severe cracks at the time of maximum deflection. This is assumed to be due to the accidental drop of the weight on the beam from approximately 2 m before the testing. Note that the maximum deflection noticed in the table is the value it was deflected in the intended impact, the deflection for the accidental impact is not included. All the beams also obtained the initial cracks in the top of the beams; i.e. similar to that obtained in the I10-beams.




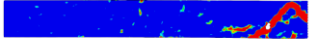




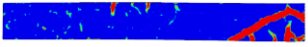
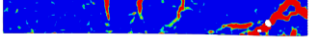

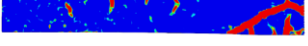

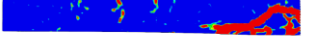
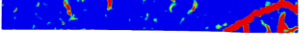
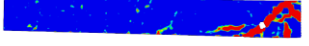


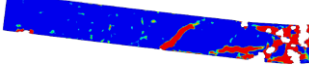
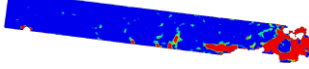
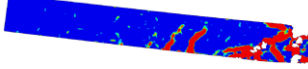

Table 9.17 Strain fields during the first two milliseconds and at the maximum deflection for beams with undamaged reinforcement dynamically loaded with 20 kg drop-weight.

[ms]	I20-UD-B2-13	I20-UD-B2-14	I20-UD-B2-15
0.2			
0.4			
0.6			
0.8			
1.0			
2.0			
u_{max}	 $t = 26.2 \text{ ms}$ $u_{max} = 82.1 \text{ mm}$	 $t = 25.4 \text{ ms}$ $u_{max} = 82.1 \text{ mm}$	 $t = 19.2 \text{ ms}$ $u_{max} = 73.8 \text{ mm}$
[%]	 1.2 1.3 1.4 1.5 1.6 1.7 1.8 1.9 2.0		

9.3.7.4 I20-D

The strain fields for Series I20-D are presented in Table 9.18. The three beams show similar crack patterns and shows the initial cracks in the top as the previous beams.

Table 9.18 Strain fields during the first two milliseconds and at the maximum deflection for beams with damaged reinforcement dynamically loaded with 20 kg drop-weight.

[ms]	I20-D-B2-16	I20-D-B2-17	I20-D-B2-18
0.2			
0.4			
0.6			
0.8			
1.0			
2.0			
u_{max}	 $t = 24.2 \text{ ms}$ $u_{max} = 74.7 \text{ mm}$	 $t = 25.4 \text{ ms}$ $u_{max} = 77.9 \text{ mm}$	 $t = 22.4 \text{ ms}$ $u_{max} = 70.0 \text{ mm}$
[%]	 1.2 1.3 1.4 1.5 1.6 1.7 1.8 1.9 2.0		

9.3.7.5 Comparison

As previously mentioned, all the beams show the initial cracks in the top at approximately one fourth of the span from the support.

The largest difference in the crack patterns is that the I20-beams show larger cracks than the I10 ones.

During the first two milliseconds there does not seem to be any difference between the beams containing undamaged reinforcement compared to the ones with damaged. This is coherent with the deformed shape of the beams which showed the same thing. However, as known from the shear velocities that is not the case, yet the difference does not seem to be visible for the naked eye. The reinforcement show a larger influence on the maximum deflection, which in general was somewhat smaller for the D-beams, see Section 9.3.4.5.

9.4 Static testing of beams

This section treats the results of the static testing of the beams. The purpose of testing the beams statically after they were tested dynamically was to analyse their static response compared to non-impacted beams (Series S) and also to evaluate their residual load and deformation capacity. The section presents the static results for beams in Series S, Series I10 and Series I20.

9.4.1 Method

The results were obtained from both the static testing machine and the 3D view analysed in GOM Correlate. In case of beams from Series I10 or Series I20, the deflection extracted from the testing machine was corrected to include the plastic deformation due to the drop-weight impact.

The 3D view analysed in GOM Correlate was done using a facet size of 17 pixels and a point distance of 14 pixels. The strain fields were displayed against the reference stage, namely the first picture in the film.

9.4.2 Results for Series S

This section presents the results for beams in Series S regarding curves for load-deflection relationship and strain fields at a total deformation of 30 mm. The load-deflection curves describe the structural behaviour and were used to calculate plastic rotation capacity, internal work and stiffness at different stages. The results obtained for Series S were later used as reference when evaluating the static results from the impacted beams.

9.4.2.1 Load-deflection relationship

The load-deflection relationship of the beams in Series S, i.e. the beams subjected to static loading only, is shown in Figure 9.23. Comparison is made between beams with undamaged reinforcement (solid line) and beams with damaged reinforcement (dashed line). Additionally, outer envelopes and average load-deflection relationship are presented in Figure 9.24 for beams with undamaged reinforcement and Figure 9.25 for beams with damaged reinforcement.

Initially, all beams in Series S show a similar behaviour independently on whether they have undamaged or damaged reinforcement. It is visible that Series S-UD reaches yielding slightly earlier than Series S-D. Furthermore, beams in Series S-UD show a more ductile behaviour compared to Series S-D. Comparing the average curves in Figure 9.24 and Figure 9.25, the beams with undamaged reinforcement reaches a somewhat lower maximum load than the beams with damaged reinforcement.

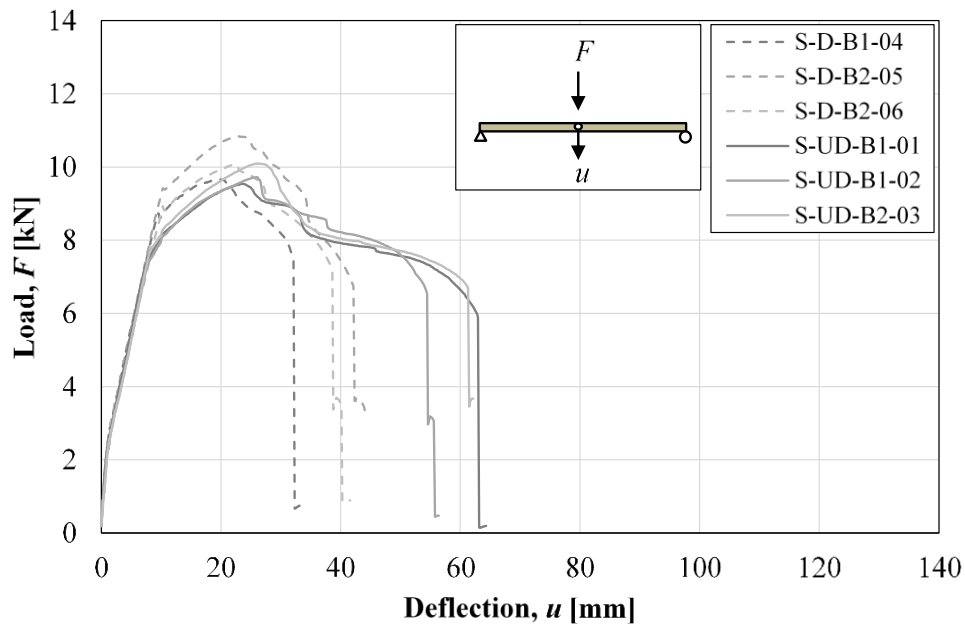


Figure 9.23 Load-deflection relationship for statically loaded beams with damaged and undamaged reinforcement. The experimental set-up was in this case static three point loading.

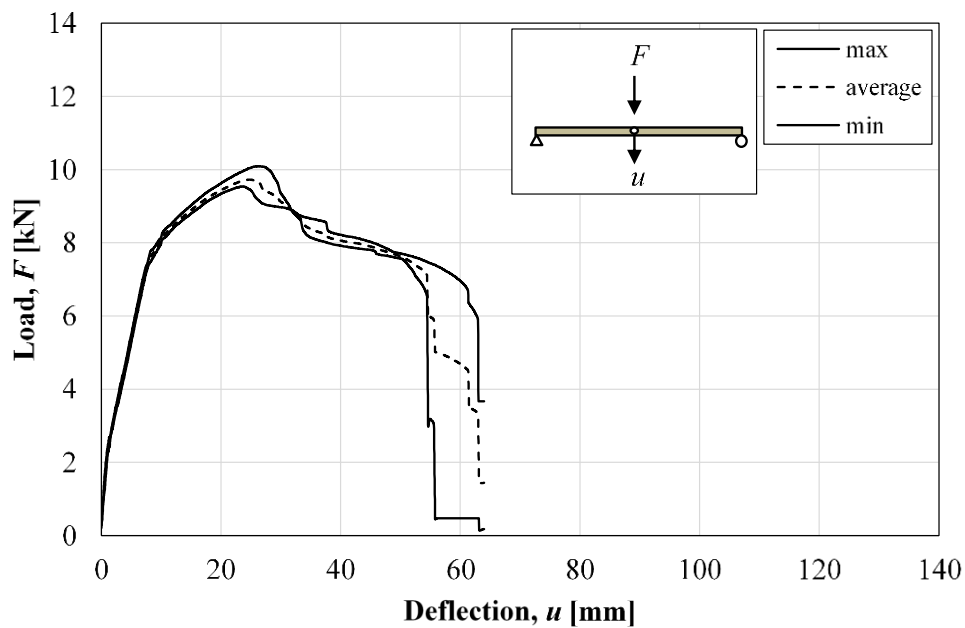


Figure 9.24 Outer envelopes and average load-deflection relationship for statically loaded beams with undamaged reinforcement.

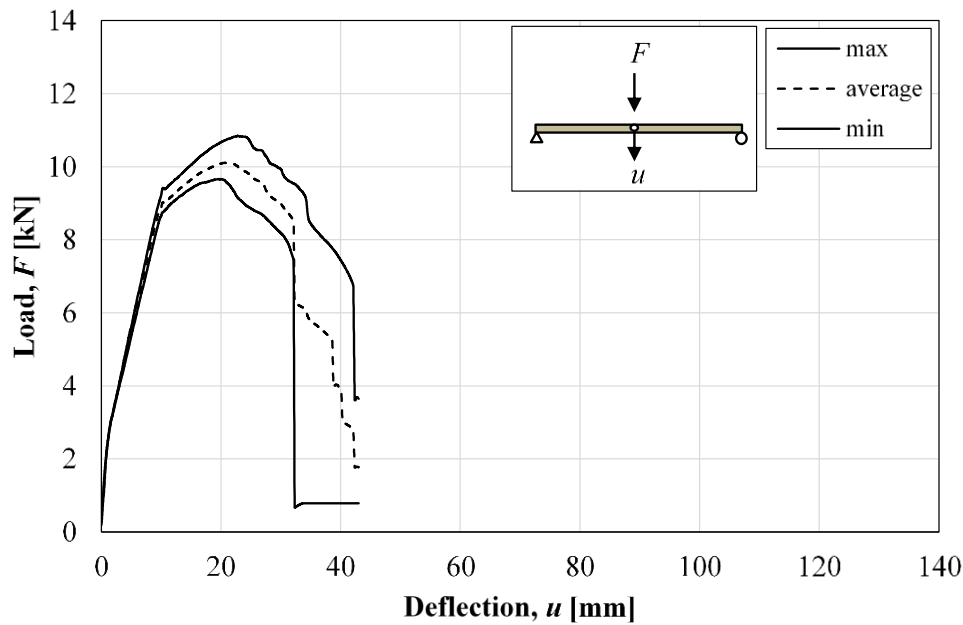


Figure 9.25 Outer envelopes and average load-deflection relationship for statically loaded beams with damaged reinforcement.

Values for maximum deflection before failure, maximum load and ratio between ultimate moment and yield moment are presented in Table 9.19 for beams with undamaged reinforcement and in Table 9.20 for beams with damaged reinforcement. A beam was in this thesis considered to reach failure when the descending branch of the load-deflection curve reached 50 % of the average value of the maximum load, F_{max} . That is at the load 4.90 kN for beams with undamaged reinforcement and at 5.10 kN for beams with damaged reinforcement. A decrease in the ratio $\eta_M = M_u/M_y$ of about 12 % is noticed for beams with damaged reinforcement compared to undamaged. Furthermore, it is noticed that η_M is considerably higher than η_f obtained in Section 9.2.1 for both undamaged and damaged reinforcement.

Table 9.19 Maximum deflection, maximum load and quotient between ultimate moment and yield moment for statically loaded beams with undamaged reinforcement.

Beam	u_{fail} [mm]	F_{max} [kN]	F_y [kN]	M_u / M_y [-]
S-UD-B1-01	63.0	9.54	7.37	1.29
S-UD-B1-02	54.4	9.73	7.49	1.30
S-UD-B2-03	61.3	10.1	7.81	1.29
Average	59.6	9.79	7.56	1.30

Table 9.20 Maximum deflection, maximum load and quotient between ultimate moment and yield moment for statically loaded beams with damaged reinforcement.

Beam	u_{fail} [mm]	F_{max} [kN]	F_y [kN]	M_u / M_y [-]
S-D-B1-04	32.1	9.66	8.63	1.12
S-D-B2-05	42.1	10.8	9.38	1.16
S-D-B2-06	38.6	10.1	8.82	1.14
Average	37.6	10.2	8.94	1.14

By looking at the load-deflection curves it is possible to distinguish the three different stages that the reinforced concrete exhibits during static loading; state I, state II and state III. The stiffness of the beams during these stages is calculated and presented in Table 9.21 for beams with undamaged reinforcement and in Table 9.22 for beams with damaged reinforcement. Two different values for the state II stiffness are presented, $k_{II,s}$ refers to the secant stiffness in state II while $k_{II,t}$ refers to the tangent stiffness in state II. All stiffnesses were calculated by dividing the difference in load by the difference in deflection. For further description of the different stiffnesses see Appendix I. There is no major difference in the stiffnesses in the different stages comparing undamaged and damaged reinforcement.

Table 9.21 Stiffnesses in different stages for statically loaded beams with undamaged reinforcement.

Beam	k_I [MN/m]	$k_{II,s}$ [MN/m]	$k_{II,t}$ [MN/m]	k_{III} [MN/m]
S-UD-B1-01	2.38	0.947	0.783	0.132
S-UD-B1-02	2.03	0.900	0.747	0.126
S-UD-B2-03	1.85	0.930	0.768	0.125
Average	2.09	0.926	0.766	0.128

Table 9.22 Stiffnesses in different stages for statically loaded beams with damaged reinforcement.

Beam	k_I [MN/m]	$k_{II,s}$ [MN/m]	$k_{II,t}$ [MN/m]	k_{III} [MN/m]
S-D-B1-04	1.86	0.885	0.743	0.094
S-D-B2-05	2.02	0.897	0.753	0.117
S-D-B2-06	2.31	0.845	0.687	0.104
Average	2.06	0.875	0.728	0.105

The plastic rotation at different load levels is presented in Table 9.23 for beams with undamaged reinforcement and in Table 9.24 for beams with damaged reinforcement. The values are calculated according to Section 4.3.3 using the secant state II stiffness, $k_{II,s}$. In comparison to beams with undamaged reinforcement, the plastic rotation is consistently lower for beams with damaged reinforcement. By looking at the load-deflection curves, this can be explained by the steep drop in load that occurs earlier for

beams with damaged reinforcement and thus resulting in a decreased value of plastic rotation capacity.

Table 9.23 Plastic rotation at different load levels for statically loaded beams with undamaged reinforcement.

Beam	$\theta_{pl,100\%}$ [mrad]	$\theta_{pl,95\%}$ [mrad]	$\theta_{pl,90\%}$ [mrad]	$\theta_{pl,85\%}$ [mrad]	$\theta_{pl,80\%}$ [mrad]
S-UD-B1-01	20.9	27.0	37.3	41.7	61.7
S-UD-B1-02	23.3	25.7	36.0	45.5	61.2
S-UD-B2-03	24.0	29.5	32.9	37.3	46.9
Average	22.7	27.4	35.4	41.5	56.6

Table 9.24 Plastic rotation at different load levels for statically loaded beams with damaged reinforcement.

Beam	$\theta_{pl,100\%}$ [mrad]	$\theta_{pl,95\%}$ [mrad]	$\theta_{pl,90\%}$ [mrad]	$\theta_{pl,85\%}$ [mrad]	$\theta_{pl,80\%}$ [mrad]
S-D-B1-04	13.9	18.9	26.1	31.6	35.2
S-D-B2-05	16.5	24.6	30.1	36.4	38.1
S-D-B2-06	16.2	23.8	26.5	34.1	39.9
Average	15.5	22.4	27.6	34.0	37.8

The rotation capacity is also presented in terms of relative rotation capacity in Figure 9.26 and Figure 9.27. The presented values are average values at different load levels that are normalized in relation to the load level corresponding to 100 % of the maximum load, F_{max} . Both beams with undamaged reinforcement and beams with damaged reinforcement obtain larger plastic rotation capacity when considering lower load levels. It is also noticed that the beams with damaged reinforcement obtain lower rotation capacity than undamaged at all load levels.

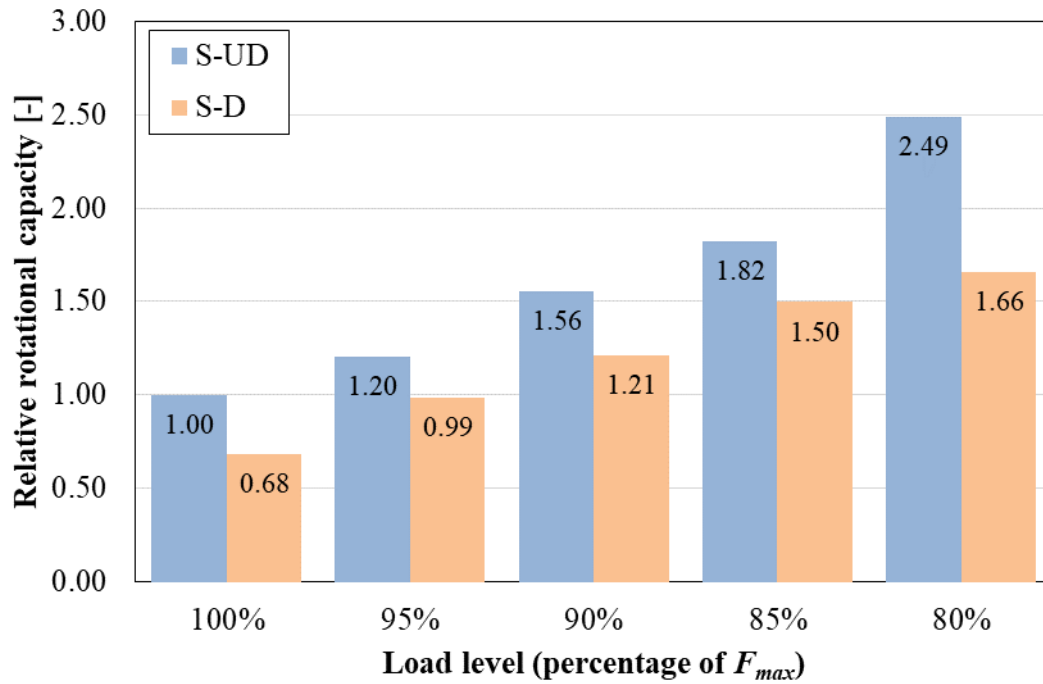


Figure 9.26 *Relative plastic rotation capacity at different load levels. The values refer to average values of statically loaded beams and are normalized in relation to the load level corresponding to 100 % of F_{max} for the undamaged reinforcement.*

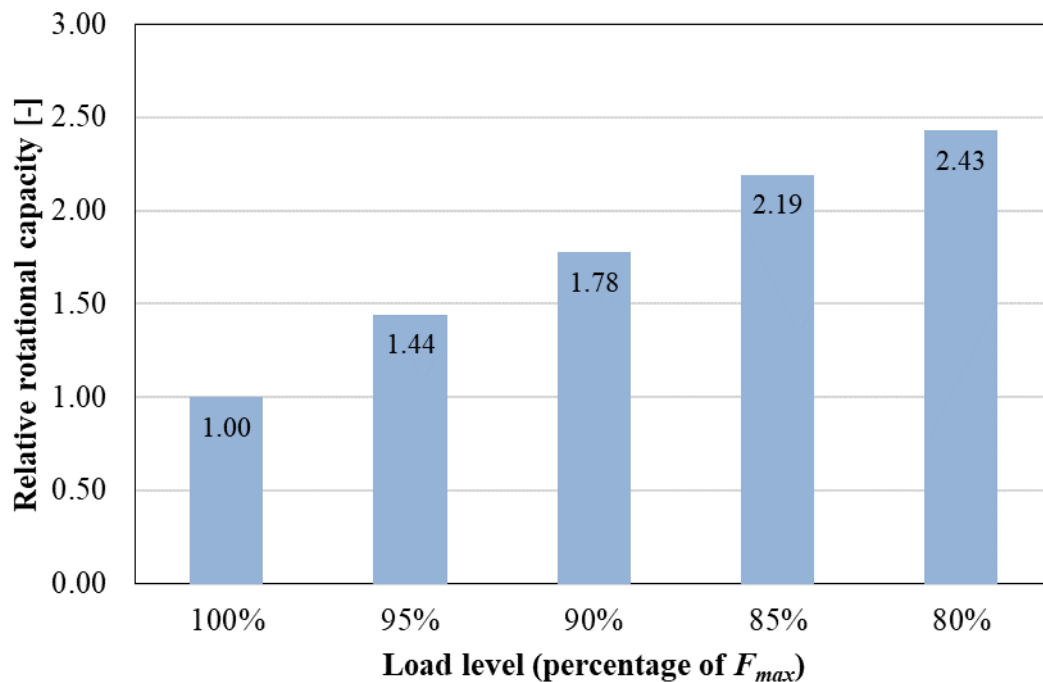


Figure 9.27 *Relative plastic rotation capacity at different load percentages. The values refer to average values of statically loaded beams with damaged reinforcement and they are normalized in relation to the load level corresponding to 100 % of F_{max} .*

The ratio between average values for the plastic rotation capacity of beams with damaged reinforcement and beams with undamaged reinforcement for different load levels can be seen in Figure 9.28. The figure shows that there is no clear correlation between the different load levels but the plastic rotation is, as stated before, lower for beams with damaged reinforcement than for beams with undamaged reinforcement. The plastic rotation capacity for the beams with damaged reinforcement is around 75 % of the one measured for the undamaged beams on all load levels.

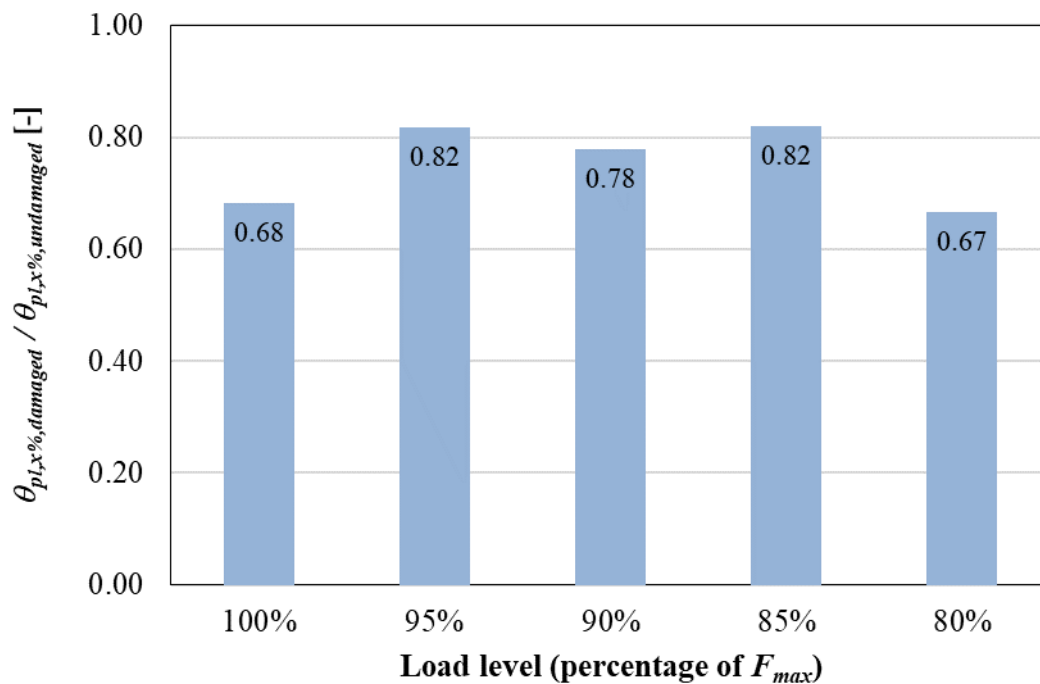


Figure 9.28 Ratio between plastic rotation capacity of beams with damaged reinforcement and beams with undamaged reinforcement. The values refer to average values of statically loaded beams.

The total internal work, W_{tot} , and internal work at different load levels, $W_{pl,x\%}$, are listed in Table 9.25 for beams with undamaged reinforcement and in Table 9.26 for beams with damaged reinforcement. The methodology of internal work is described in Section 3.3. A schematic illustration of how the internal work is interpreted and calculated can be found in Appendix J. The same conclusions as made for the comparison of the plastic rotation capacity can be made for the internal work. The internal work at different load levels is correlated to the plastic rotation at the same load level. This is reasonable since the calculation procedures for internal work and plastic rotation capacity are based on the same methodology.

Table 9.25 *Internal work at different load levels for statically loaded beams with undamaged reinforcement.*

Beam	W_{tot} [Nm]	$W_{pl,100\%}$ [Nm]	$W_{pl,95\%}$ [Nm]	$W_{pl,90\%}$ [Nm]	$W_{pl,85\%}$ [Nm]	$W_{pl,80\%}$ [Nm]
S-UD-B1-01	486	123	160	218	242	344
S-UD-B1-02	432	138	152	213	266	348
S-UD-B2-03	488	148	183	203	227	279
Average	469	136	165	211	245	324

Table 9.26 *Internal work at different load levels for statically loaded beams with damaged reinforcement.*

Beam	W_{tot} [Nm]	$W_{pl,100\%}$ [Nm]	$W_{pl,95\%}$ [Nm]	$W_{pl,90\%}$ [Nm]	$W_{pl,85\%}$ [Nm]	$W_{pl,80\%}$ [Nm]
S-D-B1-04	254	86.2	116	158	188	208
S-D-B2-05	364	112	166	203	242	252
S-D-B2-06	315	103	150	167	209	242
Average	311	100	144	176	213	234

Furthermore, the total internal work calculated based on the average load-deflection curve for Series S-UD and S-D, is presented in Table 9.27. This parameter is later used in Section 9.4.3.3.2. It is visible that there is no big difference between the average value of the total internal work for the three beams in a series compared to the total internal work based on the average curve for the same series.


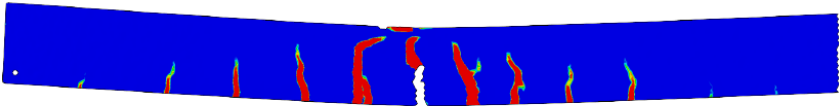
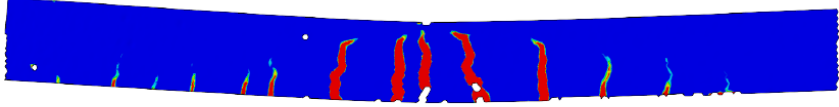
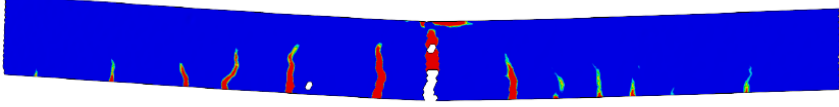

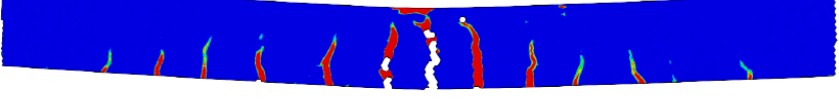

Table 9.27 *Total internal work, W_{static} , based on the average load-deflection curve for Series S.*

Series	W_{static} [Nm]
S-UD	450
S-D	303

9.4.2.2 Strain fields

The strain fields at a deformation of 30 mm for beams in Series S are presented in Table 9.28. At this stage all beams have reached their maximum load, F_{max} , and all the major cracks have appeared. All beams show similar crack patterns with clear bending cracks along the bottom of the beams. There is no distinct difference in crack pattern between beams in Series S-UD and Series S-D. Note that the colour white in the strain fields indicate areas where information is lost. This could be either due to lost contact with the surface component or loss of concrete due to spalling. For the beams in Series S the white areas are mainly due to spalling of the concrete surface close to wide cracks. Pictures of all beams at a total deformation of 30 mm can be found in Appendix K.

Table 9.28 Visualisation of strain fields at a total deformation of 30 mm of beams subjected to static testing only.

Force [kN]	Strain fields of beams in Series S
Beam S-UD-B1-01 $F_{30mm} = 8.97$	
Beam S-UD-B1-02 $F_{30mm} = 9.05$	
Beam S-UD-B2-03 $F_{30mm} = 9.34$	
Beam S-D-B1-04 $F_{30mm} = 8.19$	
Beam S-D-B2-05 $F_{30mm} = 9.89$	
Beam S-D-B2-06 $F_{30mm} = 8.83$	
[%]	 1.2 1.3 1.4 1.5 1.6 1.7 1.8 1.9 2.0

9.4.3 Results for Series I10

This section presents the results for beams in Series I10 regarding curves for load-deflection relationship and strain fields at a total deformation of 30 mm. The load-deflection curves describe the structural behaviour and are used to calculate the internal work and stiffness at different stages. Furthermore, the results obtained for Series I10 are compared to the results obtained for Series S.

9.4.3.1 Load-deflection relationship

The load-deflection relationship of the beams in Series I10, i.e. beams dynamically loaded with 10 kg drop-weight prior to the static testing, can be seen in Figure 9.29. Comparison is made between beams with undamaged reinforcement (solid line) and beams with damaged reinforcement (dashed line). Additionally, outer envelopes and average load-deflection relationship are presented in Figure 9.30 for beams with undamaged reinforcement and Figure 9.31 for beams with damaged reinforcement.

Initially, all beams in Series I10 show a similar behaviour independently on whether they have undamaged or damaged reinforcement. It is visible that Series I10-UD yields slightly earlier than Series I10-D. Furthermore, beams in Series I10-UD show a considerably larger ductility compared to Series I10-D. Comparing the average curves in Figure 9.30 and Figure 9.31, the beams with undamaged reinforcement reaches a somewhat lower maximum load than the beams with damaged reinforcement, just as for Series S.

It should be noted that the curves for outer envelopes and average load-deflection relationships for Series I10 and Series I20 can be somewhat misleading. At some places, especially at the end part of the curves, one can see that the average curve is not laying within the outer envelopes, which may seem unreasonable. This is due to the fact that the load in the outer envelopes and average curves are here based on a given deformation. Another way to display average and envelope curves could be to base the values of the deflection on given load. However, the curves displayed in this thesis are considered to be sufficient to represent the tested beams.

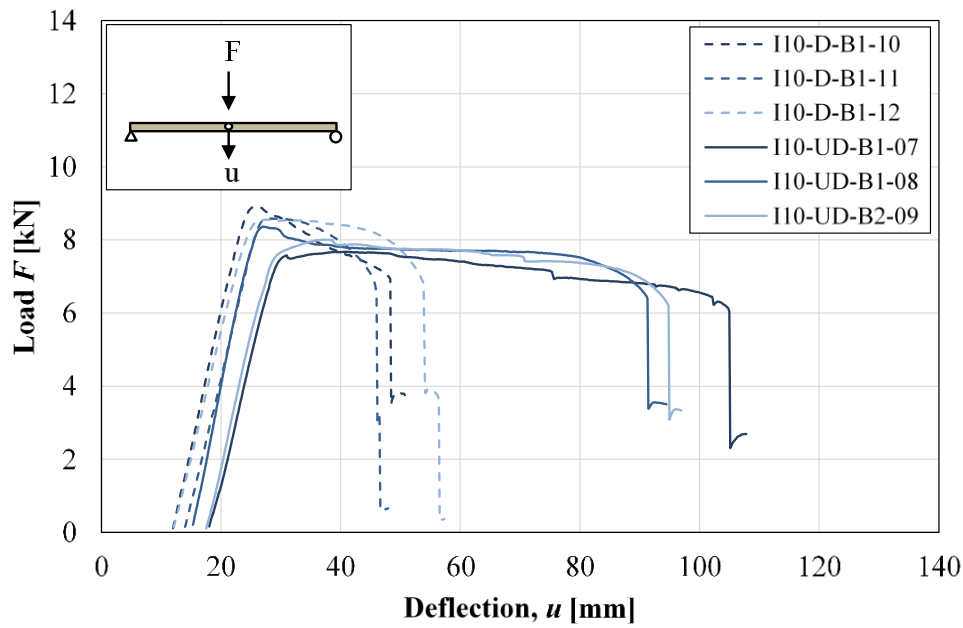


Figure 9.29 Load-deflection relationship for beams with damaged and undamaged reinforcement dynamically loaded with 10 kg drop-weight prior to the static test. The experimental set-up was in this case static three point loading.

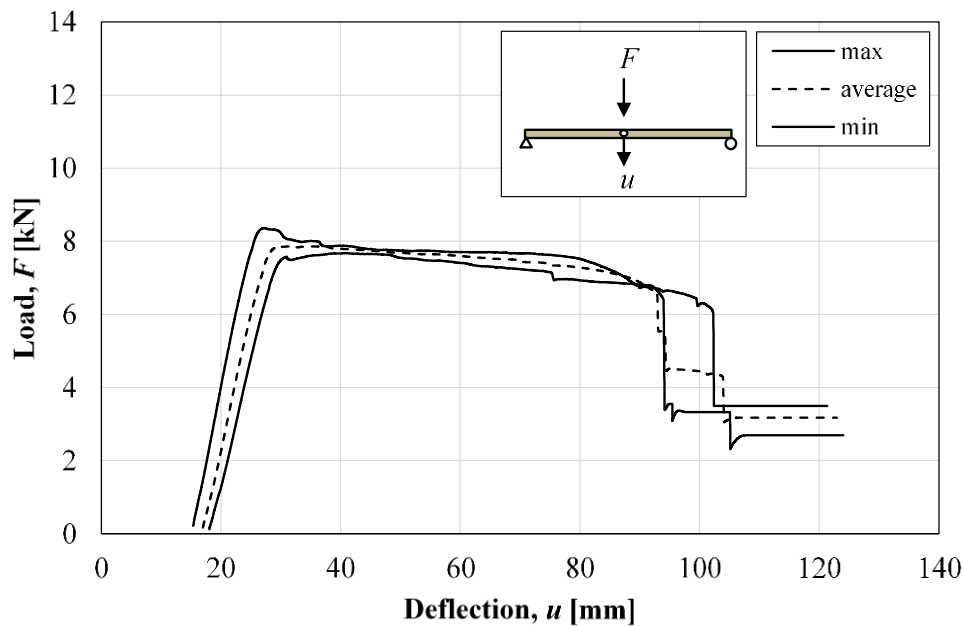


Figure 9.30 Outer envelopes and average load-deflection relationship for beams with undamaged reinforcement dynamically loaded with 10 kg drop-weight prior to the static test. The experimental set-up was in this case static three point loading.

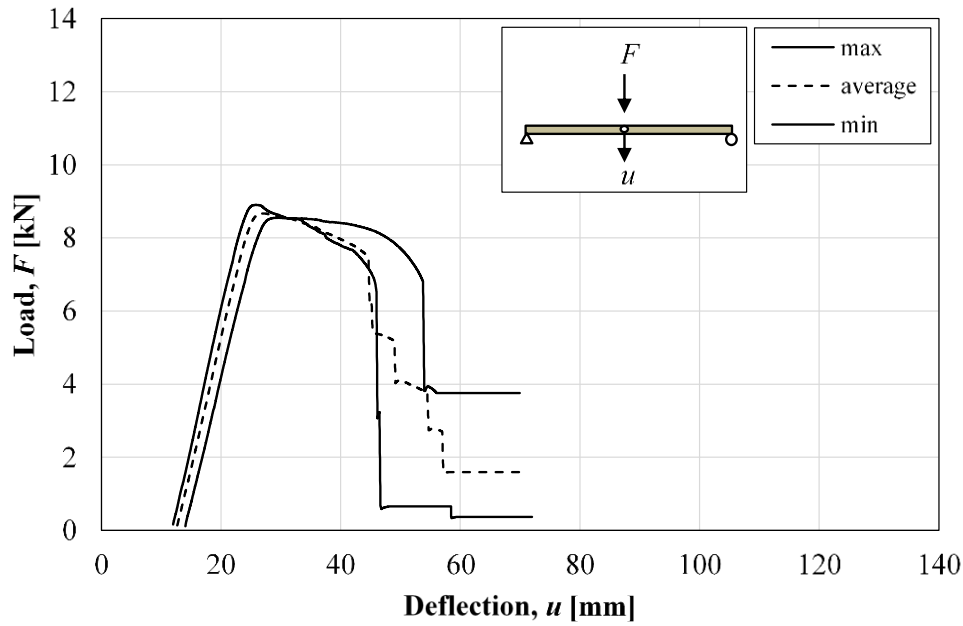


Figure 9.31 Outer envelopes and average load-deflection relationship for beams with damaged reinforcement dynamically loaded with 10 kg drop-weight prior to the static test. The experimental set-up was in this case static three point loading.

Values for maximum deflection before failure, maximum load, ratio between ultimate moment and yield moment and finally the stiffness are presented in Table 9.29 for beams with undamaged reinforcement and in Table 9.30 for beams with damaged reinforcement. There is no noticeable difference in stiffness or ratio between ultimate moment and yield moment when comparing Series I10-UD and Series I10-D.

Table 9.29 Maximum deflection, maximum load, ratio between ultimate moment and yield moment and stiffness for beams with undamaged reinforcement dynamically loaded with 10 kg drop-weight.

Beam	u_{fail} [mm]	F_{max} [kN]	M_u / M_y [-]	k_{dam} [MN/m]
I10-UD-B1-07	87.0	7.68	1.01	0.633
I10-UD-B1-08	76.0	8.36	1.00	0.761
I10-UD-B1-09	77.3	8.01	1.06	0.676
Average	80.1	8.02	1.03	0.690

Table 9.30 Maximum deflection, maximum load, ratio between ultimate moment and yield moment and stiffness for beams with damaged reinforcement dynamically loaded with 10 kg drop-weight.

Beam	u_{fail} [mm]	F_{max} [kN]	M_u / M_y [-]	k_{dam} [MN/m]
I10-D-B1-10	36.3	8.91	1.01	0.701
I10-D-B1-11	32.0	8.59	1.03	0.681
I10-D-B1-12	41.8	8.56	1.01	0.652
Average	36.7	8.68	1.01	0.678

The total internal work, W_{tot} , is tabulated in Table 9.31 for beams with undamaged reinforcement and in Table 9.32 for beams with damaged reinforcement. The methodology of internal work is described in Section 3.3. The total internal work is, compared to Series I10-D, markedly larger for beams in Series I10-UD. This is reasonable since the beams with undamaged reinforcement are considerably more ductile than the beams with damaged reinforcement.

Table 9.31 Total internal work for beams with undamaged reinforcement dynamically loaded with 10 kg drop-weight.

Beam	W_{tot} [Nm]
I10-UD-B1-07	587
I10-UD-B1-08	549
I10-UD-B1-09	544
Average	560

Table 9.32 Total internal work for beams with damaged reinforcement dynamically loaded with 10 kg drop-weight.

Beam	W_{tot} [Nm]
I10-D-B1-10	250
I10-D-B1-11	214
I10-D-B1-12	296
Average	253

9.4.3.2 Strain fields

The strain fields at a total deformation of 30 mm for beams in Series I10 are presented in Table 9.33. At this stage all beams have reached their maximum load, F_{max} , and all the major cracks have appeared. All beams show similar crack patterns with bending cracks along the bottom and two inclined and one vertical crack in the mid span where the drop-weight have hit. There is no distinct difference in crack pattern between beams in Series I10-UD and Series I10-D. However, there are distinct differences compared to Series S, where all cracks are vertical. This indicates that all the cracks in Series I10 appeared during the drop-weight impact. Note that the colour white in the strain fields mark areas where information is lost. This could be either due to lost contact with the

surface component or loss of concrete due to spalling. For the beams in Series I10 the white areas mainly correspond to spalling of the concrete surface close to wide cracks. Pictures of all beams at a deformation of 30 mm can be found in Appendix K.

Table 9.33 Visualization of strain fields at a total deformation of 30 mm of beams subjected to a 10 kg drop-weight impact prior to the static testing.

Force [kN]	Strain fields of beams in Series I10
Beam I10-UD-B1-07 $F_{30mm} = 7.50$	
Beam I10-UD-B1-08 $F_{30mm} = 8.22$	
Beam I10-UD-B1-09 $F_{30mm} = 7.68$	
Beam I10-D-B1-10 $F_{30mm} = 8.61$	
Beam I10-D-B1-11 $F_{30mm} = 8.56$	
Beam I10-D-B1-12 $F_{30mm} = 8.53$	
[%]	 1.2 1.3 1.4 1.5 1.6 1.7 1.8 1.9 2.0

9.4.3.3 Comparison with Series S

In this section a comparison between Series I10 and Series S is made regarding both load-deflection relationship and internal work. Additionally, an approximation of the internal work during the impact for Series I10 is done.

9.4.3.3.1 Load-deflection relationship

The load-deflection relationships of the beams in Series S and Series I10 are compared in Figure 9.32 for beams with undamaged reinforcement and Figure 9.33 for beams with damaged reinforcement.

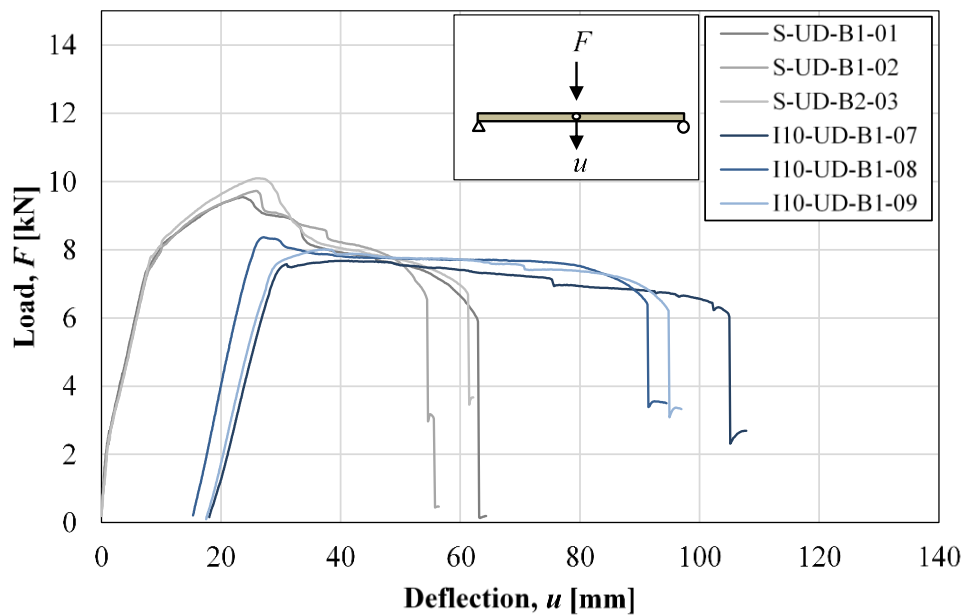


Figure 9.32 Load-deflection relationship for beams with undamaged reinforcement subjected to static load only and beams with undamaged reinforcement subjected to 10 kg drop-weight prior to static loading.

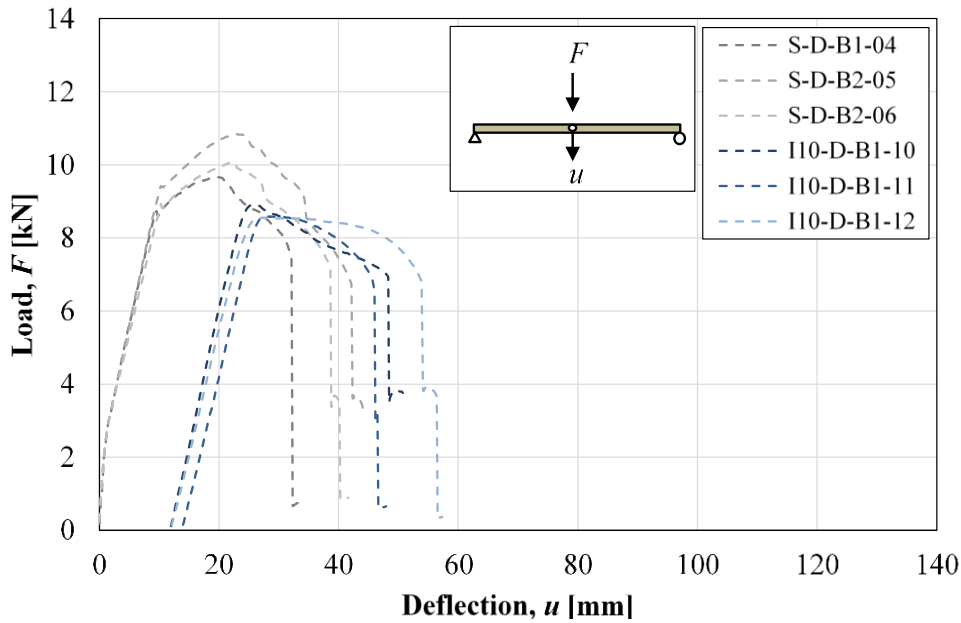


Figure 9.33 Load-deflection relationship for beams with damaged reinforcement subjected to static load only and beams with damaged reinforcement subjected to 10 kg drop-weight prior to static loading.

A comparison between average results of the key parameters obtained from the load-deflection relations from Series S and Series I10 is made in Table 9.34 and Table 9.36 for beams with undamaged reinforcement and Table 9.35 and Table 9.37 for beams with damaged reinforcement.

One can see that, independently of undamaged or damaged reinforcement, beams impacted by a drop-weight experience a reduction in ultimate static load capacity, F_{max} . The reason for this could be due to reduction of the compressive zone, after the impact. Beams with undamaged reinforcement that are impacted by a drop-weight experience an increase in both total internal work, W_{tot} , and deflection until considered failed, u_{fail} (i.e. u at 50 % of F_{max} for Series S, see Section 9.4.2.1), when tested statically. This indicates that those beams can be expected to have a larger plastic rotation capacity than beams not impact loaded prior to the static test. In contrast, beams with damaged reinforcement experience a reduction in the same parameters which indicates that those beams instead can be expected to have lower plastic rotation capacity than beams that are not dynamically impacted by a drop-weight prior to the static testing.

Furthermore, the stiffness of impacted beams, k_{dam} , corresponds best with the tangent stiffness in state II, $k_{II,t}$, of the reference beams (beams in Series S). This applies to both undamaged and damaged reinforcement. Moreover, the stiffness of impacted beams is lower than both the secant and the tangent state II stiffness of non impacted beams. This reduction may come from a decrease of the compressive zone due to spalling of concrete in the impact zone during the dynamical test.

Table 9.34 Comparison of average results for beams in Series S-UD and beams in Series I10-UD. The results presented refer to beams with undamaged reinforcement.

Series	u_{fail} [mm]	F_{max} [kN]	W_{tot} [Nm]
S-UD	59.6	9.79	469
I10-UD	80.1	8.02	560
Difference [%]	+34	-18	+19

Table 9.35 Comparison of average results for beams in Series S-D and beams in Series I10-D. The results presented refer to beams with damaged reinforcement.

Series	u_{fail} [mm]	F_{max} [kN]	W_{tot} [Nm]
S-D	37.6	10.2	311
I10-D	36.7	8.68	253
Difference [%]	-2	-15	-19

Table 9.36 Comparison of average results for beams in Series S-UD and beams in Series I10-UD. The results presented refer to beams with undamaged reinforcement.

Series	k_I (k_{dam}) [MN/m]	$k_{II,s}$ (k_{dam}) [MN/m]	$k_{II,t}$ (k_{dam}) [MN/m]	k_{III} (k_{dam}) [MN/m]
S-UD	2.09	0.926	0.766	0.128
I10-UD	0.690	0.690	0.690	0.690
Difference [%]	-67	-26	-10	+439

Table 9.37 Comparison of average results for beams in Series S-D and beams in Series I10-D. The results presented refer to beams with damaged reinforcement.

Series	k_I (k_{dam}) [MN/m]	$k_{II,s}$ (k_{dam}) [MN/m]	$k_{II,t}$ (k_{dam}) [MN/m]	k_{III} (k_{dam}) [MN/m]
S-D	2.06	0.875	0.728	0.105
I10-D	0.678	0.678	0.678	0.678
Difference [%]	-67	-23	-7	+546

9.4.3.3.2 Approximation of internal work during impact

It is of interest to investigate the internal work during the impact of the beams. However, the load-deflection relationship during the dynamic test is not known. To get an idea of the structural response during the dynamic testing, the load-deflection relation during the impact could be assumed to act as the static response of the reference beams (Series S), up to a point where unloading coincide with the static response of the impacted beams (Series I10).

Load-deflection curves for beams in Series I10 together with the average curve for Series S can be seen in Figure 9.34 and Figure 9.35 for undamaged and damaged reinforcement, respectively.

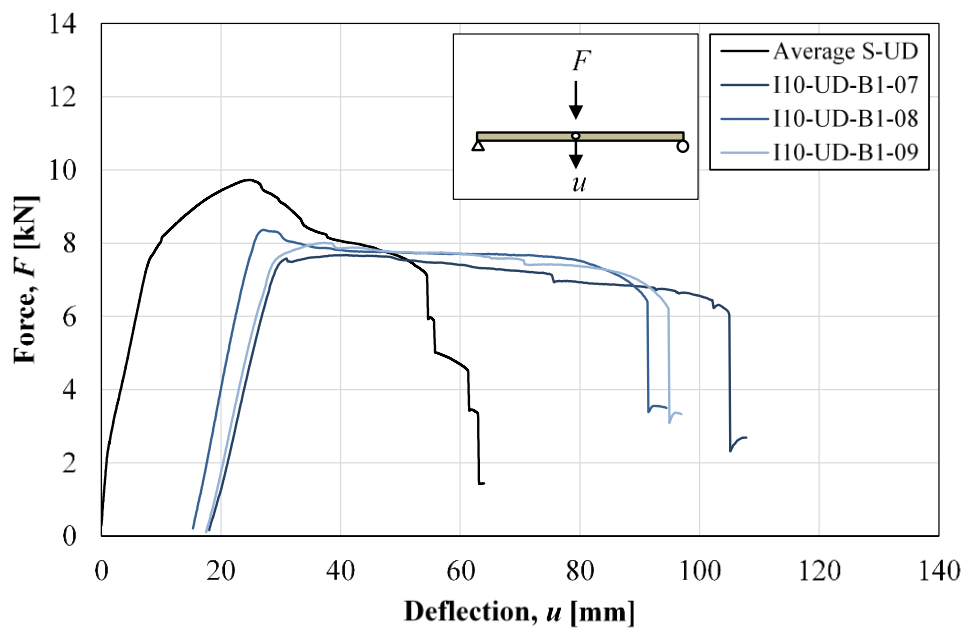


Figure 9.34 Load-deflection relationship for beams in Series I10-UD and the average curve for Series S-UD. The curves refer to beams with undamaged reinforcement.

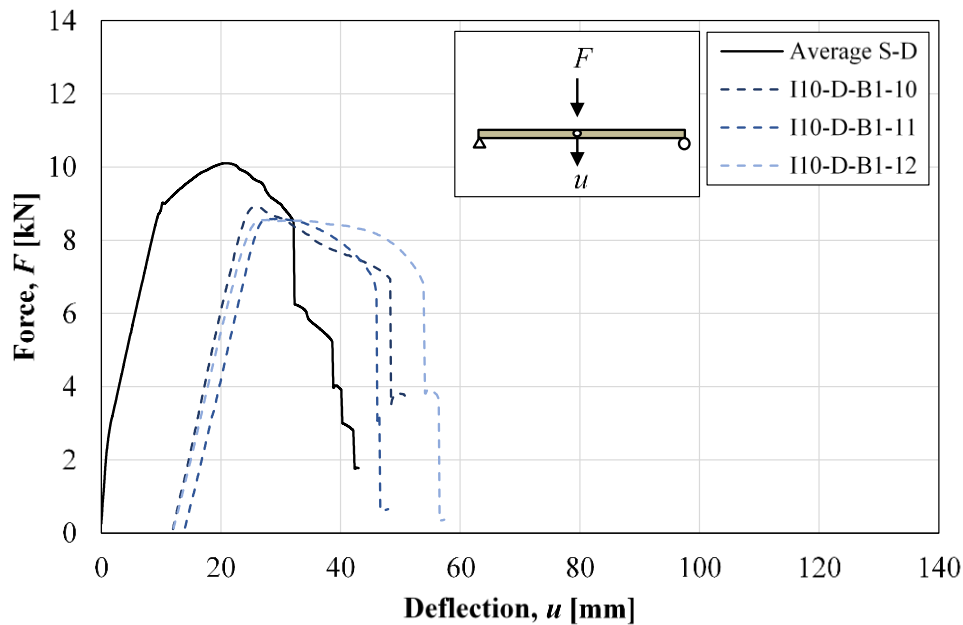


Figure 9.35 Load-deflection relationship for beams in Series I10-D and the average curve for Series S-D. The curves refer to beams with damaged reinforcement.

Based on the curves in Figure 9.34 and Figure 9.35, some key parameters regarding internal work were calculated, tabulated in Table 9.39 and Table 9.40. The total internal work, W_{static} , based on the average load-deflection curve for Series S can be found in Table 9.38. These values are used for the comparison in Table 9.39 and Table 9.40. Additionally, a comparison between beams with undamaged and damaged reinforcement is made in Table 9.41.

$W_{dynamic}$ is assumed to represent the energy consumed during the impact. $W_{impact+static}$ is interpreted as the energy consumed during both the impact and the static test. Finally, the ratio between $W_{impact+static}$ and W_{static} can be regarded as an indication of the increase in internal work due to the impact. A graphical interpretation of the different parameters in the tables can be found in Appendix L.

It is visible that the total internal work is increased substantially due to the impact. This yields for both beams with undamaged and damaged reinforcement. However, the increase is largest when undamaged reinforcement is used.

Table 9.38 Total internal work, W_{static} , based on the average load-deflection curve for Series S.

Series	W_{static} [Nm]
S-UD	450
S-D	303

Table 9.39 Parameters used to approximate the internal work due to impact for beams in Series I10-UD, based on the average load-deflection curve for Series S-UD. The results presented refer to beams with undamaged reinforcement.

Beam	$W_{dynamic}$	$W_{impact+static}$	$\frac{W_{impact+static}}{W_{static}}$
I10-UD-B1-07	249	785	1.74
I10-UD-B1-08	217	710	1.58
I10-UD-B1-09	242	731	1.62
Average	236	742	1.65

Table 9.40 Parameters used to approximate the internal work due to impact for beams in Series I10-D, based on the average load-deflection curve for Series S-D. The results presented refer to beams with damaged reinforcement.

Beam	$W_{dynamic}$	$W_{impact+static}$	$\frac{W_{impact+static}}{W_{static}}$
I10-D-B1-10	203	388	1.28
I10-D-B1-11	227	375	1.23
I10-D-B1-12	214	442	1.46
Average	215	402	1.32

Table 9.41 Comparison of average results of parameters used to approximate the internal work due to impact for beams in Series I10-UD and beams in Series I10-D.

Series	$W_{dynamic}$	$W_{impact+static}$	$\frac{W_{impact+static}}{W_{static}}$
I10-UD	236	742	1.65
I10-D	215	402	1.32
Difference [%]	-9	-46	-20

9.4.4 Results for Series I20

This section presents the results for beams in Series I20 regarding curves for load-deflection relationship and strain fields at maximum load. The load-deflection curves describe the structural behaviour and are used to calculate the internal work and stiffness at different stages. Since the beams in Series I20 were statically tested by four point bending, the results are difficult to compare to both Series S and Series I10. Hence, the static results for Series I20 is only compared to the predicted results, see Section 10.2.3.

It should be noted that beam I20-UD-B2-15 was accidentally hit by the drop-weight from a height of approximately two meters before the real intended impact test started.

This beam experienced a lot of concrete spalling after the intentional impact test (i.e. drop from 5.0 m) and was considered to more or less have consumed all its load bearing capacity and was therefore determined to not be tested statically. A picture of beam I20-UD-B2-15 after the intended impact can be seen in Appendix K.

9.4.4.1 Load-deflection relationship

The load-deflection relationship of the beams in Series I20 can be seen in Figure 9.36. Comparison is made between beams with undamaged reinforcement (solid line) and beams with damaged reinforcement (dashed line). Additionally, outer envelopes and average load-deflection relationship are presented in Figure 9.37 for beams with undamaged reinforcement and Figure 9.38 for beams with damaged reinforcement.

Initially, all beams in Series I20 show a similar behaviour independently on whether they have undamaged or damaged reinforcement. Additionally, comparing the average curves in Figure 9.37 and Figure 9.38, there is no distinct difference in neither ductility nor reached maximum load.

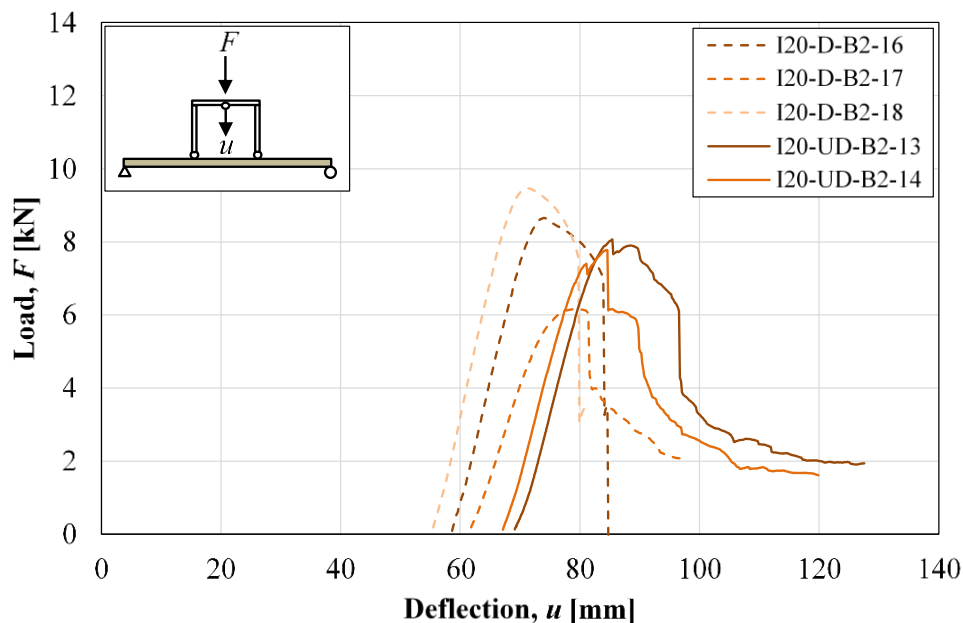


Figure 9.36 Load-deflection relationship for beams with damaged and undamaged reinforcement dynamically loaded with 20 kg drop-weight prior to the static test. Note that the experimental set-up in this case was static four point loading.

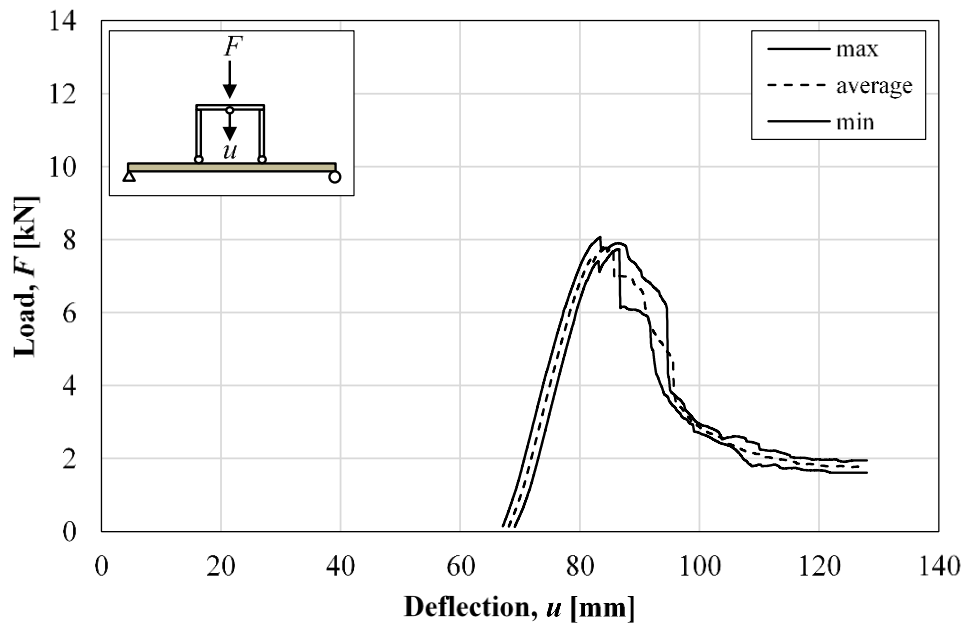


Figure 9.37 Outer envelopes and average load-deflection relationship for beams with undamaged reinforcement dynamically loaded with 20 kg drop-weight prior to the static test. The experimental set-up was in this case static four point loading.

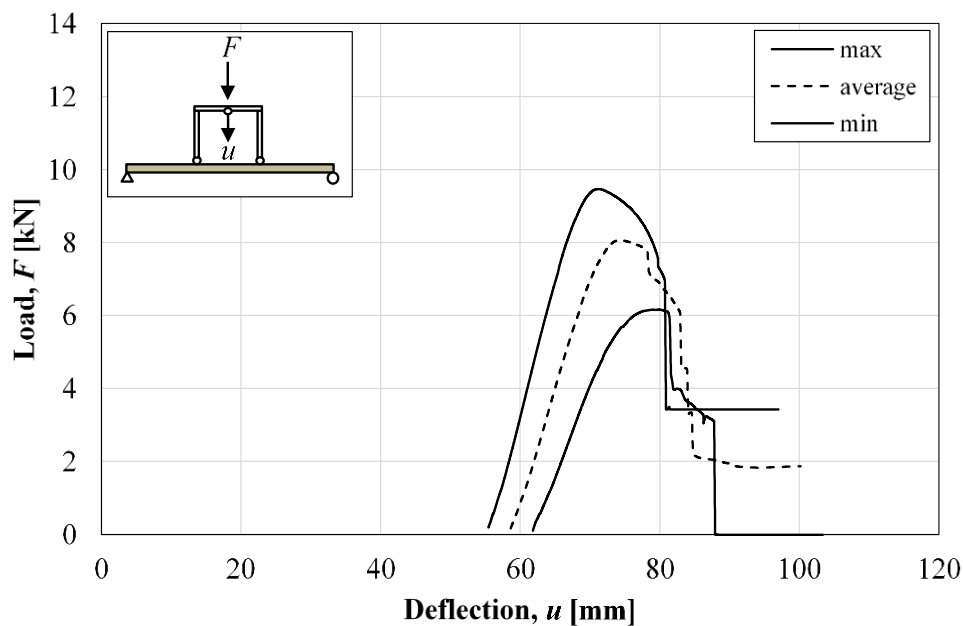


Figure 9.38 Outer envelopes and average load-deflection relationship for beams with damaged reinforcement dynamically loaded with 20 kg drop-weight prior to the static test. The experimental set-up was in this case static four point loading.

Values for maximum deflection before failure (i.e. u at 50 % of F_{max} for Series S, see Section 9.4.2.1),, maximum load, ratio between ultimate moment and yield moment and finally the stiffness are presented in Table 9.42 for beams with undamaged reinforcement and in Table 9.43 for beams with damaged reinforcement. There is no

noticeable difference in stiffness or ratio between ultimate moment and yield moment when comparing Series I20-UD and Series I20-D.

Table 9.42 Maximum deflection, maximum load, ratio between ultimate moment and yield moment and stiffness for beams with undamaged reinforcement dynamically loaded with 20 kg drop-weight.

Beam	u_{fail} [mm]	F_{max} [kN]	M_u / M_y [-]	k_{dam} [MN/m]
I20-UD-B2-13	27.6	8.07	1.02	0.551
I20-UD-B2-14	22.6	7.78	1.06	0.543
I20-UD-B2-15	-	-	-	-
Average	25.1	7.93	1.04	0.547

Table 9.43 Maximum deflection, maximum load, ratio between ultimate moment and yield moment and stiffness for beams with damaged reinforcement dynamically loaded with 20 kg drop-weight.

Beam	u_{fail} [mm]	F_{max} [kN]	M_u / M_y [-]	k_{dam} [MN/m]
I20-D-B2-16	25.3	8.66	1.00	0.621
I20-D-B2-17	19.6	6.16	1.01	0.456
I20-D-B2-18	24.3	9.46	1.00	0.685
Average	23.1	8.09	1.01	0.587

The total internal work, W_{tot} , is tabulated in Table 9.44 for beams with undamaged reinforcement and in Table 9.45 for beams with damaged reinforcement. The methodology of internal work is described in Section 3.3. There is no noticeable difference in total internal work between beams with undamaged or damaged reinforcement. This is reasonable since, as mentioned before, there is no distinguished difference in ductility either.

Table 9.44 Total internal work for beams with undamaged reinforcement dynamically loaded with 20 kg drop-weight.

Beam	W_{tot} [Nm]
I20-UD-B2-13	156
I20-UD-B2-14	115
I20-UD-B2-15	-
Average	135

Table 9.45 Total internal work for beams with damaged reinforcement dynamically loaded with 20 kg drop-weight.

Beam	W_{tot} [Nm]
I20-D-B2-16	156
I20-D-B2-17	82
I20-D-B2-18	162
Average	133

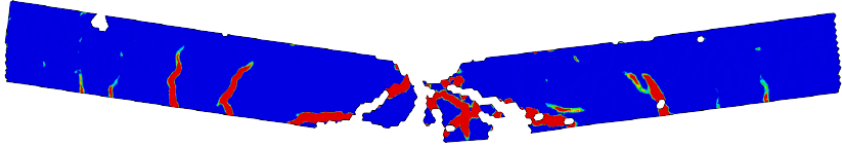
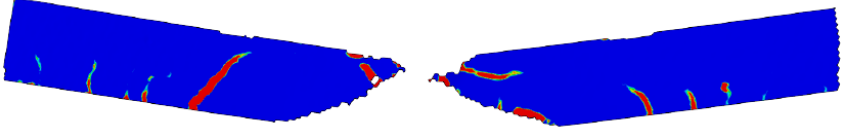
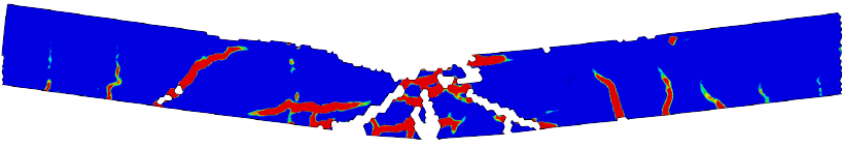
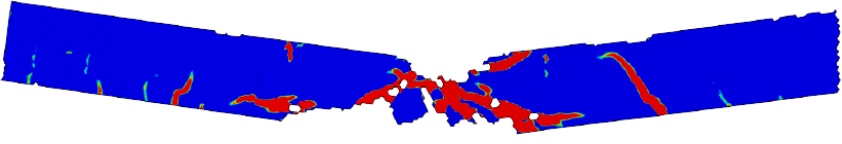
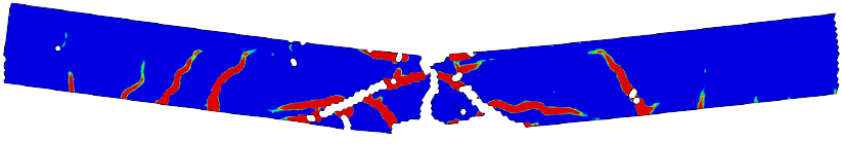

9.4.4.2 Strain fields

The strain fields at maximum load, F_{max} , for beams in Series I20 are presented in Table 9.46. The reason for displaying the strain fields at maximum load instead of at a total deflection of 30 mm is that the beams in Series I20 already have an initial deflection far above that due to the impact test. However, a comparison of crack pattern with Series S is reasonable since most cracks appeared during the drop-weight impact. Therefore, the difference in load case does not have large effects on the pattern.

All beams show similar crack patterns although it is hard to evaluate since there are lots of white areas in the pictures. This could be either due to lost contact with the surface component, excessive spalling of concrete or just spalling of the surface concrete layer. For the beams in Series I20 the white areas primarily corresponds to excessive spalling of the concrete surface. In one case, for beam I20-UD-B2-14, the white areas mainly correspond to lost contact with the surface component. Pictures of all beams at maximum load can be found in Appendix K. There is no distinct difference in crack pattern between beams in Series I20-UD and Series I20-D.

Series I20 shows great differences in crack pattern compared to Series S. The cracks are inclined which is not the case for Series S. This indicates, as for Series I10, that the cracks appeared during the impact. Furthermore, Series I20 shows similar patterns as Series I10, however, there are more cracks close to where the drop-weight impacted the beam.

Table 9.46 Visualization of strain fields at maximum load, F_{max} , of beams subjected to a 20 kg drop-weight impact prior to the static testing.

Deflection [mm]	Strain fields of beams in Series I20
Beam I20-UD-B2-13 $u_{Fmax} = 85.2$	
Beam I20-UD-B2-14 $u_{Fmax} = 84.5$	
Beam I20-UD-B2-15 $u_{Fmax} = ^{(1)}$	(1)
Beam I20-D-B2-16 $u_{Fmax} = 74.1$	
Beam I20-D-B2-17 $u_{Fmax} = 78.9$	
Beam I20-D-B2-18 $u_{Fmax} = 71.3$	
[%]	 1.2 1.3 1.4 1.5 1.6 1.7 1.8 1.9 2.0

⁽¹⁾Not tested statically due to excessive spalling of concrete in the dynamic test.

9.4.4.3 Comparison with Series S

As mentioned before, the beams in Series I20 were statically tested by four point bending. This makes the response difficult to compare to Series S (apart from the crack patterns) which were statically tested by three point bending. Therefore, Series I20 is only compared to predicted results in Section 10.2.3.

10 Comparison between experimental results and predictions

This section exhibit several comparisons between the predicted and experimental results, and is based on Chapter 8 and 9. This is aimed for comparing the results through all the steps of the beams' lives.

10.1 Dynamic response

This part is mainly aimed for comparing the 2DOF model to the beam experiments. However, it also includes the initial shear velocity.

10.1.1 2DOF

The main parts studied in the comparison between the 2DOF model and the experimental results are the deflections of the beam along with the velocity of the drop-weight. Such results are presented in Figure 10.1 to Figure 10.4 for all the series. A detailed comparison of some deflections of interest is made in Table 10.1 to Table 10.4. The comparisons are made with both the predicted R_2 and the one measured in the results to see which yields results closest to reality.

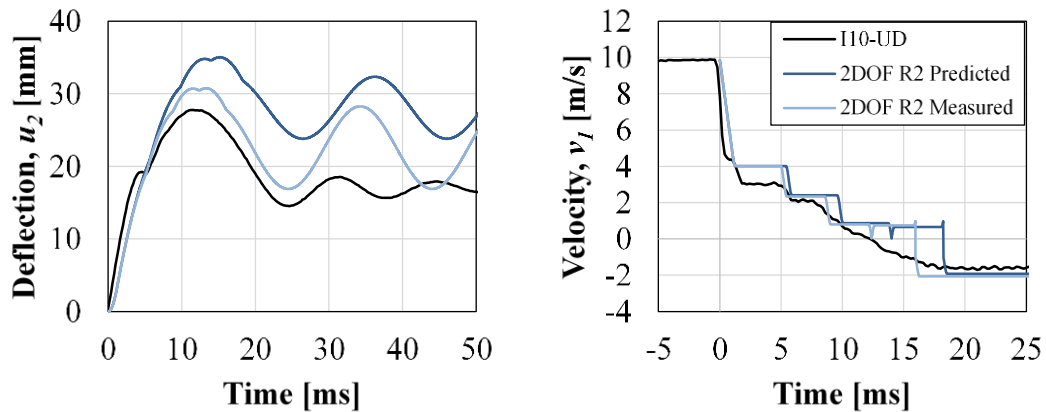


Figure 10.1 Comparison between experimental results and 2DOF model of deflection of beam, u_2 , and velocity of drop-weight, v_1 , after impact for I10-UD.

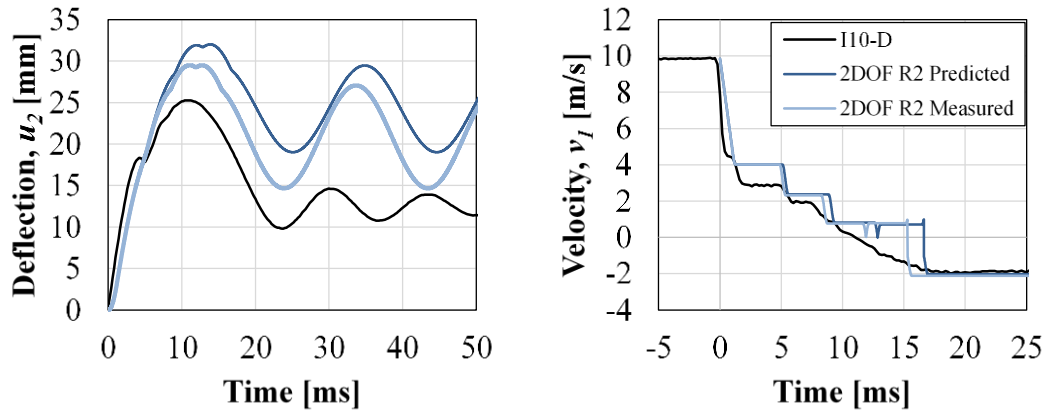


Figure 10.2 Comparison between experimental results and 2DOF model of deflection of beam, u_2 , and velocity of drop-weight, v_1 , after impact for I10-D.

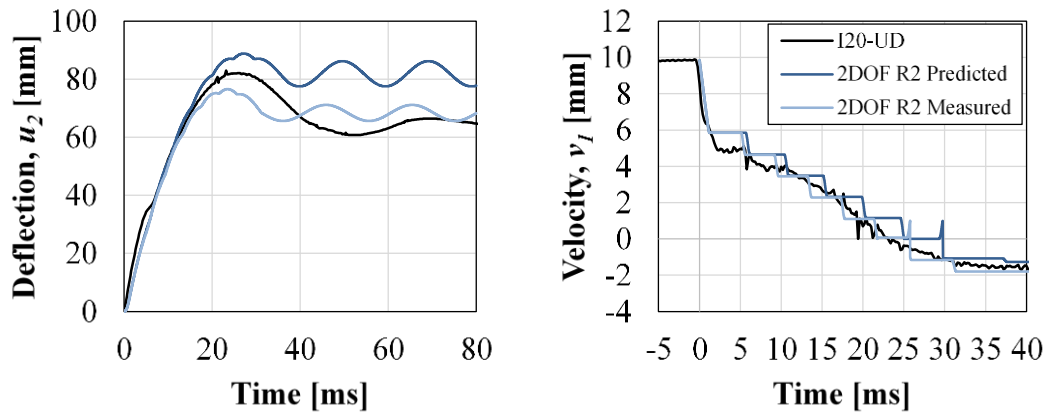


Figure 10.3 Comparison between experimental results and 2DOF model of deflection of beam, u_2 , and velocity of drop-weight, v_1 , after impact for I20-UD.

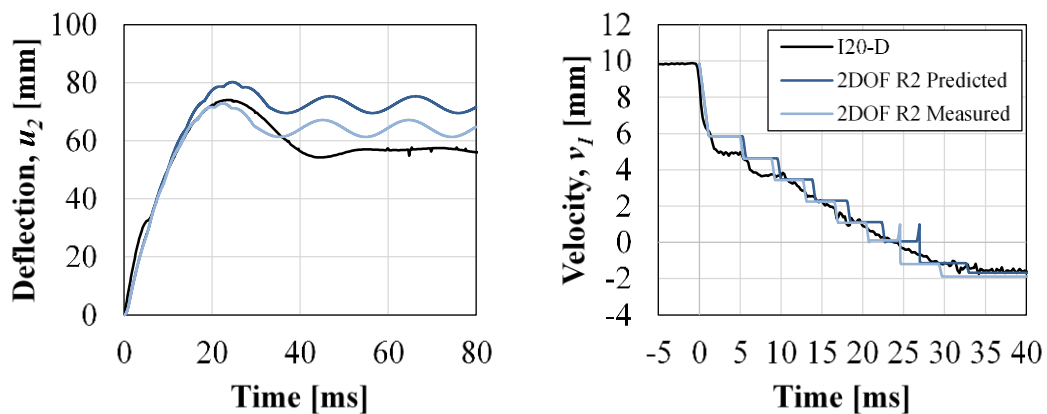


Figure 10.4 Comparison between experimental results and 2DOF model of deflection of beam, u_2 , and velocity of drop-weight, v_1 , after impact for I20-D.

The velocity of the drop-weight in the 2DOF model shows a behaviour not far away from the real one for all series.

The deflections on the other hand are slightly different compared to the real behaviour. It is evident that the 2DOF model gives too large plastic deflection for all cases; except for series I20-UD when the 2DOF has been calculated using the measured resistance R_2 ; then the results are almost equal. The maximum deflection on the other hand yields a too large result for all the series when the predicted R_2 is used in 2DOF. This is expected since the predicted ultimate load is clearly underestimated, as seen in Section 10.2. However, the predictions correspond better to the experiments for Series I20 than I10. When it comes to the maximum deflection based on the measured R_2 , there is no clear trend. As seen, the 2DOF model yields results that are slightly higher than the measured values for the I10-series. However, the maximum deflection is estimated lower than the experimental results for the I20-beams. This yields that the predicted R_2 is on the safe side to use, while the measured R_2 is slightly more unsafe to use in the 2DOF-model.

Table 10.1 Comparison of u_{max} between measured and predicted values with R_2 as predicted..

Series	Measured u_{max} [mm]	Predicted $u_{max,2DOF}$ [mm]	Difference Δu_{max}	
			[mm]	[%]
I10-UD	27.9	35.0	+8.0	+29
I10-D	25.3	32.0	+6.7	+26
I20-UD	82.1	88.8	+6.7	+8
I20-D	74.2	80.2	+6.0	+8

Table 10.2 Comparison of u_{max} between measured and predicted values with R_2 as measured.

Series	Measured u_{max} [mm]	Predicted $u_{max,2DOF}$ [mm]	Difference Δu_{max}	
			[mm]	[%]
I10-UD	27.9	30.8	+2.9	+10
I10-D	25.3	29.5	+4.2	+17
I20-UD	82.1	76.6	-5.5	-7
I20-D	74.2	72.9	-1.3	-2

Table 10.3 Comparison of u_{pl} between measured and predicted values with R_2 as predicted.

Series	Measured u_{pl} [mm]	Predicted $u_{pl,2DOF}$ [mm]	Difference Δu_{pl}	
			[mm]	[%]
I10-UD	17.0	28.1	+11	+65
I10-D	12.7	24.2	+12	+94
I20-UD	68.1	81.9	+14	+21
I20-D	58.6	72.4	+14	+24

Table 10.4 Comparison of u_{pl} between measured and predicted values with R_2 as measured.

Series	Measured u_{pl} [mm]	Predicted $u_{pl,2DOF}$ [mm]	Difference Δu_{pl}	
			[mm]	[%]
I10-UD	17.0	22.6	+5.6	+33
I10-D	12.7	20.9	+8.2	+65
I20-UD	68.1	68.4	+0.3	+0
I20-D	58.6	64.2	+5.6	+10

10.1.2 Initial shear velocity

The experimental results show that it takes the deflection to reach the end of the beam around 1.6 - 1.8 ms while the prediction according to Yi et al (2016) turn out at 0.28 ms, see Section 8.3.2. This is around 5 – 6 times smaller than the measured value which is in line with what Jönsson and Stenseke (2018) observed.

10.2 Static response

The static response of the beams is compared using the load-deflection curves for all series.

10.2.1 Series S

The load-deflection curves for series S are presented in Figure 10.5 and Figure 10.6 for beams with undamaged and damaged reinforcement respectively. The predictions used are the ones considering cracking of the concrete as a part of the evolution. Before the curve reaches ultimate capacity, the predictions overestimate the load slightly. However, the reason for the significant underestimation of the ultimate load is unknown. These observations hold for both undamaged and damaged reinforcement.

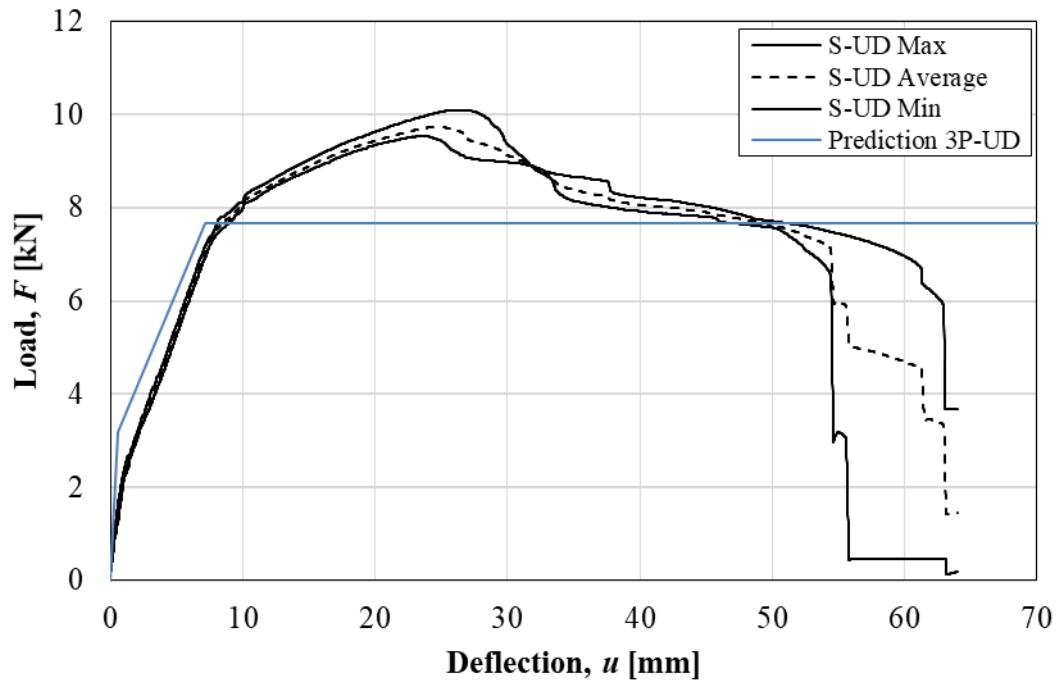


Figure 10.5 Load-deflection curves retrieved from experiments and predictions for series S-UD.

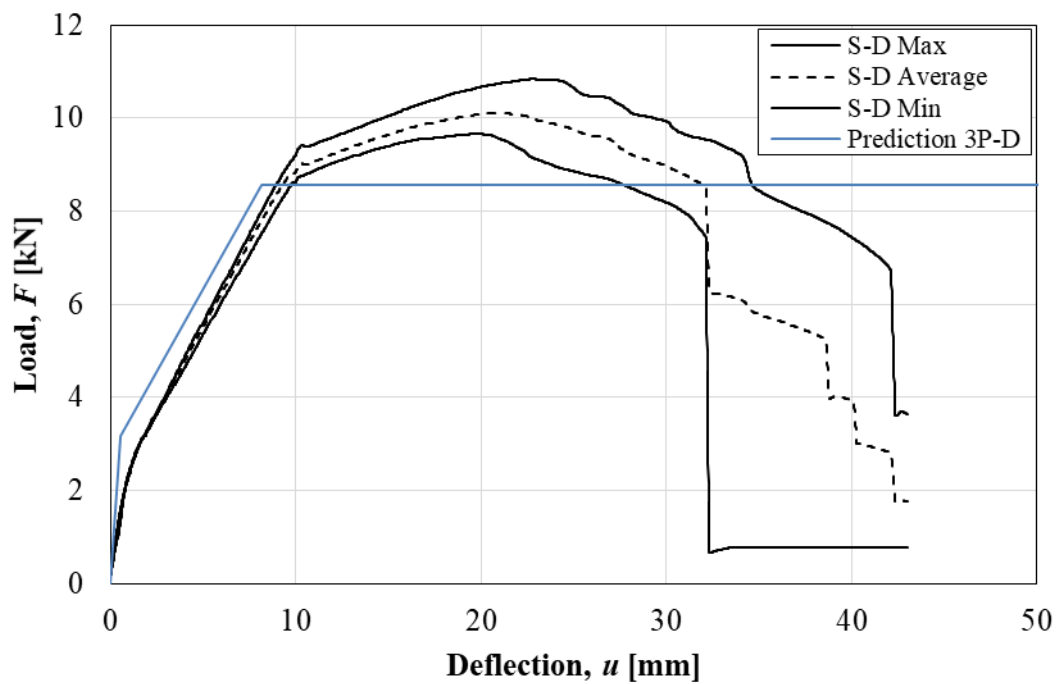


Figure 10.6 Load-deflection curves retrieved from experiments and predictions for series S-D.

For the beams in Series S, the predicted stiffness between cracking and yielding, $k_{II,t}$ or k_{cy} , corresponds well with the measured stiffness. This holds for both undamaged and damaged reinforcement. However, the predicted stiffness in state I, k_I , is markedly

higher than the measured value. This implies a stiffness prediction on the unsafe side when using the 2DOF model. This is also visible in Table 10.5.

Table 10.5 Stiffness for Series S based on experiments and predictions.

Reinforcement	Method	k_I [MN/m]	$k_{II,t}$ or k_{cy} [MN/m]
Undamaged	Measured	2.09	0.766
	Predicted	6.11	0.684
Damaged	Measured	2.06	0.728
	Predicted	6.10	0.710

10.2.2 Series I10

The load-deflection curves for series I10 are presented in Figure 10.7 and Figure 10.8 for beams with undamaged and damaged reinforcement respectively. The predictions used are the ones not considering cracking of the concrete as a part of the evolution, but the state II stiffness instead. The reason for comparing with this curve is that it was clear that the beams had already cracked during the impact.

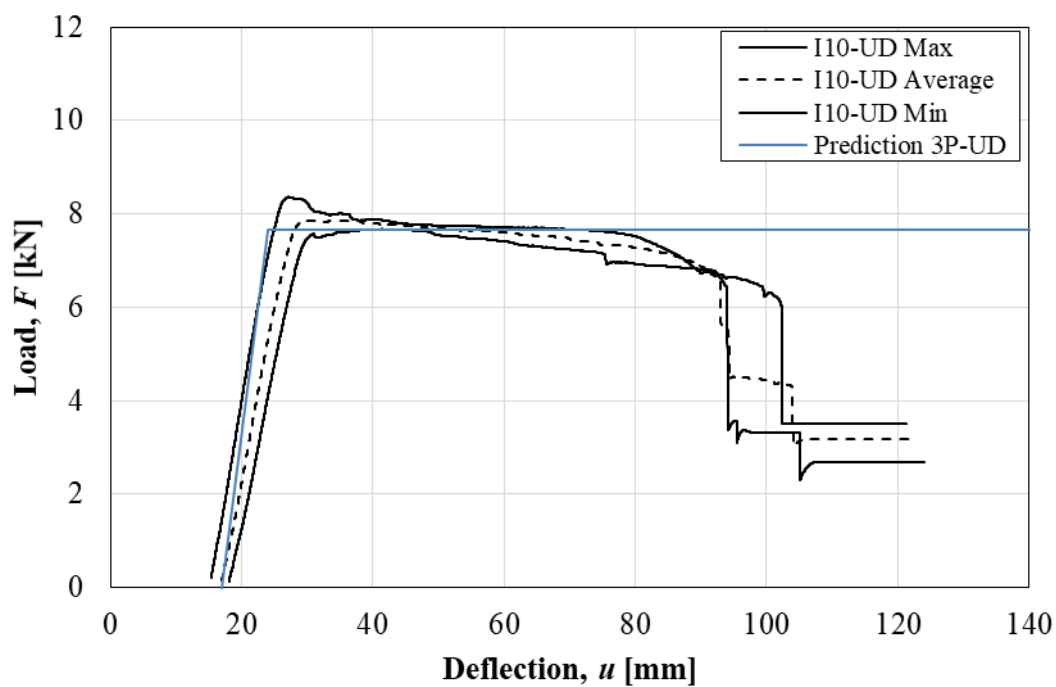


Figure 10.7 Load-deflection curves retrieved from experiments and predictions for series I10-UD.

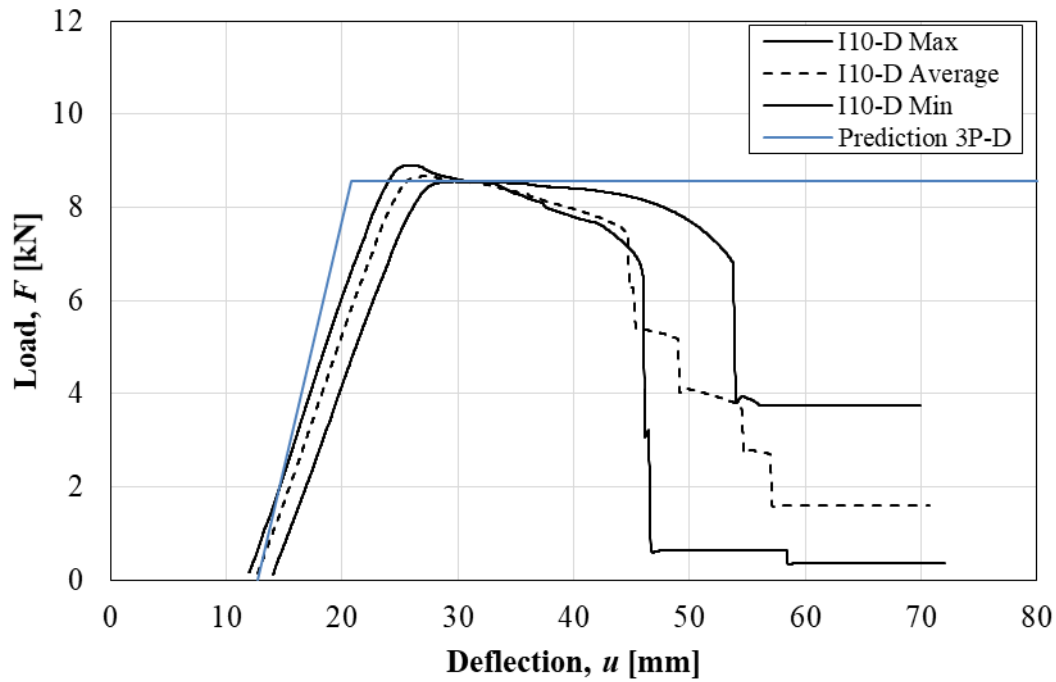


Figure 10.8 Load-deflection curves retrieved from experiments and predictions for series I10-D.

For the I10-beams, the predicted load capacity is corresponding well to the measured one. However, the stiffness in state II is slightly higher than the measured one. This could come from a reduction of the compressive zone in the impact area, which is not considered in the predictions. This is also shown in Table 10.6.

Table 10.6 Stiffness for Series I10 based on experiments and predictions.

Reinforcement	k_{dam} or k_{II} [MN/m]	
Undamaged	Measured	0.690
	Predicted	1.08
Damaged	Measured	0.678
	Predicted	1.06

Looking at the graphs, it seems that the predictions does not fully predict the influence of the damaged reinforcement. The stiffness does not seem to correspond as well in the damaged case as in the undamaged case. This could be due to the higher stress in the pre-stretched rebars which could result in greater damage of the compressive zone in the impact area.

10.2.3 Series I20

There are no pure static reference beams for the 20 kg-beams since they were tested with four point bending. However, the static three point tests showed a maximum load that was 28 % and 19 % higher than the predicted load for undamaged and damaged reinforcement, respectively. The same underestimation in the predictions is assumed here.

The load-deflection curves for series I20 are presented in Figure 10.9 and Figure 10.10 for beams with undamaged and damaged reinforcement respectively. The predictions used are the ones both considering and not considering cracking of the concrete. This is to see an approximation of how the purely static load-deflection curve may look for four point bending of the beams.

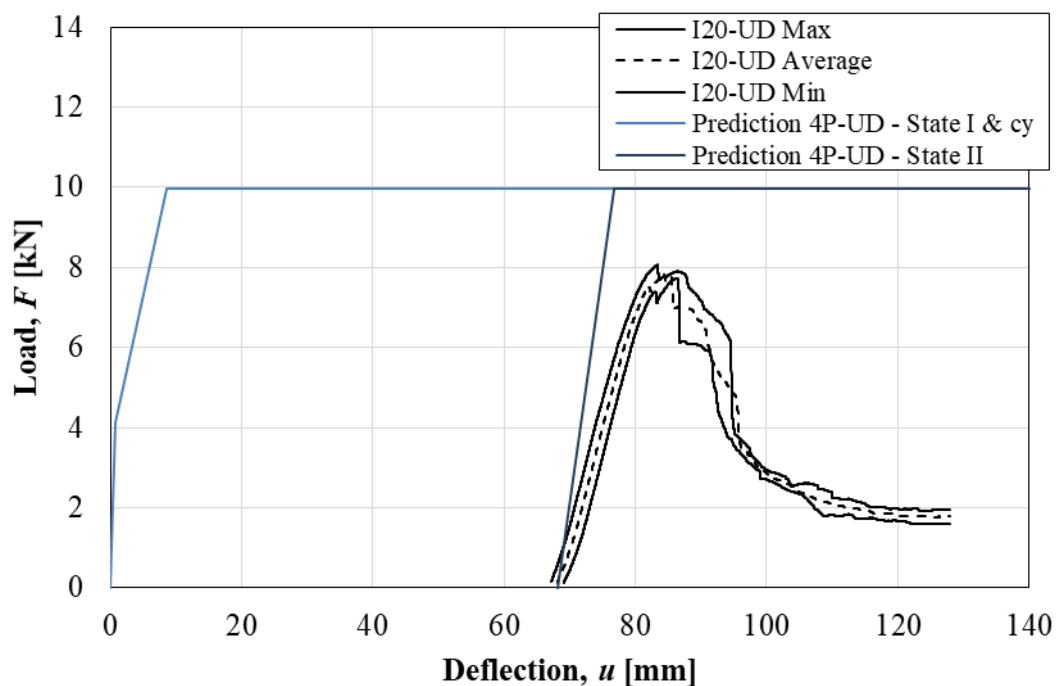


Figure 10.9 Load-deflection curves retrieved from experiments and predictions for series I20-UD. State cy is here defined as the state between cracking of the concrete and yielding of the reinforcement.

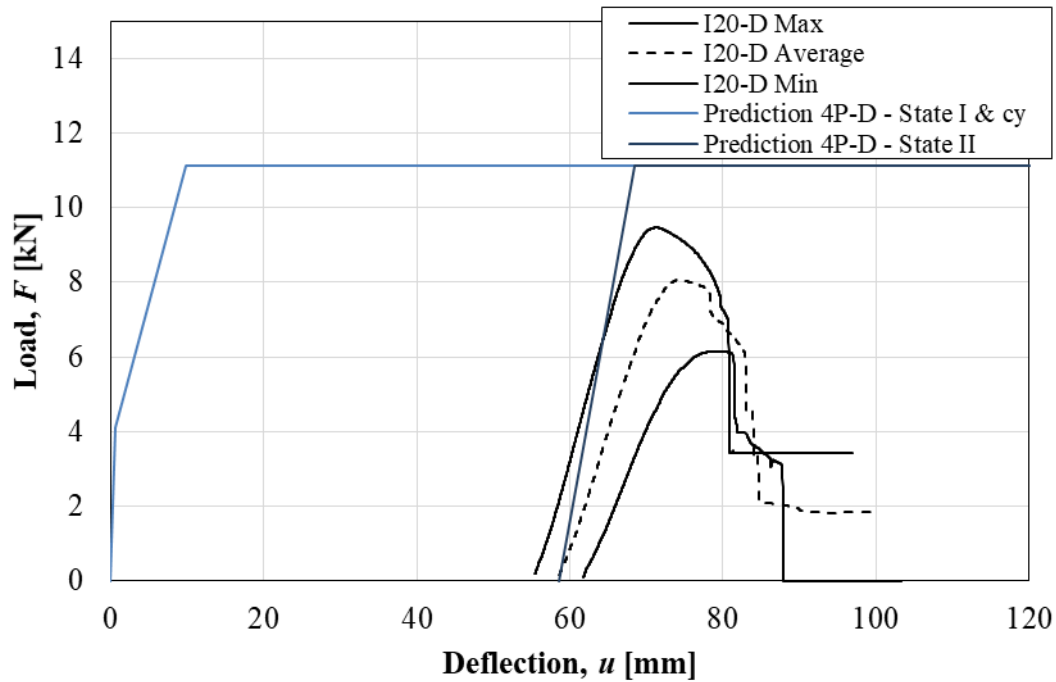


Figure 10.10 Load-deflection curves retrieved from experiments and predictions for series I20-D. State *cy* is here defined as the state between cracking of the concrete and yielding of the reinforcement.

It is clear from both graphs that the beams have consumed a large amount of their original capacity during the impact. The ultimate load capacity is significantly lower than the predicted one.

Additionally, the stiffnesses are showing the same pattern as for the I10-beams, where the predicted value is higher than the measured one. The values of the stiffnesses are listed in Table 10.7.

Table 10.7 Stiffness for Series I20 based on experiments and predictions.

Reinforcement	k_{dam} or k_{II} [kN/mm]	
Undamaged	Measured	0.547
	Predicted	1.17
Damaged	Measured	0.587
	Predicted	1.14

The measured stiffness for damaged reinforcement is slightly higher than that for undamaged reinforcement. This could be due to the greater concrete spalling in the beams with undamaged reinforcement due to larger deflections, resulting in a smaller compressive zone.

10.3 Rotation capacity

A comparison of the rotation capacity from the experiments and prediction is interpreted graphically in Figure 10.11 for undamaged reinforcement and in Figure 10.12 for damaged reinforcement. Note that this study only cares for the case of three point bending, in order to compare with the static tests.

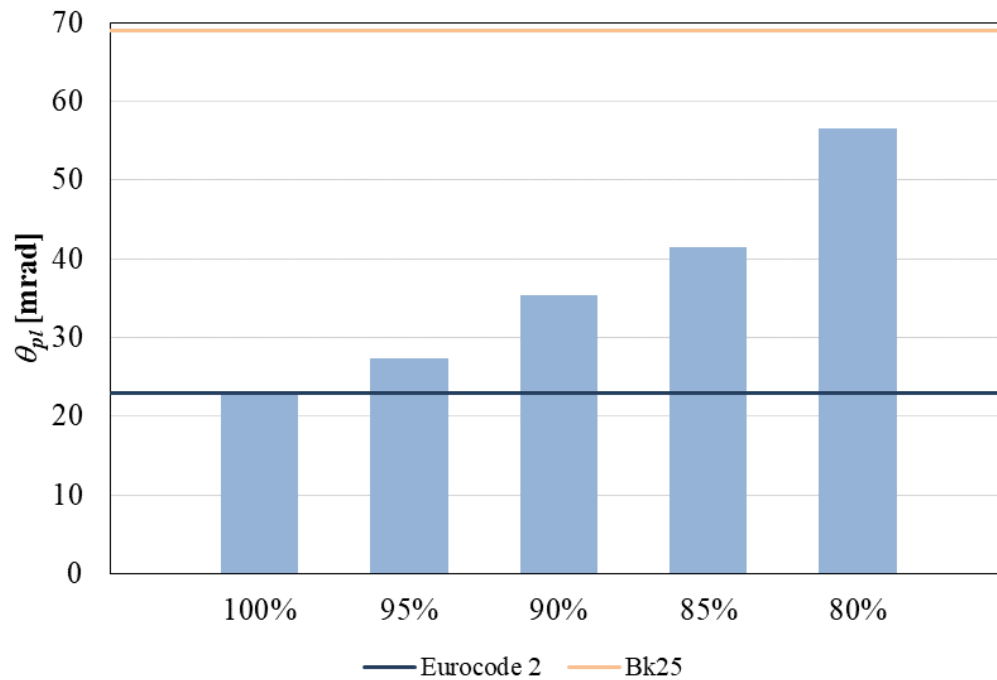


Figure 10.11 Comparison of plastic rotation capacity between experimental results and predictions when using undamaged reinforcement.

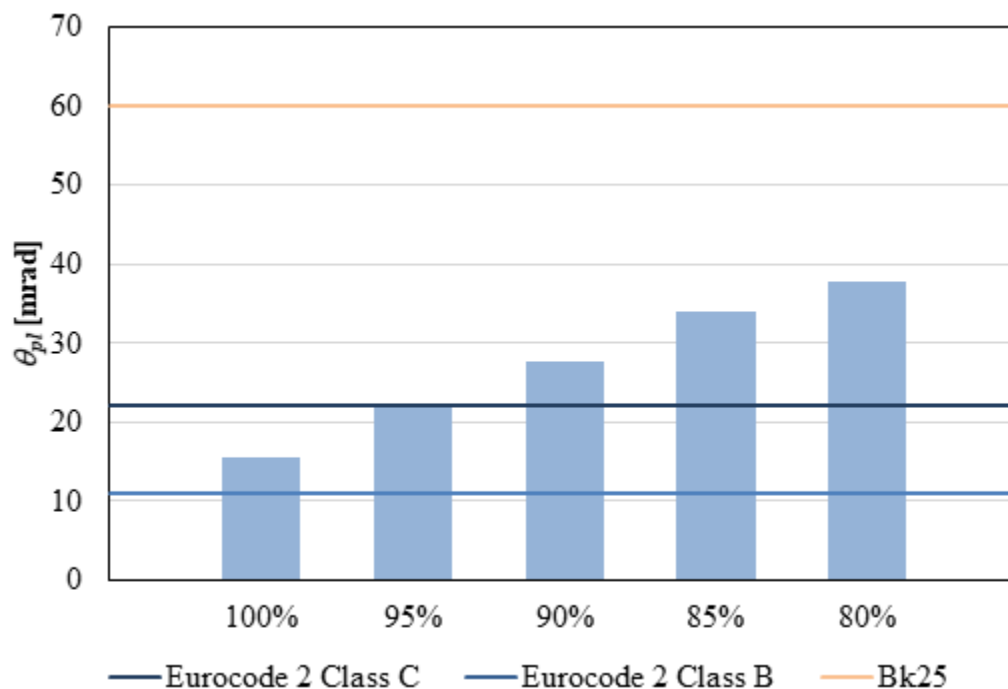


Figure 10.12 Comparison of plastic rotation capacity between experimental results and predictions when using damaged reinforcement.

It is evident that Bk25 overestimates the rotation capacity in both cases. This is assumed to partly be due to the difference in loadcase, where Bk25 is calculated for an evenly distributed load. The evenly distributed load gives a larger plastic hinge length due to the form of the moment distribution over the beam, which is beneficial for the plastic rotation capacity. Therefore, using Bk25 is incorrect in this case.

However, Eurocode 2 gives a more reasonable result, which is around the capacity for a load level of 100 %. For the beams with undamaged reinforcement, the rotation capacity is coherent for the load level 100 %. However, the damaged reinforcement does not fulfil the requirements for any of the ductility classes. It can be seen in Figure 10.12 that the experimental results show a larger rotation capacity than what is obtained for class B in Eurocode 2. The reason for this is assumed to come from the fact that the beams showed an η_M ratio that is larger than η_f obtained for the reinforcement, i.e. that the beams are more ductile than what can be observed by the reinforcement. However, according to Eurocode 2 reinforcement that is less ductile than class B should not be used in a plastic analysis.

11 Discussion

Observations made during the project are discussed in this chapter, including methods of testing and calculating, and the results.

The fact that the concrete was mixed in two different batches raise some questions regarding the results. It was shown by the material tests that the concrete from the two batches exhibited similar strength. However, to reduce possible sources of differences between the beams, it would have been preferred to mix the concrete in one batch.

Moreover, all the material tests showed a well gathered structural response, which indicated that sufficient methods during the casting and damaging (pre-stretching and bending) of the reinforcement were used. The plastic strain of the pre-stretched bars was assured in a way that the scatter would not affect the beam tests more than other dispersion in material properties. The bent bars showed a well gathered response in their stress-strain relations, which assured the method used to bend and straighten the bars. The bars were not straightened completely, which was the goal. Nonetheless, on a construction site, there are rarely means of straightening the bars completely, which is why the method used in this project is assumed to show a real case more accurately.

The material tests of the pre-stretched and bent reinforcement gave results in line with the literature study. However, the bending and straightening did not seem to have as large effect on the yield strength in the tests as in the literature. This could be due to the larger bending radius in the experiments performed in this study which may not have resulted in as large plastic deformations in the bar.

The position of the reinforcement was measured for some beams after the static tests, to assure that the predictions were describing the beams more accurately. This showed that the reinforcement indeed was placed with a concrete cover of 17 mm, which indicates that the method used to position the reinforcing bars during beam manufacturing is sufficient.

DIC proved to be a powerful tool to use in this kind of experiments, where a large amount of data could be collected from the tests afterwards. The choice to film half the beam during the dynamic tests was based on the work made by Lozano and Makdesi (2017) and Jönsson and Stenseke (2018), where it was shown that filming only half the beam would yield results with higher resolution. However, this choice has its limitations. Filming only half the beam does not capture any asymmetry of the beam response. However, this choice was assumed to be sufficient since the beams are assumed to behave symmetrically. Additionally, the cameras used in the static tests were limited to filming only one meter of the span, namely the middle. This choice was made to capture the most interesting part of the span of a beam subjected to bending, i.e. the middle part. All the results wanted were retrieved in an accurate manner, however, it may be of interest to capture the entire span.

One issue was discovered when retrieving the plastic deflection from the impact. A snapshot was taken of the beam before impact to capture this data. This snapshot was in GOM Correlate compared with the first frame captured in the film shot during the drop weight test. The film had a black frame in the top of the photo which the snapshot did not have. This was the reason for comparing the mid deflection with the support

deflection when the plastic deflection was determined, see Appendix H. However, there is an alternative way to overcome this. During the testing, a snapshot could be taken before the tests as well so that the photos used in the comparison had the same layout. Whether this would be more efficient than the method used in this project is unknown, since it would mean an extra stage during the testing. Moreover, the results are assumed to be equal independent of which method is used.

It was previously observed by Jönsson and Stenseke (2018) and Lozano and Makdesi (2017) that the predictions of the ultimate capacity of the beams was lower than the measured value, which may be due to a conservative method of calculating. This was taken into account when performing the 2DOF calculations which is why they were done with measured capacity as well. This gave a more accurate response for the beams subjected to a 10 kg-weight while it overpredicted the strength for the 20 kg-beams. This showed that the 2DOF model has shortcomings. The velocity of the drop-weight was quite accurately described compared to the experimental results. However, the predicted beam deflections were larger than the experiments, though they corresponded better with Series I20 than I10. This proves that the description of the beam response in particular could be developed further for the method to correspond even better with reality. However, the 2DOF model provides results on the safe side for this specific case.

Moreover, the 2DOF model used here does not take strain rate effects into account, which is assumed to be one reason for the difference in result from 2DOF and experiments. The dynamic tests are done at a high speed in comparison to the tests performed to obtain the material properties. It was proved for the reinforcement that the speed of testing influenced the strength and, as mentioned in Chapter 2, concrete shows even larger effects of such behaviour. This may be another reason for the too large deflections predicted with 2DOF.

When it comes to the static tests, it would have been preferred to test Series S using four point bending to compare with Series I20. The intention was to test Series I20 with three point bending, however the excessive concrete spalling averted this. It would have been a good idea to test Series S last of all. However, to save time, this was done parallel with the dynamic tests which is why it was not known during the testing of Series S that the I20-beams would suffer such damages from the impact tests.

From Series S, the plastic rotation capacity was determined and compared with the predictions based on Bk25 and Eurocode 2. For the beams with undamaged reinforcement, the rotation capacity corresponded well with the one predicted using Eurocode at a load level of 100 % for undamaged reinforcement. However, it can be seen that the beams have larger capacity if lower load levels are regarded. For damaged reinforcement, class C is not representative for the reinforcement used in the beams. However, the rotation capacity is higher than the one predicted using class B for all load levels, even though the reinforcement has a much lower η_f ratio than what is required. This is assumed to come from the fact that η_M ratio for the beams is higher than η_f for the reinforcement. Furthermore, the capacity using Bk25 was significantly higher than the measured one at all load levels studied. However, the method in Bk25 is meant to be used for a beam subjected to an evenly distributed load, which would result in a larger rotation capacity due to the more advantageous moment distribution obtained in such a load case. Therefore, Bk25 is misleading here.

12 Final Remarks

The aim of this thesis is to increase the knowledge of impact loaded reinforced concrete structures and the influence of the reinforcement properties on the structural response. This chapter gives conclusions of the results and possible future studies in the subject.

12.1 Conclusions

The study of the material properties of the reinforcement due to damages gave interesting results. For pre-stretched reinforcement, both the η_f ratio and the plastic strain capacity, ε_{pl} , were significantly decreased according to both the tests and literature survey. From the tests of the bent reinforcement, it was found that the η_f ratio was hardly affected while the ε_{pl} was reduced significantly, however the literature survey showed that the η_f ratio was increased. Welded reinforcement, which was studied through a literature survey, showed similar results with an almost indifferent η_f ratio and a significantly reduced ε_{pl} . Furthermore, the literature survey showed that for corroded reinforcement the η_f ratio was completely indifferent, however, the load capacity was reduced proportionally to the corrosion level, while the ε_{pl} was reduced significantly.

How the pre-stretching influenced the structural response of the concrete beams was studied for both the impact event and the residual capacity. During the impact, the beams containing pre-stretched reinforcement showed lower deflections than the ones containing undamaged bars, due to strain hardening. When it came to the residual capacity, the beams with pre-stretched reinforcement resulted in a significantly lower energy absorption, in terms of internal work and deformation capacity, than the ones containing undamaged bars. However, the load capacity was slightly higher for the beams with damaged compared to undamaged reinforcement.

Dynamically loaded beams showed a significantly larger deformation capacity than beams subjected to static loading only. This was true for all beams, regardless of reinforcement properties used. However, the increase was larger for undamaged than damaged reinforcement. Furthermore, looking at lower load levels in the load-deflection curves gave larger deformation capacities. Eurocode 2 (CEN, 2005) designs according to maximum load, which hence can be regarded as conservative.

The predictions of the dynamic response of the beams using the 2DOF model turned out to be conservative when using the beam resistance as predicted in the ultimate limit state calculations. However, the beam response was not described in a way that reflected reality, whereas additional strength is assumed if strain rate effects were to be taken into account.

Regarding the rotation capacity, Eurocode 2 corresponded quite well with the experiments at a load level of 100 % for the beams subjected to static loading only. Furthermore, Bk25 overestimated the rotation capacity in this study, regardless of load level or reinforcement properties.

12.2 Future studies

It would be of interest to further develop the 2DOF model in order to make it more in accordance with reality. The part of interest would be the beam response that could be described in a more detailed way, including e.g. strain rate effects, variation of initial deformed shape and loss of stiffness due to concrete spalling.

Additionally, it would be of interest to examine the behaviour studied in the experiments in a finite element analysis. Such an analysis could be compared to the experiments performed to examine if the response is predicted in an accurate way to reduce the needed amount of experiments in the matter.

13 References

- Al-Emrani, M., Engström, B., Johansson, M., Johansson, P. (2013). *Bärande konstruktioner: Del 1*. Gothenburg: Chalmers University of Technology.
- Apostolopoulos, C.A., Papadakis, V.G. (2007). Consequences of steel corrosion on the ductility properties of reinforcement bar. *Construction and Building Materials*, 22, 2316-2324, doi: 10.1016/j.conbuildmat.2007.10.006
- Biggs, J. (1964). *Introduction to Structural Dynamics*. New-York: McGraw-Hill.
- Burström, P. (2001). *Byggnadsmaterial: Uppbyggnad, tillverkning och egenskaper*. Lund: Studentlitteratur AB.
- CEN. (2005). SS-EN 1992-1-1:2005: *Design of concrete structures – Part 1-1: General rules and rules for buildings*. European Committee of Standardization.
- (2009a). SS-EN 12350-2:2009: *Testing of fresh concrete – Part 2: Slump-test*. European Committee of Standardization.
 - (2009b). SS-EN 12390-3:2009: *Testing hardened concrete – Part 3: Compressive strength of test specimens*. European Committee of Standardization.
 - (2009c). SS-EN 12390-6:2009: *Testing hardened concrete – Part 6: Tensile splitting strength of test specimens*. European Committee of Standardization.
 - (2012). SS-EN 12390-1:2012: *Testing hardened concrete – Part 1: Shape, dimension and other requirements for specimens and moulds*. European Committee of Standardization.
 - (2016). SS-EN ISO 7438: *Metallic materials – Bend test*. European Committee of Standardization.
- Chun, S.C., Ha, T. (2014) Cyclic Behavior of Wall-Slab Joints with Lap Splices of Cold-Straightened Rebars and mechanical Splices. *Journal of Structural Engineering*, 141(2), doi:10.1061/(ASCE)ST.1943-541X.0001064
- Du, Y.G., Clark, L.A., Chan, A.H.C. (2005). Effect of corrosion on ductility of reinforcing bars. *Magazine of Concrete Research*, 57(7), 407-419. Retrieved from
- Engström, B. (2011). *Bärande konstruktioner, Del 2, Chapter B7-B11*. Gothenburg: Chalmers University of Technology.
- (2015). *Design and analysis of continuous beams and columns*. Gothenburg: Chalmers University of Technology.
- Fernandez, I., Berrocal, C.G. (2019). Mechanical Properties of 30 Year-Old Naturally Corroded Steel Reinforcing Bars. *International Journal of Concrete Structures and Materials*, 13(9), doi:10.1186/s40069-018-0308-x
- Fujikake, K., Senga, T., Ueda, N., Ohno, T. and Katagiri, M. (2006). Study on Impact Response of Reactive Powder Concrete Beam and Its Analytical Model. *Journal of Advanced Concrete Technology*, 4(1), 99-108. Retrieved from https://www.jstage.jst.go.jp/article/jact/4/1/4_1_99/_pdf

- GOM. (2018). GOM Correlate Professional (Version 2018 hotfix 5) [Computer software]. Retrieved from <https://www.gom.com/3d-software/gom-correlate.html>
- Grahn, R., Jansson, P.-Å. (2013) *Mekanik – Statik och Dynamik*. Studentlitteratur AB.
- Johansson, M. (2000). *Structural behavior in concrete frame corners of civil defence shelters*. (PhD thesis, Chalmers University of Technology, Department of Structural Engineering)
- Johansson, M. (2012). *Beräkningsanvisning för strukturens respons: Central differensmetod*. (Document B03-102 from MSBs series "Beräkning av impulsbelastade konstruktioner", 2014).
- Johansson, M., Laine, L. (2012). *Bebyggelsens motståndsförmåga mot extrem dynamisk belastning, Del 3 – Kapacitet hos byggnader*. Gothenburg: Swedish Civil Contingencies Agency.
- Jönsson, J., Stenseke, A. (2018). *Concrete Beams Subjected to Repeated Drop-Weight Impact and Static Load: Assessment of structural response in experimental testing and predicted response with numerical analyses* (Master's thesis, Chalmers University of Technology, Institution of Architecture and Civil Engineering).
- Ljung, C., Saabye Ottosen, N., Ristinmaa, M. (2007). *Introduktion till hållfasthetslära: Enaxliga tillstånd*. Lund: Studentlitteratur AB.
- Lozano Mendoza, F., Makdesi Aphram, J. (2017). *Concrete Beams Subjected to Drop-Weight Impact and Static Load: Structural behavior and plastic rotation capacity from experiments and finite element analysis* (Master's thesis, Chalmers University of Technology, Institution of Architecture and Civil Engineering).
- Lovén, J., Svavarsdóttir, E. S. (2016). *Concrete Beams Subjected to Drop-weight impact* (Master's thesis, Chalmers University of Technology, Institution of Architecture and Civil Engineering).
- Lundh, H. (2000). *Grundläggande hållfasthetslära*. Stockholm: KTH Royal Institute of technology.
- Mo, Y.L., Kuo, J.Y. (1995) Effect of Welding on Ductility of Rebars. *Journal of Materials in Civil Engineering*, 7(4), 283-285, doi: 10.1061/(ASCE)0899-1561(1995)7:4(283)
- Munther, M., Runebrant, J. (2018) *Structural Response of Concrete Beams Subjected to Drop Weight Impact: A parametric study using numerical modelling* (Master's thesis, Chalmers University of Technology, Institution of Architecture and Civil Engineering).
- Tschegg, E. K. (1991). *New equipments for fracture test on concrete*. Munich: Carl Hanser Verlag.

Yi, W.J., Zhao, D.B., Kunnath, S.K. (2016) Simplified Approach for Assessing Shear Resistance of Reinforced Concrete Beams under Impact Loads. *ACI Structural Journal*, 113(4), 747-756, doi:10.14359/51688617

Appendix A Approximation of k_I in 2DOF model

As mentioned in Section 5.4.1, the stiffness of the spring between the drop weight and the beam, k_1 , is determined in an approximate way from Hertz contact theory. The expression for the impact force, F_1 , is

$$F_1 = k_1 \cdot \delta^{3/2} \quad (\text{A.1})$$

where δ is the local deformation at the impact zone, and k_1 is determined as

$$k_1 = \frac{4\sqrt{r_1}}{3} \left[\frac{1 - \nu_1^2}{E_1} + \frac{1 - \nu_2^2}{E_2} \right]^{-1} \quad (\text{A.2})$$

where r_1 is the radius of the hitting surface of the drop-weight, E_{sm} and E_{cm} are the mean modulus of elasticity of the drop-weight (steel) and the beam (concrete), respectively. ν_1 and ν_2 are the Poisson's ratio for the drop-weight (steel) and the beam (concrete), respectively. The stiffness used in this project is hereby taken as the secant of the curve yielded from Equation (A.1), see Figure A.1, at the level of the impact force of interest.

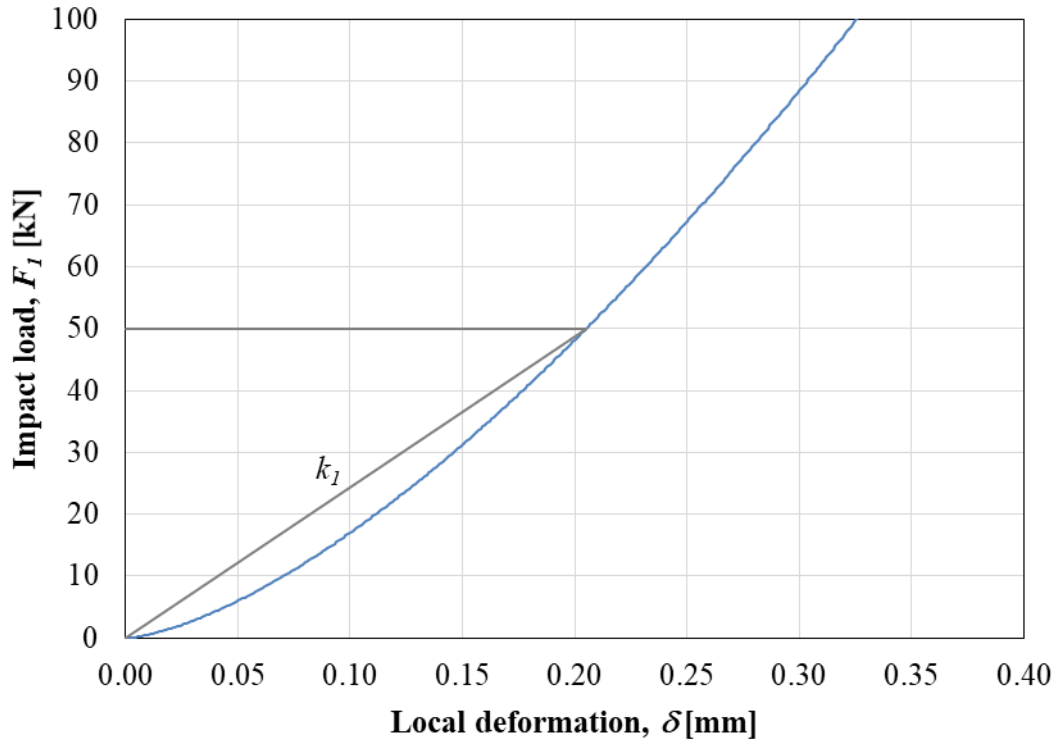


Figure A.1 Approximation of drop weight stiffness based on Hertz contact theory.

Appendix B 2DOF Convergence Study

In the 2DOF model a convergence study was performed on the variables R_I (strength of the contact) and k_I (stiffness of the contact) since those are unknown. The convergence study was performed for the series I10-UD and I20-UD to get representative values for each drop weight. Several levels of R_I were selected and then the spring stiffness was determined according to Appendix A. The parameters studied for the convergence assurance were the beam midpoint deflection and the velocity of the drop weight over time. As a comparison, the results from the study are presented in Figure B.1 to Figure B.4. In the figures, the plots of the average measured behaviours in the experiments are presented as well.

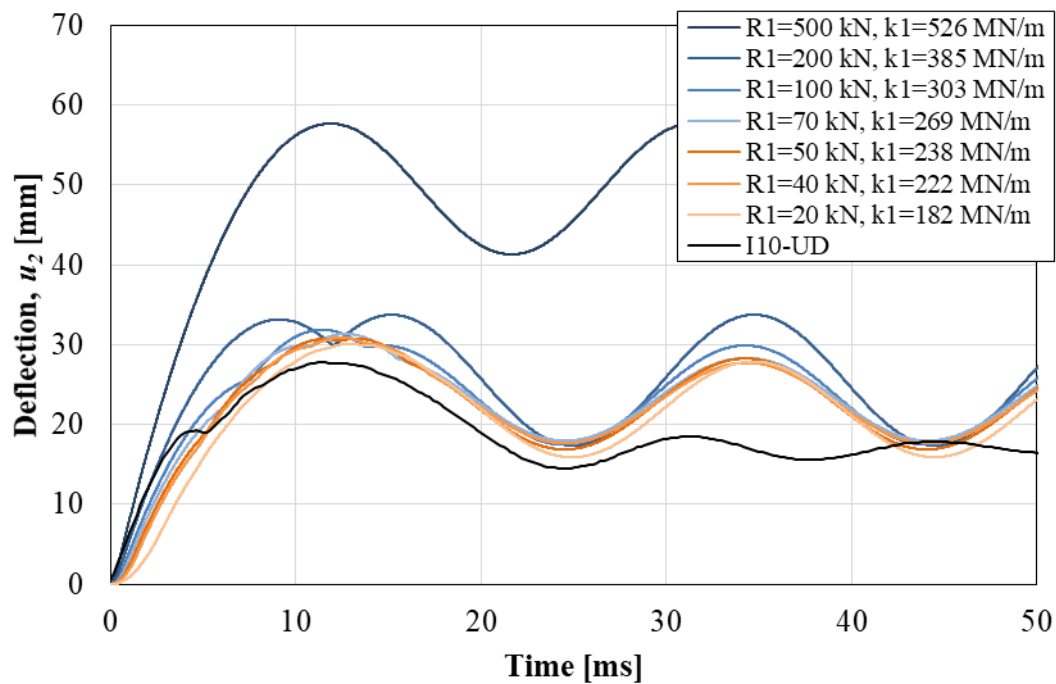


Figure B.1 Beam midpoint deflection after impact for 2DOF using different strengths and stiffnesses for the drop weight. Compared with I10-UD from experiments.

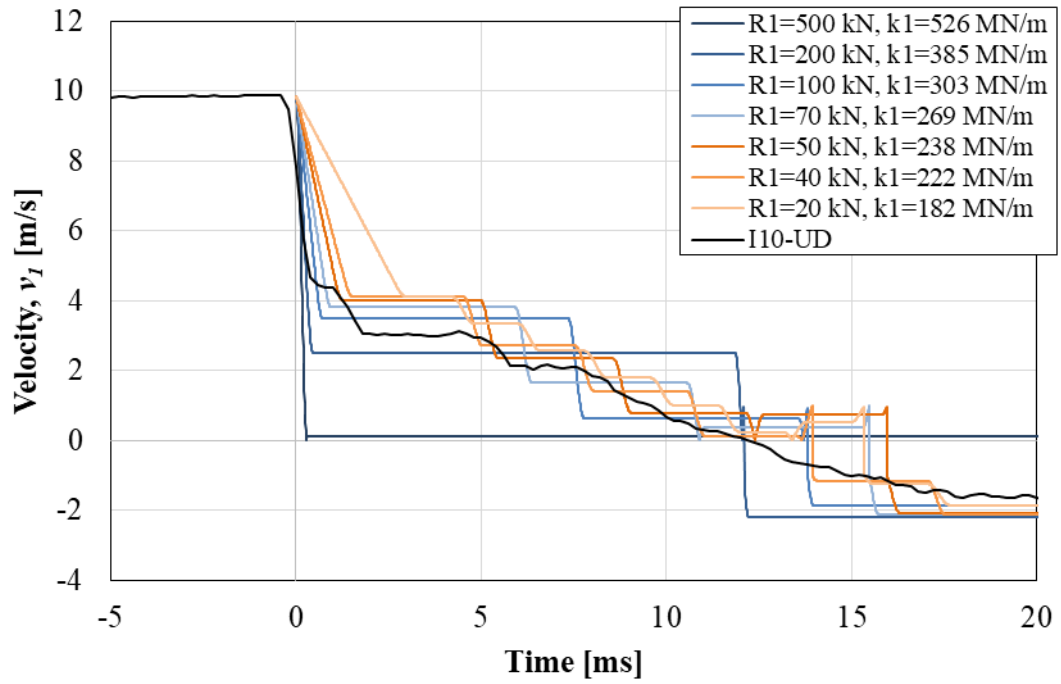


Figure B.2 Velocity of drop weight after impact for 2DOF using different strengths and stiffnesses for the drop weight. Compared with I10-UD from experiments.

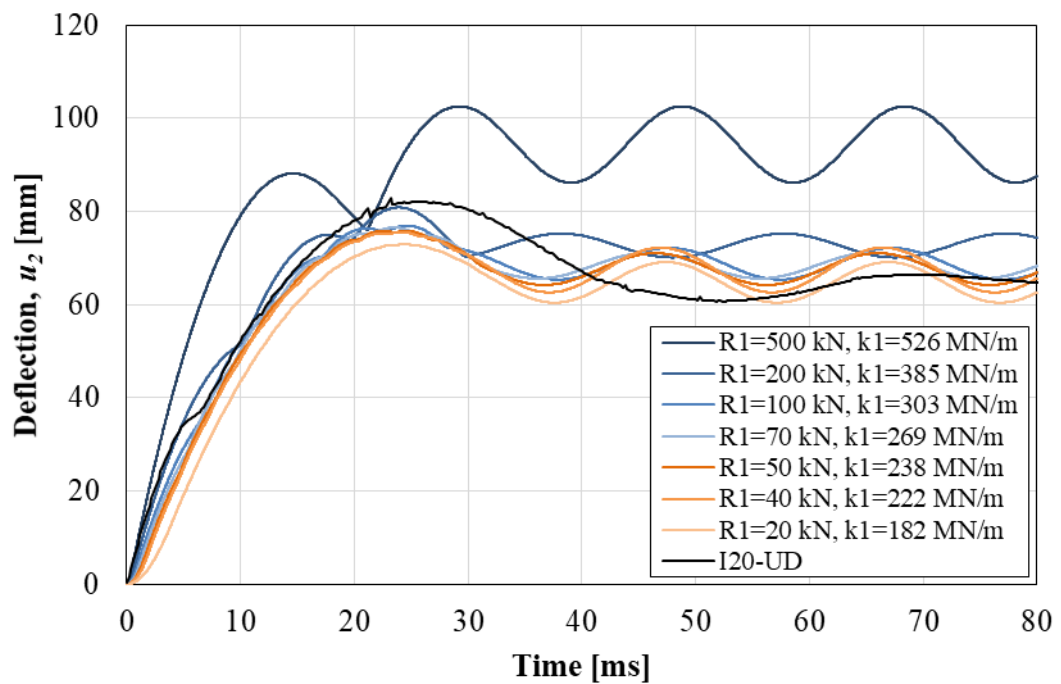


Figure B.3 Beam midpoint deflection after impact for 2DOF using different strengths and stiffnesses for the drop weight. Compared with I20-UD from experiments.

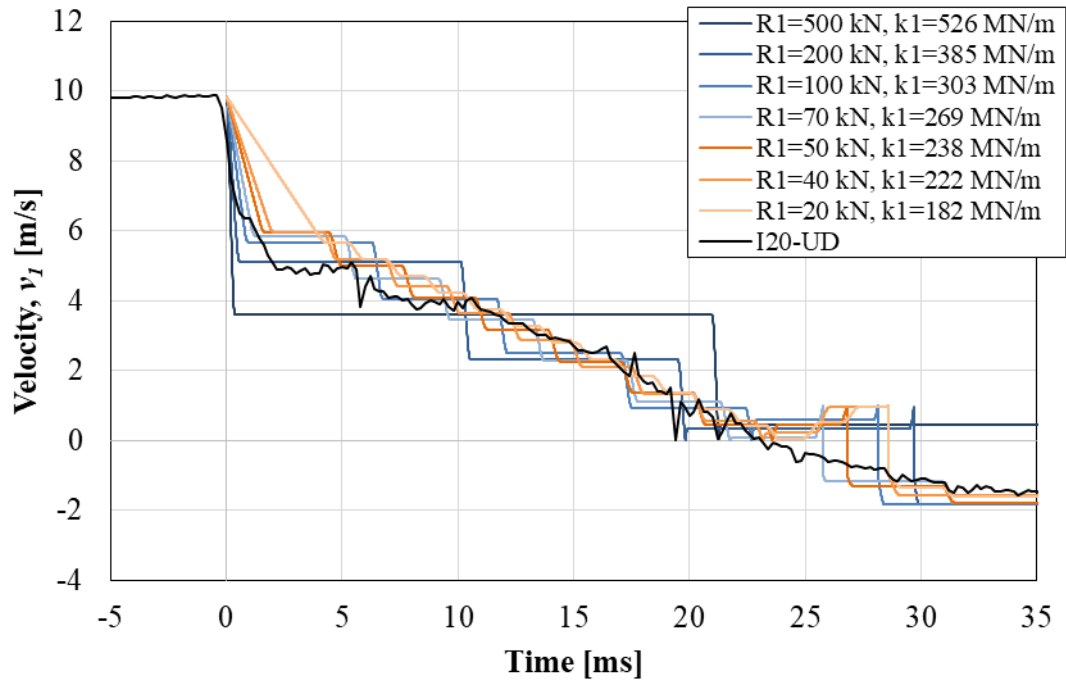


Figure B.4 Velocity of drop weight after impact for 2DOF using different strengths and stiffnesses for the drop weight. Compared with I20-UD from experiments.

The choice for the I10-beams was

$$R_1 = 50 \text{ kN}$$

$$k_1 = 238 \text{ MN/m}$$

The choice for the I20-beams was

$$R_1 = 70 \text{ kN}$$

$$k_1 = 269 \text{ MN/m}$$

Appendix C Material Properties of Concrete

The material properties of the concrete were tested both on the day of dynamic testing, after 27 days of hardening, and the day after, after 28 days of hardening. The properties tested were the cube compressive strength, the tensile splitting strength and the fracture energy.

C.1 Compressive strength

The compressive strength of the concrete was tested after both 27 and 28 days of hardening. Two specimens were tested from each batch on day 27 and on day 28 three specimens were tested from each batch. The measured values are presented in Table C.1 and Table C.2.

Table C.1 Results from compressive cube tests after 27 days of hardening.

Batch	Cube	Weight [kg]	Width [mm]	Length [mm]	Height [mm]	Density [kg/m ³]	Load [kN]	f_{cc} [MPa]
1	1	8.230	150.4	151.2	151.1	2 390	917	40.1
	2	8.262	150.3	150.7	150.3	2 430	911	40.2
2	1	8.181	150.0	150.4	150.0	2 420	952	42.2
	2	8.162	150.7	150.3	150.3	2 400	955	42.3

Table C.2 Results from compressive cube tests after 28 days of hardening.

Batch	Cube	Weight [kg]	Width [mm]	Length [mm]	Height [mm]	Density [kg/m ³]	Load [kN]	f_{cc} [MPa]
1	1	8.270	151.1	150.8	150.5	2 410	942	41.5
	2	8.240	150.5	151.0	150.5	2 410	924	40.7
	3	8.227	150.1	150.6	150.0	2 430	924	40.9
2	1	8.186	150.7	150.1	150.4	2 410	943	41.8
	2	8.239	150.1	150.1	150.1	2 430	923	41.0
	3	8.209	151.1	150.1	150.8	2 400	933	41.2

C.2 Tensile strength

The tensile splitting tests were performed after 27 days of hardening. Three specimens from each batch were tested. The measured values are presented in Table C.3.

Table C.3 Results from tensile splitting tests after 27 days of hardening.

Batch	Cube	Weight [kg]	Width [mm]	Length [mm]	Height [mm]	Density [kg/m ³]	Load [kN]	$f_{ct,sp}$ [MPa]
1	1	8.241	150.2	151.0	150.6	2 410	105	4.59
	2	8.180	150.1	149.7	149.9	2 430	113	5.03
	3	8.213	150.1	150.1	150.2	2 430	117	5.19
2	1	8.190	150.6	150.7	150.4	2 400	116	5.12
	2	8.245	151.2	151.1	150.4	2 400	104	4.59
	3	8.160	150.5	149.9	150.1	2 410	112	5.00

C.3 Fracture energy

The fracture energy of the concrete was determined using wedge splitting tests on three specimens from each batch. The tests were performed after 27 days of hardening. The geometries of the specimens are presented in Table C.4.

Table C.4 Geometric values of the specimens in the WST.

Batch	Cube	l_1 [mm]	l_2 [mm]	h_1 [mm]	h_2 [mm]	A [mm ²]
1	1	151.6	150.6	76.1	75.5	11 453
	2	150.8	151.2	76.3	75.7	11 476
	3	150.9	150.6	74.9	75.9	11 367
2	1	151.0	151.8	76.2	74.7	11 423
	2	151.3	152.0	75.9	74.7	11 419
	3	151.0	151.6	76.0	75.8	11 484

In Figure C.1, the splitting load-CMOD diagram is shown for the six cubes. It appears that the curves from cube 2.1 and 2.3 were not sufficient to represent the fracture energy of the concrete since the other four curves show a much more gathered behaviour. It is assumed that an error in the testing occurred and therefore cube 2.1 and 2.3 are not further considered.

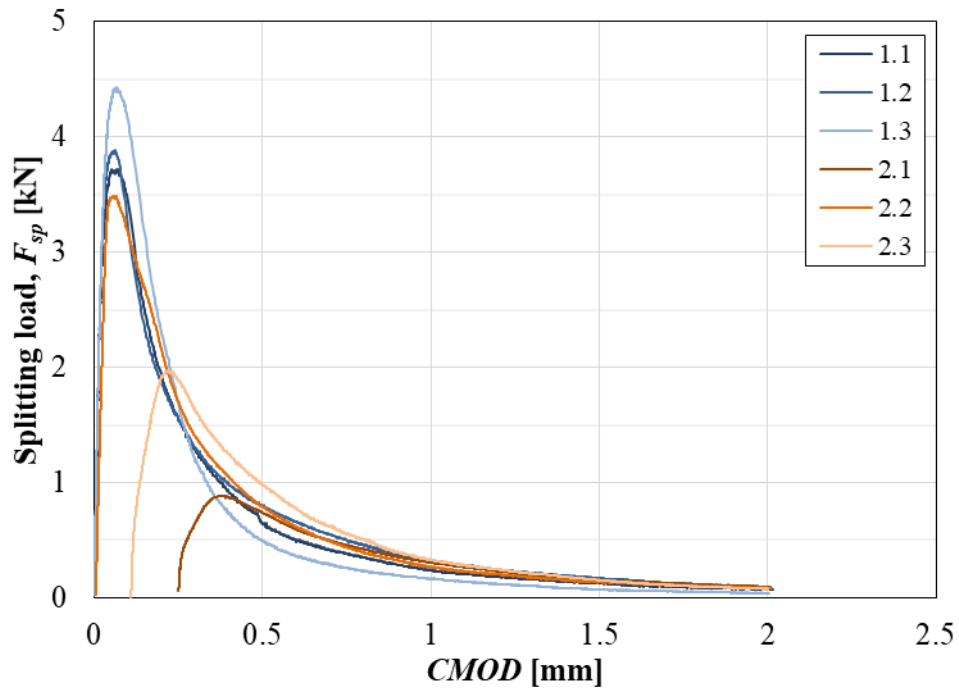


Figure C.1 Splitting force – CMOD diagram from WST. In the legend, the cubes are specimen are presented with batch number and cube number.

The parameters extracted from the behaviour seen in Figure C.1, such as the fracture energy, are listed in Table C.5.

Table C.5 Results from the WST.

Batch	Cube	Accumulated G_F [Nm/m ²]	Maximum F_{sp} [kN]	Maximum CMOD [mm]	CMOD at $F_{sp,max}$ [mm]
1	1	109	3.72	2.02	0.069
	2	119	3.88	2.01	0.061
	3	108	4.43	2.01	0.067
2	1	52*	0.88*	2.01*	0.383*
	2	114	3.49	2.01	0.060
	3	88*	1.97*	2.00*	0.218*

*Values not considered in the report.

Appendix D Material properties of reinforcement

This appendix contains all the results from the testing of the reinforcement.

D.1 Undamaged reinforcement

The stress-strain curves for the undamaged reinforcement are presented in Figure D.1 and the measured parameters based on these curves are listed in Table D.1.

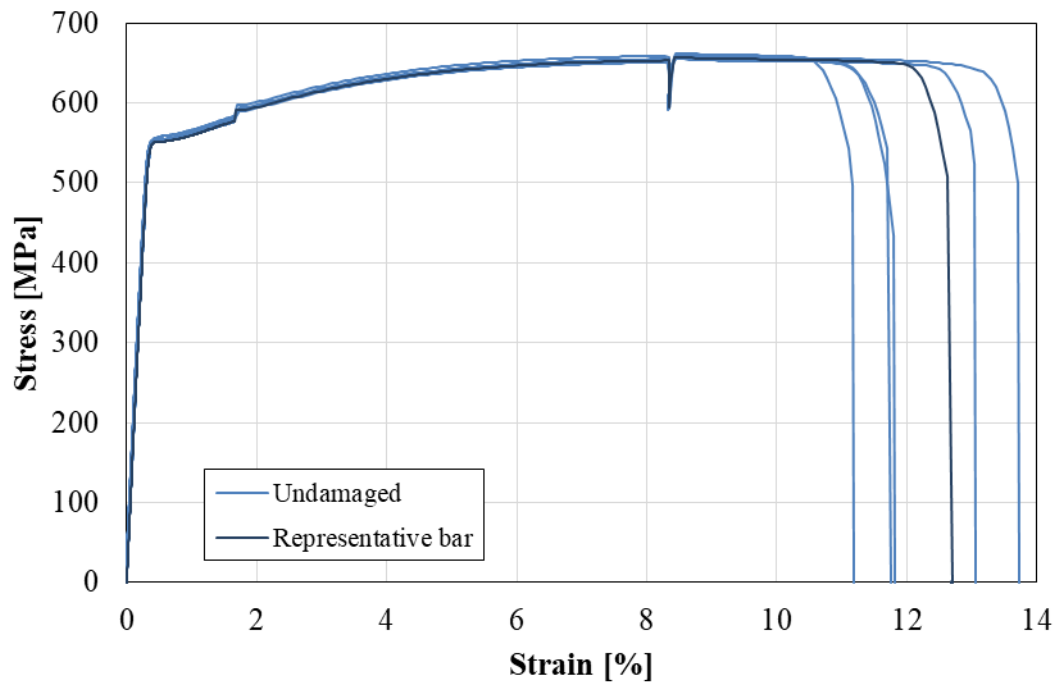


Figure D.1 Stress-strain curves for undamaged bars tested with high speed.

Table D.1 Material properties of undamaged reinforcement bars tested with high speed.

Bar	$f_{0.2}$ [MPa]	f_u [MPa]	ϵ_u [%]	E [GPa]
1	555	655	9.33	199
2	554	653	9.38	208
3	552	655	9.36	200
4	553	655	9.16	197
5	555	657	9.71	205
6	560	660	9.31	203
Average	555	656	9.38	202

D.2 Undamaged reinforcement tested with low speed

The stress-strain curves for the undamaged reinforcement tested with low speed are presented in Figure D.2 and the measured parameters based on these curves are listed in Table D.2.

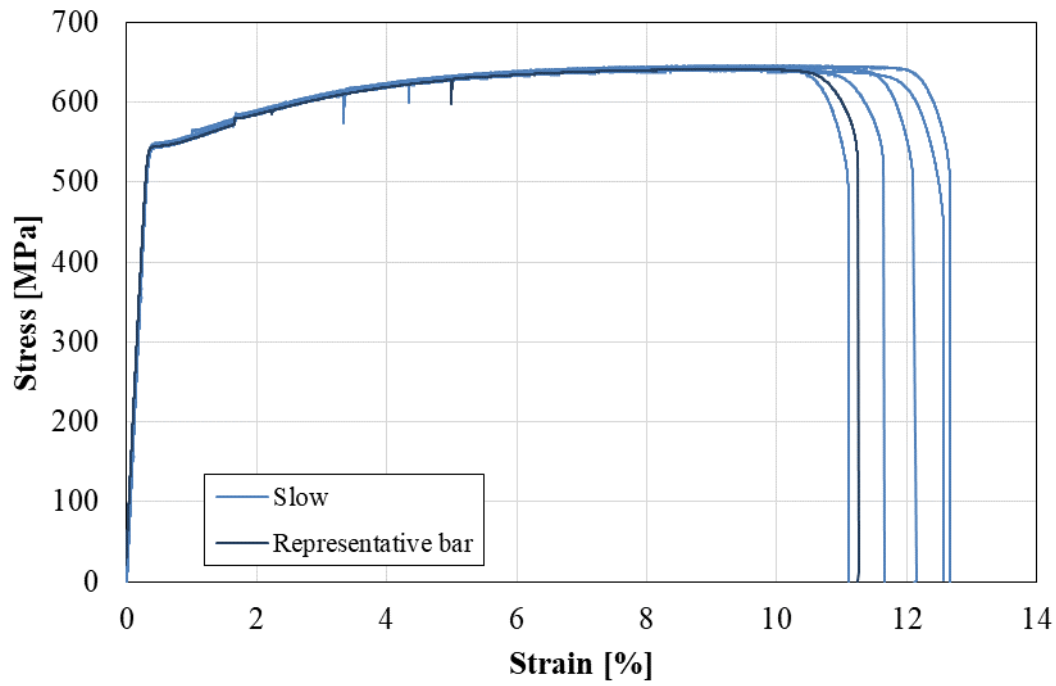


Figure D.2 Stress-strain curves for undamaged bars tested with low speed.

Table D.2 Material properties of undamaged bars tested with low speed.

Bar	$f_{0.2}$ [MPa]	f_u [MPa]	ϵ_u [%]	E [GPa]
1	545	641	9.26	204
2	546	644	8.69	197
3	544	640	9.21	203
4	549	646	9.79	193
5	547	644	9.51	210
6	544	640	8.98	210
Average	546	643	9.24	203

D.3 Pre-stretched reinforcement

The stress-strain curves for the pre-stretched reinforcement are presented in Figure D.3 and the measured parameters based on these curves are listed in Table D.3.

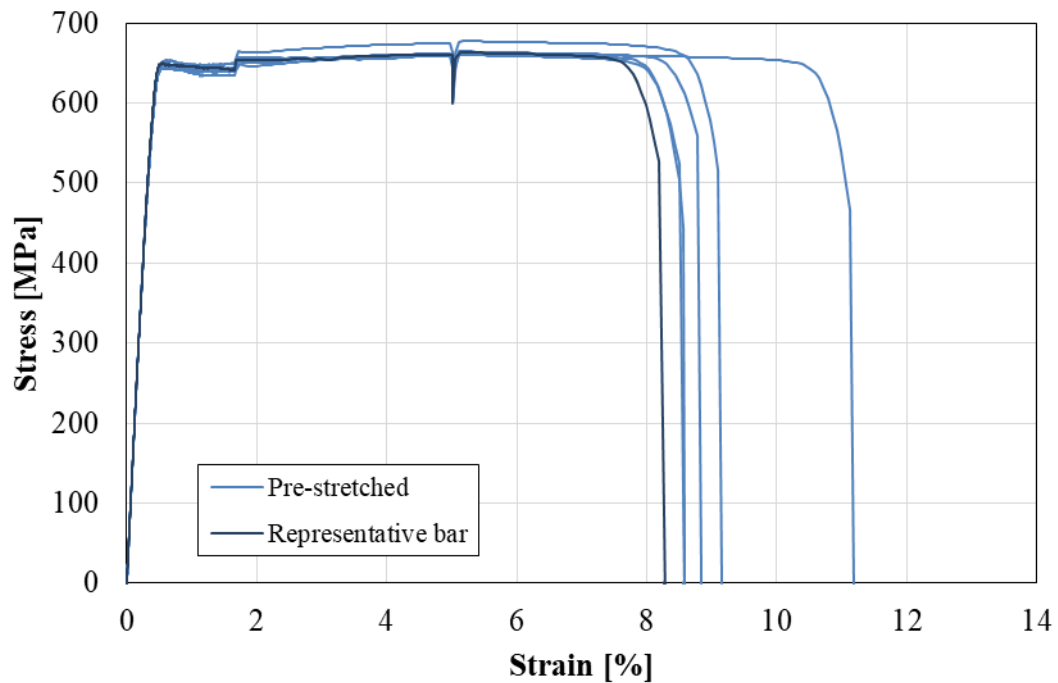


Figure D.3 Stress-strain curves for pre-stretched bars.

Table D.3 Material properties of pre-stretched bars.

Bar	$f_{0.2}$ [MPa]	f_u [MPa]	ϵ_u [%]	E [GPa]
1	647	659	5.63	191
2	652	676	5.85	190
3	643	663	5.78	188
4	643	662	5.84	219
5	643	662	5.66	191
6	641	661	6.07	195
Average	645	664	5.80	196

D.4 Bent reinforcement

The stress-strain curves for the reinforcement bent one time are presented in Figure D.4 and the measured parameters based on these curves are listed in Table D.4.

The stress-strain curves for the reinforcement bent two times are presented in Figure D.5 and the measured parameters based on these curves are listed in Table D.5.

The stress-strain curves for the reinforcement bent four times are presented in Figure D.6 and the measured parameters based on these curves are listed in Table D.6.

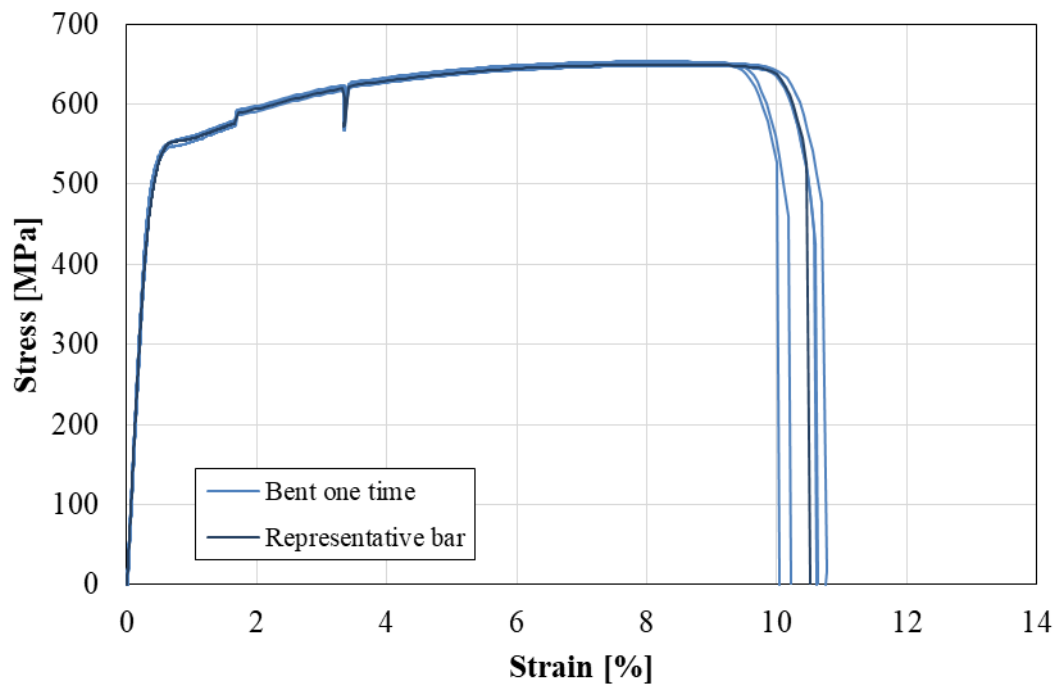


Figure D.4 Stress-strain curves for bars bent one time.

Table D.4 Material properties of bars bent one time.

Bar	f_y [MPa]	f_u [MPa]	ϵ_u [%]	E [GPa]
1	553	652	8.60	163
2	553	652	8.29	153
3	552	653	8.06	165
4	547	648	8.32	190
5	558	654	8.11	193
6	554	650	8.33	133
Average	553	651	8.29	166

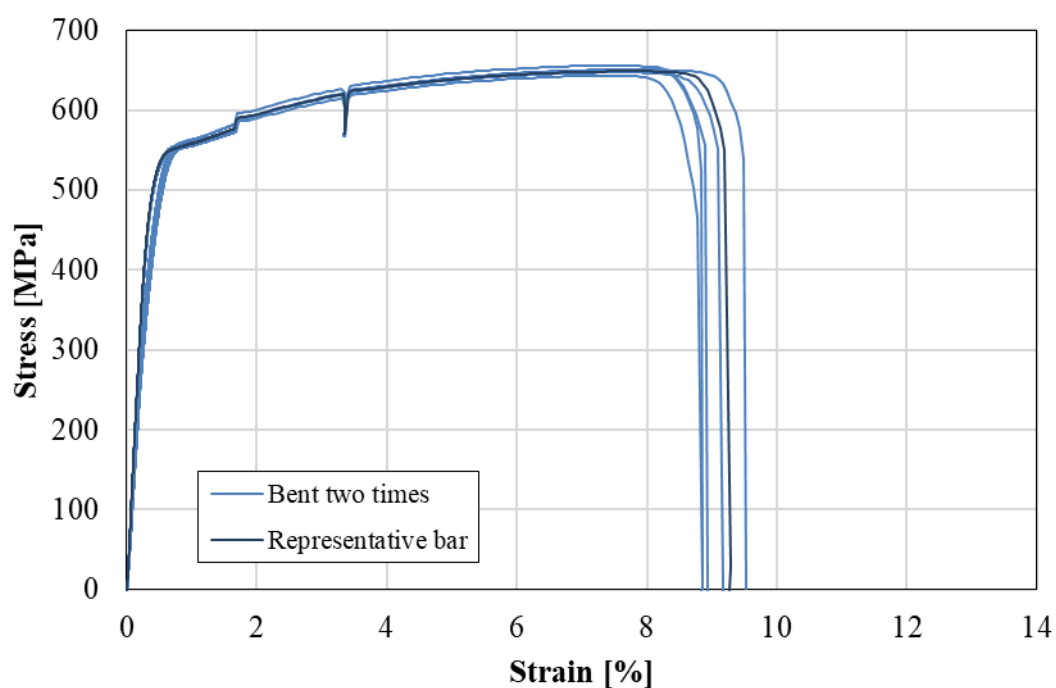


Figure D.5 Stress-strain curves for bars bent two times.

Table D.5 Material properties of bars bent two times.

Bar	f_y [MPa]	f_u [MPa]	ϵ_u [%]	E [GPa]
1	552	650	7.52	122
2	555	647	7.50	133
3	563	656	7.49	91
4	552	643	7.45	164
5	552	651	7.77	141
6	561	649	7.73	145
Average	556	649	7.58	133

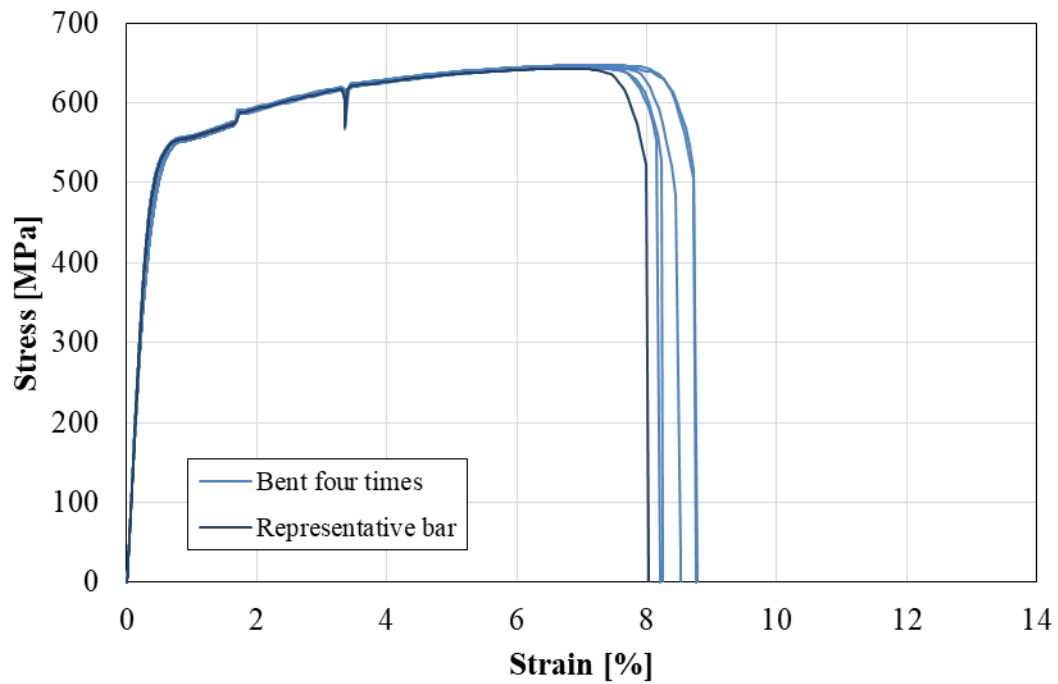


Figure D.6 Stress-strain curves for bars bent four times.

Table D.6 Material properties of bars bent four times.

Bar	f_y [MPa]	f_u [MPa]	ϵ_u [%]	E [GPa]
1	552	644	7.27	297 ⁽¹⁾
2	554	647	6.98	270 ⁽¹⁾
3	554	644	6.83	165
4	554	648	7.05	111
5	557	646	6.96	199
6	554	643	6.72	110
Average	554	645	6.97	146

⁽¹⁾ Not included in the average value.

D.5 Reinforcement tested at RISE

To assure the method of testing, some bars were tested at the Research Institutes of Sweden (RISE). The stress-strain curves for the reinforcement tested there are presented in Figure D.7 and Figure D.8 and the measured parameters based on these curves are tabulated in Table D.7 and Table D.8. These tests gave results in line with those tested at Chalmers, which is why they are not considered further.

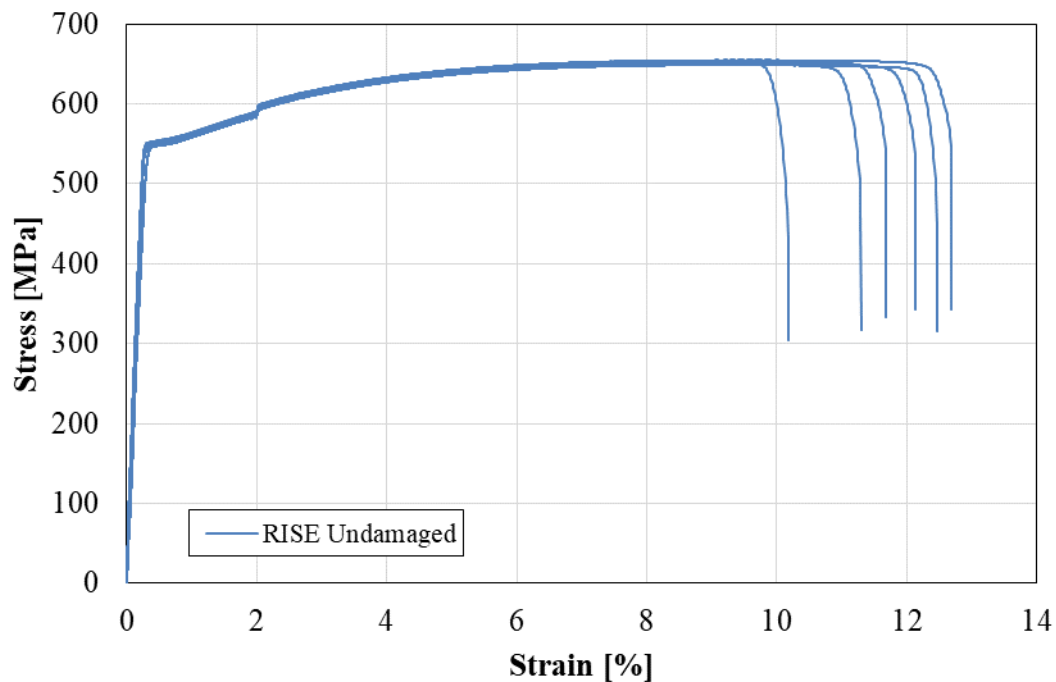


Figure D.7 Stress-strain curves for undamaged bars tested at RISE.

Table D.7 Material properties of undamaged bars tested at RISE.

Bar	$f_{0.2}$ [MPa]	f_u [MPa]	ϵ_u [%]	E [GPa]
1	554	654	8.60	209
2	553	655	8.95	200
3	551	652	8.81	212
4	547	649	9.14	205
5	550	651	9.29	205
6	550	655	9.60	189
Average	551	652	9.06	203

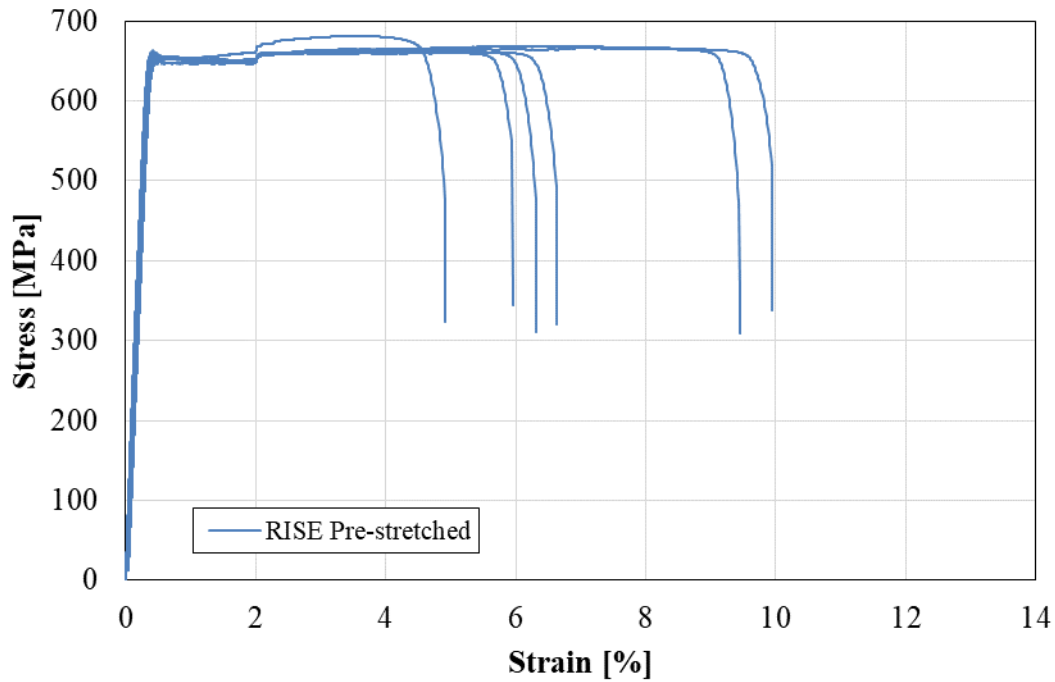


Figure D.8 Stress-strain curves for pre-stretched bars tested at RISE.

Table D.8 Material properties of pre-stretched bars tested at RISE.

Bar	$f_{0.2}$ [MPa]	f_u [MPa]	ϵ_u [%]	E [GPa]
1	653	668	6.46	190
2	656	666	7.20	197
3	649	661	5.04	196
4	649	662	4.39	211
5	652	661	3.17	188
6	653	682	3.56	187
Average	652	667	4.97	195

D.6 Modulus of elasticity

The moduli of elasticity from the tests are listed in Table D.9. The modulus of elasticity presented in the report was based on measurements from the extensometer. Though this appeared to give quite low values for the bent bars even though the curves were quite similar to the undamaged ones. It is of importance to mention that the stress-strain curves above are presented using the strain based on the displacement measured in the machine and not the extensometer. Retrieving the modulus of elasticity based on the strain from the machine gave unreasonable values overall. Though, it proved that the E-modulus for the bent bars gave similar results to the other specimens which is assumed to be why the curves are similar. It seems as though the extensometer may have been more sensitive to the straightening of the bars (the extensometer was placed in the middle of the bar, where the bend also was placed) which is why those values do not quite correspond to the form in the stress-strain curve.

Table D.9 Modulus of elasticity for the different bar groups based on extensometer and the displacement from the testing machine.

Bar group	E_{ext} [GPa]	E_{disp} [GPa]
Undamaged	202	167
Pre-stretched	196	161
Bent one time	166	166
Bent two times	133	149
Bent four times	146	159
Undamaged slow	203	166

Appendix E DIC facet analysis

In GOM Correlate Professional 2018 a triangular mesh is used for the DIC. The mesh is built based on facet size (length of a side [pixels]) and point distance (distance between midpoint of each facet [pixels]). To find an appropriate combination of facet size and point distance, a facet analysis was made on beam I10-D-B1-10 evaluating the major strains. To avoid undesirable noise, the colour scale limit was set to 5 % as upper limit and 1 % as lower limit. High accuracy computation was used. The strain fields for different settings of facet size and point distance can be seen in Table E.1 to Table E.4. Based on these strain fields, it was determined that a facet size of 15 pixels and a point distance of 5 pixels gave satisfactory results without too much noise but still clearly showing the cracks.

Table E.1 Strain fields with a point distance of 5 pixels.

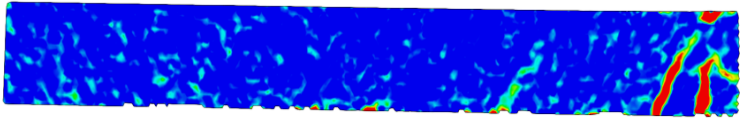
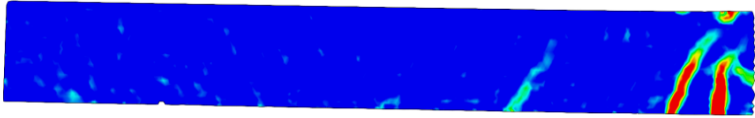


Facet size [pixels]	Point distance = 5 pixels
10	
15	
20	
25	

Table E.2 Strain fields with a point distance of 10 pixels.




Facet size [pixels]	Point distance = 10 pixels
15	
20	
25	

Table E.3 Strain fields with a point distance of 15 pixels.




Facet size [pixels]	Point distance = 15 pixels
20	
25	

Table E.4 Strain fields with a point distance of 20 pixels.

Facet size [pixels]	Point distance = 20 pixels
25	

Appendix F Impact Force - Alternative Method

An alternative way to determine the impact force was performed and is presented in this appendix. The idea was to base the force on the measured velocity at the time of impact. The time for the velocity curve was reduced to 0.6 ms before impact and 0.6 ms after. Then a trendline was retrieved from Microsoft Excel 2016 using a polynomial of grade 6. Then the polynomial was derivated to get the acceleration and the acceleration was transformed into a force using the mass of the drop weight. This was done for beam I10-UD-B1-07, -08 and -09. The resulting force-time curves are presented in Figure F.1 to Figure F.3.

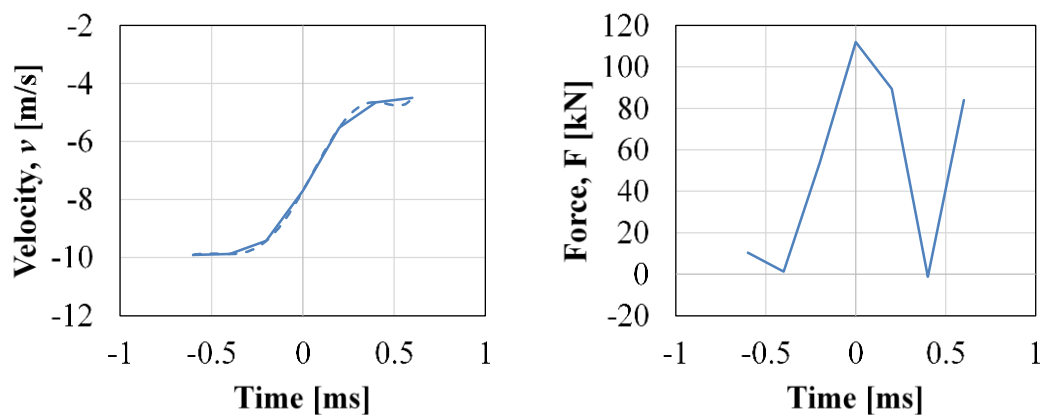


Figure F.1 Velocity and derived force for beam I10-UD-B1-07.

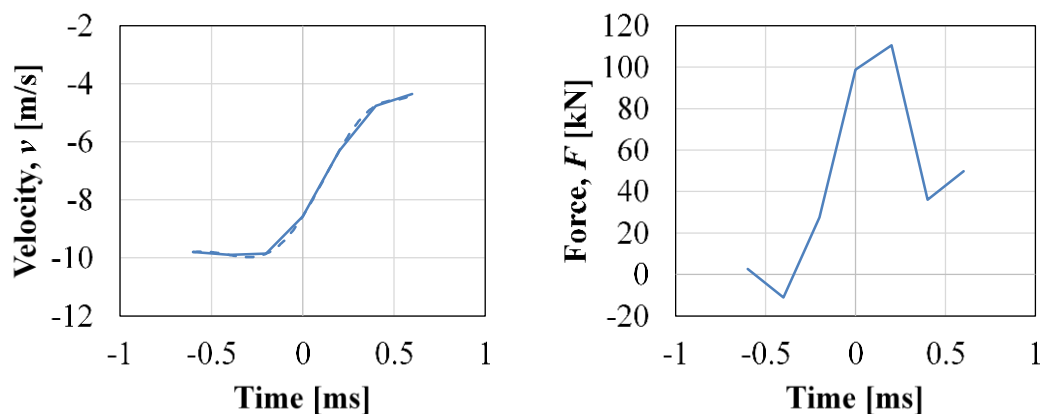


Figure F.2 Velocity and derived force for beam I10-UD-B1-08.

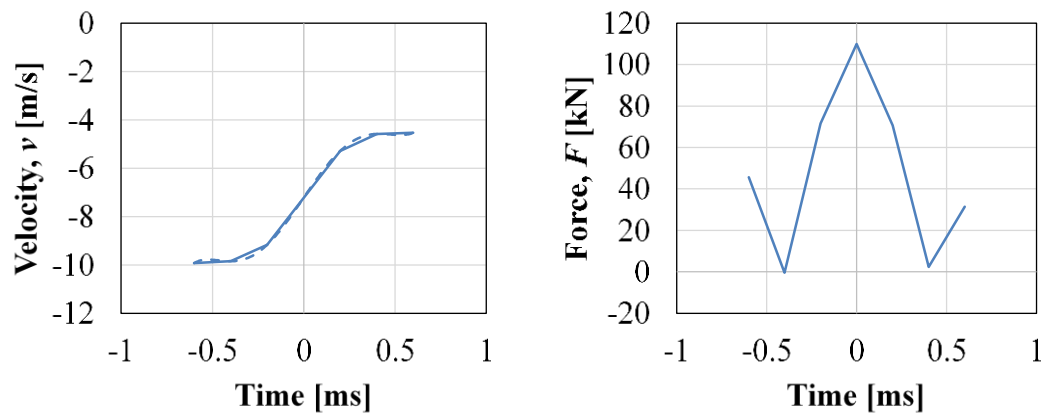


Figure F.3 Velocity and derived force for beam I10-UD-B1-09.

The study yielded about 15 % larger maximum forces than those extracted from GOM Correlate.

Appendix G Velocity of Drop Weight

The measured velocities of the drop weight during the experiments are presented for each beam in Figure G.1 to Figure G.4.

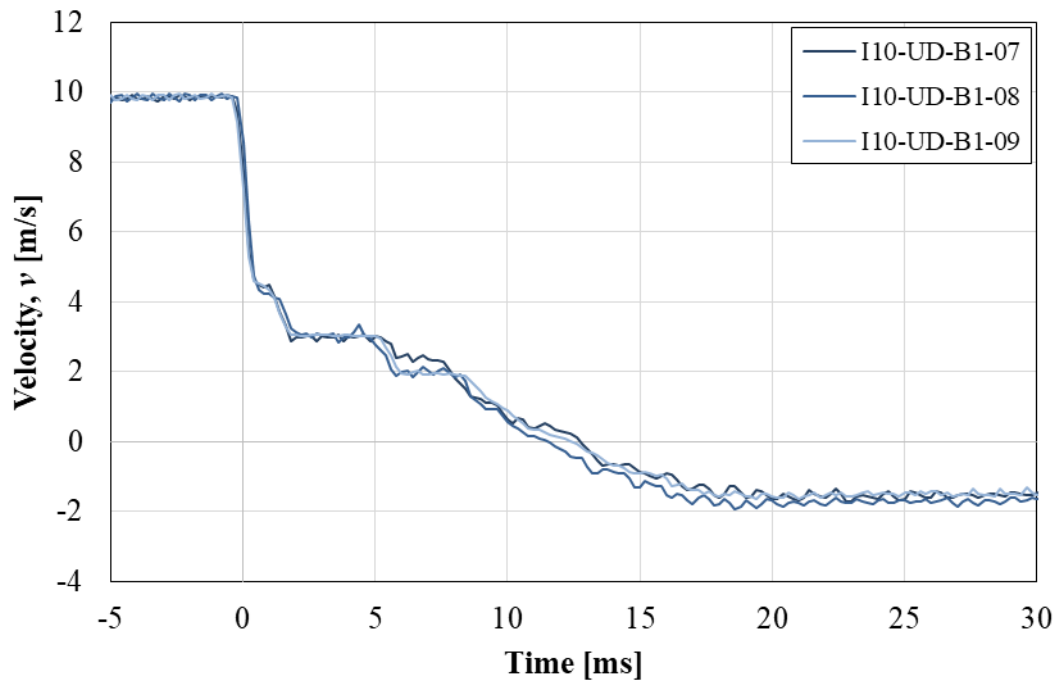


Figure G.1 Velocity of drop weight for series I10-UD.

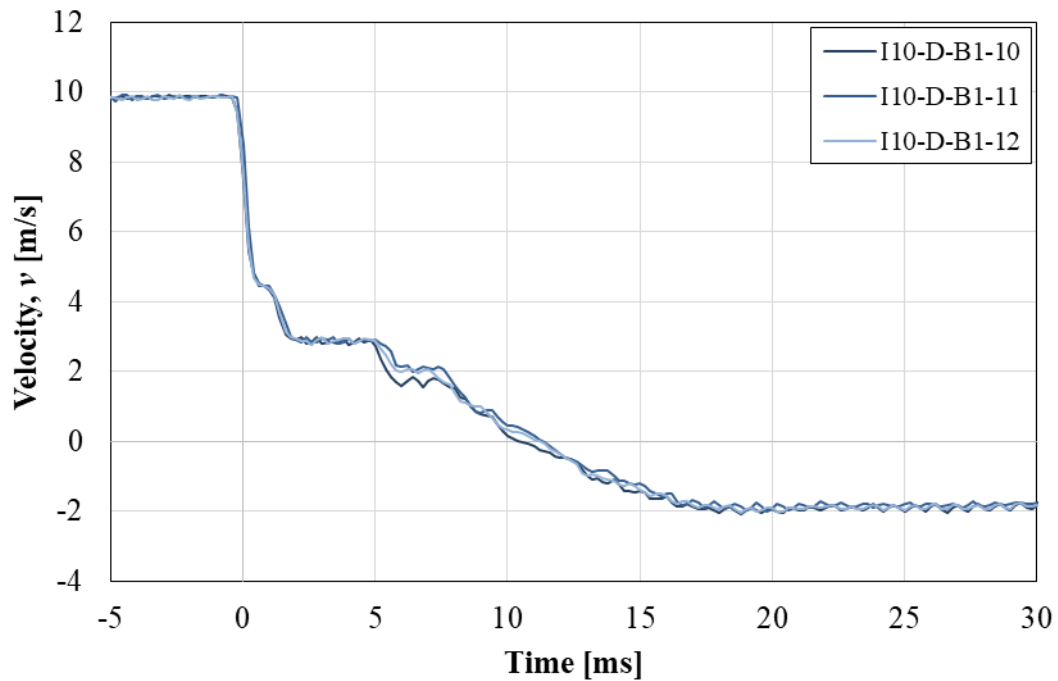


Figure G.2 Velocity of drop weight for series I10-D.

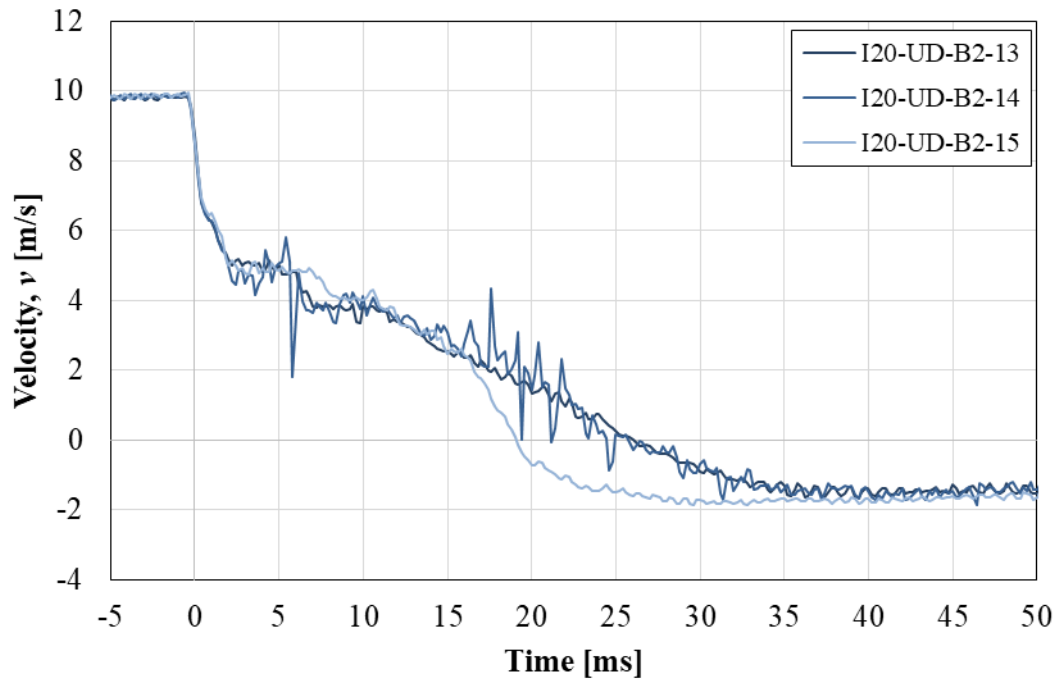


Figure G.3 Velocity of drop weight for series I20-UD.

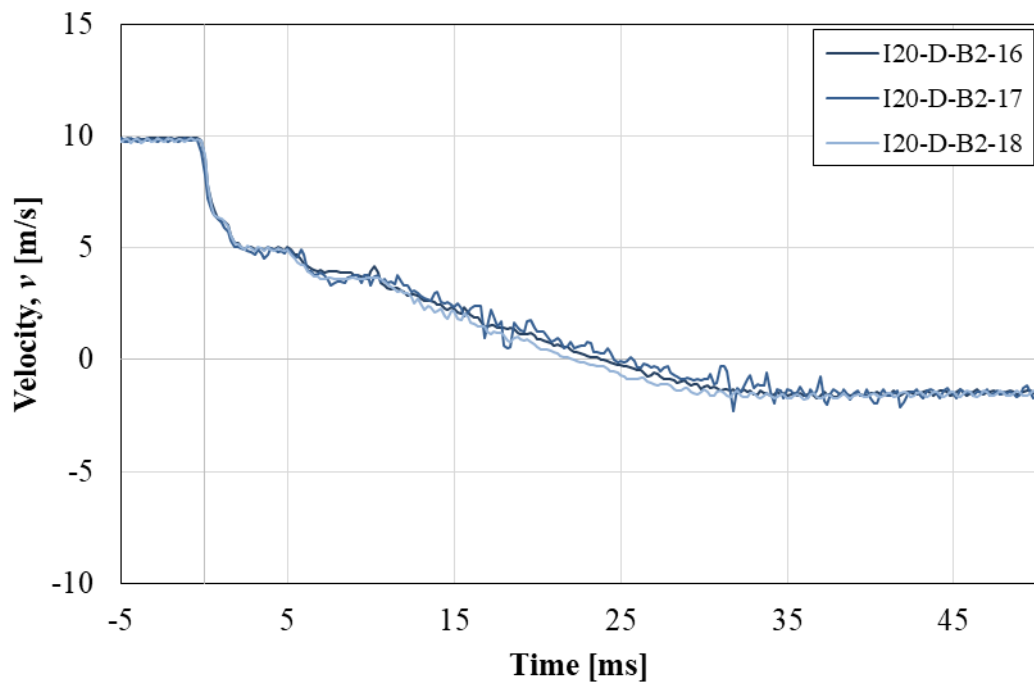


Figure G.4 Velocity of drop weight for series I20-D.

As seen the velocity of beam I20-UD-B2-14 was disturbed by large noise in GOM Correlate.

Appendix H Determination of plastic deflection using DIC

The plastic mid-span deflection after the impact was determined in GOM Correlate Professional 2018, using DIC. After the impact, the beam was put back into the correct place on the supports and another photo was taken. This photo was later correlated in GOM Correlate Professional 2018 with the first image sequence from the film of the dynamic test, and the plastic deflection was determined.

A problem that was noticed during the evaluation of the photos was that the reference photo automatically had a black area with some informational text on it while the last photo of the beam lacked this area, see Figure H.1 and Figure H.2. This results in a size difference between the two images which causes problems when correlating the pixels in them and hence also when determining the plastic deflection. As can be seen in Figure H.2, the measured deflection at the support according to GOM Correlate is +17.093 mm. Though, in reality the deflection at the support should be close to zero. The measured deflection at the support from GOM Correlate appears due to the size difference of the reference image and the photo after impact. To correct for this effect, the plastic deformation in mid-span, u_{pl} , was calculated based on the measured values from GOM Correlate as

$$u_{pl} = u_{2,mid} - u_{2,support} \quad (H.1)$$

where $u_{2,mid}$ is the deflection at mid-span in the second photo and $u_{2,support}$ is the deflection at the support in the second photo.

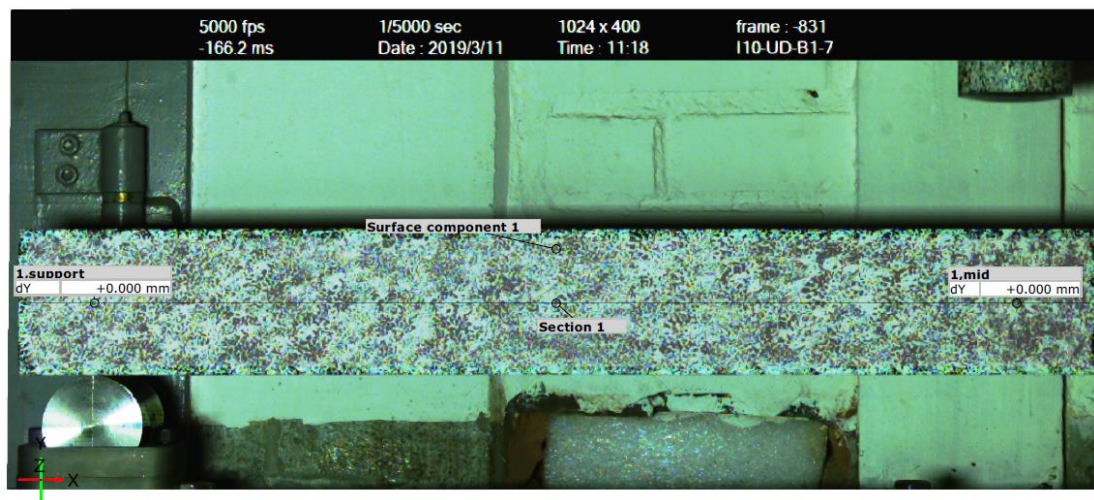


Figure H.1 Image of the beam before the impact, used as reference. Here beam I10-UD-B1-07 serves as an example.



Figure H.2 Photo of the beam after the impact. Here beam I10-UD-B1-07 serves as an example.

Appendix I Calculation of stiffness

In this thesis four different stiffnesses have been calculated; k_I , $k_{II,t}$, $k_{II,s}$ and k_{III} . What is meant by the different stiffnesses is illustrated Figure I.1 and Figure I.2. All stiffnesses are calculated based on the load-deflection curves gained from the static testing by dividing the difference in load, ΔF , by the difference in deflection, Δu , see Equation (I.1).

$$k_i = \frac{\Delta F}{\Delta u} \quad (\text{I.1})$$

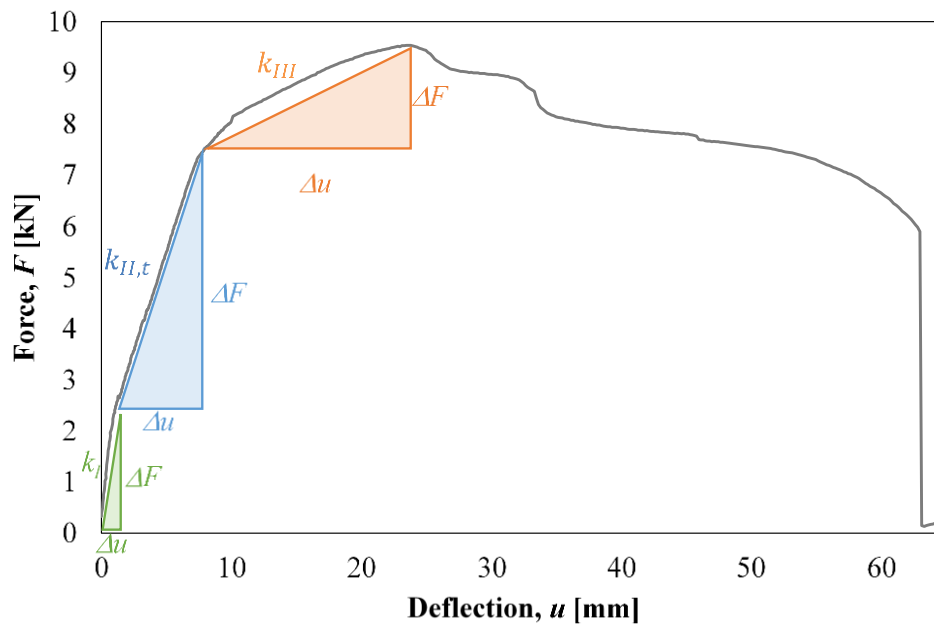


Figure I.1 Principal illustration of k_I , $k_{II,t}$ and k_{III} .

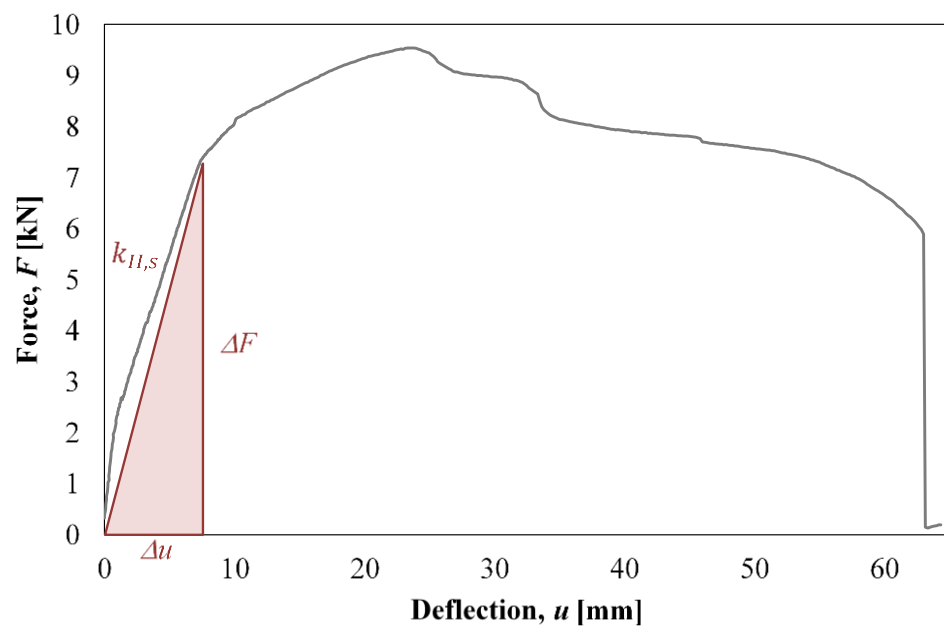


Figure I.2 Principal illustration of $k_{II,S}$.

Appendix J Calculation of internal work

The internal work at different load levels is calculated as the area under the load-deflection curve, see Figure J.1. Secant state II stiffness is assumed. The total internal work, W_{tot} , is calculated as the area under the whole load-deflection curve. Prior to the calculation of internal work, the load-deflection curve is truncated at the point where the beam is considered to have reached its full capacity. In this thesis that point was considered to be when the descending branch of the load-deflection reached a load corresponding to 50 % of the average maximum load of the beams in Series S.

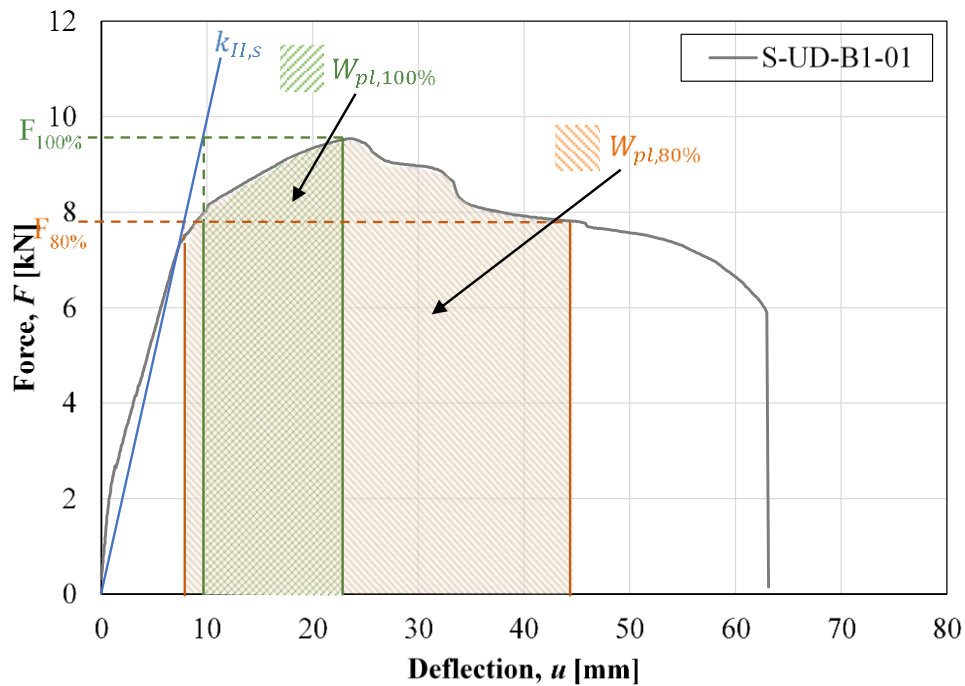


Figure J.1 Method for calculating the internal work at different load levels. Here beam S-UD-B1-01 serves as an example.

Appendix K Strain fields from static test displayed on beams

The strain fields from the static testing, extracted from GOM Correlate Professional 2018, are in this appendix displayed on real photos of the beams. Note that two cameras were used to capture the static response. This is photos from the left camera, but the right camera show similar results.

K.1 Series S

The strain fields at a deformation of 30 mm, displayed on beams in Series S, are presented in Figure K.1 to Figure K.6.

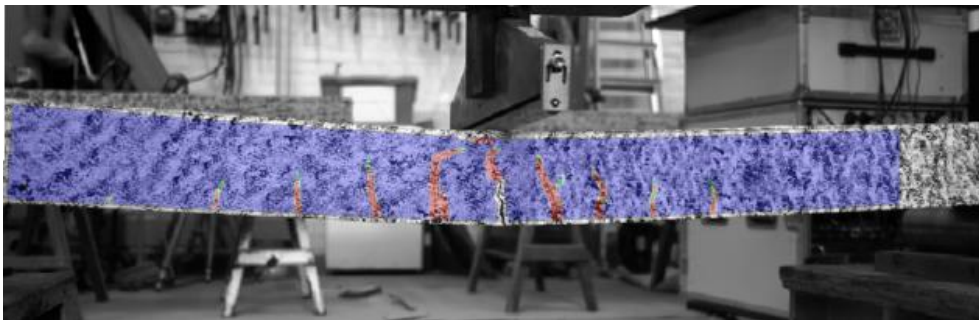


Figure K.1 Strain field displayed on beam S-UD-B1-01.

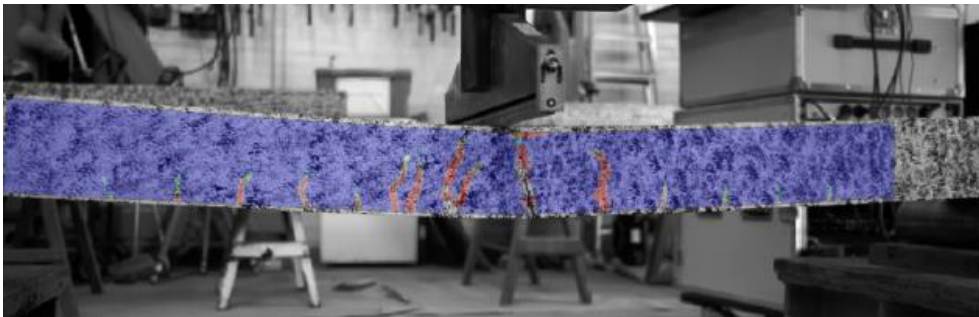


Figure K.2 Strain field displayed on beam S-UD-B1-02.

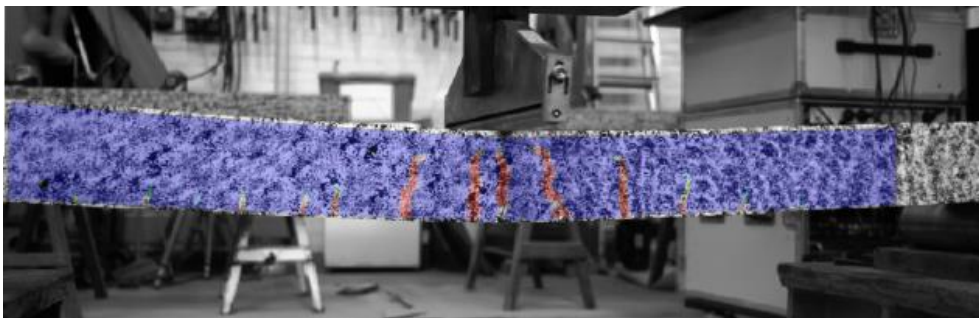


Figure K.3 Strain field displayed on beam S-UD-B2-03.

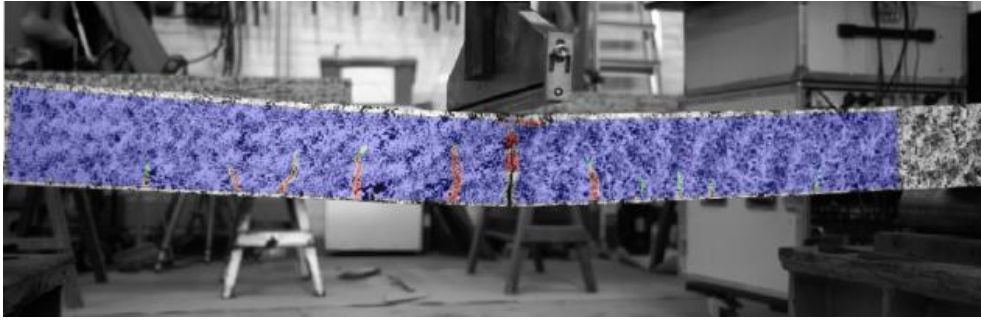


Figure K.4 Strain field displayed on beam S-D-B1-04.

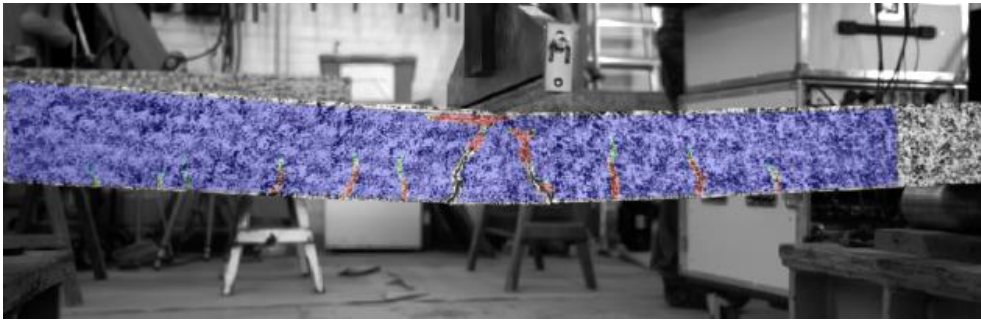


Figure K.5 Strain field displayed on beam S-D-B2-05.

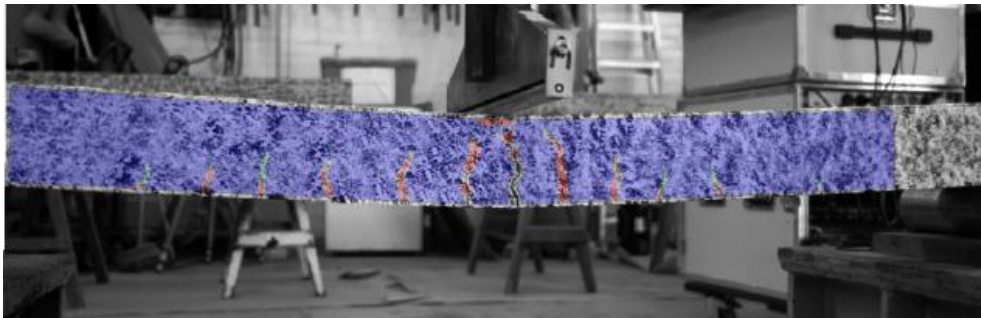


Figure K.6 Strain field displayed on beam S-D-B2-06.

K.2 Series I10

The strain fields at a deformation of 30 mm, displayed on beams in Series I10, are presented in Figure K.7 to Figure K.12.

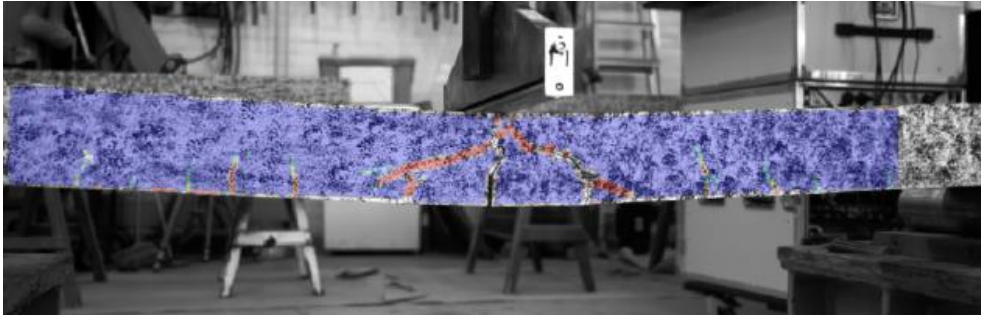


Figure K.7 Strain field displayed on beam I10-UD-B1-07.

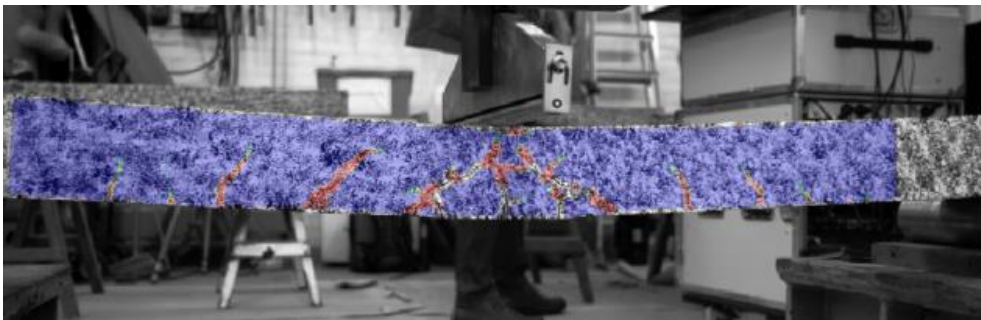


Figure K.8 Strain field displayed on beam I10-UD-B1-08.

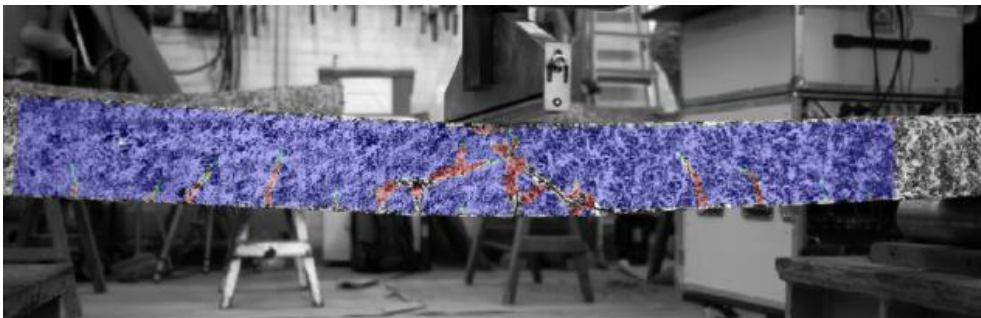


Figure K.9 Strain field displayed on beam I10-UD-B1-09.

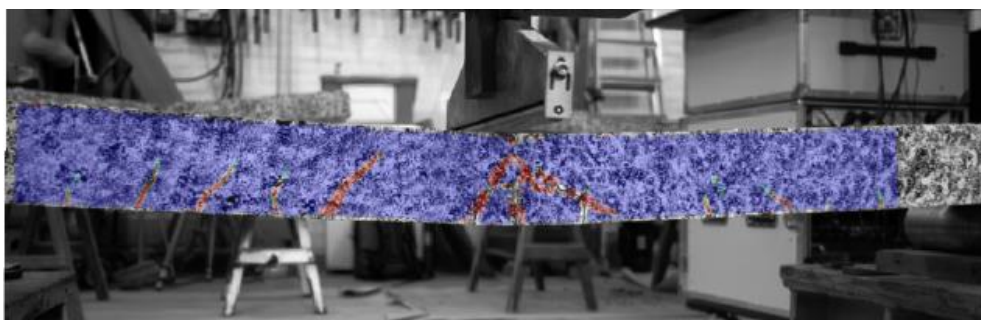


Figure K.10 Strain field displayed on beam I10-D-B1-10.

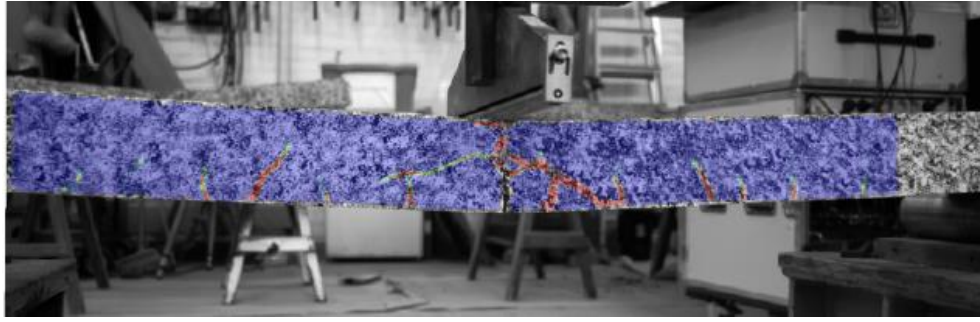


Figure K.11 Strain field displayed on beam I10-D-B1-11.

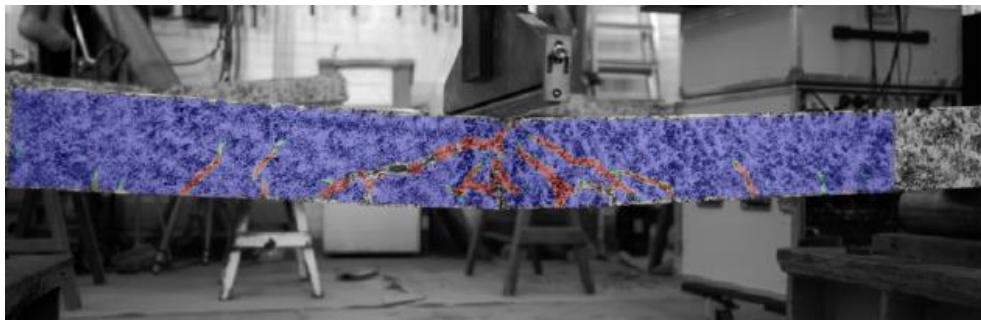


Figure K.12 Strain field displayed on beam I10-D-B1-12.

K.3 Series I20

The strain fields at maximum load, displayed on beams in Series I20, are presented in Figure K.13 to Figure K.18. Note that beam I20-UD-B2-15 experienced excessive spalling of concrete during the dynamic test and was therefore not tested statically. However, a photo of this beam after the dynamic loading test can be seen in Figure K.15.



Figure K.13 Strain field displayed on beam I20-UD-B2-13.

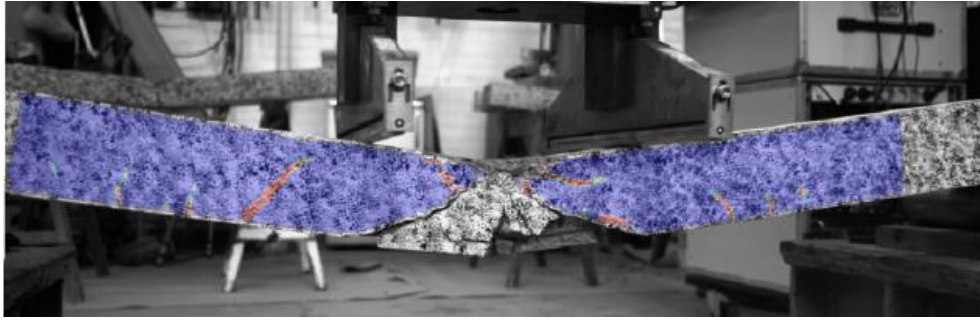


Figure K.14 Strain field displayed on beam I20-UD-B2-14.

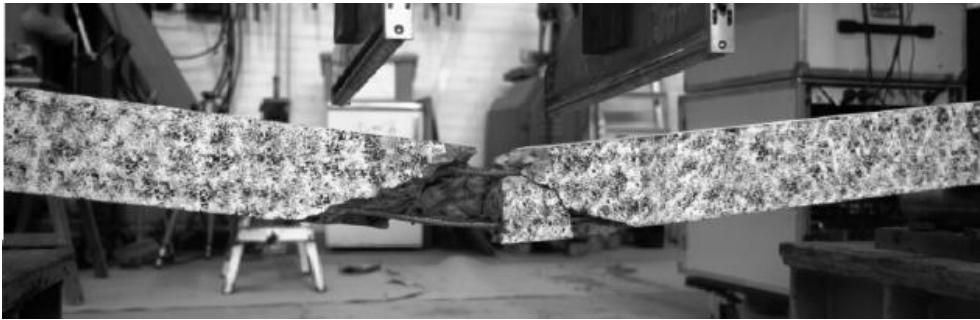


Figure K.15 Photo of beam I20-UD-B2-15 after the dynamic loading test.

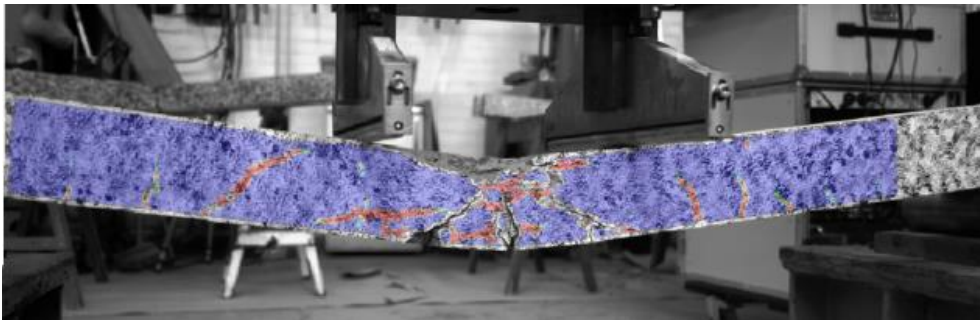


Figure K.16 Strain field displayed on beam I20-D-B2-16.

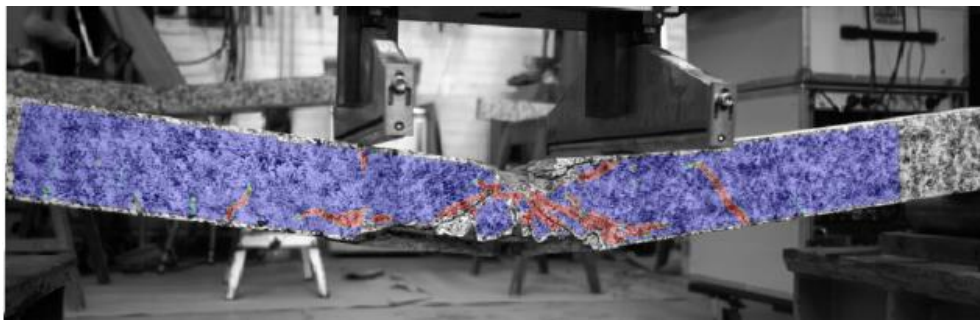


Figure K.17 Strain field displayed on beam I20-D-B2-17.

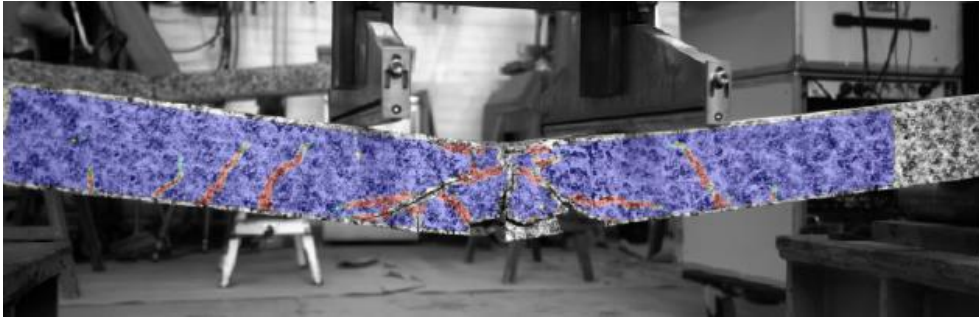


Figure K.18 Strain field displayed on beam I20-D-B2-18.

Appendix L Approximation of internal work during impact

Graphical interpretations of the internal work parameters discussed in Section 9.4.3.3.2 are illustrated in Figure L.1 to Figure L.3. All the load-deflection curves were truncated at the point where they were considered to have utilized their full capacity prior to the calculation of internal work.

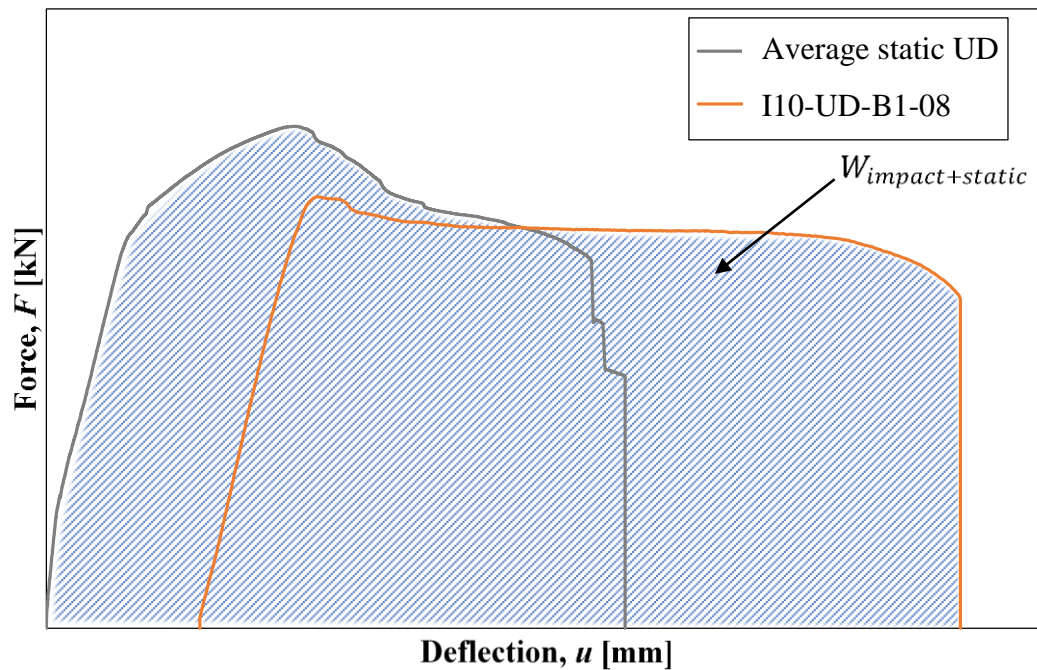


Figure L.1 Graphical interpretation of $W_{\text{impact+static}}$. Here the average static curve for undamaged reinforcement together with beam I10-UD-B1-08 serve as example.

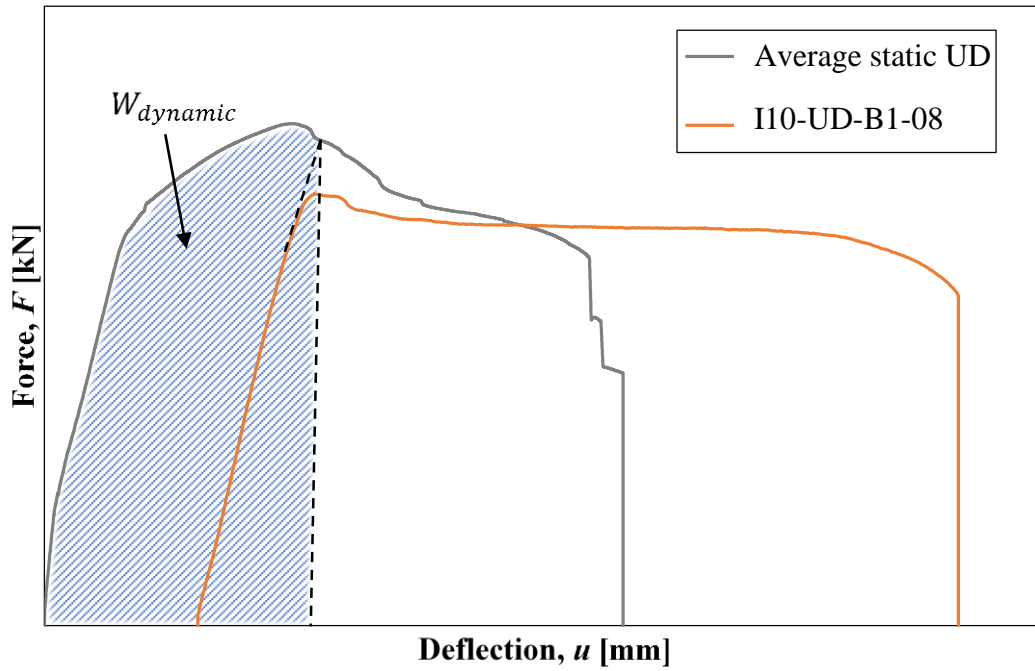


Figure L.2 Graphical interpretation of $W_{dynamic}$. Here the average static curve for undamaged reinforcement together with beam I10-UD-B1-08 serve as example.

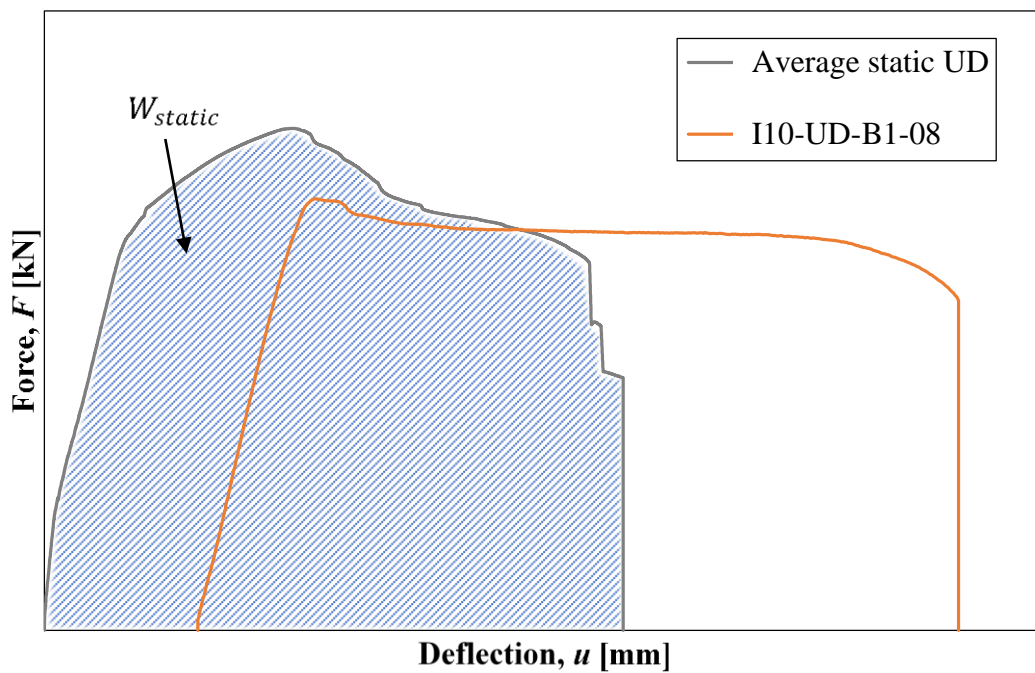


Figure L.3 Graphical interpretation of W_{static} . Here the average static curve for undamaged reinforcement together with beam I10-UD-B1-08 serve as example.

Appendix M Matlab Script for 2DOF model

```
%%%%%%%%%%%%%%%%%%%%%%%%%%%%%%%%%%%%%%%%%%%%%%%%%%%%%%%%%%%%%%%%%%%%%%%%%%%%%%
%%%%%%%%%%%%%%%%%%%%%%%%%%%%%%%%%%%%%%%%%%%%%%%%%%%%%%%%%%%%%%%%%%%%%%%%%%%%%% Simplified 2DOF System
%%%%%%%%%%%%%%%%%%%%%%%%%%%%%%%%%%%%%%%%%%%%%%%%%%%%%%%%%%%%%%%%%%%%%%%%%%%%%%
%%%%%%%%%%%%%%%%%%%%%%%%%%%%%%%%%%%%%%%%%%%%%%%%%%%%%%%%%%%%%%%%%%%%%%%%%%%%%% Malin Andersson
%%%%%%%%%%%%%%%%%%%%%%%%%%%%%%%%%%%%%%%%%%%%%%%%%%%%%%%%%%%%%%%%%%%%%%%%%%%%%% Emma Pettersson
%%%%%%%%%%%%%%%%%%%%%%%%%%%%%%%%%%%%%%%%%%%%%%%%%%%%%%%%%%%%%%%%%%%%%%%%%%%%%% Modified from the version made by
%%%%%%%%%%%%%%%%%%%%%%%%%%%%%%%%%%%%%%%%%%%%%%%%%%%%%%%%%%%%%%%%%%%%%%%%%%%%%% Fabio Lozano Mendoza & Josef Makdesi Aphram
%%%%%%%%%%%%%%%%%%%%%%%%%%%%%%%%%%%%%%%%%%%%%%%%%%%%%%%%%%%%%%%%%%%%%%%%%%%%%% Chalmers University of Technology
%%%%%%%%%%%%%%%%%%%%%%%%%%%%%%%%%%%%%%%%%%%%%%%%%%%%%%%%%%%%%%%%%%%%%%%%%%%%%% 16 - May - 2019
%%%%%%%%%%%%%%%%%%%%%%%%%%%%%%%%%%%%%%%%%%%%%%%%%%%%%%%%%%%%%%%%%%%%%%%%%%%%%%
%%%%%%%%%%%%%%%%%%%%%%%%%%%%%%%%%%%%%%%%%%%%%%%%%%%%%%%%%%%%%%%%%%%%%%%%%%%%%%

clear all
close all
clc

conditions=2;          % Indata for different impact conditions.
                        % 1 - 10 kg
                        % 2 - 20 kg

resistance=4;          % Indata for resistance
                        % 1 - calculated resistance, undamaged
                        % 2 - measured resistance, undamaged
                        % 3 - calculated resistance, damaged
                        % 4 - measured resistance, damaged

%%%%%%%%%%%%%%%%%%%%%%%%%%%%%%%%%%%%%%%%%%%%%%%%%%%%%%%%%%%%%%%%%%%%%%%%%%%%%%

if conditions==1
    m_1 = 10;          % [kg] mass of the drop-weight
    L_d = 0.250;       % [m] Length Drop-weight
elseif conditions==2
    m_1 = 20;          % [kg] mass of the drop-weight
    L_d = 0.500;       % [m] Length Drop-weight
end

if resistance==1
    R_u=7.675e3;        % Calculated resistance, undamaged
elseif resistance==2
    R_u=9.00e3;         % Measured resistance, undamaged
elseif resistance==3
    R_u=8.559e3;        % Calculated resistance, damaged
elseif resistance==4
    R_u=9.50e3;         % Measured resistance, damaged
end

%% MATERIAL PROPERTIES

% Concrete
r_c = 2420;            % [kg/m^3] Mass density
E_c = 31.5e9;          % [Pa] Modulus of elasticity
```

```

% Steel
r_s = 7800;           % [kg/m^3] Mass density
E_s = 200e9;          % [Pa] Modulus of elasticity

%% GEOMETRY

A_1 = 5027e-6;        % [m^2] Area dropweight
A_2 = 0.1*0.1;        % [m^2] Area beam
L_b = 1.3;            % [m] Length Beam

%% TRANSFORMATION FACTORS

% Transformation factors for the beam
k_b_m_el = 0.486;     % Elastic mass transformation factor
k_b_m_pl = 0.333;     % Plastic mass transformation factor

k_b_F_el = 1;         % Elastic load transformation factor
k_b_F_pl = 1;         % Plastic load transformation factor

k_b_K_el = 1;         % Elastic stiffness transformation factor
k_b_K_pl = 1;         % Plastic stiffness transformation factor

% Transformation factors for the drop-weight
k_d_m = 1;            % Plastic mass transformation factor
k_d_F = 1;            % Plastic load transformation factor
k_d_K = 1;            % Plastic stiffness transformation factor

%% MASS PROPERTIES

m_2 = r_c*A_2*L_b;    % [kg] mass of the beam

% Mass matrix
M = [m_1*k_d_m 0; 0 m_2*k_b_m_pl];

%% STIFFNESS PROPERTIES

I_b_ii = 1.571e-6;    % [m^4] Second moment of inertia of the beam
                    % corresponding to the stiffness in state II.

K_el_1 = 2.69e+8;     % [N/m] Elastic stiffness of the
                    % drop-weight, according to Hertz
%K_el_1 = A_1*E_s/L_d; % [N/m] Elastic stiffness of the
drop-weight
K_el_2 = 48*E_c*I_b_ii/L_b^3; % [N/m] Elastic stiffness of the beam

% Initial stiffness matrix
K_el = [K_el_1 -K_el_1;
-K_el_1 K_el_1+K_el_2];

%% MATERIAL RESPONSE

% Drop-weight
R_1 = 70e+3;          % [N] Plastic resistance
u_el_1 = R_1/K_el_1;  % [m] Limit of elastic deformation
u_rd_1 = 50;          % [m] Limit of plastic deformation

```

```

% Beam
R_2_sw = r_c*9.81*A_2*L_b/2; % [N] Reduction of plastic resistance
                                % due to self-weight

R_2 = R_u - R_2_sw; % [N] Plastic resistance.

u_el_2 = R_2/K_el_2; % [m] Limit of elastic deformation
u_rd_2 = 50; % [m] Limit of plastic deformation

%% DETERMINATION OF EIGENFREQUENCIES

[L,X] = eig(K_el, M); % "L" is a matrix containing the
eigenvectors % "X" is a matrix containing the
eigenvalues

% Maximum eigenfrequency
w_max = sqrt(max(max(X)));

%% CRITICAL TIME STEP

h_crit = 2/w_max; % [s] Maximum admissible value
h = 0.1e-4; % [s] Chosen time step

t_end = 80e-3; % [s] End of sequence
t = linspace(0,t_end,t_end/h); % Time vector

if h >= h_crit
disp('ERROR, chosen time step too large')
end

%% INITIAL CONDITIONS

% Empty matrices
dofs = 2; % Number of degree of freedom
u = zeros(dofs, length(t)); % Empty matrix storing displacement
vectors
v = zeros(dofs, length(t)-1); % Velocity vectors
a = zeros(dofs, length(t)-1); % Acceleration vectors

% Assigning initial values
u(:,1) = [0;0]; % Initial Displacement

height = 5.0; % [m] Drop height
v_d = 9.84; % [m/s] Initial velocity of drop-
weight % [measured value]

% v_d = sqrt(2*9.81*height); % [m/s] Initial velocity of drop-
weight % [theoretical value]

v(:,1) = [v_d; 0]; % Velocities at time t = 0

a_0 = inv(M)*(-K_el*u(:,1)); % Initial acceleration vector
a(:,1) = a_0; % Initial acceleration as calculated
before

```

```

u_b0 = u(:,1)-h*v(:,1)+h^2/2*a(:,1);    % Displacement at time step
n-1

% Initial plastic deformation
u_pl_1 = 0;                               % Plastic deformation of rod
u_pl_2_pos = 0;                           % Plastic deformation of beam in
compression
u_pl_2_neg = 0;                           % Plastic deformation of beam in
tension

%% CENTRAL DIFFERENCE METHOD

for i =2:length(t)
    du = u(1,i-1)-u(2,i-1);               % [m] Relative displacement between
beam
                                           % and drop-weight
    u2 = u(2,i-1);                       % [m] Downwards beam displacement

    % Determining resistance and stiffness of fictitious spring
between
    % drop-weight and beam

    % If du = 0, set stiffness equal to elastic stiffness
    if du == 0;
        K_1 = K_el_1;
    % If spring is in tension, set stiffness to 0
    elseif du < u_pl_1;
        K_1 = 0;
    % If spring is in elastic range
    elseif du > u_pl_1 && du <= u_pl_1+u_el_1;
        R = K_el_1*(du-u_pl_1);
        K_1 = R/du;
    % If spring is in plastic range
    elseif du > u_pl_1+u_el_1
        K_1 = R_1/du;
        u_pl_1 = du-u_el_1;
    end

    % Determining resistance and stiffness of beam spring

    % If u2 = 0, set stiffness equal to elastic stiffness
    if u2 == 0;
        K_2 = K_el_2;
    % If spring is in elastic tension/compression
    elseif u2 > u_pl_2_pos - u_el_2 && u2 <= u_pl_2_pos + u_el_2
        R = K_el_2*(u2-u_pl_2_pos);
        K_2 = R/u2;
    % If spring is in plastic compression
    elseif u2 > u_pl_2_pos + u_el_2;
        K_2 = R_2/u2;
        u_pl_2_pos = u2-u_el_2;
    % If spring is in plastic tension
    elseif u2 <= u_pl_2_pos - u_el_2
        K_2 = -R_2/u2;
        u_pl_2_neg = abs(u2+u_el_2-u_pl_2_pos);
        u_pl_2_pos = u_pl_2_pos - u_pl_2_neg;
    end
end

```

```

% Storing values of resistance for all time steps
Res(1,i-1) = K_1*du;
Res(2,i-1) = K_2*u2;

% Computing stiffness matrix
K = [(K_1) -(K_1); -(K_1) (K_1)+(K_2)];

% Calculation of displacement, velocity and acceleration
if i==2
    u(:,i) = inv(M/h^2)*(-(K-2*M/h^2)*u(:,i-1)-(M/h^2)*u_b0);
else
    u(:,i) = inv(M/h^2)*(-(K-2*M/h^2)*u(:,i-1)-(M/h^2)*u(:,i-2));
    v(:,i-1) = (u(:,i)-u(:,i-2))/(2*h);
    a(:,i-1) = (u(:,i)-2*u(:,i-1)+u(:,i-2))/h^2;
end
end

%% CALCULATION OF ENERGY

% External Work of Beam
DeltaWe(1) = 0;
We(1) = 0;

for i = 2:(length(t)-1)
    DeltaWe(i) = 0.5*(Res(1,i-1)+Res(1,i))*(u(2,i)-u(2,i-1));
    We(i) = We(i-1)+DeltaWe(i);
end

% Internal Work of Beam
DeltaWi(1) = 0;
Wi(1) = 0;

for i = 2:(length(t)-1)
    DeltaWi(i) = 0.5*(Res(2,i-1)+Res(2,i))*(u(2,i)-u(2,i-1));
    Wi(i) = Wi(i-1)+DeltaWi(i);
end

% Kinetic Energy
Wk(1)=0;

for i = 2:(length(t)-1)
    Wk(i) = m_2*k_b_m_pl*0.5*v(2,i-1)^2;
end

% Total Energy
Wt(1)=0;

for i = 2:(length(t)-1)
    Wt(i) = Wi(i)+Wk(i);
end

%% CREATING PLOTS

% Displacement vs Time plots
figure(1)
plot(t*1000,u(1,:)*1000,'LineWidth',3);
set(gca,'fontsize',16)
title('Displacement of mass 1', 'FontSize', 30)

```

```

xlabel('Time [ms]'); ylabel('Displacement [mm]');

figure(2)
plot(t*1000,u(2,:)*1000,'LineWidth',3);
set(gca,'fontsize',16)
title('Displacement of mass 2', 'FontSize', 30)
xlabel('Time [ms]'); ylabel('Displacement [mm]');

% Resistance vs Displacement
figure(3)
plot(u(2,1:length(u)-1)*1000,Res(2,+)/1000,'LineWidth',3);
set(gca,'fontsize',16)
title('Internal Resistance vs Displacement - Body 2', 'FontSize', 30)
xlabel('Displacement [mm]'); ylabel('Resistance [kN]');

figure(4)
plot(u(1,1:1500)*1000-
u(2,1:1500)*1000,Res(1,1:1500)/1000,'LineWidth',3);
set(gca,'fontsize',16)
title('Internal Resistance vs Displacement - Body 1', 'FontSize', 30)
xlabel('Displacement [mm]'); ylabel('Resistance [kN]');

% Resistance vs Time
figure(5)
plot(t(1:length(t)-1)*1000,Res(2,+)/1000,'LineWidth',3);
set(gca,'fontsize',16)
title('Internal Resistance vs Time - Body 2', 'FontSize', 30)
xlabel('Time [ms]'); ylabel('Resistance [kN]');

figure(6)
plot(t(1:1500)*1000,Res(1,1:1500)/1000,'LineWidth',3);
set(gca,'fontsize',16)
title('Internal Resistance vs Time - Body 1', 'FontSize', 30)
xlabel('Time [ms]'); ylabel('Resistance [kN]');

% Velocity vs Time
figure(7)
plot(t(1:(length(t)-1))*1000,v(1,:), 'LineWidth',3);
set(gca,'fontsize',16)
title('Velocity of Body 1', 'FontSize', 30)
xlabel('Time [ms]'); ylabel('Velocity [m/s]');

figure(8)
plot(t(1:(length(t)-1))*1000,v(2,:), 'LineWidth',3);
set(gca,'fontsize',16)
title('Velocity of Body 2', 'FontSize', 30)
xlabel('Time [ms]'); ylabel('Velocity [m/s]');

% Work vs Time
figure(9)
plot(t(1:(length(t)-1))*1000,We(:), 'LineWidth',3);
hold on
plot(t(1:(length(t)-1))*1000,Wi(:), 'LineWidth',3);
hold on
plot(t(1:(length(t)-1))*1000,Wk(:), 'LineWidth',3);
hold on
plot(t(1:(length(t)-1))*1000,Wt(:), 'LineWidth',3);
set(gca,'fontsize',16)
title('External Work of Body 2', 'FontSize', 30)
xlabel('Time [ms]'); ylabel('Velocity [m/s]');

```



```
height;  
v_init = v(1,2);  
maxdisp = max(max(u(2,:)));  
u_pl = maxdisp - u_el_2;  
[height v_init maxdisp u_pl]
```


Appendix N Mathcad Calculations

1. Three point bending and undamaged reinforcement

1.1 Load Capacity of Reinforced Concrete Beam

The load capacity of a reinforced concrete beam is determined for a given cross section.

$$\text{kN} := \text{N} \cdot 10^3 \quad \text{MPa} := \text{Pa} \cdot 10^6$$

1.1.1 Input Data

1.1.1.1 Geometry

Beam height: $h := 0.1\text{m}$

Beam width: $b := 0.1\text{m}$

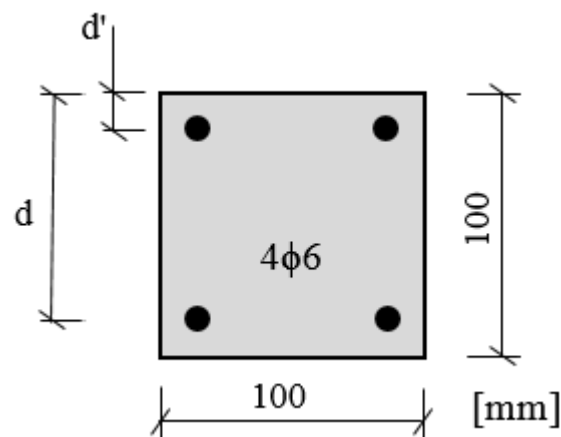
Effective span length: $L := 1.3\text{m}$

Nominal bar diameter: $\Phi := 6\text{mm}$

Area of reinforcement bar: $A_{\text{bar}} := \pi \cdot \frac{\Phi^2}{4} = 28.274 \text{mm}^2$

Stirrup dimension: $\Phi_s := 0\text{mm}$

Note: No stirrups



Number of bars in the top: $n' := 2$

Number of bars in the bottom: $n := 2$

Area of top reinforcement: $A_s := n \cdot A_{\text{bar}} = 56.549 \text{mm}^2$

Area of bottom reinforcement: $A'_s := n' \cdot A_{\text{bar}} = 56.549 \text{mm}^2$

Concrete cover:

$$c := 0.02m - \frac{\Phi}{2} = 17 \cdot \text{mm}$$

Distance from top edge to bottom reinforcement:

$$d := h - \left(\frac{\Phi}{2} + c \right) = 80 \cdot \text{mm}$$

Distance from top edge to top reinforcement:

$$d' := \frac{\Phi}{2} + c = 20 \cdot \text{mm}$$

1.1.1.2 Material properties

Concrete:

Mean compressive strength:

$$f_{cm} := 33.0 \text{MPa}$$

Mean tensile strength

$$f_{ctm} := 4.43 \cdot \text{MPa}$$

Mean modulus of elasticity

$$E_{cm} := 31.5 \text{GPa}$$

Reinforcing steel:

Mean yield strength:

$$f_{ym} := 555 \text{MPa}$$

Ultimate tensile stress:

$$f_t := 656 \text{MPa}$$

Mean modulus of elasticity:

$$E_{sm} := 202 \cdot \text{GPa}$$

1.1.2. Stress-strain Relationship of Concrete

1.1.2.1 Mathematic formulation

The parabola-rectangle stress-strain diagram for concrete under compression (according to EN 1992-1-1) is adopted.

Parameters for all concrete classes:

Concrete strain at maximum strength:

$$\varepsilon_{c2} := 2 \cdot 10^{-3}$$

Ultimate concrete strain:

$$\varepsilon_{cu2} := 3.5 \cdot 10^{-3}$$

Exponent:

$$n := 2$$

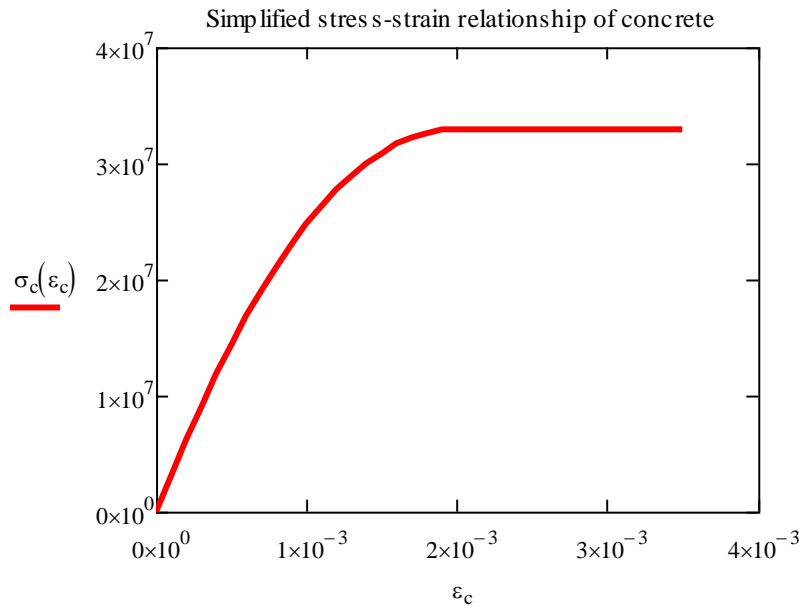
Stress-strain relationship:

$$\sigma_c(\varepsilon_c) := \begin{cases} \left[1 - \left(1 - \frac{\varepsilon_c}{\varepsilon_{c2}} \right)^n \right] \cdot f_{cm} & \text{if } 0 \leq \varepsilon_c \leq \varepsilon_{c2} \\ f_{cm} & \text{if } \varepsilon_{c2} < \varepsilon_c \leq \varepsilon_{cu2} \end{cases}$$

Create a vector with different values of strain:

$$\varepsilon_c := 0, 0.0001 \dots \varepsilon_{cu2}$$

Graphic representation of the stress-strain relationship:



1.1.2.2 Determination of block factors

Area under the curve for a given value of strain:

$$\text{Area}(\epsilon_c) := \int_0^{\epsilon_c} \sigma_c(\epsilon_c) d\epsilon_c$$

Area under the curve multiplied by the distance from the origin to the center of gravity of the area:

$$A_{-\epsilon}(\epsilon_c) := \int_0^{\epsilon_c} \sigma_c(\epsilon_c) \cdot \epsilon_c d\epsilon_c$$

Determination of factors $\alpha_{R,S}$ and $\beta_{R,S}$

$$\alpha_{R,S}(\epsilon_c) := \frac{\text{Area}(\epsilon_c)}{f_{cm} \cdot \epsilon_c} \quad \alpha_{R,S}(\epsilon_{cu2}) = 0.81$$

$$\beta_{R,S}(\epsilon_c) := \frac{\epsilon_c - \frac{A_{-\epsilon}(\epsilon_c)}{\text{Area}(\epsilon_c)}}{\epsilon_c} \quad \beta_{R,S}(\epsilon_{cu2}) = 0.416$$

1.1.3 Stress-strain Relationship of Reinforcing Steel

1.1.3.1 Mathematic formulation

Ultimate steel strain: $\varepsilon_{su} := 0.0938$

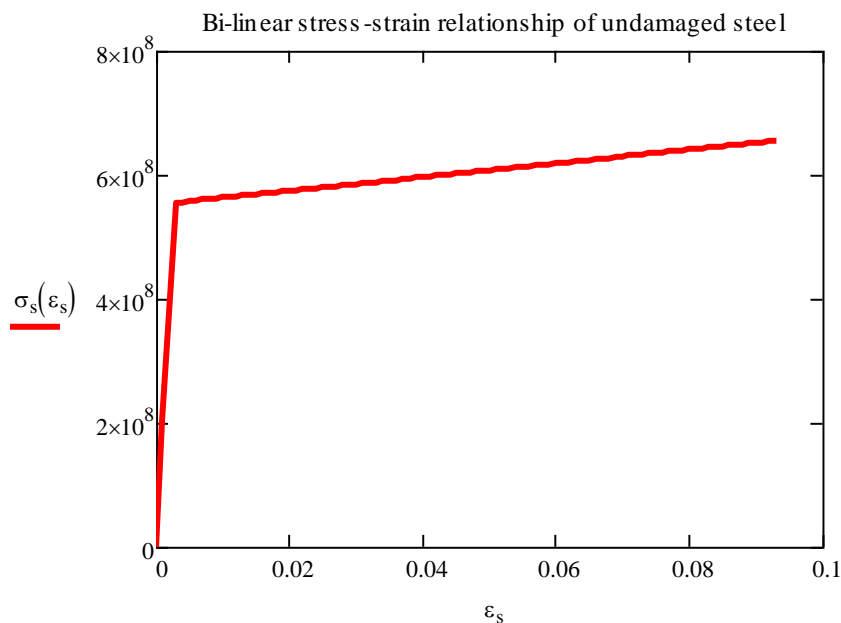
Yield strain: $\varepsilon_{sy} := \frac{f_{ym}}{E_{sm}} \quad \varepsilon_{sy} = 2.748 \times 10^{-3}$

Relationship parameters: $p_1(\varepsilon_s) := \frac{\varepsilon_s - \varepsilon_{sy}}{\varepsilon_{su} - \varepsilon_{sy}}$

Stress-strain relationship:
$$\sigma_s(\varepsilon_s) := \begin{cases} E_{sm} \cdot \varepsilon_s & \text{if } \varepsilon_s \leq \varepsilon_{sy} \\ f_{ym} + p_1(\varepsilon_s) \cdot (f_t - f_{ym}) & \text{if } \varepsilon_s > \varepsilon_{sy} \end{cases}$$

$$\varepsilon_s := 0, 0.001.. \varepsilon_{su}$$

Graphic representation of the stress-strain relationship for reinforcing steel:



1.1.4. Design Strength Values

1.1.4.1 Concrete

Partial factor: $\gamma_C := 1.0$

Design compressive strength: $f_{cd} := \frac{f_{cm}}{\gamma_C} \quad f_{cd} = 33 \cdot \text{MPa}$

Concrete ultimate strain: $\varepsilon_{cu} := 0.0035$

Stress block factors:

$$\alpha_R := \alpha_{R,S}(\epsilon_{cu}) = 0.81$$

$$\beta_R := \beta_{R,S}(\epsilon_{cu2}) = 0.416$$

5%-fractile tensile strength:

$$f_{ctk0.05} := 0.7 \cdot f_{ctm} = 3.101 \cdot \text{MPa}$$

Flexural tensile strength:

$$\kappa := 0.6 + \frac{0.4}{\sqrt[4]{\frac{h}{m}}} = 1.311$$

$$f_{ct,fl} := \kappa \cdot f_{ctm} = 5.809 \cdot \text{MPa}$$

1.1.4.2 Reinforcing steel

Partial factor:

$$\gamma_S := 1.0$$

Design yield stress:

$$f_{yd} := \frac{f_{ym}}{\gamma_S} \quad f_{yd} = 555 \cdot \text{MPa}$$

1.1.5. Load Capacity in Ultimate Limit State

1.1.5.1 Analysis of field section without top reinforcement

Number of bars in the top: $n' := 0$

Number of bars in the bottom: $n = 2$

Assume yielding: $\epsilon_{s,1} > \epsilon_{sy}$ $\epsilon_{s,1} = \frac{d - x_{u,1}}{x_{u,1}} \epsilon_{cu}$

Position of neutral axis:

Initial guess: $x_{u,1} := 20 \text{ mm}$

Calculated value: $x_{u,1} := \text{root} \left(\alpha_R \cdot f_{cd} \cdot b \cdot x_{u,1} - \sigma_s \left(\frac{d - x_{u,1}}{x_{u,1}} \epsilon_{cu} \right) \cdot n \cdot A_{bar, x_{u,1}} \right)$
 $x_{u,1} = 12.143 \text{ mm}$

Check the strain in the reinforcement bars:

$$\epsilon_{s,1} := \frac{d - x_{u,1}}{x_{u,1}} \epsilon_{cu} = 0.02 \quad \epsilon_{sy} = 2.748 \times 10^{-3} \quad \epsilon_{s,1} > \epsilon_{sy} = 1$$

Calculation of load capacity:

$$M_{u,1} := \alpha_R \cdot f_{cd} \cdot b \cdot x_{u,1} \cdot (d - \beta_R \cdot x_{u,1}) \quad M_{u,1} = 2.431 \cdot \text{kN} \cdot \text{m}$$

$$F_{u,1} := \frac{4 \cdot M_{u,1}}{L} \quad F_{u,1} = 7.481 \cdot \text{kN}$$

Calculation of stress in the steel bars:

$$\sigma_{s,1} := \sigma_s(\epsilon_{s,1}) \quad \sigma_{s,1} = 573.648 \cdot \text{MPa}$$

Calculation of curvature at failure:

$$\epsilon_{s,1} = 0.02 \quad \varphi_{u,1} := \frac{\epsilon_{s,1}}{d - x_{u,1}} = 0.288 \cdot \text{m}^{-1}$$

1.1.5.2 Analysis of field section including top reinforcement

Number of bars in the top: $n' := 2$

Number of bars in the bottom: $n = 2$

Assume tension in top and bottom and that the neutral axis is located above the top reinforcement.

$$\text{Strain in bottom reinforcement:} \quad \epsilon_{s,2} = \frac{d - x_{u,2}}{x_{u,2}} \epsilon_{cu}$$

$$\text{Strain in top reinforcement:} \quad \epsilon'_{s,2} = \frac{d' - x_{u,2}}{x_{u,2}} \epsilon_{cu}$$

Position of neutral axis:

Initial guess: $x_{u,2} := 20 \text{ mm}$

Calculated value:

$$x_{u,2} := \text{root} \left(\alpha_R \cdot f_{cd} \cdot b \cdot x_{u,2} - \sigma_s \left(\frac{d' - x_{u,2}}{x_{u,2}} \epsilon_{cu} \right) \cdot A'_s - \sigma_s \left(\frac{d - x_{u,2}}{x_{u,2}} \epsilon_{cu} \right) \cdot A_s, x_{u,2} \right)$$

$$x_{u,2} = 15.888 \text{ mm}$$

Note: The neutral axis is indeed located above the top reinforcement. Top bars are subjected to tensile stress.

Check the strain in the reinforcement bars:

$$\varepsilon_{s,2} := \frac{d - x_{u,2}}{x_{u,2}} \varepsilon_{cu} = 0.014 \quad \varepsilon_{sy} = 2.748 \times 10^{-3} \quad \varepsilon_{s,2} > \varepsilon_{sy} = 1$$

$$\varepsilon'_{s,2} := \frac{d' - x_{u,2}}{x_{u,2}} \varepsilon_{cu} = 9.058 \times 10^{-4} \quad \varepsilon'_{s,2} > \varepsilon_{sy} = 0$$

Calculation of moment capacity:

$$M_{u,2} := \alpha_R \cdot f_{cd} \cdot b \cdot x_{u,2} \cdot (d - \beta_R \cdot x_{u,2}) - \sigma_s \left(\frac{d' - x_{u,2}}{x_{u,2}} \varepsilon_{cu} \right) \cdot A'_s \cdot (d - d') \quad M_{u,2} = 2.494 \cdot \text{kN} \cdot \text{m}$$

$$F_{u,2} := \frac{4 \cdot M_{u,2}}{L} \quad F_{u,2} = 7.675 \cdot \text{kN}$$

Calculation of stress in the steel bars:

$$\sigma'_{s,2} := \sigma_s(\varepsilon'_{s,2}) \quad \sigma'_{s,2} = 182.963 \cdot \text{MPa}$$

$$\sigma_{s,2} := \sigma_s(\varepsilon_{s,2}) \quad \sigma_{s,2} = 567.618 \cdot \text{MPa}$$

Calculation of curvature at failure:

$$\varepsilon_{s,2} = 0.014 \quad \varphi_{u,2} := \frac{\varepsilon_{s,2}}{d - x_{u,2}} = 0.22 \text{ m}^{-1}$$

1.1.6. Moment and Curvature at Onset of Yielding

1.1.6.1 Analysis of field section without top reinforcement

Yielding strain: $\varepsilon_{sy} = 2.748 \times 10^{-3}$

Definition of strain in the compressed edge:

$$\varepsilon_{cc,y,1} = \frac{x_{y,1}}{d - x_{y,1}} \cdot \varepsilon_{sy}$$

Tensile force in the bottom reinforcement:

$$F_{sy} := f_{yd} \cdot n \cdot A_{\text{bar}} = 31.385 \cdot \text{kN}$$

Equivalent compressive force in concrete

$$F_{C,y,1} = \alpha_{R,y} \cdot f_{cd} \cdot b \cdot x_{y,1} \quad \alpha_{R,y} = \alpha_{R,S}(\varepsilon_{cc,y,1})$$

Horizontal equilibrium condition:

$$F_{sy} = F_{C,y}$$

Assume $x_{y,1} := 22.042\text{mm}$

Total tensile force: $F_{sy} = 31.385\text{ kN}$

Total compressive force: $F_{C,y,1} := \alpha_{R,S} \left(\frac{x_{y,1}}{d - x_{y,1}} \cdot \varepsilon_{sy} \right) \cdot f_{cd} \cdot b \cdot x_{y,1} = 31.384\text{ kN}$

$$\Delta F := F_{C,y,1} - F_{sy} = -7.021 \times 10^{-5} \cdot \text{kN}$$

Note: Check that $\Delta F \approx 0$

Calculation of strains

$$\varepsilon_{cc,y,1} := \frac{x_{y,1}}{d - x_{y,1}} \cdot \varepsilon_{sy} = 1.045 \times 10^{-3} \quad \varepsilon_{cc,y,1} < \varepsilon_{c2} = 1$$

Calculation of moment at yielding:

$$\alpha_{R,y} := \alpha_{R,S}(\varepsilon_{cc,y,1}) = 0.431 \quad \beta_{R,y} := \beta_{R,S}(\varepsilon_{cc,y,1}) = 0.351$$

$$M_{y,1} := \alpha_{R,y} \cdot f_{cd} \cdot b \cdot x_{y,1} \cdot (d - \beta_{R,y} \cdot x_{y,1}) \quad M_{y,1} = 2.268 \cdot \text{kN} \cdot \text{m} \quad F_{y,1} := \frac{4 \cdot M_{y,1}}{L} = 6.978 \cdot \text{kN}$$

Determination of stresses in the reinforcement bars:

$$\sigma_{s,y,1} := \sigma_s(\varepsilon_{sy}) \quad \sigma_{s,y,1} = 555 \cdot \text{MPa}$$

Curvature at yielding

$$\varepsilon_{sy} = 2.748 \times 10^{-3} \quad \phi_{y,1} := \frac{\varepsilon_{sy}}{d - x_{y,1}} = 0.047 \text{ m}^{-1}$$

1.1.6.2 Analysis of field section including top reinforcement

Assume tension in the top reinforcement bars

Yielding strain: $\varepsilon_{sy} = 2.748 \times 10^{-3}$

Definition of strain in the compressed edge and top reinforcement:

$$\varepsilon_{cc,y,2} = \frac{x_{y,2}}{d - x_{y,2}} \cdot \varepsilon_{sy} \quad \varepsilon'_{s,y,2} = \frac{x_{y,2} - d'}{d - x_{y,2}} \cdot \varepsilon_{sy}$$

Tensile force in the reinforcement:

Top reinforcement: $F'_{sy,2} = \sigma_s(\varepsilon'_{s,y,2}) \cdot A'_s$

Bottom reinforcement: $F_{sy} := f_{yd} \cdot A_s = 31.385 \text{ kN}$

Equivalent compressive force in concrete

$$F_{C,y,2} = \alpha_{R,y} \cdot f_{cd} \cdot b \cdot x_{y,2} \quad \alpha_{R,y} = \alpha_{R,S}(\varepsilon_{cc,y,2})$$

Horizontal equilibrium condition:

$$F_{sy} = F_{C,y,2} + F'_{sy,2}$$

Assume $x_{y,2} := 21.725 \text{ mm}$

Total tensile force: $F_{T,y,2} := F_{sy} = 31.385 \text{ kN}$

Total compressive force: $F_{C,y,2} := \alpha_{R,S} \left(\frac{x_{y,2}}{d - x_{y,2}} \cdot \varepsilon_{sy} \right) \cdot f_{cd} \cdot b \cdot x_{y,2} + \sigma_s \left(\frac{x_{y,2} - d'}{d - x_{y,2}} \cdot \varepsilon_{sy} \right) \cdot A'_s$

$$F_{C,y,2} = 31.378 \text{ kN}$$

$$\Delta F := F_{C,y,2} - F_{T,y,2} = -6.889 \times 10^{-3} \text{ kN}$$

Note: Check that $\Delta F \approx 0$

Calculation of strains

$$\varepsilon_{cc,y,2} := \frac{x_{y,2}}{d - x_{y,2}} \cdot \varepsilon_{sy} = 1.024 \times 10^{-3}$$

$$\varepsilon_{cc,y,2} < \varepsilon_{c2} = 1$$

$$\varepsilon'_{s,y,2} := \frac{x_{y,2} - d'}{x_{y,2}} \cdot \varepsilon_{cc,y,2} = 8.133 \times 10^{-5}$$

Note: The strains are in fact negative though they are positive here to be able to use the stress-strain curve.

Calculation of moment at yielding:

$$\alpha_{R,y} := \alpha_{R,s}(\varepsilon_{cc,y,2}) = 0.425 \quad \beta_{R,y} := \beta_{R,s}(\varepsilon_{cc,y,2}) = 0.35$$

$$M_{y,2} := \alpha_{R,y} \cdot f_{cd} \cdot b \cdot x_{y,2} \cdot (d - \beta_{R,y} \cdot x_{y,2}) + \sigma_s \left(\frac{x_{y,2} - d'}{x_{y,2}} \varepsilon_{cc,y,2} \right) \cdot A'_s \cdot (d - d')$$

$$M_{y,2} = 2.26 \cdot \text{kN} \cdot \text{m} \quad F_{y,2} := \frac{4 \cdot M_{y,2}}{L} = 6.953 \cdot \text{kN}$$

Determination of stresses in the reinforcement bars:

$$\text{Top reinforcement:} \quad \sigma'_{s,y,2} := -\sigma_s(\varepsilon'_{s,y,2}) \quad \sigma'_{s,y,2} = -16.429 \cdot \text{MPa}$$

$$\text{Bottom reinforcement:} \quad \sigma_{s,y,2} := \sigma_s(\varepsilon_{sy}) \quad \sigma_{s,y,2} = 555 \cdot \text{MPa}$$

Curvature at yielding

$$\varepsilon_{sy} = 2.748 \times 10^{-3} \quad \varphi_{y,2} := \frac{\varepsilon_{sy}}{d - x_{y,2}} = 0.047 \text{ m}^{-1}$$

1.1.7 Summary

1.1.7.1 Moment and curvature at yielding without consideration of top reinforcement

$$M_{y,1} = 2.268 \cdot \text{kN} \cdot \text{m} \quad x_{y,1} = 22.042 \cdot \text{mm}$$

$$F_{y,1} = 6.978 \cdot \text{kN} \quad \varphi_{y,1} = 0.047 \text{ m}^{-1}$$

1.1.7.2 Moment and curvature at yielding considering both top and bottom reinforcement

$$M_{y,2} = 2.26 \cdot \text{kN} \cdot \text{m} \quad x_{y,2} = 21.725 \cdot \text{mm}$$

$$F_{y,2} = 6.953 \cdot \text{kN} \quad \varphi_{y,2} = 0.047 \text{ m}^{-1}$$

1.1.7.3 Load Capacity at Ultimate State without consideration of top reinforcement

$$M_{u,1} = 2.431 \cdot \text{kN} \cdot \text{m} \quad x_{u,1} = 12.143 \cdot \text{mm}$$

$$F_{u,1} = 7.481 \cdot \text{kN} \quad \varphi_{u,1} = 0.288 \text{ m}^{-1}$$

1.1.7.4 Load Capacity at Ultimate State considering both top and bottom reinforcement

$$M_{u,2} = 2.494 \text{ kN}\cdot\text{m}$$

$$x_{u,2} = 15.888 \text{ mm}$$

$$F_{u,2} = 7.675 \text{ kN}$$

$$\varphi_{u,2} = 0.22 \text{ m}^{-1}$$

Increase in load capacity if top reinforcement is considered:

$$\frac{F_{u,2} - F_{u,1}}{F_{u,1}} = 2.591\%$$

1.2 Theoretical Load vs Deformation Relationship

1.2.1. Determination of Cracking Moment and Cracking Curvature:

Modular ratio: $\alpha_s := \frac{E_{sm}}{E_{cm}} = 6.413$

Moment of inertia in State I: $I_I := \frac{b \cdot h^3}{12} + (\alpha_s - 1) 2n \cdot A_{bar} \cdot \left(d - \frac{h}{2}\right)^2 = 8.884 \times 10^6 \cdot \text{mm}^4$

Cracking stress: $f_{ct,fl} = \frac{M_{cr} \cdot \left(\frac{h}{2}\right)}{I_I}$

Cracking moment: $M_{cr} := \frac{f_{ct,fl} \cdot I_I}{\frac{h}{2}} = 1.032 \cdot \text{kN} \cdot \text{m}$

Cracking force: $F_{cr} := \frac{4 \cdot M_{cr}}{L} = 3.176 \cdot \text{kN}$

1.2.2. Determination of Moment of Inertia in State II

Calculation of position of neutral axis:

Number of bars in the top: $n' = 2$

Number of bars in the bottom: $n = 2$

Consider first moment of area around the neutral axis:

$$\frac{b \cdot x_{II}^2}{2} + (\alpha_s - 1) \cdot A'_s \cdot (x_{II} - d') = \alpha_s \cdot A_s \cdot (d - x_{II})$$

Initial guess:

$$x_{II} := 50 \text{ mm}$$

Calculated value:

$$x_{II} := \text{root} \left[\frac{b \cdot x_{II}^2}{2} - (\alpha_s) \cdot A'_s \cdot (d' - x_{II}) - \alpha_s \cdot A_s \cdot (d - x_{II}), x_{II} \right]$$

$$x_{II} = 20.638 \text{ mm}$$

Moment of inertia:

$$I_{II} := \frac{b \cdot x_{II}^3}{3} + (\alpha_s) \cdot A'_s \cdot (d' - x_{II})^2 + \alpha_s \cdot A_s \cdot (d - x_{II})^2$$

$$I_{II} = 1.571 \times 10^{-6} \text{ m}^4$$

1.2.3. Load-Deformation plot

1.2.3.1 Determination of equivalent stiffness

Stiffness in State I:

$$K_I := \frac{48 \cdot E_{cm} \cdot I_I}{L^3} = 6.114 \cdot \frac{\text{kN}}{\text{mm}}$$

Stiffness in State II:

$$K_{II} := \frac{48 \cdot E_{cm} \cdot I_{II}}{L^3} = 1.081 \cdot \frac{\text{kN}}{\text{mm}}$$

1.2.3.2 Deformation considering only State II until ultimate load

Peak load:

$$F_{u,2} = 7.675 \cdot \text{kN}$$

Deflection at peak load:

$$u_{II} := \frac{F_{u,2}}{K_{II}} = 7.098 \cdot \text{mm}$$

Load as a function of displacement:

$$\text{Force}_2(u) := \begin{cases} u \cdot K_{II} & \text{if } u < u_{II} \\ F_{u,2} & \text{if } u > u_{II} \end{cases}$$

1.2.3.3 Deformation considering State I and State II

Cracking load:

$$F_{cr} = 3.176 \cdot \text{kN}$$

Deflection when cracking occurs:

$$u_{cr} := \frac{F_{cr}}{K_I} = 0.519 \cdot \text{mm}$$

Peak load:

$$F_{u,2} = 7.675 \cdot \text{kN}$$

Deflection at peak load:

$$u_{II} = 7.098 \cdot \text{mm}$$

Stiffness between cracking and yielding:

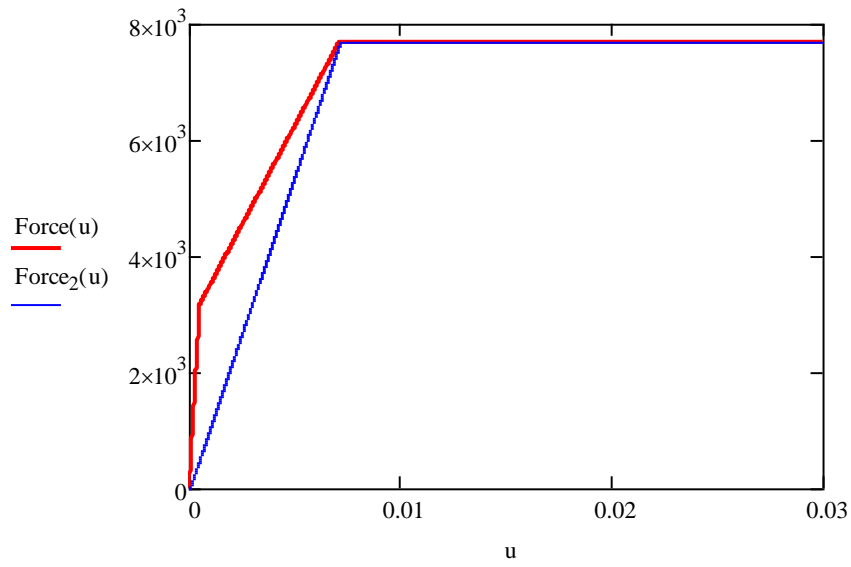
$$K_{cy} := \frac{F_{u,2} - F_{cr}}{u_{II} - u_{cr}} = 0.684 \cdot \frac{\text{kN}}{\text{mm}}$$

Load as a function of displacement:

$$\text{Force}(u) := \begin{cases} (K_I \cdot u) & \text{if } u \leq u_{cr} \\ [F_{cr} + (u - u_{cr}) \cdot K_{cy}] & \text{if } u > u_{cr} \\ F_{u,2} & \text{if } u > u_{II} \end{cases}$$

$$u := 0\text{mm}, 0.01\text{mm}.. 30\text{mm}$$

1.2.3.4 Load-deformation curves



1.3 Prediction of Plastic Rotational Capacity

1.3.1 Input Data

1.3.1.1 Geometry

Beam height: $h = 0.1 \text{ m}$

Beam width: $b = 0.1 \text{ m}$

Effective span length: $L = 1.3 \text{ m}$

Distance to critical section from support: $l_0 := \frac{L}{2} = 650 \text{ mm}$

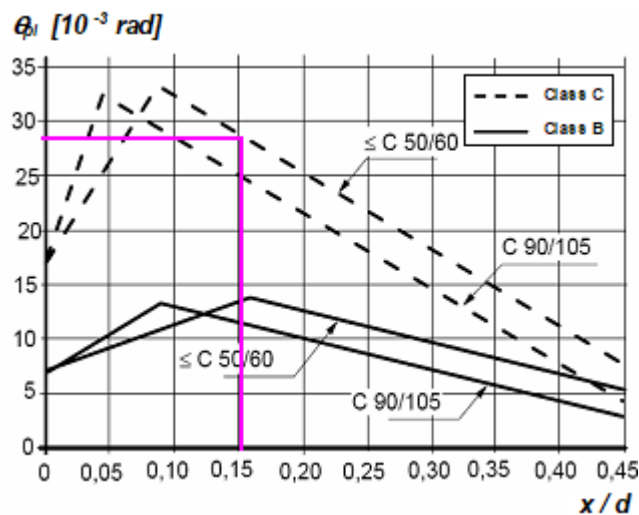
Effective height: $d = 0.08 \text{ m}$

1.3.2. Rotation Capacity According to Eurocode 2

Determine allowable rotation for reference beam ($\eta = 3$):

$x_u := x_{u,1} = 12.143 \text{ mm}$ **Note:** Position of neutral axis considering only bottom reinforcement.

$$\frac{x_u}{d} = 0.152$$



Rotation capacity from the chart:

$$\Theta_{\text{total.Eur.R}} := 0.028$$

Correction for different values of shear slenderness:

$$\lambda := \frac{l_0}{d} = 8.125 \quad \kappa_\lambda := \sqrt{\frac{\lambda}{3}} = 1.646$$

$$\Theta_{\text{total.Eur}} := \kappa_{\lambda} \cdot \Theta_{\text{total.Eur.R}} = 0.046$$

Consider:

$$\Theta_{\text{total.Eur}} = 2 \cdot \theta_{\text{pl.Eur}}$$

Rotational capacity according to Eurocode 2:

$$\theta_{\text{pl.Eur}} := \frac{\Theta_{\text{total.Eur}}}{2} = 0.023$$

$$u_{\text{pl.Eur}} := \frac{\theta_{\text{pl.Eur}} \cdot L}{2} = 14.976 \text{ mm}$$

1.3.3 Rotation Capacity According to Bk 25

Empirical expression:

$$l_{\text{p.Bk25}} = 0.5 \cdot d + 0.15L \quad \text{Plastic hinge on the field}$$

Plastic hinge length:

$$l_{\text{p.Bk25}} := 0.5 \cdot d + 0.15L = 235 \cdot \text{mm}$$

Area of tensile reinforcement:

$$A_s = 56.549 \cdot \text{mm}^2$$

$$\omega_s := \frac{A_s}{b \cdot d} \cdot \frac{f_{ym}}{f_{cm}} = 0.119$$

Since no stirrups were included, the contribution of the top bars can be disregarded

Area of compression reinforcement:

$$A_c := 0 \quad \textbf{Note:} \text{ the top reinforcement has been proved to be subjected to tensile stress.}$$

$$\omega'_s := \frac{A_c}{b \cdot d} \cdot \frac{f_{ym}}{f_{cm}} = 0$$

Dominant failure mode:

$$\omega_{s,\text{crit}} := \frac{0.8 \cdot \varepsilon_{cu}}{\varepsilon_{cu} + \varepsilon_{su}} = 0.029 \quad \omega_s = 0.119$$

$$\omega_s > \omega_{s,\text{crit}} = 1$$

Note: The dominant failure mode is concrete crushing

Determination of plastic rotation capacity:

$$\theta_{\text{pl.Bk25}} := \frac{0.4 \cdot \varepsilon_{cu}}{\omega_s} \left(1 + 0.3 \cdot \frac{L}{d} \right) = 0.0692$$

$$u_{\text{pl.Bk25}} := \frac{\theta_{\text{pl.Bk25}} \cdot L}{2} = 44.972 \text{ mm}$$

1.3.4. Summary

Eurocode 2:

$$\theta_{\text{pl.Eur}} = 0.023 \cdot \text{rad}$$

Bk25 method:

$$\theta_{\text{pl.Bk25}} = 0.069 \cdot \text{rad}$$

2. Three point bending and damaged reinforcement

2.1 Load Capacity of Reinforced Concrete Beam

The load capacity of a reinforced concrete beam is determined for a given cross section.

$$\text{kN} := \text{N} \cdot 10^3 \quad \text{MPa} := \text{Pa} \cdot 10^6$$

2.1.1 Input Data

2.1.1.1 Geometry

Beam height: $h := 0.1\text{m}$

Beam width: $b := 0.1\text{m}$

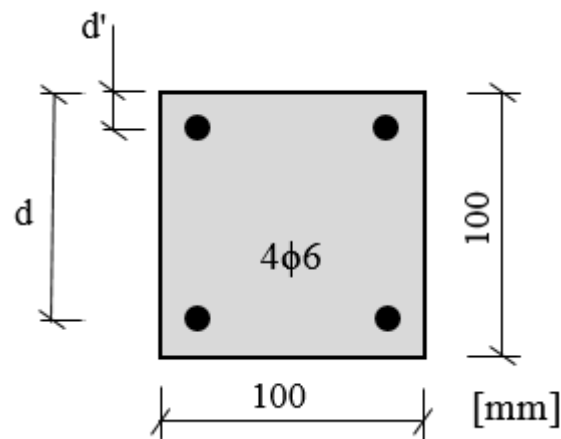
Effective span length: $L := 1.3\text{m}$

Nominal bar diameter: $\Phi := 6\text{mm}$

Area of reinforcement bar: $A_{\text{bar}} := \pi \cdot \frac{\Phi^2}{4} = 28.274\text{mm}^2$

Stirrup dimension: $\Phi_s := 0\text{mm}$

Note: No stirrups



Number of bars in the top: $n' := 2$

Number of bars in the bottom: $n := 2$

Area of top reinforcement: $A_s := n \cdot A_{\text{bar}} = 56.549\text{mm}^2$

Area of bottom reinforcement: $A'_s := n' \cdot A_{\text{bar}} = 56.549\text{mm}^2$

Concrete cover:

$$c := 0.02\text{m} - \frac{\Phi}{2} = 0.017\text{m}$$

Distance from top edge to bottom reinforcement:

$$d := h - \left(\frac{\Phi}{2} + c \right) = 80\cdot\text{mm}$$

Distance from top edge to top reinforcement:

$$d' := \frac{\Phi}{2} + c = 20\cdot\text{mm}$$

2.1.1.2 Material properties

Concrete:

Mean compressive strength:

$$f_{cm} := 33.0\text{MPa}$$

Mean tensile strength

$$f_{ctm} := 4.43\cdot\text{MPa}$$

Mean modulus of elasticity

$$E_{cm} := 31.5\text{GPa}$$

Reinforcing steel:

Mean yield strength:

$$f_{ym} := 645\text{MPa}$$

Ultimate tensile stress:

$$f_t := 664\text{MPa}$$

Mean modulus of elasticity:

$$E_{sm} := 196\cdot\text{GPa}$$

2.1.2. Stress-strain Relationship of Concrete

2.1.2.1 Mathematic formulation

The parabola-rectangle stress-strain diagram for concrete under compression (according to EN 1992-1-1) is adopted.

Parameters for all concrete classes:

Concrete strain at maximum strength:

$$\varepsilon_{c2} := 2 \cdot 10^{-3}$$

Ultimate concrete strain:

$$\varepsilon_{cu2} := 3.5 \cdot 10^{-3}$$

Exponent:

$$n := 2$$

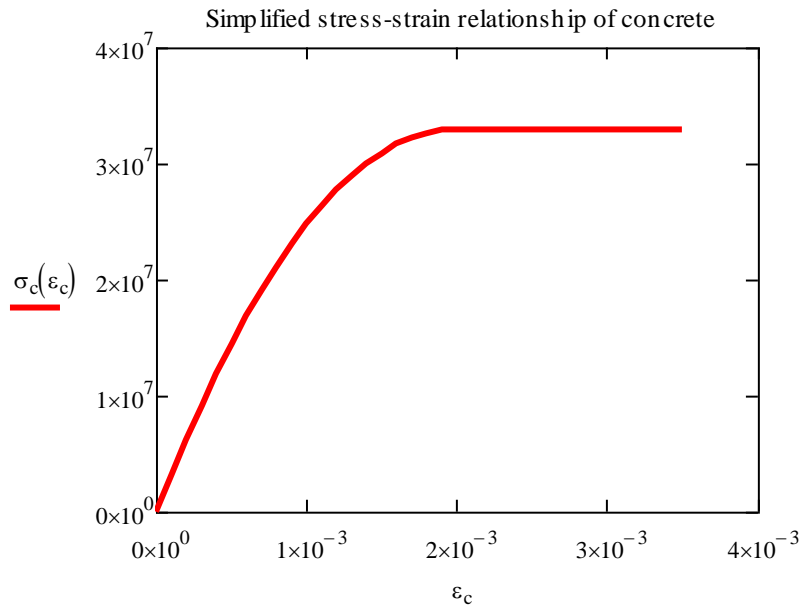
Stress-strain relationship:

$$\sigma_c(\varepsilon_c) := \begin{cases} \left[1 - \left(1 - \frac{\varepsilon_c}{\varepsilon_{c2}} \right)^n \right] \cdot f_{cm} & \text{if } 0 \leq \varepsilon_c \leq \varepsilon_{c2} \\ f_{cm} & \text{if } \varepsilon_{c2} < \varepsilon_c \leq \varepsilon_{cu2} \end{cases}$$

Create a vector with different values of strain:

$$\varepsilon_c := 0, 0.0001.. \varepsilon_{cu2}$$

Graphic representation of the stress-strain relationship:



2.1.2.2 Determination of block factors

Area under the curve for a given value of strain:

$$\text{Area}(\varepsilon_c) := \int_0^{\varepsilon_c} \sigma_c(\varepsilon_c) d\varepsilon_c$$

Area under the curve multiplied by the distance from the origin to the center of gravity of the area:

$$A_{-\varepsilon}(\varepsilon_c) := \int_0^{\varepsilon_c} \sigma_c(\varepsilon_c) \cdot \varepsilon_c d\varepsilon_c$$

Determination of factors $\alpha_{R.S}$ and $\beta_{R.S}$

$$\alpha_{R.S}(\varepsilon_c) := \frac{\text{Area}(\varepsilon_c)}{f_{cm} \cdot \varepsilon_c} \quad \alpha_{R.S}(\varepsilon_{cu2}) = 0.81$$

$$\beta_{R.S}(\varepsilon_c) := \frac{\varepsilon_c - \frac{A_{-\varepsilon}(\varepsilon_c)}{\text{Area}(\varepsilon_c)}}{\varepsilon_c} \quad \beta_{R.S}(\varepsilon_{cu2}) = 0.416$$

2.1.3 Stress-strain Relationship of Reinforcing Steel

2.1.3.1 Mathematic formulation

Ultimate steel strain: $\varepsilon_{su} := 0.0580$

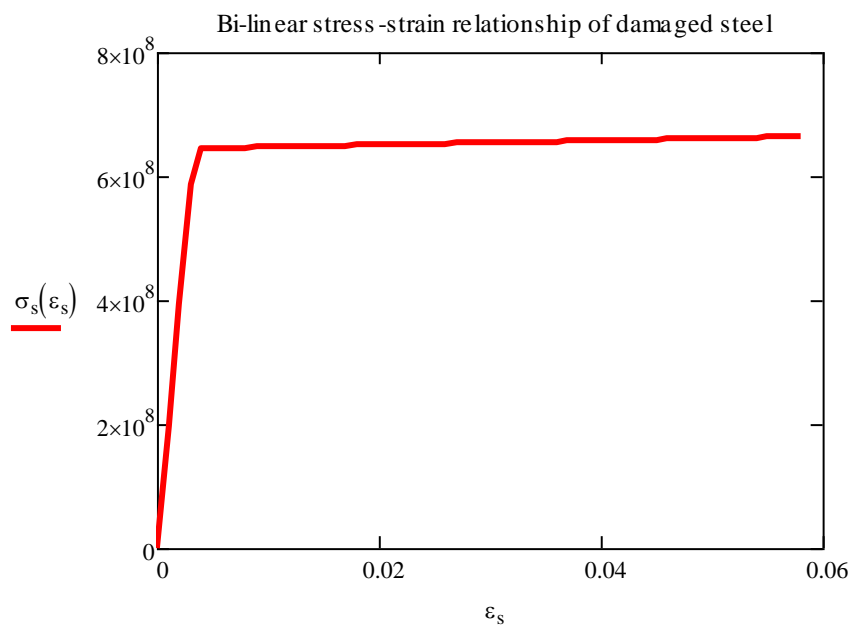
Yield strain: $\varepsilon_{sy} := \frac{f_{ym}}{E_{sm}} \quad \varepsilon_{sy} = 3.291 \times 10^{-3}$

Relationship parameters: $p_1(\varepsilon_s) := \frac{\varepsilon_s - \varepsilon_{sy}}{\varepsilon_{su} - \varepsilon_{sy}}$

Stress-strain relationship:
$$\sigma_s(\varepsilon_s) := \begin{cases} E_{sm} \cdot \varepsilon_s & \text{if } \varepsilon_s \leq \varepsilon_{sy} \\ f_{ym} + p_1(\varepsilon_s) \cdot (f_t - f_{ym}) & \text{if } \varepsilon_s > \varepsilon_{sy} \end{cases}$$

$\varepsilon_s := 0, 0.001 \dots \varepsilon_{su}$

Graphic representation of the stress-strain relationship for reinforcing steel:



2.1.4. Design Strength Values

2.1.4.1 Concrete

Partial factor:

$$\gamma_C := 1.0$$

Design compressive strength:

$$f_{cd} := \frac{f_{cm}}{\gamma_C} \quad f_{cd} = 33 \cdot \text{MPa}$$

Concrete ultimate strain:

$$\varepsilon_{cu} := 0.0035$$

Stress block factors:

$$\alpha_R := \alpha_{R.S}(\varepsilon_{cu}) = 0.81$$

$$\beta_R := \beta_{R.S}(\varepsilon_{cu2}) = 0.416$$

5%-fractile tensile strength:

$$f_{ctk0.05} := 0.7 \cdot f_{ctm} = 3.101 \cdot \text{MPa}$$

Flexural tensile strength:

$$\kappa := 0.6 + \frac{0.4}{\sqrt[4]{\frac{h}{m}}} = 1.311$$

$$f_{ct.fl} := \kappa \cdot f_{ctm} = 5.809 \cdot \text{MPa}$$

2.1.4.2 Reinforcing steel

Partial factor:

$$\gamma_S := 1.0$$

Design yield stress:

$$f_{yd} := \frac{f_{ym}}{\gamma_S} \quad f_{yd} = 645 \cdot \text{MPa}$$

2.1.5. Load Capacity in Ultimate Limit State

2.1.5.1 Analysis of field section without top reinforcement

Number of bars in the top:

$$n' := 0$$

Number of bars in the bottom:

$$n = 2$$

Assume yielding:

$$\varepsilon_{s,1} > \varepsilon_{sy}$$

$$\varepsilon_{s,1} = \frac{d - x_1}{x_1} \varepsilon_{cu}$$

Position of neutral axis:

Initial guess: $x_{u,1} := 20\text{mm}$

Calculated value: $x_{u,1} := \text{root}\left(\alpha_R \cdot f_{cd} \cdot b \cdot x_{u,1} - \sigma_s \left(\frac{d - x_{u,1}}{x_{u,1}} \varepsilon_{cu}\right) \cdot n \cdot A_{bar}, x_{u,1}\right)$
 $x_{u,1} = 13.753\text{mm}$

Check the strain in the reinforcement bars:

$$\varepsilon_{s,1} := \frac{d - x_{u,1}}{x_{u,1}} \varepsilon_{cu} = 0.017 \quad \varepsilon_{sy} = 3.291 \times 10^{-3} \quad \varepsilon_{s,1} > \varepsilon_{sy} = 1$$

Calculation of load capacity:

$$M_{u,1} := \alpha_R \cdot f_{cd} \cdot b \cdot x_{u,1} \cdot (d - \beta_R \cdot x_{u,1}) \quad M_{u,1} = 2.729\text{ kN}\cdot\text{m}$$

$$F_{u,1} := \frac{4 \cdot M_{u,1}}{L} \quad F_{u,1} = 8.397\text{ kN}$$

Calculation of stress in the steel bars:

$$\sigma_{s,1} := \sigma_s(\varepsilon_{s,1}) \quad \sigma_{s,1} = 649.712\text{ MPa}$$

Calculation of curvature at failure:

$$\varepsilon_{s,1} = 0.017 \quad \varphi_{u,1} := \frac{\varepsilon_{s,1}}{d - x_{u,1}} = 0.254\text{ m}^{-1}$$

2.1.5.2 Analysis of field section including top reinforcement

Number of bars in the top: $n' := 2$

Number of bars in the bottom: $n = 2$

Assume tension in top and bottom and that the neutral axis is located above the top reinforcement.

Strain in bottom reinforcement: $\varepsilon_{s,2} = \frac{d - x_{u,2}}{x_{u,2}} \varepsilon_{cu}$

Strain in top reinforcement: $\varepsilon'_{s,2} = \frac{d' - x_{u,2}}{x_{u,2}} \varepsilon_{cu}$

Position of neutral axis:

Initial guess: $x_{u,2} := 20\text{mm}$

Calculated value:

$$x_{u,2} := \text{root}\left(\alpha_R \cdot f_{cd} \cdot b \cdot x_{u,2} - \sigma_s \left(\frac{d' - x_{u,2}}{x_{u,2}} \varepsilon_{cu} \right) \cdot A'_s - \sigma_s \left(\frac{d - x_{u,2}}{x_{u,2}} \varepsilon_{cu} \right) \cdot A_s, x_{u,2} \right)$$

$$x_{u,2} = 16.649\text{mm}$$

Note: The neutral axis is indeed located above the top reinforcement. Top bars are subjected to tensile stress.

Check the strain in the reinforcement bars:

$$\varepsilon_{s,2} := \frac{d - x_{u,2}}{x_{u,2}} \varepsilon_{cu} = 0.013 \quad \varepsilon_{sy} = 3.291 \times 10^{-3} \quad \varepsilon_{s,2} > \varepsilon_{sy} = 1$$

$$\varepsilon'_{s,2} := \frac{d' - x_{u,2}}{x_{u,2}} \varepsilon_{cu} = 7.044 \times 10^{-4} \quad \varepsilon'_{s,2} > \varepsilon_{sy} = 0$$

Calculation of moment capacity:

$$M_{u,2} := \alpha_R \cdot f_{cd} \cdot b \cdot x_{u,2} \cdot (d - \beta_R \cdot x_{u,2}) - \sigma_s \left(\frac{d' - x_{u,2}}{x_{u,2}} \varepsilon_{cu} \right) \cdot A'_s \cdot (d - d') \quad M_{u,2} = 2.782 \cdot \text{kN} \cdot \text{m}$$

$$F_{u,2} := \frac{4 \cdot M_{u,2}}{L} \quad F_{u,2} = 8.559 \cdot \text{kN}$$

Calculation of stress in the steel bars:

$$\sigma'_{s,2} := \sigma_s(\varepsilon'_{s,2}) \quad \sigma'_{s,2} = 138.054 \text{ MPa}$$

$$\sigma_{s,2} := \sigma_s(\varepsilon_{s,2}) \quad \sigma_{s,2} = 648.482 \text{ MPa}$$

Calculation of curvature at failure:

$$\varepsilon_{s,2} = 0.013 \quad \varphi_{u,2} := \frac{\varepsilon_{s,2}}{d - x_{u,2}} = 0.21 \text{ m}^{-1}$$

2.1.6. Moment and Curvature at Onset of Yielding

2.1.6.1 Analysis of field section without top reinforcement

Yielding strain: $\varepsilon_{sy} = 3.291 \times 10^{-3}$

Definition of strain in the compressed edge:

$$\varepsilon_{cc,y,1} = \frac{x_{y,1}}{d - x_{y,1}} \cdot \varepsilon_{sy}$$

Tensile force in the bottom reinforcement:

$$F_{sy} := f_{yd} \cdot n \cdot A_{bar} = 36.474 \text{ kN}$$

Equivalent compressive force in concrete

$$F_{C,y,1} = \alpha_{R,y} \cdot f_{cd} \cdot b \cdot x_{y,1} \quad \alpha_{R,y} = \alpha_{R,S}(\varepsilon_{cc,y,1})$$

Horizontal equilibrium condition:

$$F_{sy} = F_{C,y}$$

Assume $x_{y,1} := 22.18 \text{ mm}$

Total tensile force: $F_{sy} = 36.474 \text{ kN}$

Total compressive force: $F_{C,y,1} := \alpha_{R,S} \left(\frac{x_{y,1}}{d - x_{y,1}} \cdot \varepsilon_{sy} \right) \cdot f_{cd} \cdot b \cdot x_{y,1} = 36.479 \text{ kN}$

$$\Delta F := F_{C,y,1} - F_{sy} = 5.062 \times 10^{-3} \cdot \text{kN}$$

Note: Check that $\Delta F \approx 0$

Calculation of strains

$$\varepsilon_{cc,y,1} := \frac{x_{y,1}}{d - x_{y,1}} \cdot \varepsilon_{sy} = 1.262 \times 10^{-3} \quad \varepsilon_{cc,y,1} < \varepsilon_{c2} = 1$$

Calculation of moment at yielding:

$$\alpha_{R,y} := \alpha_{R,S}(\varepsilon_{cc,y,1}) = 0.498 \quad \beta_{R,y} := \beta_{R,S}(\varepsilon_{cc,y,1}) = 0.356$$

$$M_{y,1} := \alpha_{R,y} \cdot f_{cd} \cdot b \cdot x_{y,1} \cdot (d - \beta_{R,y} \cdot x_{y,1}) \quad M_{y,1} = 2.631 \cdot \text{kN} \cdot \text{m} \quad F_{y,1} := \frac{4 \cdot M_{y,1}}{L} = 8.094 \cdot \text{kN}$$

Determination of stresses in the reinforcement bars:

$$\sigma_{s,y,1} := \sigma_s(\varepsilon_{sy}) \quad \sigma_{s,y,1} = 645 \cdot \text{MPa}$$

Curvature at yielding

$$\varepsilon_{sy} = 3.291 \times 10^{-3} \quad \phi_{y,1} := \frac{\varepsilon_{sy}}{d - x_{y,1}} = 0.057 \text{ m}^{-1}$$

2.1.6.2 Analysis of field section including top reinforcement

Assume tension in the top reinforcement bars

Yielding strain: $\varepsilon_{sy} = 3.291 \times 10^{-3}$

Definition of strain in the compressed edge and top reinforcement:

$$\varepsilon_{cc,y,2} = \frac{x_{y,2}}{d - x_{y,2}} \cdot \varepsilon_{sy} \quad \varepsilon'_{s,y,2} = \frac{x_{y,2} - d'}{d - x_{y,2}} \cdot \varepsilon_{sy}$$

Tensile force in the reinforcement:

$$\text{Top reinforcement:} \quad F'_{sy,2} = \sigma_s(\varepsilon'_{s,y,2}) \cdot A'_s$$

$$\text{Bottom reinforcement:} \quad F_{sy} := f_{yd} \cdot A_s = 36.474 \text{ kN}$$

Equivalent compressive force in concrete

$$F_{C,y,2} = \alpha_{R,y} \cdot f_{cd} \cdot b \cdot x_{y,2} \quad \alpha_{R,y} = \alpha_{R,S}(\varepsilon_{cc,y,2})$$

Horizontal equilibrium condition:

$$F_{sy} = F_{C,y,2} + F'_{sy,2}$$

Assume $x_{y,2} := 21.83 \text{ mm}$

Total tensile force: $F_{T,y,2} := F_{sy} = 36.474 \text{ kN}$

Total compressive force:

$$F_{C,y,2} := \alpha_{R,s} \left(\frac{x_{y,2}}{d - x_{y,2}} \cdot \varepsilon_{sy} \right) \cdot f_{cd} \cdot b \cdot x_{y,2} + \sigma_s \left(\frac{x_{y,2} - d'}{d - x_{y,2}} \cdot \varepsilon_{sy} \right) \cdot A'_s = 36.475 \cdot \text{kN}$$

$$\Delta F := F_{C,y,2} - F_{T,y,2} = 8.149 \times 10^{-4} \cdot \text{kN}$$

Note: Check that $\Delta F \approx 0$

Calculation of strains

$$\varepsilon_{cc,y,2} := \frac{x_{y,2}}{d - x_{y,2}} \cdot \varepsilon_{sy} = 1.235 \times 10^{-3} \quad \varepsilon_{cc,y,2} < \varepsilon_{c2} = 1$$

$$\varepsilon'_{s,y,2} := \frac{x_{y,2} - d'}{x_{y,2}} \cdot \varepsilon_{cc,y,2} = 1.035 \times 10^{-4}$$

Note: The strains are in fact negative though they are positive here to be able to use the stress-strain curve.

Calculation of moment at yielding:

$$\alpha_{R,y} := \alpha_{R,s}(\varepsilon_{cc,y,2}) = 0.49 \quad \beta_{R,y} := \beta_{R,s}(\varepsilon_{cc,y,2}) = 0.355$$

$$M_{y,2} := \alpha_{R,y} \cdot f_{cd} \cdot b \cdot x_{y,2} \cdot (d - \beta_{R,y} \cdot x_{y,2}) + \sigma_s \left(\frac{x_{y,2} - d'}{x_{y,2}} \varepsilon_{cc,y,2} \right) \cdot A'_s \cdot (d - d')$$

$$M_{y,2} = 2.621 \cdot \text{kN} \cdot \text{m} \quad F_{y,2} := \frac{4 \cdot M_{y,2}}{L} = 8.066 \cdot \text{kN}$$

Determination of stresses in the reinforcement bars:

$$\text{Top reinforcement:} \quad \sigma'_{s,y,2} := -\sigma_s(\varepsilon'_{s,y,2}) \quad \sigma'_{s,y,2} = -20.291 \cdot \text{MPa}$$

$$\text{Bottom reinforcement:} \quad \sigma_{s,y,2} := \sigma_s(\varepsilon_{sy}) \quad \sigma_{s,y,2} = 645 \cdot \text{MPa}$$

Curvature at yielding

$$\varepsilon_{sy} = 3.291 \times 10^{-3} \quad \varphi_{y,2} := \frac{\varepsilon_{sy}}{d - x_{y,2}} = 0.057 \text{ m}^{-1}$$

2.1.8. Summary

2.1.8.1 Moment and curvature at yielding without consideration of top reinforcement

$$M_{y,1} = 2.631 \cdot \text{kN} \cdot \text{m} \quad x_{y,1} = 22.18 \cdot \text{mm}$$

$$F_{y,1} = 8.094 \cdot \text{kN} \quad \varphi_{y,1} = 0.057 \text{ m}^{-1}$$

2.1.8.2 Moment and curvature at yielding consider ring both top and bottom reinforcement

$$M_{y,2} = 2.621 \cdot \text{kN} \cdot \text{m} \quad x_{y,2} = 21.83 \cdot \text{mm}$$

$$F_{y,2} = 8.066 \cdot \text{kN} \quad \varphi_{y,2} = 0.057 \text{ m}^{-1}$$

2.1.8.3 Load Capacity at Ultimate State without consideration of top reinforcement

$$M_{u,1} = 2.729 \cdot \text{kN} \cdot \text{m} \quad x_{u,1} = 13.753 \cdot \text{mm}$$

$$F_{u,1} = 8.397 \cdot \text{kN} \quad \varphi_{u,1} = 0.254 \text{ m}^{-1}$$

2.1.8.4 Load Capacity at Ultimate State considering both top and bottom reinforcement

$$M_{u,2} = 2.782 \cdot \text{kN} \cdot \text{m} \quad x_{u,2} = 16.649 \cdot \text{mm}$$

$$F_{u,2} = 8.559 \cdot \text{kN} \quad \varphi_{u,2} = 0.21 \text{ m}^{-1}$$

Increase in load capacity if top reinforcement is considered:

$$\frac{F_{u,2} - F_{u,1}}{F_{u,1}} = 1.932 \cdot \%$$

2.2 Theoretical Load vs Deformation Relationship

2.2.1. Determination of Cracking Moment and Cracking Curvature:

Modular ratio:
$$\alpha_s := \frac{E_{sm}}{E_{cm}} = 6.222$$

Moment of inertia in State I:
$$I_I := \frac{b \cdot h^3}{12} + (\alpha_s - 1) 2n \cdot A_{bar} \cdot \left(d - \frac{h}{2}\right)^2 = 8.865 \times 10^6 \cdot \text{mm}^4$$

Cracking stress:
$$f_{ct,fl} = \frac{M_{cr} \cdot \left(\frac{h}{2}\right)}{I_I}$$

Cracking moment:
$$M_{cr} := \frac{f_{ct,fl} \cdot I_I}{\frac{h}{2}} = 1.03 \cdot \text{kN} \cdot \text{m}$$

Cracking force:
$$F_{cr} := \frac{4 \cdot M_{cr}}{L} = 3.169 \cdot \text{kN}$$

2.2.2. Determination of Moment of Inertia in State II

Calculation of position of neutral axis:

Number of bars in the top: $n' = 2$

Number of bars in the bottom: $n = 2$

Consider first moment of area around the neutral axis:

$$\frac{b \cdot x_{II}^2}{2} + (\alpha_s - 1) \cdot A'_s \cdot (x_{II} - d') = \alpha_s \cdot A_s \cdot (d - x_{II})$$

Initial guess:

$$x_{II} := 50 \text{ mm}$$

Calculated value:

$$x_{II} := \text{root} \left[\frac{b \cdot x_{II}^2}{2} - (\alpha_s) \cdot A'_s \cdot (d' - x_{II}) - \alpha_s \cdot A_s \cdot (d - x_{II}), x_{II} \right]$$

$$x_{II} = 20.408 \text{ mm}$$

Moment of inertia:

$$I_{II} := \frac{b \cdot x_{II}^3}{3} + (\alpha_s) \cdot A'_s \cdot (d' - x_{II})^2 + \alpha_s \cdot A_s \cdot (d - x_{II})^2$$

$$I_{II} = 1.533 \times 10^{-6} \text{ m}^4$$

2.2.3. Load-Deformation plot

2.2.3.1 Determination of equivalent stiffness

Stiffness in State I: $K_I := \frac{48 \cdot E_{cm} \cdot I_I}{L^3} = 6.101 \cdot \frac{\text{kN}}{\text{mm}}$

Stiffness in State II: $K_{II} := \frac{48 \cdot E_{cm} \cdot I_{II}}{L^3} = 1.055 \cdot \frac{\text{kN}}{\text{mm}}$

2.2.3.2 Deformation considering only State II until ultimate load

Peak load: $F_{u,2} = 8.559 \cdot \text{kN}$

Deflection at peak load: $u_{II} := \frac{F_{u,2}}{K_{II}} = 8.113 \cdot \text{mm}$

Load as a function of displacement: $\text{Force}_2(u) := \begin{cases} u \cdot K_{II} & \text{if } u < u_{II} \\ F_{u,2} & \text{if } u > u_{II} \end{cases}$

2.2.3.3 Deformation considering State I and State II

Cracking load: $F_{cr} = 3.169 \cdot \text{kN}$

Deflection when cracking occurs: $u_{cr} := \frac{F_{cr}}{K_I} = 0.519 \cdot \text{mm}$

Peak load: $F_{u,2} = 8.559 \cdot \text{kN}$

Deflection at peak load: $u_{II} = 8.113 \cdot \text{mm}$

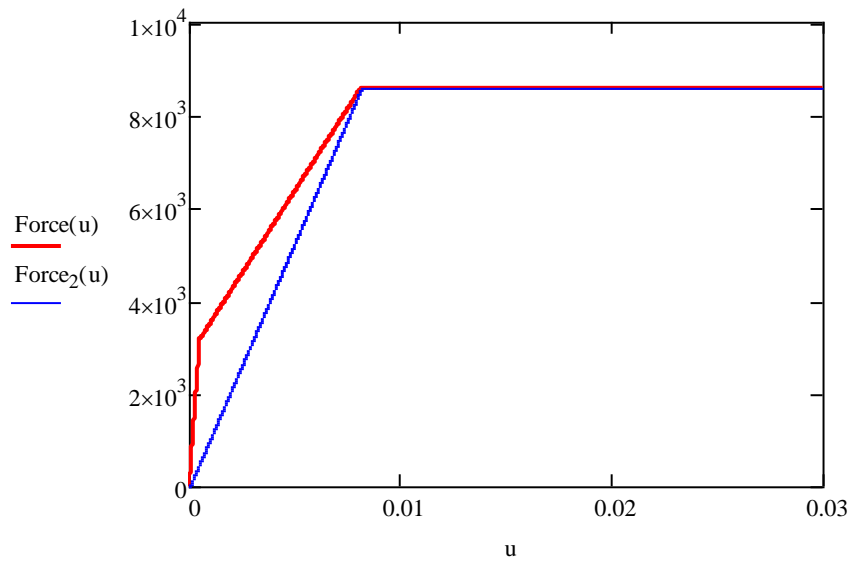
Stiffness between cracking and yielding: $K_{cy} := \frac{F_{u,2} - F_{cr}}{u_{II} - u_{cr}} = 0.71 \cdot \frac{\text{kN}}{\text{mm}}$

Load as a function of displacement:

$$\text{Force}(u) := \begin{cases} (K_I \cdot u) & \text{if } u \leq u_{cr} \\ [F_{cr} + (u - u_{cr}) \cdot K_{cy}] & \text{if } u > u_{cr} \\ F_{u,2} & \text{if } u > u_{II} \end{cases}$$

$$u := 0\text{mm}, 0.01\text{mm}.. 30\text{mm}$$

2.2.3.4 Load-deformation curves



2.3 Prediction of Plastic Rotational Capacity

2.3.1 Input Data

2.3.1.1 Geometry

Beam height:	$h = 0.1 \text{ m}$
Beam width:	$b = 0.1 \text{ m}$
Effective span length:	$L = 1.3 \text{ m}$
Distance to critical section from support:	$l_0 := \frac{L}{2} = 650 \text{ mm}$
Effective height:	$d = 0.08 \text{ m}$

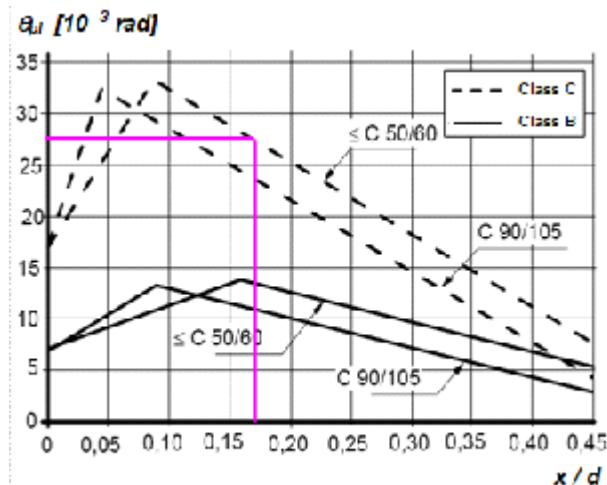
2.3.2. Rotation Capacity According to Eurocode 2

Determine allowable rotation for reference beam ($\eta = 3$):

$$x_u := x_{u,1} = 13.753 \text{ mm} \quad \textbf{Note:} \text{ Position of neutral axis considering only bottom reinforcement.}$$

$$\frac{x_u}{d} = 0.172$$

Reinforcement class C



Rotation capacity from the chart:

$$\Theta_{\text{total.Eur.R.C}} := 0.027$$

Correction for different values of shear slenderness:

$$\lambda_C := \frac{l_0}{d} = 8.125 \quad \kappa_{\lambda_C} := \sqrt{\frac{\lambda_C}{3}} = 1.646$$

$$\Theta_{\text{total.Eur.C}} := \kappa_{\lambda C} \cdot \Theta_{\text{total.Eur.R.C}} = 0.044$$

Consider:

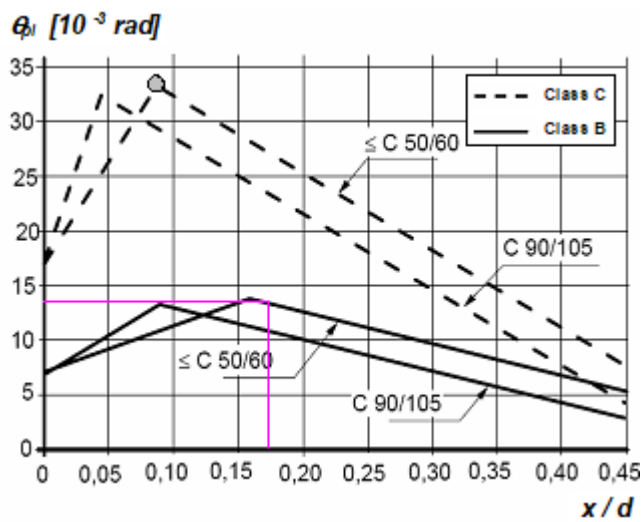
$$\Theta_{\text{total.Eur.C}} = 2 \cdot \theta_{\text{pl.Eur.C}}$$

Rotational capacity according to Eurocode 2:

$$\theta_{\text{pl.Eur.C}} := \frac{\Theta_{\text{total.Eur.C}}}{2} = 0.0222$$

$$u_{\text{pl.Eur.C}} := \frac{\theta_{\text{pl.Eur.C}} \cdot L}{2} = 14.441 \cdot \text{mm}$$

Reinforcement class B



Rotation capacity from the chart:

$$\Theta_{\text{total.Eur.R.B}} := 0.0135$$

Correction for different values of shear slenderness:

$$\lambda_B := \frac{l_0}{d} = 8.125 \quad \kappa_{\lambda B} := \sqrt{\frac{\lambda_B}{3}} = 1.646$$

$$\Theta_{\text{total.Eur.B}} := \kappa_{\lambda B} \cdot \Theta_{\text{total.Eur.R.B}} = 0.022$$

Consider:

$$\Theta_{\text{total.Eur.B}} = 2 \cdot \theta_{\text{pl.Eur.B}}$$

Rotational capacity according to Eurocode 2:

$$\theta_{\text{pl.Eur.B}} := \frac{\Theta_{\text{total.Eur.B}}}{2} = 0.0111$$

$$u_{\text{pl.Eur.B}} := \frac{\theta_{\text{pl.Eur.B}} \cdot L}{2} = 7.221 \cdot \text{mm}$$

2.3.3 Rotation Capacity According to Bk 25

Empirical expression:

$$l_{\text{p.Bk25}} = 0.5 \cdot d + 0.15L \quad \text{Plastic hinge on the field}$$

Plastic hinge length:

$$l_{\text{p.Bk25}} := 0.5 \cdot d + 0.15L = 235 \cdot \text{mm}$$

Area of tensile reinforcement:

$$A_s = 56.549 \cdot \text{mm}^2$$

$$\omega_s := \frac{A_s}{b \cdot d} \cdot \frac{f_{ym}}{f_{cm}} = 0.138$$

Since no stirrups were included, the contribution of the top bars can be disregarded

Area of compression reinforcement:

$$A_c := 0 \quad \textbf{Note:} \text{ the top reinforcement has been proved to be subjected to tensile stress.}$$

$$\omega'_s := \frac{A_c}{b \cdot d} \cdot \frac{f_{ym}}{f_{cm}} = 0$$

Dominant failure mode:

$$\omega_{s,\text{crit}} := \frac{0.8 \cdot \epsilon_{cu}}{\epsilon_{cu} + \epsilon_{su}} = 0.046 \quad \omega_s = 0.138$$

$$\omega_s > \omega_{s,\text{crit}} = 1$$

Note: The dominant failure mode is concrete crushing

Determination of plastic rotation capacity:

$$\theta_{\text{pl.Bk25}} := \frac{0.4 \cdot \epsilon_{cu}}{\omega_s} \left(1 + 0.3 \cdot \frac{L}{d} \right) = 0.0595$$

$$u_{\text{pl.Bk25}} := \frac{\theta_{\text{pl.Bk25}} \cdot L}{2} = 38.696 \cdot \text{mm}$$

2.3.4. Summary

Eurocode 2:

$$\theta_{pl.Eur.C} = \cdot \text{rad}$$

$$\theta_{pl.Eur.B} = \cdot \text{rad}$$

Bk25 method:

$$\theta_{pl.Bk25} = \cdot \text{rad}$$

3 Four point bending and undamaged reinforcement

3.1 Load Capacity of Reinforced Concrete Beam

The load capacity of a reinforced concrete beam is determined for a given cross section.

$$\text{kN} := \text{N} \cdot 10^3 \quad \text{MPa} := \text{Pa} \cdot 10^6$$

3.1.1 Input Data

3.1.1.1 Geometry

Beam height:

$$h := 0.1\text{m}$$

Beam width:

$$b := 0.1\text{m}$$

Effective span length:

$$L := 1.3\text{m}$$

Distance to load application from support:

$$L_F := 0.5\text{m}$$

Nominal bar diameter:

$$\Phi := 6\text{mm}$$

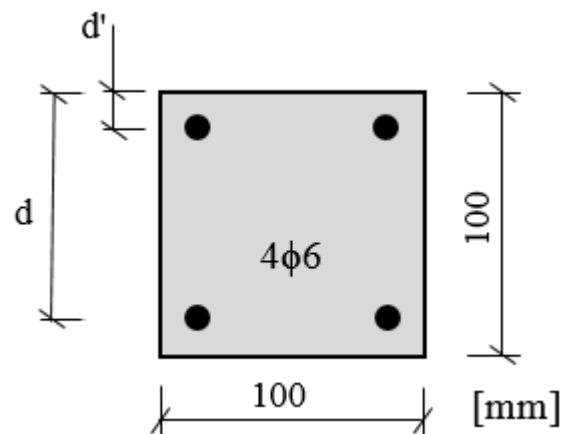
Area of reinforcement bar:

$$A_{\text{bar}} := \pi \cdot \frac{\Phi^2}{4} = 28.274 \cdot \text{mm}^2$$

Stirrup dimension:

$$\Phi_s := 0\text{mm}$$

Note: No stirrups



Number of bars in the top:

$$n' := 2$$

Number of bars in the bottom:

$$n := 2$$

Area of top reinforcement:

$$A_s := n \cdot A_{\text{bar}} = 56.549 \cdot \text{mm}^2$$

Area of bottom reinforcement:

$$A'_s := n' \cdot A_{\text{bar}} = 56.549 \cdot \text{mm}^2$$

Concrete cover:

$$c := 0.02\text{m} - \frac{\Phi}{2} = 0.017\text{m}$$

Distance from top edge to bottom reinforcement:

$$d := h - \left(\frac{\Phi}{2} + c \right) = 80\cdot\text{mm}$$

Distance from top edge to top reinforcement:

$$d' := \frac{\Phi}{2} + c = 20\cdot\text{mm}$$

3.1.1.2 Material properties

Concrete:

Mean compressive strength:

$$f_{cm} := 33.0\text{MPa}$$

Mean tensile strength

$$f_{ctm} := 4.43\cdot\text{MPa}$$

Mean modulus of elasticity

$$E_{cm} := 31.5\text{GPa}$$

Reinforcing steel:

Mean yield strength:

$$f_{ym} := 555\text{MPa}$$

Ultimate tensile stress:

$$f_t := 656\text{MPa}$$

Mean modulus of elasticity:

$$E_{sm} := 202\cdot\text{GPa}$$

3.1.2. Stress-strain Relationship of Concrete

3.1.2.1 Mathematic formulation

The parabola-rectangle stress-strain diagram for concrete under compression (according to EN 1992-1-1) is adopted.

Parameters for all concrete classes:

Concrete strain at maximum strength:

$$\varepsilon_{c2} := 2 \cdot 10^{-3}$$

Ultimate concrete strain:

$$\varepsilon_{cu2} := 3.5 \cdot 10^{-3}$$

Exponent:

$$n := 2$$

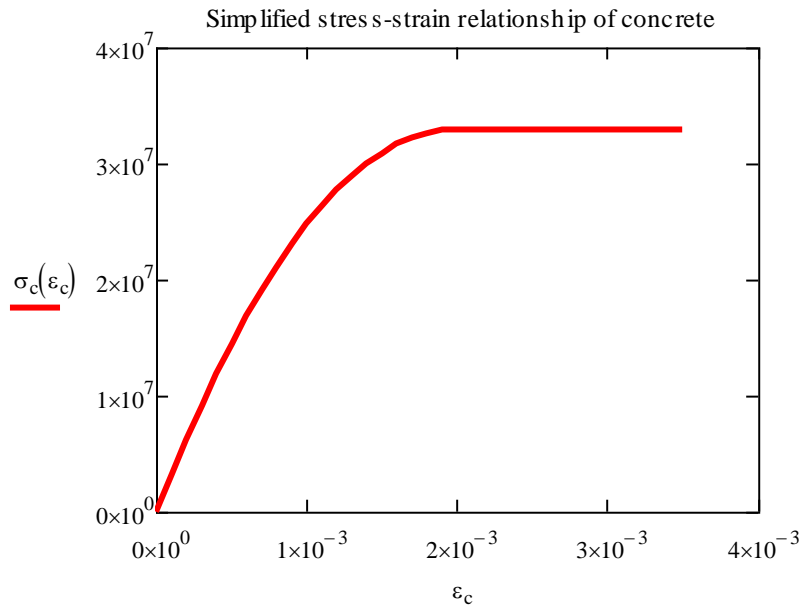
Stress-strain relationship:

$$\sigma_c(\varepsilon_c) := \begin{cases} \left[1 - \left(1 - \frac{\varepsilon_c}{\varepsilon_{c2}} \right)^n \right] \cdot f_{cm} & \text{if } 0 \leq \varepsilon_c \leq \varepsilon_{c2} \\ f_{cm} & \text{if } \varepsilon_{c2} < \varepsilon_c \leq \varepsilon_{cu2} \end{cases}$$

Create a vector with different values of strain:

$$\varepsilon_c := 0.0001, \varepsilon_{c2}, \varepsilon_{cu2}$$

Graphic representation of the stress-strain relationship:



3.1.2.2 Determination of block factors

Area under the curve for a given value of strain:

$$\text{Area}(\epsilon_c) := \int_0^{\epsilon_c} \sigma_c(\epsilon_c) d\epsilon_c$$

Area under the curve multiplied by the distance from the origin to the center of gravity of the area:

$$A_{-\epsilon}(\epsilon_c) := \int_0^{\epsilon_c} \sigma_c(\epsilon_c) \cdot \epsilon_c d\epsilon_c$$

Determination of factors $\alpha_{R.S}$ and $\beta_{R.S}$

$$\alpha_{R.S}(\epsilon_c) := \frac{\text{Area}(\epsilon_c)}{f_{cm} \cdot \epsilon_c} \quad \alpha_{R.S}(\epsilon_{cu2}) = 0.81$$

$$\beta_{R.S}(\epsilon_c) := \frac{\epsilon_c - \frac{A_{-\epsilon}(\epsilon_c)}{\text{Area}(\epsilon_c)}}{\epsilon_c} \quad \beta_{R.S}(\epsilon_{cu2}) = 0.416$$

3.1.3 Stress-strain Relationship of Reinforcing Steel

3.1.3.1 Mathematic formulation

Ultimate steel strain: $\varepsilon_{su} := 0.0938$

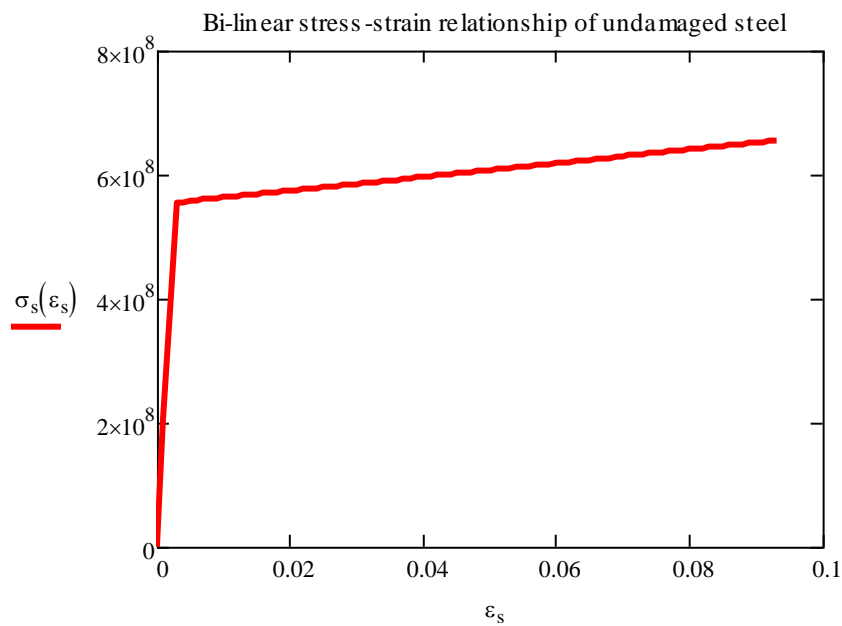
Yield strain: $\varepsilon_{sy} := \frac{f_{ym}}{E_{sm}} \quad \varepsilon_{sy} = 2.748 \times 10^{-3}$

Relationship parameters: $p_1(\varepsilon_s) := \frac{\varepsilon_s - \varepsilon_{sy}}{\varepsilon_{su} - \varepsilon_{sy}}$

Stress-strain relationship:
$$\sigma_s(\varepsilon_s) := \begin{cases} E_{sm} \cdot \varepsilon_s & \text{if } \varepsilon_s \leq \varepsilon_{sy} \\ f_{ym} + p_1(\varepsilon_s) \cdot (f_t - f_{ym}) & \text{if } \varepsilon_s > \varepsilon_{sy} \end{cases}$$

$\varepsilon_s := 0, 0.001 \dots \varepsilon_{su}$

Graphic representation of the stress-strain relationship for reinforcing steel:



3.1.4. Design Strength Values

3.1.4.1 Concrete

Partial factor:

$$\gamma_C := 1.0$$

Design compressive strength:

$$f_{cd} := \frac{f_{cm}}{\gamma_C} \quad f_{cd} = 33 \cdot \text{MPa}$$

Concrete ultimate strain:

$$\varepsilon_{cu} := 0.0035$$

Stress block factors:

$$\alpha_R := \alpha_{R.S}(\varepsilon_{cu}) = 0.81$$

$$\beta_R := \beta_{R.S}(\varepsilon_{cu2}) = 0.416$$

5%-fractile tensile strength:

$$f_{ctk0.05} := 0.7 \cdot f_{ctm} = 3.101 \cdot \text{MPa}$$

Flexural tensile strength:

$$\kappa := 0.6 + \frac{0.4}{\sqrt[4]{\frac{h}{m}}} = 1.311$$

$$f_{ct.fl} := \kappa \cdot f_{ctm} = 5.809 \cdot \text{MPa}$$

3.1.4.2 Reinforcing steel

Partial factor:

$$\gamma_S := 1.0$$

Design yield stress:

$$f_{yd} := \frac{f_{ym}}{\gamma_S} \quad f_{yd} = 555 \cdot \text{MPa}$$

3.1.5 Load Capacity in Ultimate Limit State

3.1.5.1 Analysis of field section without top reinforcement

Number of bars in the top:

$$n' := 0$$

Number of bars in the bottom:

$$n = 2$$

Assume yielding:

$$\varepsilon_{s.1} > \varepsilon_{sy}$$

$$\varepsilon_{s.1} = \frac{d - x_l}{x_l} \varepsilon_{cu}$$

Position of neutral axis:

Initial guess:

$$x_{u,1} := 20\text{mm}$$

Calculated value:

$$x_{u,1} := \text{root}\left(\alpha_R \cdot f_{cd} \cdot b \cdot x_{u,1} - \sigma_s \left(\frac{d - x_{u,1}}{x_{u,1}} \varepsilon_{cu}\right) \cdot n \cdot A_{bar}, x_{u,1}\right)$$

$$x_{u,1} = 12.143\text{mm}$$

Check the strain in the reinforcement bars:

$$\varepsilon_{s,1} := \frac{d - x_{u,1}}{x_{u,1}} \varepsilon_{cu} = 0.02$$

$$\varepsilon_{sy} = 2.748 \times 10^{-3}$$

$$\varepsilon_{s,1} > \varepsilon_{sy} = 1$$

Calculation of load capacity:

$$M_{u,1} := \alpha_R \cdot f_{cd} \cdot b \cdot x_{u,1} \cdot (d - \beta_R \cdot x_{u,1})$$

$$M_{u,1} = 2.431 \cdot \text{kN} \cdot \text{m}$$

$$F_{u,1} := \frac{M_{u,1}}{L_F}$$

$$F_{u,1} = 4.863 \cdot \text{kN}$$

$$F_{u,1,tot} := 2 \cdot F_{u,1} = 9.725 \cdot \text{kN}$$

Calculation of stress in the steel bars:

$$\sigma_{s,1} := \sigma_s(\varepsilon_{s,1})$$

$$\sigma_{s,1} = 573.648 \text{MPa}$$

Calculation of curvature at failure:

$$\varepsilon_{s,1} = 0.02$$

$$\varphi_{u,1} := \frac{\varepsilon_{s,1}}{d - x_{u,1}} = 0.288 \text{m}^{-1}$$

3.1.5.2 Analysis of field section including top reinforcement

Number of bars in the top:

$$n' := 2$$

Number of bars in the bottom:

$$n = 2$$

Assume tension in top and bottom and that the neutral axis is located above the top reinforcement.

Strain in bottom reinforcement:

$$\varepsilon_{s,2} = \frac{d - x_{u,2}}{x_{u,2}} \varepsilon_{cu}$$

Strain in top reinforcement:

$$\varepsilon'_{s,2} = \frac{d' - x_{u,2}}{x_{u,2}} \varepsilon_{cu}$$

Position of neutral axis:

Initial guess: $x_{u,2} := 20\text{mm}$

Calculated value:

$$x_{u,2} := \text{root}\left(\alpha_R \cdot f_{cd} \cdot b \cdot x_{u,2} - \sigma_s \left(\frac{d' - x_{u,2}}{x_{u,2}} \varepsilon_{cu}\right) \cdot A'_s - \sigma_s \left(\frac{d - x_{u,2}}{x_{u,2}} \varepsilon_{cu}\right) \cdot A_s, x_{u,2}\right)$$

$$x_{u,2} = 15.888\text{ mm}$$

Note: The neutral axis is indeed located above the top reinforcement. Top bars are subjected to tensile stress.

Check the strain in the reinforcement bars:

$$\varepsilon_{s,2} := \frac{d - x_{u,2}}{x_{u,2}} \varepsilon_{cu} = 0.014$$

$$\varepsilon_{sy} = 2.748 \times 10^{-3}$$

$$\varepsilon_{s,2} > \varepsilon_{sy} = 1$$

$$\varepsilon'_{s,2} := \frac{d' - x_{u,2}}{x_{u,2}} \varepsilon_{cu} = 9.058 \times 10^{-4}$$

$$\varepsilon'_{s,2} > \varepsilon_{sy} = 0$$

Calculation of moment capacity:

$$M_{u,2} := \alpha_R \cdot f_{cd} \cdot b \cdot x_{u,2} \cdot (d - \beta_R \cdot x_{u,2}) - \sigma_s \left(\frac{d' - x_{u,2}}{x_{u,2}} \varepsilon_{cu}\right) \cdot A'_s \cdot (d - d')$$

$$M_{u,2} = 2.494 \cdot \text{kN} \cdot \text{m}$$

$$F_{u,2} := \frac{M_{u,2}}{L_F}$$

$$F_{u,2} = 4.989 \cdot \text{kN}$$

$$F_{u,2,\text{tot}} := 2 \cdot F_{u,2} = 9.977 \cdot \text{kN}$$

Calculation of stress in the steel bars:

$$\sigma'_{s,2} := \sigma_s(\varepsilon'_{s,2})$$

$$\sigma'_{s,2} = 182.963 \cdot \text{MPa}$$

$$\sigma_{s,2} := \sigma_s(\varepsilon_{s,2})$$

$$\sigma_{s,2} = 567.618 \cdot \text{MPa}$$

Calculation of curvature at failure:

$$\varepsilon_{s,2} = 0.014$$

$$\varphi_{u,2} := \frac{\varepsilon_{s,2}}{d - x_{u,2}} = 0.22 \text{ m}^{-1}$$

3.1.6. Moment and Curvature at Onset of Yielding

3.1.6.1 Analysis of field section without top reinforcement

Yielding strain: $\varepsilon_{sy} = 2.748 \times 10^{-3}$

Definition of strain in the compressed edge:

$$\varepsilon_{cc,y,1} = \frac{x_{y,1}}{d - x_{y,1}} \cdot \varepsilon_{sy}$$

Tensile force in the bottom reinforcement:

$$F_{sy} := f_{yd} \cdot n \cdot A_{bar} = 31.385 \text{ kN}$$

Equivalent compressive force in concrete

$$F_{C,y,1} = \alpha_{R,y} \cdot f_{cd} \cdot b \cdot x_{y,1} \quad \alpha_{R,y} = \alpha_{R,S}(\varepsilon_{cc,y,1})$$

Horizontal equilibrium condition:

$$F_{sy} = F_{C,y}$$

Assume $x_{y,1} := 22.042 \text{ mm}$

Total tensile force: $F_{sy} = 31.385 \text{ kN}$

Total compressive force: $F_{C,y,1} := \alpha_{R,S} \left(\frac{x_{y,1}}{d - x_{y,1}} \cdot \varepsilon_{sy} \right) \cdot f_{cd} \cdot b \cdot x_{y,1} = 31.384 \text{ kN}$

$$\Delta F := F_{C,y,1} - F_{sy} = -7.021 \times 10^{-5} \text{ kN}$$

Note: Check that $\Delta F \approx 0$

Calculation of strains

$$\varepsilon_{cc,y,1} := \frac{x_{y,1}}{d - x_{y,1}} \cdot \varepsilon_{sy} = 1.045 \times 10^{-3} \quad \varepsilon_{cc,y,1} < \varepsilon_{c2} = 1$$

Calculation of moment at yielding:

$$\alpha_{R,y} := \alpha_{R,S}(\varepsilon_{cc,y,1}) = 0.431 \quad \beta_{R,y} := \beta_{R,S}(\varepsilon_{cc,y,1}) = 0.351$$

$$M_{y,1} := \alpha_{R,y} \cdot f_{cd} \cdot b \cdot x_{y,1} \cdot (d - \beta_{R,y} \cdot x_{y,1}) \quad M_{y,1} = 2.268 \text{ kN} \cdot \text{m} \quad F_{y,1} := \frac{M_{y,1}}{L_F} = 4.536 \text{ kN}$$

$$F_{v,1 \text{ tot}} := 2 \cdot F_{v,1} = 9.072 \text{ kN}$$

Determination of stresses in the reinforcement bars:

$$\sigma_{s,y,1} := \sigma_s(\varepsilon_{sy}) \quad \sigma_{s,y,1} = 555 \cdot \text{MPa}$$

Curvature at yielding

$$\varepsilon_{sy} = 2.748 \times 10^{-3} \quad \varphi_{y,1} := \frac{\varepsilon_{sy}}{d - x_{y,1}} = 0.047 \text{ m}^{-1}$$

3.1.6.2 Analysis of field section including top reinforcement

Assume tension in the top reinforcement bars

Yielding strain: $\varepsilon_{sy} = 2.748 \times 10^{-3}$

Definition of strain in the compressed edge and top reinforcement:

$$\varepsilon_{cc,y,2} = \frac{x_{y,2}}{d - x_{y,2}} \cdot \varepsilon_{sy} \quad \varepsilon'_{s,y,2} = \frac{x_{y,2} - d'}{d - x_{y,2}} \cdot \varepsilon_{sy}$$

Tensile force in the reinforcement:

$$\text{Top reinforcement:} \quad F'_{sy,2} = \sigma_s(\varepsilon'_{s,y,2}) \cdot A'_s$$

$$\text{Bottom reinforcement:} \quad F_{sy} := f_{yd} \cdot A_s = 31.385 \text{ kN}$$

Equivalent compressive force in concrete

$$F_{C,y,2} = \alpha_{R,y} \cdot f_{cd} \cdot b \cdot x_{y,2} \quad \alpha_{R,y} = \alpha_{R,S}(\varepsilon_{cc,y,2})$$

Horizontal equilibrium condition:

$$F_{sy} = F_{C,y,2} + F'_{sy,2}$$

Assume $x_{y,2} := 21.725 \text{ mm}$

Total tensile force: $F_{T,y,2} := F_{sy} = 31.385 \text{ kN}$

$$\text{Total compressive force:} \quad F_{C,y,2} := \alpha_{R,S} \left(\frac{x_{y,2}}{d - x_{y,2}} \cdot \varepsilon_{sy} \right) \cdot f_{cd} \cdot b \cdot x_{y,2} + \sigma_s \left(\frac{x_{y,2} - d'}{d - x_{y,2}} \cdot \varepsilon_{sy} \right) \cdot A'_s = 31.378 \text{ kN}$$

$$\Delta F := F_{C,y,2} - F_{T,y,2} = -6.889 \times 10^{-3} \cdot \text{kN}$$

Note: Check that $\Delta F \approx 0$

Calculation of strains

$$\varepsilon_{cc,y,2} := \frac{x_{y,2}}{d - x_{y,2}} \cdot \varepsilon_{sy} = 1.024 \times 10^{-3}$$

$$\varepsilon_{cc,y,2} < \varepsilon_{c2} = 1$$

$$\varepsilon'_{s,y,2} := \frac{x_{y,2} - d'}{x_{y,2}} \cdot \varepsilon_{cc,y,2} = 8.133 \times 10^{-5}$$

Note: The strains are in fact negative though they are positive here to be able to use the stress-strain curve.

Calculation of moment at yielding:

$$\alpha_{R,y} := \alpha_{R,s}(\varepsilon_{cc,y,2}) = 0.425 \quad \beta_{R,y} := \beta_{R,s}(\varepsilon_{cc,y,2}) = 0.35$$

$$M_{y,2} := \alpha_{R,y} \cdot f_{cd} \cdot b \cdot x_{y,2} \cdot (d - \beta_{R,y} \cdot x_{y,2}) + \sigma_s \left(\frac{x_{y,2} - d'}{x_{y,2}} \varepsilon_{cc,y,2} \right) \cdot A'_s \cdot (d - d')$$

$$M_{y,2} = 2.26 \cdot \text{kN} \cdot \text{m} \quad F_{y,2} := \frac{M_{y,2}}{L_F} = 4.52 \cdot \text{kN}$$

$$F_{y,2,tot} := 2 \cdot F_{y,2} = 9.039 \cdot \text{kN}$$

Determination of stresses in the reinforcement bars:

$$\text{Top reinforcement:} \quad \sigma'_{s,y,2} := -\sigma_s(\varepsilon'_{s,y,2}) \quad \sigma'_{s,y,2} = -16.429 \cdot \text{MPa}$$

$$\text{Bottom reinforcement:} \quad \sigma_{s,y,2} := \sigma_s(\varepsilon_{sy}) \quad \sigma_{s,y,2} = 555 \cdot \text{MPa}$$

Curvature at yielding

$$\varepsilon_{sy} = 2.748 \times 10^{-3} \quad \varphi_{y,2} := \frac{\varepsilon_{sy}}{d - x_{y,2}} = 0.047 \text{ m}^{-1}$$

3.1.8. Summary

3.1.8.1 Moment and curvature at yielding without consideration of top reinforcement

$$M_{y,1} = 2.268 \cdot \text{kN} \cdot \text{m} \quad x_{y,1} = 22.042 \cdot \text{mm}$$

$$F_{y,1,tot} = 9.072 \cdot \text{kN} \quad \varphi_{y,1} = 0.047 \text{ m}^{-1}$$

3.1.8.2 Moment and curvature at yielding considering both top and bottom reinforcement

$$M_{y,2} = 2.26 \cdot \text{kN} \cdot \text{m} \quad x_{y,2} = 21.725 \cdot \text{mm}$$

$$F_{y,2,tot} = 9.039 \cdot \text{kN} \quad \varphi_{y,2} = 0.047 \text{ m}^{-1}$$

3.1.8.3 Load Capacity at Ultimate State without consideration of top reinforcement

$$M_{u,1} = 2.431 \cdot \text{kN} \cdot \text{m}$$

$$x_{u,1} = 12.143 \cdot \text{mm}$$

$$F_{u,1,\text{tot}} = 9.725 \cdot \text{kN}$$

$$\varphi_{u,1} = 0.288 \text{ m}^{-1}$$

3.1.8.4 Load Capacity at Ultimate State considering both top and bottom reinforcement

$$M_{u,2} = 2.494 \cdot \text{kN} \cdot \text{m}$$

$$x_{u,2} = 15.888 \cdot \text{mm}$$

$$F_{u,2,\text{tot}} = 9.977 \cdot \text{kN}$$

$$\varphi_{u,2} = 0.22 \text{ m}^{-1}$$

Increase in load capacity if top reinforcement is considered:

$$\frac{F_{u,2,\text{tot}} - F_{u,1,\text{tot}}}{F_{u,1,\text{tot}}} = 2.591 \cdot \%$$

3.2 Theoretical Load vs Deformation Relationship

3.2.1. Determination of Cracking Moment and Cracking Curvature:

Modular ratio:
$$\alpha_s := \frac{E_{sm}}{E_{cm}} = 6.413$$

Moment of inertia in State I:
$$I_I := \frac{b \cdot h^3}{12} + (\alpha_s - 1) 2n \cdot A_{bar} \cdot \left(d - \frac{h}{2}\right)^2 = 8.884 \times 10^6 \cdot \text{mm}^4$$

Cracking stress:
$$f_{ct,fl} = \frac{M_{cr} \cdot \left(\frac{h}{2}\right)}{I_I}$$

Cracking moment:
$$M_{cr} := \frac{f_{ct,fl} \cdot I_I}{\frac{h}{2}} = 1.032 \cdot \text{kN} \cdot \text{m}$$

Cracking force:
$$F_{cr} := \frac{M_{cr}}{L_F} = 2.064 \cdot \text{kN} \quad F_{cr,tot} := 2 \cdot F_{cr} = 4.129 \cdot \text{kN}$$

3.2.2. Determination of Moment of Inertia in State II

Calculation of position of neutral axis:

Number of bars in the top: $n' = 2$

Number of bars in the bottom: $n = 2$

Consider first moment of area around the neutral axis:

$$\frac{b \cdot x_{II}^2}{2} + (\alpha_s - 1) \cdot A'_s \cdot (x_{II} - d') = \alpha_s \cdot A_s \cdot (d - x_{II})$$

Initial guess:

$$x_{II} := 50 \text{ mm}$$

Calculated value:

$$x_{II} := \text{root} \left[\frac{b \cdot x_{II}^2}{2} - (\alpha_s) \cdot A'_s \cdot (d' - x_{II}) - \alpha_s \cdot A_s \cdot (d - x_{II}), x_{II} \right]$$

$$x_{II} = 20.638 \text{ mm}$$

Moment of inertia:

$$I_{II} := \frac{b \cdot x_{II}^3}{3} + (\alpha_s) \cdot A'_s \cdot (d' - x_{II})^2 + \alpha_s \cdot A_s \cdot (d - x_{II})^2$$

$$I_{II} = 1.571 \times 10^{-6} \text{ m}^4$$

3.2.3. Load-Deformation plot

3.2.3.1 Determination of equivalent stiffness

Stiffness in State I:

$$K_I := \frac{48 \cdot E_{cm} \cdot I_I}{L_F \cdot L^2 \left(3 - \frac{4 \cdot L_F^2}{L^2} \right)} = 6.601 \cdot \frac{\text{kN}}{\text{mm}}$$

Stiffness in State II:

$$K_{II} := \frac{48 \cdot E_{cm} \cdot I_{II}}{L_F \cdot L^2 \left(3 - \frac{4 \cdot L_F^2}{L^2} \right)} = 1.167 \cdot \frac{\text{kN}}{\text{mm}}$$

3.2.3.2 Deformation considering only State II until ultimate load

Peak load:

$$F_{u.2.tot} = 9.977 \cdot \text{kN}$$

Deflection at peak load:

$$u_{II} := \frac{F_{u.2.tot}}{K_{II}} = 8.547 \cdot \text{mm}$$

Load as a function of displacement:

$$\text{Force}_2(u) := \begin{cases} u \cdot K_{II} & \text{if } u < u_{II} \\ F_{u.2.tot} & \text{if } u > u_{II} \end{cases}$$

3.2.3.3 Deformation considering State I and State II

Cracking load:

$$F_{cr.tot} = 4.129 \cdot \text{kN}$$

Deflection when cracking occurs:

$$u_{cr} := \frac{F_{cr.tot}}{K_I} = 0.625 \cdot \text{mm}$$

Peak load:

$$F_{u.2.tot} = 9.977 \cdot \text{kN}$$

Deflection at peak load:

$$u_{II} = 8.547 \cdot \text{mm}$$

Stiffness between cracking and yielding:

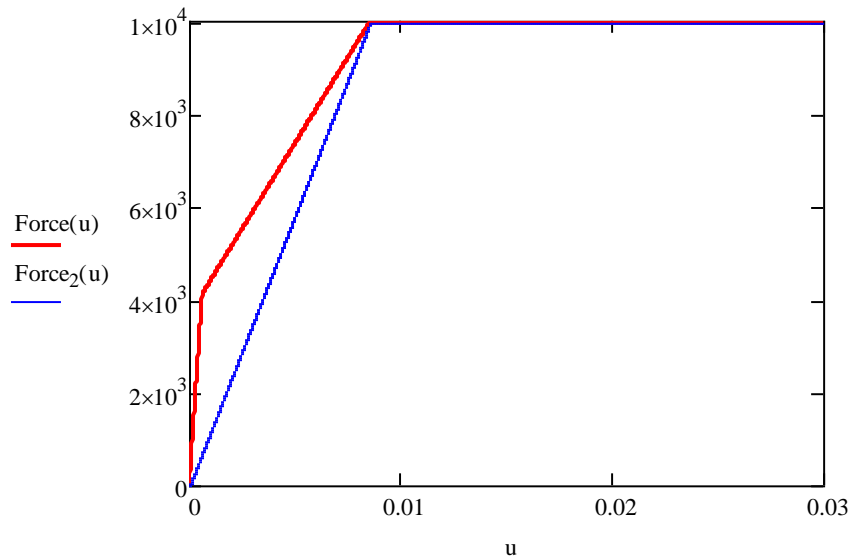
$$K_{cy} := \frac{F_{u.2.tot} - F_{cr.tot}}{u_{II} - u_{cr}} = 0.738 \cdot \frac{\text{kN}}{\text{mm}}$$

Load as a function of displacement:

$$\text{Force}(u) := \begin{cases} (K_I \cdot u) & \text{if } u \leq u_{cr} \\ [F_{cr.tot} + (u - u_{cr}) \cdot K_{cy}] & \text{if } u > u_{cr} \\ F_{u.2.tot} & \text{if } u > u_{II} \end{cases}$$

$$u := 0\text{mm}, 0.01\text{mm}.. 30\text{mm}$$

3.2.3.4 Load-deformation curves



3.3 Prediction of Plastic Rotational Capacity

3.3.1 Input Data

3.3.1.1 Geometry

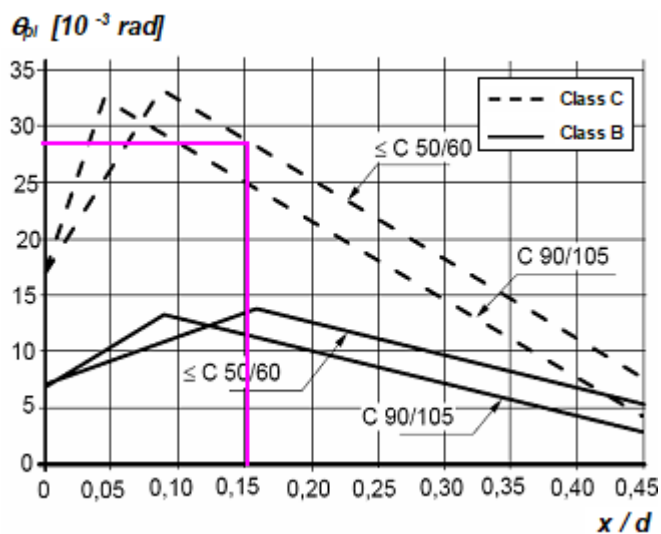
Beam height:	$h = 0.1 \text{ m}$
Beam width:	$b = 0.1 \text{ m}$
Effective span length:	$L = 1.3 \text{ m}$
Distance to critical section from support:	$l_0 := L_F = 0.5 \text{ m}$
Effective height:	$d = 0.08 \text{ m}$

3.3.2. Rotation Capacity According to Eurocode 2

Determine allowable rotation for reference beam ($\eta = 3$):

$$x_u := x_{u,1} = 12.143 \text{ mm} \quad \textbf{Note:} \text{ Position of neutral axis considering only bottom reinforcement.}$$

$$\frac{x_u}{d} = 0.152$$



Rotation capacity from the chart:

$$\Theta_{\text{total.Eur.R}} := 0.028$$

Correction for different values of shear slenderness:

$$\lambda := \frac{l_0}{d} = 6.25 \quad \kappa_\lambda := \sqrt{\frac{\lambda}{3}} = 1.443$$

$$\Theta_{\text{total.Eur}} := \kappa_{\lambda} \cdot \Theta_{\text{total.Eur.R}} = 0.04$$

Consider:

$$\Theta_{\text{total.Eur}} = 2 \cdot \theta_{\text{pl.Eur}}$$

Rotational capacity according to Eurocode 2:

$$\theta_{\text{pl.Eur}} := \frac{\Theta_{\text{total.Eur}}}{2} = 0.0202$$

$$u_{\text{pl.Eur}} := \theta_{\text{pl.Eur}} \cdot l_0 = 10.104 \text{ mm}$$

3.3.3 Rotation Capacity According to Bk 25

Empirical expression:

$$l_{\text{p.Bk25}} = 0.5 \cdot d + 0.15L \quad \text{Plastic hinge in the field}$$

Plastic hinge length:

$$l_{\text{p.Bk25}} := 0.5 \cdot d + 0.15L = 235 \text{ mm}$$

Area of tensile reinforcement:

$$A_s = 56.549 \text{ mm}^2$$

$$\omega_s := \frac{A_s}{b \cdot d} \cdot \frac{f_{ym}}{f_{cm}} = 0.119$$

Since no stirrups were included, the contribution of the top bars can be disregarded

Area of compression reinforcement:

$$A_c := 0 \quad \textbf{Note:} \text{ the top reinforcement has been proved to be subjected to tensile stress.}$$

$$\omega'_s := \frac{A_c}{b \cdot d} \cdot \frac{f_{ym}}{f_{cm}} = 0$$

Dominant failure mode:

$$\omega_{s,\text{crit}} := \frac{0.8 \cdot \varepsilon_{cu}}{\varepsilon_{cu} + \varepsilon_{su}} = 0.029 \quad \omega_s = 0.119$$

$$\omega_s > \omega_{s,\text{crit}} = 1$$

Note: The dominant failure mode is concrete crushing

Determination of plastic rotation capacity:

$$\theta_{\text{pl.Bk25}} := \frac{0.4 \cdot \varepsilon_{cu}}{\omega_c} \left(1 + 0.3 \cdot \frac{L}{d} \right) = 0.0692$$

$$u_{\text{pl.Bk25}} := \theta_{\text{pl.Bk25}} \cdot l_0 = 34.593 \text{ mm}$$

3.3.4. Summary

Eurocode 2:

$$\theta_{\text{pl.Eur}} = 0.02 \cdot \text{rad}$$

Bk25 method:

$$\theta_{\text{pl.Bk25}} = 0.069 \cdot \text{rad}$$

4. Four point bending and damaged reinforcement

4.1 Load Capacity of Reinforced Concrete Beam

The load capacity of a reinforced concrete beam is determined for a given cross section.

$$\text{kN} := \text{N} \cdot 10^3 \quad \text{MPa} := \text{Pa} \cdot 10^6$$

4.1.1 Input Data

4.1.1.1 Geometry

Beam height:

$$h := 0.1\text{m}$$

Beam width:

$$b := 0.1\text{m}$$

Effective span length:

$$L := 1.3\text{m}$$

Distance to load application from support:

$$L_F = 0.5\text{m}$$

Nominal bar diameter:

$$\Phi := 6\text{mm}$$

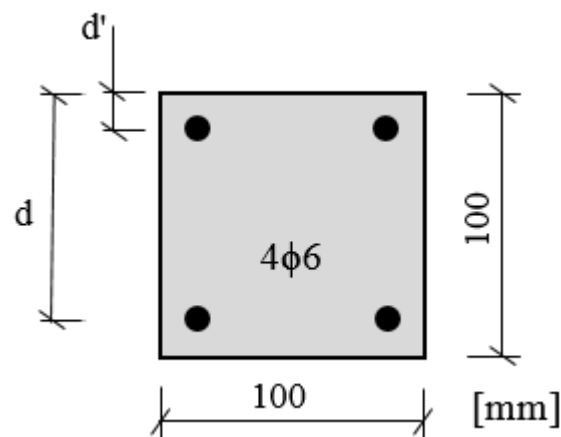
Area of reinforcement bar:

$$A_{\text{bar}} := \pi \cdot \frac{\Phi^2}{4} = 28.274 \cdot \text{mm}^2$$

Stirrup dimension:

$$\Phi_s := 0\text{mm}$$

Note: No stirrups



Number of bars in the top:

$$n' := 2$$

Number of bars in the bottom:

$$n := 2$$

Area of top reinforcement:

$$A_s := n \cdot A_{\text{bar}} = 56.549 \cdot \text{mm}^2$$

Area of bottom reinforcement:

$$A'_s := n' \cdot A_{\text{bar}} = 56.549 \cdot \text{mm}^2$$

Concrete cover:

$$c := 0.02\text{m} - \frac{\Phi}{2} = 0.017\text{m}$$

Distance from top edge to bottom reinforcement:

$$d := h - \left(\frac{\Phi}{2} + c \right) = 80\cdot\text{mm}$$

Distance from top edge to top reinforcement:

$$d' := \frac{\Phi}{2} + c = 20\cdot\text{mm}$$

4.1.1.2 Material properties

Concrete:

Mean compressive strength:

$$f_{cm} := 33.0\text{MPa}$$

Mean tensile strength

$$f_{ctm} := 4.43\cdot\text{MPa}$$

Mean modulus of elasticity

$$E_{cm} := 31.5\text{GPa}$$

Reinforcing steel:

Mean yield strength:

$$f_{ym} := 645\text{MPa}$$

Ultimate tensile stress:

$$f_t := 664\text{MPa}$$

Mean modulus of elasticity:

$$E_{sm} := 196\cdot\text{GPa}$$

4.1.2. Stress-strain Relationship of Concrete

4.1.2.1 Mathematic formulation

The parabola-rectangle stress-strain diagram for concrete under compression (according to EN 1992-1-1) is adopted.

Parameters for all concrete classes:

Concrete strain at maximum strength:

$$\varepsilon_{c2} := 2 \cdot 10^{-3}$$

Ultimate concrete strain:

$$\varepsilon_{cu2} := 3.5 \cdot 10^{-3}$$

Exponent:

$$n := 2$$

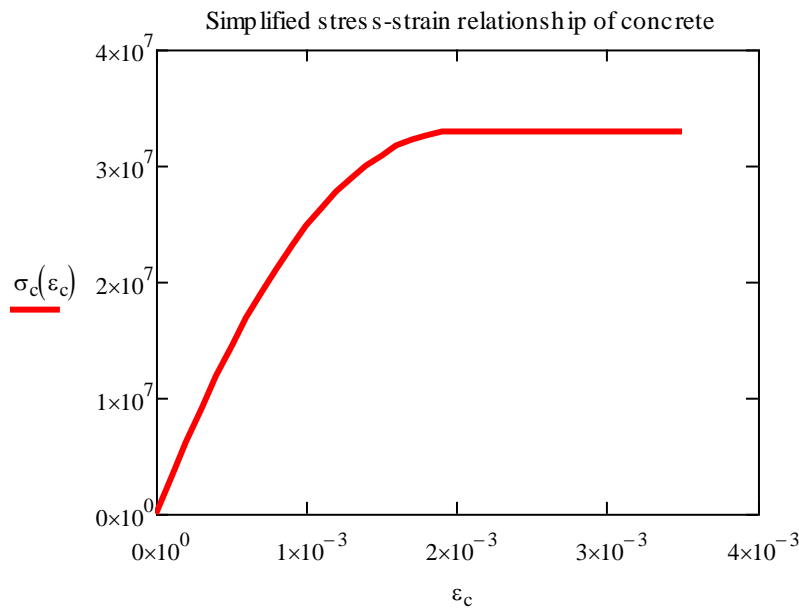
Stress-strain relationship:

$$\sigma_c(\varepsilon_c) := \begin{cases} \left[1 - \left(1 - \frac{\varepsilon_c}{\varepsilon_{c2}} \right)^n \right] \cdot f_{cm} & \text{if } 0 \leq \varepsilon_c \leq \varepsilon_{c2} \\ f_{cm} & \text{if } \varepsilon_{c2} < \varepsilon_c \leq \varepsilon_{cu2} \end{cases}$$

Create a vector with different values of strain:

$$\varepsilon_c := 0, 0.0001, \dots, \varepsilon_{cu2}$$

Graphic representation of the stress-strain relationship:



4.1.2.2 Determination of block factors

Area under the curve for a given value of strain:

$$\text{Area}(\epsilon_c) := \int_0^{\epsilon_c} \sigma_c(\epsilon_c) d\epsilon_c$$

Area under the curve multiplied by the distance from the origin to the center of gravity of the area:

$$A_{-\epsilon}(\epsilon_c) := \int_0^{\epsilon_c} \sigma_c(\epsilon_c) \cdot \epsilon_c d\epsilon_c$$

Determination of factors $\alpha_{R,S}$ and $\beta_{R,S}$

$$\alpha_{R,S}(\epsilon_c) := \frac{\text{Area}(\epsilon_c)}{f_{cm} \cdot \epsilon_c} \quad \alpha_{R,S}(\epsilon_{cu2}) = 0.81$$

$$\beta_{R,S}(\epsilon_c) := \frac{\epsilon_c - \frac{A_{-\epsilon}(\epsilon_c)}{\text{Area}(\epsilon_c)}}{\epsilon_r} \quad \beta_{R,S}(\epsilon_{cu2}) = 0.416$$

4.1.3 Stress-strain Relationship of Reinforcing Steel

4.1.3.1 Mathematic formulation

Ultimate steel strain: $\varepsilon_{su} := 0.0580$

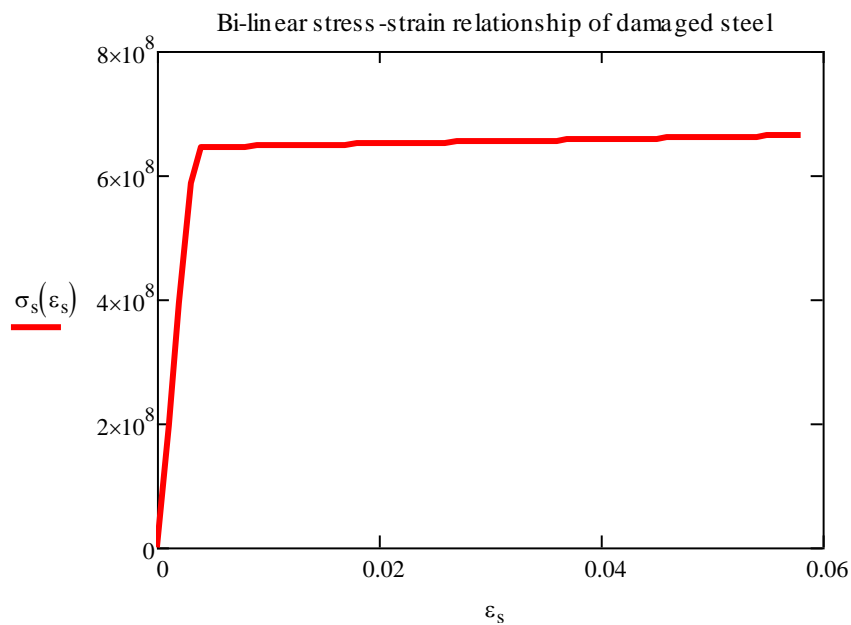
Yield strain: $\varepsilon_{sy} := \frac{f_{ym}}{E_{sm}} \quad \varepsilon_{sy} = 3.291 \times 10^{-3}$

Relationship parameters: $p_1(\varepsilon_s) := \frac{\varepsilon_s - \varepsilon_{sy}}{\varepsilon_{su} - \varepsilon_{sy}}$

Stress-strain relationship:
$$\sigma_s(\varepsilon_s) := \begin{cases} E_{sm} \cdot \varepsilon_s & \text{if } \varepsilon_s \leq \varepsilon_{sy} \\ f_{ym} + p_1(\varepsilon_s) \cdot (f_t - f_{ym}) & \text{if } \varepsilon_s > \varepsilon_{sy} \end{cases}$$

$\varepsilon_s := 0, 0.001 .. \varepsilon_{su}$

Graphic representation of the stress-strain relationship for reinforcing steel:



4.1.4. Design Strength Values

4.1.4.1 Concrete

Partial factor:

$$\gamma_C := 1.0$$

Design compressive strength:

$$f_{cd} := \frac{f_{cm}}{\gamma_C} \quad f_{cd} = 33 \cdot \text{MPa}$$

Concrete ultimate strain:

$$\varepsilon_{cu} := 0.0035$$

Stress block factors:

$$\alpha_R := \alpha_{R.S}(\varepsilon_{cu}) = 0.81$$

$$\beta_R := \beta_{R.S}(\varepsilon_{cu2}) = 0.416$$

5%-fractile tensile strength:

$$f_{ctk0.05} := 0.7 \cdot f_{ctm} = 3.101 \cdot \text{MPa}$$

Flexural tensile strength:

$$\kappa := 0.6 + \frac{0.4}{\sqrt[4]{\frac{h}{m}}} = 1.311$$

$$f_{ct.fl} := \kappa \cdot f_{ctm} = 5.809 \cdot \text{MPa}$$

4.1.4.2 Reinforcing steel

Partial factor:

$$\gamma_S := 1.0$$

Design yield stress:

$$f_{yd} := \frac{f_{ym}}{\gamma_S} \quad f_{yd} = 645 \cdot \text{MPa}$$

4.1.5. Load Capacity in Ultimate Limit State

4.1.5.1 Analysis of field section without top reinforcement

Number of bars in the top: $n' := 0$

Number of bars in the bottom: $n = 2$

Assume yielding:

$$\varepsilon_{s.1} > \varepsilon_{sy}$$

$$\varepsilon_{s.1} = \frac{d - x_l}{x_l} \varepsilon_{cu}$$

Position of neutral axis:

Initial guess: $x_{u,1} := 20\text{mm}$

Calculated value: $x_{u,1} := \text{root}\left(\alpha_R \cdot f_{cd} \cdot b \cdot x_{u,1} - \sigma_s \left(\frac{d - x_{u,1}}{x_{u,1}} \varepsilon_{cu}\right) \cdot n \cdot A_{bar}, x_{u,1}\right)$
 $x_{u,1} = 13.753\text{mm}$

Check the strain in the reinforcement bars:

$$\varepsilon_{s,1} := \frac{d - x_{u,1}}{x_{u,1}} \varepsilon_{cu} = 0.017 \quad \varepsilon_{sy} = 3.291 \times 10^{-3} \quad \varepsilon_{s,1} > \varepsilon_{sy} = 1$$

Calculation of load capacity:

$$M_{u,1} := \alpha_R \cdot f_{cd} \cdot b \cdot x_{u,1} \cdot (d - \beta_R \cdot x_{u,1}) \quad M_{u,1} = 2.729\text{ kN}\cdot\text{m}$$

$$F_{u,1} := \frac{M_{u,1}}{L_F} \quad F_{u,1} = 5.458\text{ kN} \quad F_{u,1,tot} := 2 \cdot F_{u,1} = 10.916\text{ kN}$$

Calculation of stress in the steel bars:

$$\sigma_{s,1} := \sigma_s(\varepsilon_{s,1}) \quad \sigma_{s,1} = 649.712\text{ MPa}$$

Calculation of curvature at failure:

$$\varepsilon_{s,1} = 0.017 \quad \varphi_{u,1} := \frac{\varepsilon_{s,1}}{d - x_{u,1}} = 0.254\text{ m}^{-1}$$

4.1.5.2 Analysis of field section including top reinforcement

Number of bars in the top: $n' := 2$

Number of bars in the bottom: $n = 2$

Assume tension in top and bottom and that the neutral axis is located above the top reinforcement.

Strain in bottom reinforcement: $\varepsilon_{s,2} = \frac{d - x_{u,2}}{x_{u,2}} \varepsilon_{cu}$

Strain in top reinforcement: $\varepsilon'_{s,2} = \frac{d' - x_{u,2}}{x_{u,2}} \varepsilon_{cu}$

Position of neutral axis:

Initial guess: $x_{u,2} := 20\text{mm}$

Calculated value:

$$x_{u,2} := \text{root} \left(\alpha_R \cdot f_{cd} \cdot b \cdot x_{u,2} - \sigma_s \left(\frac{d' - x_{u,2}}{x_{u,2}} \varepsilon_{cu} \right) \cdot A'_s - \sigma_s \left(\frac{d - x_{u,2}}{x_{u,2}} \varepsilon_{cu} \right) \cdot A_s, x_{u,2} \right)$$

$$x_{u,2} = 16.649\text{mm}$$

Note: The neutral axis is indeed located above the top reinforcement. Top bars are subjected to tensile stress.

Check the strain in the reinforcement bars:

$$\varepsilon_{s,2} := \frac{d - x_{u,2}}{x_{u,2}} \varepsilon_{cu} = 0.013 \quad \varepsilon_{sy} = 3.291 \times 10^{-3} \quad \varepsilon_{s,2} > \varepsilon_{sy} = 1$$

$$\varepsilon'_{s,2} := \frac{d' - x_{u,2}}{x_{u,2}} \varepsilon_{cu} = 7.044 \times 10^{-4} \quad \varepsilon'_{s,2} > \varepsilon_{sy} = 0$$

Calculation of moment capacity:

$$M_{u,2} := \alpha_R \cdot f_{cd} \cdot b \cdot x_{u,2} \cdot (d - \beta_R \cdot x_{u,2}) - \sigma_s \left(\frac{d' - x_{u,2}}{x_{u,2}} \varepsilon_{cu} \right) \cdot A'_s \cdot (d - d') \quad M_{u,2} = 2.782 \cdot \text{kN} \cdot \text{m}$$

$$F_{u,2} := \frac{M_{u,2}}{L_F} \quad F_{u,2} = 5.564 \cdot \text{kN} \quad F_{u,2,\text{tot}} := 2 \cdot F_{u,2} = 11.127 \cdot \text{kN}$$

Calculation of stress in the steel bars:

$$\sigma'_{s,2} := \sigma_s(\varepsilon'_{s,2}) \quad \sigma'_{s,2} = 138.054 \text{MPa}$$

$$\sigma_{s,2} := \sigma_s(\varepsilon_{s,2}) \quad \sigma_{s,2} = 648.482 \text{MPa}$$

Calculation of curvature at failure:

$$\varepsilon_{s,2} = 0.013 \quad \varphi_{u,2} := \frac{\varepsilon_{s,2}}{d - x_{u,2}} = 0.21 \text{m}^{-1}$$

4.1.6. Moment and Curvature at Onset of Yielding

4.1.6.1 Analysis of field section without top reinforcement

Yielding strain: $\varepsilon_{ev} = 3.291 \times 10^{-3}$

Definition of strain in the compressed edge:

$$\varepsilon_{cc,y,1} = \frac{x_{y,1}}{d - x_{y,1}} \cdot \varepsilon_{sy}$$

Tensile force in the bottom reinforcement:

$$F_{sy} := f_{yd} \cdot n \cdot A_{bar} = 36.474 \text{ kN}$$

Equivalent compressive force in concrete

$$F_{C,y,1} = \alpha_{R,y} \cdot f_{cd} \cdot b \cdot x_{y,1} \quad \alpha_{R,y} = \alpha_{R,S}(\varepsilon_{cc,y,1})$$

Horizontal equilibrium condition:

$$F_{sy} = F_{C,y}$$

Assume $x_{y,1} := 22.18 \text{ mm}$

Total tensile force: $F_{sy} = 36.474 \text{ kN}$

Total compressive force: $F_{C,y,1} := \alpha_{R,S} \left(\frac{x_{y,1}}{d - x_{y,1}} \cdot \varepsilon_{sy} \right) \cdot f_{cd} \cdot b \cdot x_{y,1} = 36.479 \text{ kN}$

$$\Delta F := F_{C,y,1} - F_{sy} = 5.062 \times 10^{-3} \cdot \text{kN}$$

Note: Check that $\Delta F \approx 0$

Calculation of strains

$$\varepsilon_{cc,y,1} := \frac{x_{y,1}}{d - x_{y,1}} \cdot \varepsilon_{sy} = 1.262 \times 10^{-3} \quad \varepsilon_{cc,y,1} < \varepsilon_{c2} = 1$$

Calculation of moment at yielding:

$$\alpha_{R,y} := \alpha_{R,S}(\varepsilon_{cc,y,1}) = 0.498 \quad \beta_{R,y} := \beta_{R,S}(\varepsilon_{cc,y,1}) = 0.356$$

$$M_{y,1} := \alpha_{R,y} \cdot f_{cd} \cdot b \cdot x_{y,1} \cdot (d - \beta_{R,y} \cdot x_{y,1}) \quad M_{y,1} = 2.631 \cdot \text{kN} \cdot \text{m}$$

$$F_{y,1} := \frac{M_{y,1}}{L_F} = 5.261 \cdot \text{kN} \quad F_{y,1,tot} := 2 \cdot F_{y,1} = 10.523 \cdot \text{kN}$$

Determination of stresses in the reinforcement bars:

$$\sigma_{s,v,1} := \sigma_s(\varepsilon_{sv}) \quad \sigma_{s,v,1} = 645 \cdot \text{MPa}$$

Curvature at yielding

$$\varepsilon_{sy} = 3.291 \times 10^{-3} \quad \phi_{y.1} := \frac{\varepsilon_{sy}}{d - x_{y.1}} = 0.057 \text{ m}^{-1}$$

4.1.6.2 Analysis of field section including top reinforcement

Assume tension in the top reinforcement bars

Yielding strain: $\varepsilon_{sy} = 3.291 \times 10^{-3}$

Definition of strain in the compressed edge and top reinforcement:

$$\varepsilon_{cc.y.2} = \frac{x_{y.2}}{d - x_{y.2}} \cdot \varepsilon_{sy} \quad \varepsilon'_{s.y.2} = \frac{x_{y.2} - d'}{d - x_{y.2}} \cdot \varepsilon_{sy}$$

Tensile force in the reinforcement:

$$\text{Top reinforcement:} \quad F'_{sy.2} = \sigma_s(\varepsilon'_{s.y.2}) \cdot A'_s$$

$$\text{Bottom reinforcement:} \quad F_{sy} := f_{yd} \cdot A_s = 36.474 \text{ kN}$$

Equivalent compressive force in concrete

$$F_{C.y.2} = \alpha_{R.y} \cdot f_{cd} \cdot b \cdot x_{y.2} \quad \alpha_{R.y} = \alpha_{R.S}(\varepsilon_{cc.y.2})$$

Horizontal equilibrium condition:

$$F_{sy} = F_{C.y.2} + F'_{sy.2}$$

Assume $x_{y.2} := 21.83 \text{ mm}$

$$\text{Total tensile force:} \quad F_{T.y.2} := F_{sy} = 36.474 \text{ kN}$$

$$\text{Total compressive force:} \quad F_{C.y.2} := \alpha_{R.S} \left(\frac{x_{y.2}}{d - x_{y.2}} \cdot \varepsilon_{sy} \right) \cdot f_{cd} \cdot b \cdot x_{y.2} + \sigma_s \left(\frac{x_{y.2} - d'}{d - x_{y.2}} \cdot \varepsilon_{sy} \right) \cdot A'_s = 36.475 \text{ kN}$$

$$\Delta F := F_{C.y.2} - F_{T.y.2} = 8.149 \times 10^{-4} \cdot \text{kN}$$

Note: Check that $\Delta F \approx 0$

Calculation of strains

$$\varepsilon_{cc,y,2} := \frac{x_{y,2}}{d - x_{y,2}} \cdot \varepsilon_{sy} = 1.235 \times 10^{-3}$$

$$\varepsilon_{cc,y,2} < \varepsilon_{c2} = 1$$

$$\varepsilon'_{s,y,2} := \frac{x_{y,2} - d'}{x_{y,2}} \cdot \varepsilon_{cc,y,2} = 1.035 \times 10^{-4}$$

Note: The strains are in fact negative though they are positive here to be able to use the stress-strain curve.

Calculation of moment at yielding:

$$\alpha_{R,y} := \alpha_{R,S}(\varepsilon_{cc,y,2}) = 0.49 \quad \beta_{R,y} := \beta_{R,S}(\varepsilon_{cc,y,2}) = 0.355$$

$$M_{y,2} := \alpha_{R,y} \cdot f_{cd} \cdot b \cdot x_{y,2} \cdot (d - \beta_{R,y} \cdot x_{y,2}) + \sigma_s \left(\frac{x_{y,2} - d'}{x_{y,2}} \varepsilon_{cc,y,2} \right) \cdot A'_s \cdot (d - d')$$

$$M_{y,2} = 2.621 \cdot \text{kN} \cdot \text{m} \quad F_{y,2} := \frac{M_{y,2}}{L_F} = 5.243 \cdot \text{kN} \quad F_{y,2,\text{tot}} := 2 \cdot F_{y,2} = 10.485 \cdot \text{kN}$$

Determination of stresses in the reinforcement bars:

$$\text{Top reinforcement:} \quad \sigma'_{s,y,2} := -\sigma_s(\varepsilon'_{s,y,2}) \quad \sigma'_{s,y,2} = -20.291 \cdot \text{MPa}$$

$$\text{Bottom reinforcement:} \quad \sigma_{s,y,2} := \sigma_s(\varepsilon_{sy}) \quad \sigma_{s,y,2} = 645 \cdot \text{MPa}$$

Curvature at yielding

$$\varepsilon_{sy} = 3.291 \times 10^{-3} \quad \varphi_{y,2} := \frac{\varepsilon_{sy}}{d - x_{y,2}} = 0.057 \text{ m}^{-1}$$

4.1.8. Summary

4.1.8.1 Moment and curvature at yielding without consideration of top reinforcement

$$M_{y,1} = 2.631 \cdot \text{kN} \cdot \text{m} \quad x_{y,1} = 22.18 \cdot \text{mm}$$

$$F_{y,1,\text{tot}} = 10.523 \cdot \text{kN} \quad \varphi_{y,1} = 0.057 \text{ m}^{-1}$$

4.1.8.2 Moment and curvature at yielding considering both top and bottom reinforcement

$$M_{y,2} = 2.621 \cdot \text{kN} \cdot \text{m} \quad x_{y,2} = 21.83 \cdot \text{mm}$$

$$F_{y,2,\text{tot}} = 10.485 \cdot \text{kN} \quad \varphi_{y,2} = 0.057 \text{ m}^{-1}$$

4.1.8.3 Load Capacity at Ultimate State without consideration of top reinforcement

$$M_{u,1} = 2.729 \cdot \text{kN} \cdot \text{m} \quad x_{u,1} = 13.753 \cdot \text{mm}$$

$$F_{u,1.\text{tot}} = 10.916 \cdot \text{kN} \quad \varphi_{u,1} = 0.254 \text{m}^{-1}$$

4.1.8.4 Load Capacity at Ultimate State considering both top and bottom reinforcement

$$M_{u,2} = 2.782 \cdot \text{kN} \cdot \text{m} \quad x_{u,2} = 16.649 \cdot \text{mm}$$

$$F_{u,2.\text{tot}} = 11.127 \cdot \text{kN} \quad \varphi_{u,2} = 0.21 \text{m}^{-1}$$

Increase in load capacity if top reinforcement is considered:

$$\frac{F_{u,2.\text{tot}} - F_{u,1.\text{tot}}}{F_{u,1.\text{tot}}} = 1.932 \cdot \%$$

4.2 Theoretical Load vs Deformation Relationship

4.2.1. Determination of Cracking Moment and Cracking Curvature:

Modular ratio:
$$\alpha_s := \frac{E_{sm}}{E_{cm}} = 6.222$$

Moment of inertia in State I:
$$I_I := \frac{b \cdot h^3}{12} + (\alpha_s - 1) 2n \cdot A_{bar} \cdot \left(d - \frac{h}{2}\right)^2 = 8.865 \times 10^6 \cdot \text{mm}^4$$

Cracking stress:
$$f_{ct,fl} = \frac{M_{cr} \cdot \left(\frac{h}{2}\right)}{I_I}$$

Cracking moment:
$$M_{cr} := \frac{f_{ct,fl} \cdot I_I}{\frac{h}{2}} = 1.03 \cdot \text{kN} \cdot \text{m}$$

Cracking force:
$$F_{cr} := \frac{M_{cr}}{L_F} = 2.06 \cdot \text{kN} \quad F_{cr,tot} := 2 \cdot F_{cr} = 4.12 \cdot \text{kN}$$

4.2.2. Determination of Moment of Inertia in State II

Calculation of position of neutral axis:

Number of bars in the top: $n' = 2$

Number of bars in the bottom: $n = 2$

Consider first moment of area around the neutral axis:

$$\frac{b \cdot x_{II}^2}{2} + (\alpha_s - 1) \cdot A'_s \cdot (x_{II} - d') = \alpha_s \cdot A_s \cdot (d - x_{II})$$

Initial guess:

$$x_{II} := 50 \text{ mm}$$

Calculated value:

$$x_{II} := \text{root} \left[\frac{b \cdot x_{II}^2}{2} - (\alpha_s) \cdot A'_s \cdot (d' - x_{II}) - \alpha_s \cdot A_s \cdot (d - x_{II}), x_{II} \right]$$

$$x_{II} = 20.408 \text{ mm}$$

Moment of inertia:

$$I_{II} := \frac{b \cdot x_{II}^3}{3} + (\alpha_s) \cdot A'_s \cdot (d' - x_{II})^2 + \alpha_s \cdot A_s \cdot (d - x_{II})^2$$

$$I_{II} = 1.533 \times 10^{-6} \text{ m}^4$$

4.2.3. Load-Deformation plot

4.2.3.1 Determination of equivalent stiffness

Stiffness in State I:

$$K_I := \frac{48 \cdot E_{cm} \cdot I_I}{L_F \cdot L^2 \cdot \left(3 - \frac{4 \cdot L_F^2}{L^2} \right)} = 6.587 \cdot \frac{\text{kN}}{\text{mm}}$$

Stiffness in State II:

$$K_{II} := \frac{48 \cdot E_{cm} \cdot I_{II}}{L_F \cdot L^2 \cdot \left(3 - \frac{4 \cdot L_F^2}{L^2} \right)} = 1.139 \cdot \frac{\text{kN}}{\text{mm}}$$

4.2.3.2 Deformation considering only State II until ultimate load

Peak load:

$$F_{u,2,tot} = 11.127 \cdot \text{kN}$$

Deflection at peak load:

$$u_{II} := \frac{F_{u,2,tot}}{K_{II}} = 9.77 \cdot \text{mm}$$

Load as a function of displacement:

$$\text{Force}_2(u) := \begin{cases} u \cdot K_{II} & \text{if } u < u_{II} \\ F_{u,2,tot} & \text{if } u > u_{II} \end{cases}$$

4.2.3.3 Deformation considering State I and State II

Cracking load:

$$F_{cr,tot} = 4.12 \cdot \text{kN}$$

Deflection when cracking occurs:

$$u_{cr} := \frac{F_{cr,tot}}{K_I} = 0.625 \cdot \text{mm}$$

Peak load:

$$F_{u,2,tot} = 11.127 \cdot \text{kN}$$

Deflection at peak load:

$$u_{II} = 9.77 \cdot \text{mm}$$

Stiffness between cracking and yielding:

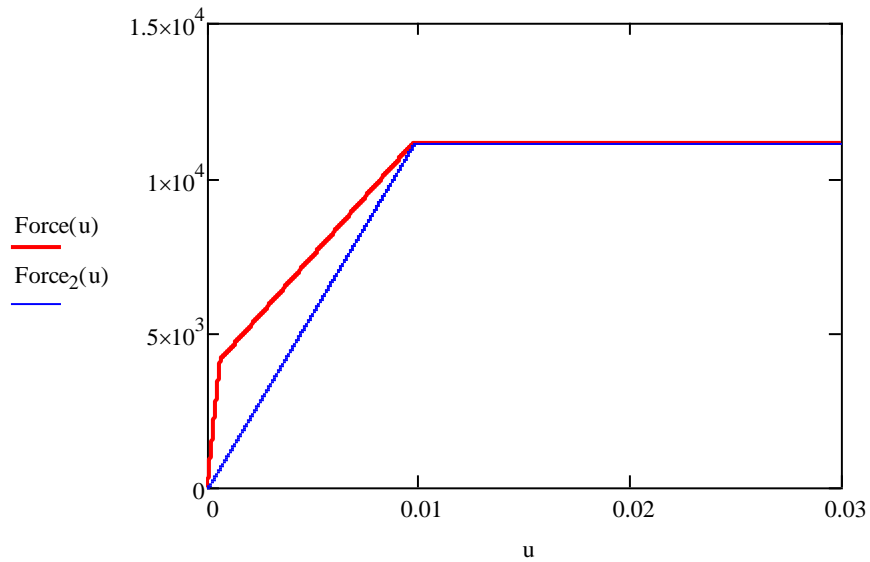
$$K_{cy} := \frac{F_{u,2,tot} - F_{cr,tot}}{u_{II} - u_{cr}} = 0.766 \cdot \frac{\text{kN}}{\text{mm}}$$

Load as a function of displacement:

$$\text{Force}(u) := \begin{cases} (K_I \cdot u) & \text{if } u \leq u_{cr} \\ [F_{cr.tot} + (u - u_{cr}) \cdot K_{cy}] & \text{if } u > u_{cr} \\ F_{u.2.tot} & \text{if } u > u_{II} \end{cases}$$

$$u := 0\text{mm}, 0.01\text{mm}.. 30\text{mm}$$

4.2.3.4 Load-deformation curves



4.3 Prediction of Plastic Rotational Capacity

4.3.1 Input Data

4.3.1.1 Geometry

Beam height: $h = 0.1 \text{ m}$

Beam width: $b = 0.1 \text{ m}$

Effective span length: $L = 1.3 \text{ m}$

Distance to critical section from support: $l_0 := L_F = 0.5 \text{ m}$

Effective height: $d = 0.08 \text{ m}$

4.3.2. Rotation Capacity According to Eurocode 2

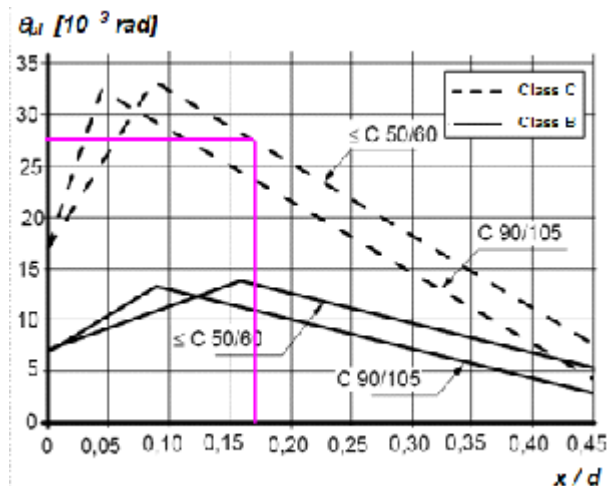
Determine allowable rotation for reference beam ($\eta = 3$):

$$x_u := x_{u,1} = 13.753 \text{ mm}$$

Note: Position of neutral axis considering only bottom reinforcement.

$$\frac{x_u}{d} = 0.172$$

Reinforcement class C



Rotation capacity from the chart:

$$\Theta_{\text{total Eur R C}} := 0.027$$

Correction for different values of shear slenderness

$$\lambda_C := \frac{l_0}{d} = 6.25 \quad \kappa_{\lambda_C} := \sqrt{\frac{\lambda_C}{3}} = 1.443$$

$$\Theta_{\text{total.Eur.C}} := \kappa_{\lambda_C} \cdot \Theta_{\text{total.Eur.R.C}} = 0.039$$

Consider:

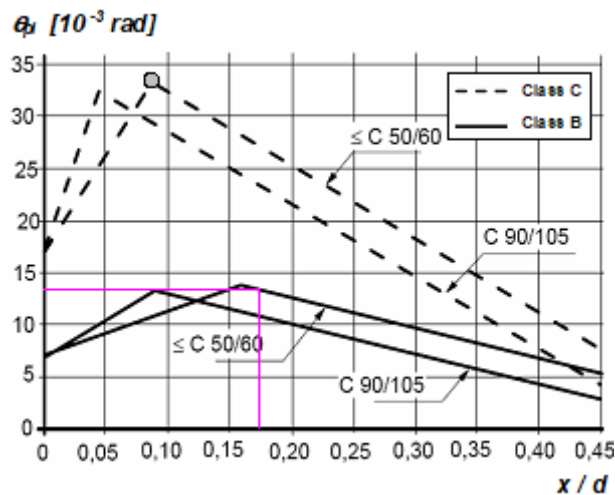
$$\Theta_{\text{total.Eur.C}} = 2 \cdot \theta_{\text{pl.Eur.C}}$$

Rotational capacity according to Eurocode 2:

$$\theta_{\text{pl.Eur.C}} := \frac{\Theta_{\text{total.Eur.C}}}{2} = 0.0195$$

$$u_{\text{pl.Eur.C}} := \theta_{\text{pl.Eur.C}} \cdot l_0 = 9.743 \cdot \text{mm}$$

Reinforcement class B



Rotation capacity from the chart:

$$\Theta_{\text{total.Eur.R.B}} := 0.0135$$

Correction for different values of shear slenderness:

$$\lambda_B := \frac{l_0}{d} = 6.25 \quad \kappa_{\lambda_B} := \sqrt{\frac{\lambda_B}{3}} = 1.443$$

$$\Theta_{\text{total.Eur.R}} := \kappa_{\lambda_B} \cdot \Theta_{\text{total.Eur.R.B}} = 0.019$$

Consider:

$$\Theta_{\text{total.Eur.B}} = 2 \cdot \theta_{\text{pl.Eur.B}}$$

Rotational capacity according to Eurocode 2:

$$\theta_{\text{pl.Eur.B}} := \frac{\Theta_{\text{total.Eur.B}}}{2} = 9.7428 \times 10^{-3}$$

$$u_{\text{pl.Eur.B}} := \theta_{\text{pl.Eur.B}} \cdot l_0 = 4.871 \cdot \text{mm}$$

4.3.3 Rotation Capacity According to Bk 25

Empirical expression:

$$l_{\text{p.Bk25}} = 0.5 \cdot d + 0.15L \quad \text{Plastic hinge on the field}$$

Plastic hinge length:

$$l_{\text{p.Bk25}} := 0.5 \cdot d + 0.15L = 235 \cdot \text{mm}$$

Area of tensile reinforcement:

$$A_s = 56.549 \cdot \text{mm}^2$$

$$\omega_s := \frac{A_s}{b \cdot d} \cdot \frac{f_{ym}}{f_{cm}} = 0.138$$

Since no stirrups were included, the contribution of the top bars can be disregarded

Area of compression reinforcement:

$$A_c := 0 \quad \textbf{Note:} \text{ the top reinforcement has been proved to be subjected to tensile stress.}$$

$$\omega'_s := \frac{A_c}{b \cdot d} \cdot \frac{f_{ym}}{f_{cm}} = 0$$

Dominant failure mode:

$$\omega_{s,\text{crit}} := \frac{0.8 \cdot \varepsilon_{cu}}{\varepsilon_{cu} + \varepsilon_{su}} = 0.046 \quad \omega_s = 0.138$$

$$\omega_s > \omega_{s,\text{crit}} = 1$$

Note: The dominant failure mode is concrete crushing

Determination of plastic rotation capacity:

$$\theta_{\text{pl.Bk25}} := \frac{0.4 \cdot \varepsilon_{cu}}{\omega_s} \left(1 + 0.3 \cdot \frac{L}{d} \right) = 0.0595$$

$$u_{\text{pl.Bk25}} := \theta_{\text{pl.Bk25}} \cdot l_0 = 29.766 \cdot \text{mm}$$

4.3.4. Summary

Eurocode 2:

$$\theta_{\text{pl.Eur.C}} = 0.019 \cdot \text{rad}$$

$$\theta_{\text{pl.Eur.B}} = 9.743 \times 10^{-3} \cdot \text{rad}$$

Bk25 method:

$$\theta_{\text{pl.Bk25}} = 0.06 \cdot \text{rad}$$

5. Initial shear velocity

$$\nu := 0.2$$

$$G := \frac{E_{cm}}{2(1 + \nu)} = 13.125 \text{ GPa}$$

$$\rho := 2420 \text{ kg}$$

$$v_s := \sqrt{\frac{G}{\rho}} \cdot m^{1.5} = 2.329 \times 10^3 \cdot \frac{\text{m}}{\text{s}}$$

$$t_0 := \frac{L}{2 \cdot v_s} = 0.279 \cdot \text{ms}$$